Vaasan yliopisto
UNIVERSITY OF VAASA

OMAR ALI ABU-ELLA

Interference Mitigation Using Group Decoding in Multiantenna Systems

ACTA WASAENSIA 308

COMPUTER SCIENCE 11
TELECOMMUNICATION ENGINEERING

ISBN 978–952–476–555–8 (print)
ISBN 978–952–476–556–5 (online)

ISSN 0355–2667 (Acta Wasaensia 308, print)
ISSN 2323–9123 (Acta Wasaensia 308, online)

ISSN 1455–7339 (Acta Wasaensia. Computer Science 11, print)
ISSN 2342–0693 (Acta Wasaensia. Computer Science 11, online)

Julkaisija	**Julkaisupäivämäärä**
Vaasan yliopisto	Syyskuu 2014

Tekijä(t) Omar Ali Abu-Ella	**Julkaisun tyyppi** Monografia	
	Julkaisusarjan nimi, osan numero Acta Wasaensia, 308	
Yhteystiedot Vaasan yliopisto Teknillinen tiedekunta Tietotekniikan laitos PL 700 FI-65101 Vaasa	**ISBN** ISBN 978–952–476–555–8 (print) ISBN 978–952–476–556–5 (online)	
	ISSN ISSN 0355–2667 (Acta Wasaensia 308, print) ISSN 2323–9123 (Acta Wasaensia 308, online) ISSN 1455–7339 (Acta Wasaensia. Computer Science 11, print) ISSN 2342–0693 (Acta Wasaensia. Computer Science 11, online)	
	Sivumäärä 202	**Kieli** Englanti

Julkaisun nimike
Interferenssin alentaminen käyttäen ryhmädekoodausta moniantennissa systeemeissä

Tiivistelmä
Langattomien viestintäjärjestelmien nopea yleistyminen ja jatkuva vaatimus yhä suuremmasta tiedonvälityskapasiteetista sekä paremmasta suorituskyvystä ovat tehneet tehokkaan interferenssin alentamistrategian käyttöönoton välttämättömäksi kaikissa nykyisissä ja tulevissa viestintäjärjestelmissä.

Tässä väitöskirjassa tutkitaan perättäisten ryhmädekoodaustekniikoiden käyttämistä interferenssin alentamiseksi ja moniantennisten systeemien suorituskyvyn parantamiseksi. Tutkimuksessa tarkastellaan laaja-alaisesti erilaisia mahdollisuuksia, ehdotetaan uusia systeemeitä ja pohditaan erilaisten ratkaisuvaihtoehtojen hyviä ja huonoja puolia useissa eri tiedonsiirtojärjestelmissä sekä erilaisissa langattomissa käyttöolosuhteissa.

Tulokset osoittavat että tutkitut perättäiset ryhmädekoodaus menetelmät yhdessä moniantennisten systeemien kanssa voivat suuresti parantaa energia- ja spektritehokkuutta, mahdollistaen joustavamman liikkuvuuden langattomissa tiedonsiirtojärjestelmissä. Tutkimuksen mukaan ne ovat lupaavia tekniikoita seuraavan sukupolven tiedonsiirtoverkkoihin (NGN).

Asiasanat
Interferenssin (keskinäishäiriön) alentaminen, kapsiteetti, ryhmädekoodaus, moniantenniset systeemit, MIMO.

Publisher	**Date of publication**
Vaasan yliopisto	September 2014

Author(s)	**Type of publication**
Omar Ali Abu-Ella	Monograph
	Name and number of series
	Acta Wasaensia, 308
Contact information	**ISBN**
University of Vaasa Faculty of Technology Department of Computer Science P.O. Box 700 FI-65101 Vaasa Finland	ISBN 978–952–476–555–8 (print) ISBN 978–952–476–556–5 (online)
	ISSN ISSN 0355–2667 (Acta Wasaensia 308, print) ISSN 2323–9123 (Acta Wasaensia 308, online) ISSN 1455–7339 (Acta Wasaensia. Computer Science 11, print) ISSN 2342–0693 (Acta Wasaensia. Computer Science 11, online)
	Number of pages: 202 — **Language**: English

Title of publication
Interference Mitigation Using Group Decoding in Multiantenna Systems

Abstract

The rapid growth of wireless communication systems and the continuing demand for higher data rate and better performance have made the deployment of an efficient interference mitigation strategy an inevitable necessity in every current or future communication system.

This thesis has studied the use of successive group decoding techniques to mitigate interference and improve the performance of multiantenna systems. I have extensively investigated the opportunities, proposed new systems, and discussed the advantages as well as the challenges of employing such approaches in several communication systems and for different wireless environments.

The results of this work show that the explored successive group decoding schemes along with the multiantenna systems have potentially improved the energy and spectral efficiency, allowing for more flexible mobility in wireless communication systems. According to the research, they can be considered as promising technologies for the next-generation networks (NGN).

Keywords

Interference mitigation, capacity, group decoding, multiantenna systems, MIMO.

ACKNOWLEDGEMENT

First and foremost, praise be to Allah almighty through whose mercy (and favors) all good things are accomplished.

Here, I would like to express my sincere gratitude to my advisor Prof. Mohammed Elmusrati for the continuous support of my doctoral study and research, also for his patience, motivation, enthusiasm, and immense knowledge. His friendly attitude and guidance helped me in all the time of research and writing of this thesis. I could not have imagined having a better advisor and mentor for my doctoral study.

I would like to thank Prof. Timo Mantere for the flexibility of the department which facilitate my study here in the University of Vaasa, and for his assistance to translate the abstract of this thesis to the Finnish language. Likewise, I would thank Mr. Virrankoski for his support to ease my work trips during my stay in Vaasa. Also, I thank Juha Miettinen for his swift ICT assistance. My sincere thanks also go to Dr. Ruifeng Duan for his friendship and all of the stimulating discussion that helped me through my journey in University of Vaasa. Also, I would thank all of my friends especially, Ahmad Elgargori and Tobias Glocker.

Last but not least, I would like to express my heartfelt gratitude to my family: my parents, my wive's parents, my sisters and brothers, for their support and taking care of my wife and daughter during the period of my study here in Finland. Finally, I would thank my wife for her patience and her limitless effort encouraging me to complete my doctoral study.

This thesis is specially dedicated to the souls of the martyrs in my beloved city of Misurata and all over my dear country Libya.

Special Acknowledgments to Pre-examiners:

I am grateful for pre-examinars, Prof. Riku Jäntti, Aalto University, Finland, and Prof. Majdi Ashibani, College of Industrial Technology, Libya, for their highly appreciated comments, which greatly improved the quality of this thesis.

Omar Abu-Ella
September 17, 2014
Vaasa, Finland

Contents

Figures

Tables

LIST OF ABBREVIATION

BER Bit Error Rate

BLAST Bell-Labs Layered Space-Time Architecture

bps/Hz bit per second per Hertz

BS Base-Station

BWC Broadband Wireless Communication

CDMA Code Division Multiple Access

CIC Cooperative Interference Cancellation

CPGD Constrained Partial Group Decoding

CSI Channel State Information

CSIT Channel State Information at the Transmitter

CoMP Coordinated multi-point

dB Decibel

DoF Degree of Freedom

DPC Dirty Paper Coding

EC Effective Capacity

FDD Frequency Division Duplex

FDMA Frequency Division Multiple Access

GD Group Decoding

ICh Interference Channel

ICT Information and Communication Technology

INR Interference-to-Noise Power Ratio

INR-MIN Interference-to-Noise Power Ratio Minimization

LSAS Large-Scale Antenna Systems

ISR Interference-to-Signal Power Ratio

LDPC Low Density Parity Check

LOS Line of Sight

LS-MIMO Large-Scale MIMO

LTE Long Term Evolution

MAC Multiple Access Channel

MCP Multi-Cell Processing

MIL Minimum Interference Leakage

MIMO Multiple-Input Multiple-Output

ML Maximum Likelihood

ML-MUD Maximum Likelihood Multi-User Detection

MMSE Minimum Mean Square Error

MSE Mean Square Error

MU-MIMO Multiple-User MIMO

NDS Norm Descent Search

NGN Next-Generation Networks

OSGD Optimal Successive Group Decoding

OSIC Ordered Successive Interference Cancellation

QoS Quality of Service

QoE Quality of Experiencece

QSA Quantum Search Algorithms

RBF Random Beamforming

SDMA Spatial Division Multiple Access

SIC Successful Interference Cancellation

SGD Successive Group Decoding

SINR Signal-to-Interference plus Noise Power Ratio

SINR-MAX Signal-to-Interference plus Noise Power Ratio Maximization

SIR Signal-to-Interference Power Ratio

SISO Single-Input Single-Output

SNR Signal-to-Noise Power Ratio

SU Signal-User

SU-MIMO Single-User MIMO

SUM-MSE-MIN Minimization of the Total Sum of the Mean Square Errors

TDD Time Division Duplex

TDMA Time Division Multiple Access

UT User-Terminals

ZF Zero-Forcing

NOTATION

Scalars represented in this thesis with lowercase italics, vectors, and matrices denoted respectively by lowercase boldface and uppercase boldface; superscripts $\cdot^{\mathcal{T}}$ and $\cdot^{\mathcal{H}}$ symbolize the transpose and Hermitian (complex-conjugate) transpose; $[\cdot]_{i,j}$ stands for the (i,j)th element of a matrix; $tr(\mathbf{A})$ implies the trace of matrix $\mathbf{A}$; $\mathtt{abs}(\cdot)$ designates the absolute value; $\|\mathbf{H}\|^2 = \sum_{i=1}^{N_r}\sum_{j=1}^{N_t}|[\mathbf{H}]_{i,j}|^2 = tr(\mathbf{H}^{\mathcal{H}}\mathbf{H})$ is the squared Frobenius norm of $\mathbf{H}$; $\mathbb{E}\{\cdot\}$ expresses the statistical average; $\sim$ denotes the distribution equivalence between the left and right random variables; $\approx$ means approximately equals; $\triangleq$ means is equal by definition to; the operator $(x)^+ \triangleq \max(0,x)$ is the projection on the nonnegative orthant; $\otimes$ indicates the kronecker product; also, $\odot$ denotes Hadammard product; uppercase calligraphic letter (e.g., $\mathcal{M}$) indicates a finite set of integers; the underlined uppercase calligraphic letter (e.g., $\underline{\mathcal{G}}$) represents the ordered partition of a set; $|\mathcal{A}|$ indicates cardinality of the set $\mathcal{A}$; $\in$ stands for: is element of; $\mathcal{B} \subseteq \mathcal{D}$ indicates that $\mathcal{B}$ is a subset of $\mathcal{D}$; $\Pr(\cdot)$ is a shorthand for the probability of; $\log(\cdot)$ expresses the logarithm term; $\mathtt{W}(\cdot)$ stands for the Lambert W-function; $\mathbb{R}$ denotes the set of real numbers; $\mathbb{R}_+$ denotes positive real plane; $\mathbb{C}$ denotes the complex plane.

LIST OF SYMBOLS

α	The interference-to-signal power ratio
α_c	Effective capacity
α_i	Stands for the cross-talk factor from the undesired transmitters
β_k	Scalar to fulfill the total virtual power constraint
$\beta(\gamma_k, K)$	The scheduling threshold
γ	SNR of the system
γ_{kl}	Scalar to account for the path-loss and shadowing effects
γ_F	FDMA transmit SNR
γ_T	TDMA transmit SNR
γ_{gap}	Represents the gap between the capacity limit using Gaussian modulation with the infinite-length random codes and the achievable capacity using practical modulation scheme with finite-length codes
δ_a	Constant depends on the service and the arrival processes
$\Delta_k(\cdot)$	Rate margin of user k
$\zeta(r,t)$	The (r,t)th element of the variance profile matrix
$\zeta_{m,k}^n$	Path-loss coefficient for the link between the kth user of the mth cell and the nth base station
η_{ch}	Channel estimation error ratio
η_1	The fraction of the time or bandwidth resources allocated to user 1 in the orthogonal transmission scheme
θ	Decaying rate of the tail of the distribution of the stationary length of the buffering queue
$\hat{\theta}$	Normalized QoS exponent
ι	Factor to consider the large-scale fading effects
λ_k	Lagrange multiplier for the kth user
μ_c	Ergodic capacity or the mean of the distribution of instantaneous achieved capacity by the desired user in the large-scale OSGD system
μ_i	Group size constraint, the maximum allowable number of users that allowable to be jointly decoded at receiver i
μ_z	Mean of Gaussian random variable Z
$\hat{\mu}_c(\gamma, N)$	Estimated capacity mean as a function of SNR and number of antennas

ξ_{rm}	Denotes the minimum rate margin
ρ	The spatial correlation factor
σ^2	Noise variance
σ_c^2	The variance of the distribution of achieved capacity by the desired user in the large-scale OSGD system
σ_z	Variance of Gaussian random variable Z
$\hat{\sigma}_c^2(\gamma, N)$	Estimated capacity variance as a function of SNR and number of antennas
Σ	Deterministic matrix
Υ	The normalized target rate
ϕ	empty set
Φ	The reflected covariance matrix of virtual channel
$\acute{\Phi}_k$	The virtual covariance matrix
$\Phi_{\mathcal{G}_l}^{(i)}$	The noise covariance matrix at the receiver i in the decoding stage l
ψ_1, ψ_2 and ψ_3	Scalars determine the scheduling threshold
$\varepsilon(\cdot)$	Denotes the minimum rate margin
ϑ_k	Scalar to fulfill the total power constraint
$\aleph_r$	Receive side spatial correlation matrix
$\aleph_t$	Transmit side spatial correlation matrix
$\aleph_{ij}$	The (i,j) element of the spatial correlation matrix
$\triangle(\cdot)$	Denotes the rate margin

$\mathcal{A}_c$	The constellation of the transmitted signal alphabet
$\mathcal{A}$ or $\mathcal{D}$, and $\mathcal{B}$	Disjoint subsets of users
$\mathcal{C}(\cdot)$	Denotes the rate region
$\mathcal{C}_d(\cdot)$	The instantaneous achievable rate region at the receiver of interest
$\mathcal{C}_k(\cdot)$	The capacity limit region of the kth receiver
$\mathcal{D}_t$	The set of all possible combinations of the transmitted data vectors
$\mathcal{E}_i^2$	Squared error of the ith estimated value
$\mathcal{E}(\sigma_c^2, \hat{\theta})$	Rate margin offset depends on the variance of the achieved capacity σ_c^2 and the system QoS constraints expressed by the metric $\hat{\theta}$
$\mathcal{G}^*$	The set of jointly decoded users corresponds to the minimum rate margin
$\mathcal{G}_l$	Set of the jointly decoded users in stage l
$\mathcal{G}_m^k$	The set of users that will be decoded jointly by receiver k at stage m
$\underline{\mathcal{G}}^k$	Valid partition of the receiver k
$\underline{\mathcal{G}}$	ordered partition
$\underline{\mathcal{G}}_{opt}$	The optimal partition
$\mathcal{K}$	Ricean factor of fading channel
$\mathcal{L}(\cdot)$	Lagrangian objective function
$\mathcal{M}$ or $\mathcal{S}$	The total set of users indices
$\mathcal{O}^{(i)}$	Stands for the outage event at the receiver i
$\mathcal{Q}^d$	The valid partition of $\mathcal{M}$ for the user of interest d
$\mathcal{Q}^k$	Valid ordered partition for the user k
$\mathcal{Q}^{d*}$	The optimal ordered partition for the receiver d which minimizes the rate margin or equivalently maximizes the rate increment
$\mathcal{Q}_{opt}^k$	Optimal ordered partition for the CPGD scheme
$\underline{\mathcal{Q}}^d$	Ensembles all the valid partitions $\mathcal{Q}^d$
$\boldsymbol{\mathcal{Q}}_i$	Valid ordered partition of all subsets of $\mathcal{M}$ which contain i
$\underline{\boldsymbol{\mathcal{Q}}}_i$	The set of all valid ordered partitions of all subsets of $\mathcal{M}$ which contain i
$\underline{\boldsymbol{\mathcal{Q}}}^k$	Set ensembles all the valid partitions for the user k
$\mathcal{S}_i$ and $\hat{\mathcal{S}}_i$	The actual and the estimated sample value of a quantity respectively
$\mathcal{U}, \mathcal{V}$	Any two disjoint partitions of the set of users' indices

a_m, b_m and c_m	Constants determine the estimated capacity mean
a_v, b_v c_v, d_v and e_v	Constants determine the estimated capacity variance
B	Stands for the system bandwidth
B_m	Set of the indices of users who have responded with the integer m as a favorable beam in the feedback stage
C	Ergodic capacity
C_{opt}	The optimal per-cell sum-rate
C_{mmse}^{FDMA}	The achievable per-cell sum-rate with FDMA and linear MMSE filtering
C_{mmse}^{TDMA}	The achievable per-cell sum-rate with TDMA and linear MMSE filtering
d_0	Reference distance
d_k	Degree of freedom assigned to the kth transmitter
D	Stands for the buffering delay of the packet at the steady-state
D_{max}	The delay bound of a connection
$d(r,t)$	Represents the distance between the kth user of the mth cell and the nth base station
$\mathbf{E}_{ch}$	Channel estimation error matrix
$f_i(\cdot)$	Bounding function for the users i
$f_Z(z)$	Probability density function of a random variable Z
$F_C(\cdot)$	The achieved capacity commutative distribution function
$F_k(x)$	The cumulative distribution function (CDF) of $SINR_{k,m}$
$\mathbf{g}_m$	The mth filtering vector.
$\mathbf{G}$	Complex Gaussian random matrix
$\mathbf{G_{mmse}}$	The MMSE filtering matrix
h_{n_s}	Sub-channel gain
$\mathbf{h}_{k,q}$	denotes the channel vector from the q base station to the user in the cell k
$\mathbf{H}$	General fading channel matrix
$\hat{\mathbf{H}}$	The estimated channel matrix
$\mathbf{H}_d$	Channel fading matrix seen by the receiver of interest from its intended transmitter
$\mathbf{H}_D$	Deterministic component of the channel matrix
$\mathbf{H}_i$	Channel fading matrix seen by the receiver of interest from the interfering transmitters
$\mathbf{H}_o$	The intra-cell orthogonalization channel matrix

$\mathbf{H}_r$	Random component of the channel matrix
$\mathbf{H}_w$	Normalized complex Gaussian random matrix
$\hat{\mathbf{H}}_k$	Estimated channel matrix of the kth user
$\mathbf{H}_{ki}$	Channel coefficient matrix between the i transmitter and the kth receiver
$\tilde{\mathbf{H}}^{(i)}$	Concatenation of the different users channel realization seen by the receiver i
$\tilde{\mathbf{H}}_m$	The channel matrix excluding the corresponding channel vectors of the previous detected streams
$\mathbf{I}$	Identity matrix
$\mathbb{I}_{n_{BS}\times n_{UT}}$	Matrix of ones with size of $n_{BS} \times n_{UT}$
J_{MSE}	MSE cost function for the total transmitted data streams
k	Index of the user of interest
K	Number of active users in the system
L	the number of array antennas
L_0	Path-loss value at the reference distance
L_{ki}	The interference power due to virtual transmitter k at virtual receiver i
$\acute{L}_k$	The total interference power due to the virtual transmitter k
m	The transmitted stream index
m_k^*	The most favorable beam for kth user
n	Symbol interval index, or the time slot index
n_s	Sub-channel index
n_k	Received noise at the terminal user at the cell k
n_{BS}	Number of antennas of base station base station
n_{UT}	Number of antennas of the terminal user
$\mathbf{n}_k$	Complex additive white Gaussian noise (AWGN) vector at receiver k
N	Number of antennas
N_c	Number of cells
N_r	Number of receive antennas
N_{r_k}	Number of receive antennas of the kth receiver
N_{t_i}	Number of transmit antennas of the ith transmitter
N_{sc}	The number of parallel sub-channels
N_0	The noise power spectral density

N_t	Number of transmit antennas
N_{rk}	Number of receive antennas of the receiving user k
N_{tk}	Number of transmit antennas of the transmuting user k
p	Number of decoding stages
P	Represents the transmit power
$\bar{P}$	The average transmit power
P_{n_s}	The allocated power to the n_sth sub-channel
$P_{n_s}^*$	The optimal power allocation which satisfies the water-filling algorithm optimality condition
P_D	The average of received power from the desired user
P_I	The average of received interference power from each interfering transmitter
P_i, P_j	The transmitted power from base station i or the allocated power to the jth transmitter
P_T	Total allocated power
$P_{outage}(R, \gamma, N)$	The rate outage probability of user for a certain target rate R_t, N antennas and SNR
q_l	The length of the buffering queue
$q_l(\infty)$	The steady length of a queue of a stationary ergodic service process
Q_l	The distribution of the buffering queue length
$\mathbf{Q}$	The interference plus noise covariance matrix at receiver k
$\mathbf{Q}_x$	Normalized input covariance matrix
r^*	Globally optimal rate increment
r_k^*	Represents the maximum tolerable rate increment for the receiver k
$r_{\mathcal{Q}^d}^*$	The maximum user rate increment at the receiver d
$r_d(\mathcal{Q}^d)$	The fair rate increment which grantee that all users in valid partition are decodable at the receiver d
$r_k(\mathcal{Q}^k)$	The fair rate increment which grantee that all users in valid partition $\mathcal{Q}^k$ are decodable at the receiver k
$\tilde{\mathbf{r}}^{(i)}$	The whitened received signal vector at user i
$\mathbf{r}_{\mathcal{G}_m^d}^*$	maximum rate increment vector for receiver d
$\mathbf{r}_{\mathcal{G}_{m^k}}^k$	Rate-increment vector of the users in the set $\mathcal{G}_{m^k}$
$\boldsymbol{R}_{\mathcal{G}_m^d}$	decodable rate vector for receiver d before the increment
$\mathbf{R}$	Users' rates
$\mathbf{R}_{\mathcal{D}}$	Rate of jointly decoding the users in the set $\mathcal{D}$
$\boldsymbol{\mathcal{R}}_k(\cdot)$	The rate region of user k

R_i	Transmission rate of the ith user
R_{di}	Cell radius
$R_s[i]$	The discrete time stationary ergodic stochastic service process
$\boldsymbol{R}_{\mathcal{G}_{m^k}}$	Rate vector of the users in the set $\mathcal{G}_{m^k}$
$\widetilde{\boldsymbol{R}}_{\mathcal{G}_{m^k}}$	Rate vector of the users in the set $\mathcal{G}_{m^k}$ after the fair increment
$\widetilde{\boldsymbol{R}}_{\mathcal{G}_m^d}$	Maximum decodable rate vector for receiver d
$\mathbf{s}_{ki}$	The interference signal due to transmitter k at the unintended receivers
$\mathbf{s}_i$	The transmitted signal vector from the base station i
$\mathbf{S}_k$	Denoting the training sequence of the kth user
S_k	The size of the transmitter k data vector
$S[t]$	The time accumulated service process
$SINR_{k,m}$	SINR of the decoded $m$he data stream SINR at the kth user
t	denotes time
$\mathbf{t}_k, \mathbf{u}_k$	The desired signal subspace of the kth user
T	Time frame duration, or block duration
T_q	Certain queue limit
$T_{q_{max}}$	The buffer size of a queue
$\mathbf{u}$	small-scale fading random vector
U	Number of the scheduled users
$\mathbf{v}_i$	The transmit filter vector at the transmitter i or the unitary random beamforming vector for transmitter i
$\mathbf{v}_k^{opt}$	The optimum transmit filter vector at the transmitter k
$\mathbf{V}_i$	Precoding matrix at transmitter i
$\mathbf{V}_k$	The linear transmitting precoding matrix for the kth user
$\mathbf{w}_k$	The receiver filter vector at the receiver k
$\mathbf{w}_k^{opt}$	The optimum receiver filter vector at the receiver k
$\mathbf{w}_k^{INR}$	The post-processing vector to minimize INR at the kth user
$\mathbf{w}_k^{SINR}$	The post-processing vector to maximize SINR at the kth user
$\mathbf{W}_k$	The linear receiving filtering matrix for the kth user
$\hat{\mathcal{W}}$	The rate margin minimizing set which among all minimizers has the smallest cardinality
$\mathtt{W}(\cdot)$	Stands for the Lambert W-function
$W_{max}(\mathbf{A})$	The eigenvector of matrix $(\mathbf{A})$ corresponding to the maximum eigenvalue $\lambda_{max}(\mathbf{A})$

$W_{min}(\mathbf{A})$	The eigenvector of matrix $(\mathbf{A})$ corresponding to the minimum eigenvalue $\lambda_{min}(\mathbf{A})$
x_m	The mth complex valued of the transmitted data symbol
$\hat{x}_m^{(f)}$	The final estimated output corresponding to the mth antenna stream
$\mathbf{x}$	Transmitted signal vector
$\mathbf{x}_d$	Represents a unit power symbol vector transmitted from the desired user
$\mathbf{x}_i$	Represents a unit power symbol vector transmitted from the ith user
$\hat{\mathbf{x}}_{\mathrm{ML}}$	the ML estimate of the transmitted vector $textbfx$
$\mathbf{x}_{\mathcal{G}_l}$	Transmitted symbol vector by the users included in the set $\mathcal{G}_l$
$\hat{\mathbf{x}}_{\mathcal{G}_l}^{(i)}$	The decision made corresponding to the codeword of the users in the set $\mathcal{G}_l$
X, Z and Γ	Denote random variables
$\mathbf{y}_k$	Received signal vector
$\mathbf{Y}_k$	Received signal matrix at receiver k
$\mathbf{z}$	The complex AWGN vector at the receiver
$\mathbf{z}_k$	AWGN vector at the receiver k
$\tilde{\mathbf{z}}^{(i)}$	Received noise vector at user i

1 INTRODUCTION

1.1 Motivations

In the whole world wide the strategy of the leading mobile communication companies is to improve their operations and enhance their quality of service, all together with their aiming towards better customer confidence. Thus, they are actively seeking for new ways and technologies to spread those services everywhere and to make them available to everyone at any time. This accelerates the expansion of wireless communication and speed up the move towards the next-generation of Information and Communication Technology (ICT). Motivated by that, researchers continuously try to create new promising developments in the field of communication systems to realize peak bit rate of multi-gigabit per second. Achieving such rate is predicted to be facilitated by the deployment of distributed Broadband Wireless Communication (BWC) systems, where interference arises everywhere, such interference environment is usually appears in most of wireless communication systems, see Figures (1, and 2). Therefore, in this thesis we decided to extensively study, investigate, and analyze the performance of new interference mitigation approaches that can be adopted in the multiantenna systems. Thus, this research work can significantly improve the currently employed communication networks and help to develop new energy-efficient techniques with higher data rates. Consequently, they can be used to support higher spectral efficiency with more flexible mobility wireless communication for the Next-Generation Networks (NGN).

Technically speaking, this thesis should be significant in the sense that it will deepen the understanding and expand the insight of the subject of interference management and mitigation using the group decoding techniques, and it will broaden the comprehension of the crucial role of the Group Decoding (GD) as a promising key strategy for the broadband wireless communication networks to resolve the challenges facing the next-generation networks beyond 4G (B4G) towards 5G.

Moreover, this work can significantly contribute to the developing of a new environmentally friendly design for the wireless communication systems. Simply, because a better interference mitigation scheme means, the communication system can work reliably with less transmitted power. This leads to better and more efficient power consumption. Consequently, following the stream which encourages the research to develop new green technologies, our work in this thesis can

contribute to explore novel techniques that have less harmful impact on the environment and the human health.

The remainder of this chapter is organized as follows: Section 1.2 gives a general review for the multiple antenna techniques. Section 1.3 discusses the most recent trends of multiple antenna techniques to mitigate interference. Section 1.4 briefly outlines the previous research work related to this thesis topic. Section 1.5 describes the general model of interference channel which have been adopted in this thesis. A brief review for the basic concepts of the effective capacity illustrated in Section 1.6. Section 1.7 gives a brief review for the fundamentals of the interference mitigation techniques addressed in this thesis and which are used later in this thesis for the performance assessment of the investigated group decoding schemes. Complexity issues related to the presented schemes are discussed in Section 1.8. Contributions of this thesis are summarized in Section 1.9. Finally, Section 1.10 presents main outlines of this thesis.

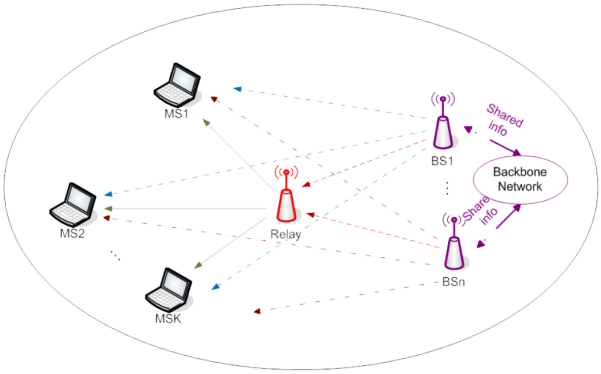

Figure 1. Interference in the distributed communication network (Vucetic, Li & Hardjawana 2013)

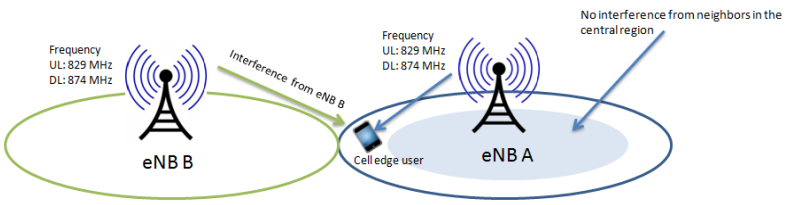

Figure 2. Interference in the cellular communication system (Basir 2013)

1.2 Multiple Antenna Techniques

The all-time question faces the researchers in the field of wireless communication is: *how to design a high speed systems with reliable connection?* in other words, how can we establish a wireless system that grantees not only a high speed bit rate but with an acceptable low bit error rate performance? Conventionally, single antenna systems try to utilize the time and frequency domains to optimize the system performance to overcome the wireless channel multipath effects. However, the rapidly increase of the wireless services and the pressing demand for higher bit rates and better error performance, have motivated the researcher to look for other new ways to utilize the available resources in communication system. Interestingly the solution came by exploiting the multipath environment which was a part of the problem. This can be achieved by utilizing the antenna system to open a new era of wireless systems to be extended into another processing space, represented as the spatial domain by using the multiple antennas.

This great opportunity of utilizing the multiantenna system started in the end of the 1990's, where it was shown to be an opening for new technologies that can substantially improve the quality of services of the wireless systems (Mietzner *et al.* 2009). The general aspects of the benefits of utilizing the multiple antennas in wireless communication system as presented in Fig. 3 can be categorized into the following main points:

1.2.1 Higher Data Rates Using Spatial Multiplexing

Spatial multiplexing means transmitting independent sequence (layer) of information simultaneously through the individual elements of the multiple antenna system. Spatial multiplexing using N-element transmit antenna can roughly increase the data rate by factor of N comparing with the single antenna system, and interestingly without any increase of the allocated power. The first spatial multiplexing schemes were published in (Paulraj & Kailath 1994; Weitzen, Kilpatrick & Mui 1992). Then, the well-known spatial multiplexing scheme Bell-Labs Layered Space-Time Architecture (BLAST) was introduced in (Foschini 1996). The main steps of all the spatial multiplexing techniques are: splitting the data bits into N layers at the transmitter (demultiplexing). Then, those bits are modulated into symbols and transmitted simultaneously over the N antenna elements. At the receiver side, interference cancellation algorithms are employed to separate

the different data sequences from the received signal. There are various types of detection algorithms. The designers of those algorithms try to keep the balance between the performance and complexity trade-offs. For instance, good examples for the low complexity detection algorithms based on linear receivers are the zero-forcing and Minimum Mean Square Error (MMSE) algorithms (Gore, Gorokhov & Paulraj 2002). As expected the error performance of such receiving algorithms are poor (Mietzner *et al.* 2009). On the other hand, the receiver designed based on the ML detection criterion has the best performance, which of course comes with the heavy cost of the exponentially growing complexity with the number of transmit antenna and the symbol size due to the exhaustive search manner of its decision making process.

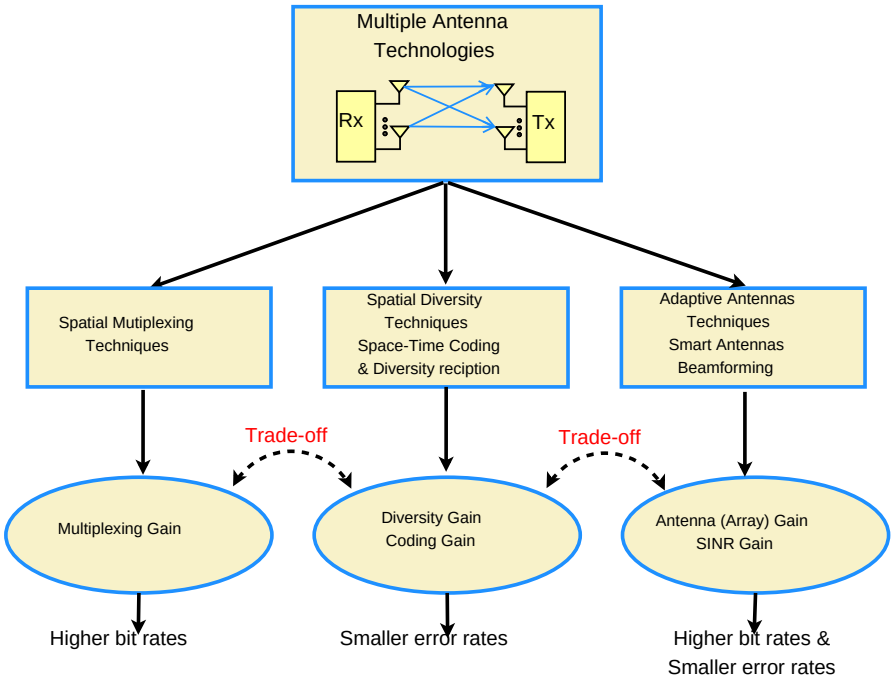

Figure 3. Benefits of multiple antenna techniques

Other, schemes stand in the middle between the linear and ML systems. They are designed to have near ML performance but with significantly reduced complexity. This goal is achieved by performing the detection process successively rather than jointly. The Successful Interference Cancellation (SIC) algorithms which were introduced as detection methods for the multi-user Code Division Multiple Access (CDMA) system (Sfar & Letaief 2003), and the similar successive detection

based BLAST schemes are good examples of this strategy (Joshi, Rukmini & Mahesh 2011). In general, those schemes provide a good trade-off between the performance and complexity, especially, for high Signal-to-Noise Power Ratio (SNR) environment, where the error propagation, the main drawback of the successive algorithms, is negligible. In Subsection 1.7.4 we will address the SIC algorithm in more detail.

1.2.2 Smaller Bit Error Rate Using Spatial Diversity

In contrast to the spatial multiplexing, if the same sequence of information is transmitted from or received by the different elements of antenna system, then the redundancy of information can be exploited to establish the diversity gain that has the same effect of the channel coding, but without reducing the bit rate comparing with the single antenna system. One of the first diversity techniques was introduced in 1950's where it exploits the linear combining techniques to achieve receiving diversity (Brennan 1959). On the other hand, it took about four decades before introducing the first transmit diversity scheme by Alamouti for wireless communication systems in the end of 1990's (Alamouti 1998). From other point of view, the spatial diversity can be classified into two types: the macroscopic and microscopic diversity. The first implies the large-scale diversity and it related to the obstructions and the shadowing effects in wireless environment. The large-scale diversity can be attained by the large spatial separation between the multiple antennas in transmit or receive side, such that the probability that all links are simultaneously obstructed is smaller than that for the single antenna system. The second is referring to the small-scale diversity which arises as a result of multipath effects in the rich scattering environment. This type of diversity is achieved by separating the multiple co-located antenna elements by a distance less than a wavelength, such that the probability of all received links are simultaneously in deep fading is smaller than that for the single antenna system (Mietzner *et al.* 2009).

1.2.3 Improving Signal-to-Noise Ratio and Co-Channel Interference Mitigation Using Adaptive Antenna Arrays

In addition to increasing the data rate or decreasing the error rate, the multiple antenna system can also be utilized to improve the SNR or to suppress the co-channel

interference (Mietzner *et al.* 2009). As presented in (Godara 1997) the adaptive array antennas, widely known as the smart antennas, can be exploited to achieve this improve SNR or SINR by utilizing beamforming techniques to reshape (steer) the array antenna pattern, by directing and maximizing the main lobe towards the direction of the desired signal. On the other hand, these techniques can also be used to null or minimize the array antenna gain at the directions correspond to the undesired signals. The SNR or SINR gain achieved through this process is often called antenna or array gain. The concept of the Antenna arrays is not new, and it dated back to the 1950's, see (Harrington & Lepage 1952; Widrow *et al.* 1967). However, at that time the main purpose of such technology was limited for the radar and aerospace application. But, similar to other multiple antennas techniques, the 1990's have witnessed the start of the intensive research of utilizing the adaptive array antenna in the field of wireless communications. Although the receive or transmit diversity can be used to establish the adaptive antenna system to mitigate interference in wireless communication system, it is still till now that these techniques are limited to be employed only by fixed station or mobile station fixed on vehicles; because of the requirements of such system. However, the recent trend of research is aiming to investigate the feasibility of equipping the end user hand mobile sets with smart antennas in micro-strip form. Here it is worthy to mention that utilizing the spatial domain by deploying the different multiple antenna interference mitigation techniques to accommodate the multiple users in the system is often known as the Spatial Division Multiple Access (SDMA). In the cellular communication literature, for instance (Luo, Shum & Zhao 2004; Petrus, Ertel & Reed 1998; Winters, Salz & Gitlin 1994), it was shown that the system capacity in terms of users per cell can be largely improved using the SDMA techniques.

1.2.4 Combined Multiple Antenna Techniques

It is obvious that the aforementioned multiple antenna techniques are different. For instance, the adaptive antenna array techniques are close to the signal processing field and aim at improving SINR. Spatial diversity schemes are related to the channel coding and modulation field, and they are designed to improve the coding gain or (diversity gain). On the other hand, spatial multiplexing techniques are more related to the field of multi-user communication and their main goal is to increase the multiplexing gain. In fact there are also other multiple antenna architectures and techniques that intended to achieve a combination of the different gains mentioned above. However, it is known that for a given number of antennas, there are a

certain trade-offs between those gains (Zheng & Tse 2003). An example for these combined techniques is that when spatial multiplexing system achieves also a diversity gain if an optimum maximum likelihood receiver is employed (Mietzner *et al.* 2009).

1.3 Recent Interference Mitigation Trends of Multiantenna Systems

Interference mitigation strategies can be defined as a number of possible means for the prevention and suppression (reduction) of interference in the communication system. In this section we review the literature of the main recent trends of future research in this field. As we interested exclusively in the multiantenna systems, we consider only four disruptive related technologies that will fundamentally change the design of future wireless communications, which are: Network Multiple-Input Multiple-Output (MIMO) or as widely known Coordinated multi-point (CoMP), smarter devices, millimeter wave communication and massive MIMO.

1.3.1 Coordinated Multi-Point MIMO

It is known that in multicell MIMO networks, the long term evolution (LTE)-advanced can eliminate the intra-cell interference based on orthogonal frequency division multiplexing (OFDM). However, the system still suffers from the effects of the inter-cell interference (ICI). A recent approach introduced as a candidate to mitigate such interference is the coordinated multi-point (CoMP) transmission/reception. Although CoMP increases the systems complexity, this approach can significantly increase the coverage and capacity of the systems, consequently, it potentially improves the average cell and the cell edge throughput of the LTE-advanced systems in downlink and uplink scenarios (Pateromichelakis *et al.* 2013; Wang *et al.* 2009). In general, the CoMP mechanism can be classified into two types:

- Joint processing/transmission (CoMP-JP)
- Coordinated scheduling and/or beamforming (CoMP-CS, CB)

The first type can broadly described as follows, the data is transmitted simultaneously to a terminal user from different cooperating transmission point in different

cells that associated with that user, i.e., from the serving cell and the non-serving cell as depicted in Fig 4. The goal of this joint transmission is to improve the quality of the received signal, i.e., to increase the SINR at the terminal user, which consequently boosts the overall system throughput.

In the second type, the transmit beamforming weights for each user are generated to reduce the unnecessary interference to other scheduled users in the same coordinated cells, as shown in Fig 5. Hence, the SINR of each user improves, and consequently the cell edge user throughput can be enhanced (Sawahashi *et al.* 2010).

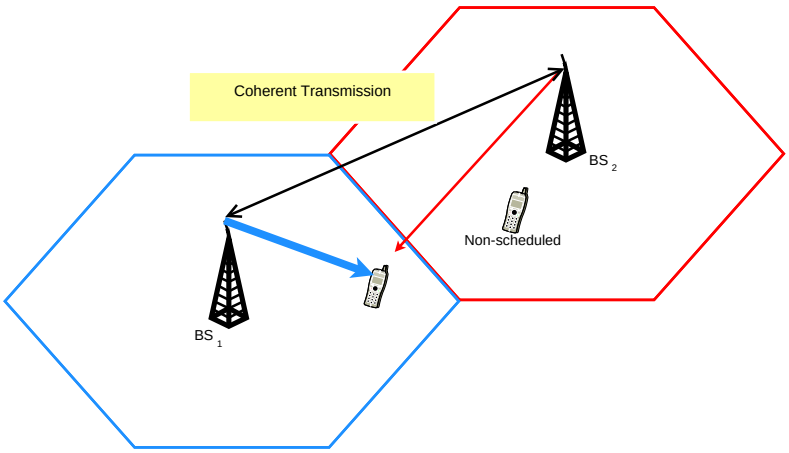

Figure 4. CoMP joint transmission

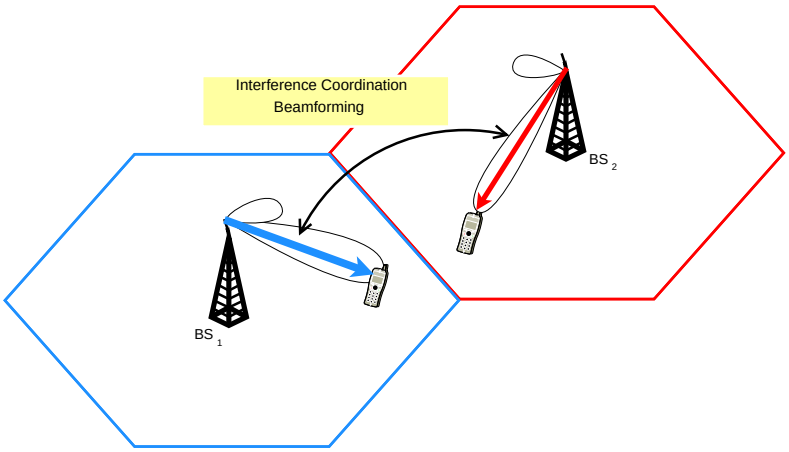

Figure 5. CoMP transmission with coordinated beamforming

As a newly introduced approach it is surly faces some critical challenges before it can be integrated in the future wireless systems (Singh *et al.* 2012). Examples of the major problems of this approach are listed below:

- Delay: the time delay, i.e., the latency associated with the back-haul system in sharing information between the transmission points causes some CSI mismatch comparing to real-time states.
- Synchronization: the shared information in CoMP system needs a high level of time and phase synchronization. This necessity put a huge pressure on the speed requirements of the back-haul system.
- CSI availability: in the systems with Time Division Duplex (TDD) operation mode, the propagation channel reciprocity between the uplink and downlink can be utilized to estimate the CSI. But, the link reciprocity is strongly associated with the match between transmit and receive frequency where they should be within the coherence bandwidth of the channel. On the other hand, in the systems with Frequency Division Duplex (FDD) operation mode, uplink and downlink uses different frequencies. Therefore, the terminal users must feedback their CSI to the transmitting points and this of course causes an overwhelming overhead in the CoMP system.
- Impact of feedback errors: the quantization or the compression errors of the feedback information can significantly affect the CoMP system performance.

1.3.2 Smarter Devices

The previous 2G and 3G cellular communication networks were built on the assumption that all control and main processing operations are done by the infrastructure side. However, this will change in the next-generation wireless communications by exploiting the intelligence of the end-user devices. The utilization of the intelligence of the terminal devices can be facilitated in several ways (Boccardi, Heath & Lozano 2014), such as:

- Allowing device-to-device connectivity.
- Adopting new advanced interference rejection techniques at the receiver side.

The last mentioned approach is one of the motivations of the research work of this thesis, where we will extensively investigate the opportunities of utilizing newly introduced group decoding schemes and also we will explore their capability for interference cancellation in different wireless environments.

1.3.2.1 Device-to-Device Communication

In future communication, it will be common to have several co-located devices that would like to wirelessly exchange and share contents e.g., digital pictures or they even interact with each other through social networking or video gaming. However, processing these kinds of connections through the network can lead to different aspects of the system inefficiency, such as: The device-to-device communication can significantly improve the performance and efficiency of the LTE networks (Doppler *et al.* 2009; Lei *et al.* 2012) by enabling mobile devices to be location aware nodes, where they can discover the presence and communicate with other mobile devices in their vicinity with the least network involvement (Brydon 2014).

- Utilizing multiple wireless hops, where it is sufficient to use a single hop to do the job. This will result huge unnecessary signaling overhead, and high latency.
- Wasting power in both uplink (fraction of watt), and downlink (several of watts) to establish what can be accomplished with only a few of milliWatts. This will result of course fast battery draining and impose unwanted interference to the other devices using the same resources in the system.
- The strong path-losses between the base station and the devices will cause a saver spectral efficiency degradation comparing with what is possible through the direct links between the co-located devices.

It might not be a new idea to have local device-to-device communication, where this kind of local data exchange can be achieved using the already deployed radio access technologies, such as, WiFi and Bluetooth, which support short-range communication. However, these technologies have some drawbacks that limit their capability to support mass market deployment (Brydon 2014):

- Unlicensed spectrum: this means there is no control of usage or interference. This is not a problem for low density usage; however, it becomes a major limit for the high density based services which of course affects the reliability, range, and throughput of such technologies.
- Manual pairing: bluetooth and WiFi are manually paired to enable devices to communicate. This will limit the dynamism of the service.
- Security: the security features of bluetooth and WiFi technologies are much less than those for cellular networks. This makes them unstable for public safety applications.
- Independence from the cellular networks: Bluetooth and WiFi operate independently from cellular network, and this make any device-to-device communication run in parallel with the cellular network operation which cause inefficiency and speed up the draining of the device battery.

1.3.2.2 Advanced Interference Cancellation

Driven by the rapidly increasing trend of the network densification and due to the increasing challenges of the network planning, interference has become the performance limiting factor in the cellular communication systems. One of the most recent introduced ideas to mitigate interference in the cellular networks is Cooperative Interference Cancellation (CIC) between the co-located users using device-to-device communication. In downlink scenario, in contrast to the noise generated in the front-end of the individual users, the undesired reserved interference is generated from the same set of base stations, therefore, it is correlated a cross all users in the same vicinity. This correlation can be exploited to cancel the interference at the victim users. This cooperative interference cancellation is the competing technique of the CoMP technology, where the interference is pre-canceled. However, the advantage of CIC technology is that there is no requirement for low latency or high speed back-haul architecture. It is important also to notice that the suitable back-haul architecture for CoMP is costly and must be implemented in the area of the high mobile traffic, without the possibility of adaptation. In contrast, CIC using device-to-device is adaptive since it does not rely on the back-infrastructure and it takes place exactly where the inter-cell interference is experienced (Tanbourgi, Jakel & Jondral 2014).

From other point of view, in future wireless networks, technology may allow for equipping devices with several antennas and then it will open much greater opportunity for interference mitigation at the user terminal. Advanced joint detection, efficient spatial multiplexing, beamforming, along with better control of transmit receive processing. All of that can significantly reduce interference effects at the receiver side, and consequently will lead to potential performance improvement in wireless communication systems (Boccardi, Heath & Lozano 2014).

The receive-side or (post-processing) interference mitigation techniques, especially the group successive decoding, will be discussed in more detail in following chapters of this thesis.

1.3.3 Millimeter Wave Communication

One of the major challenges that limit growth of wireless communication to meet the drastically expansion of wireless services demand is the scarcity of microwave spectrum. In nowadays technology there are two ways to gain more access in microwave spectrum:

- Re-regulate (re-farm) or re-purpose the occupied spectrum: e.g., the re-purposing the terrestrial TV spectrum for another application, such as, the broadband access communications. However, although the associated cost of such regulation plans is high, it has not freed more than 80 MHz of the spectrum (Boccardi, Heath & Lozano 2014).
- The shared spectrum utilization: e.g., cognitive radio technology. The high expectation and interest in this technology start to fade due to the fact that the primary users or the licensed incumbent are not willing to cooperate.

Alternatively, recent studies suggested that the millimeter wave frequencies can be the solution of the scarcity of microwave cellular spectrum problem. Millimeter wave offers order of magnitude, several tens of gigahertz of spectrum comparing with the currently available microwave spectrum which spread for only around 600 MHz and available in the saturated radio frequency band in the range of 700 MHz to 2.6 GHz (Boccardi, Heath & Lozano 2014; Rappaport *et al.* 2013). On the other hand, the available millimeter frequency bands including: 28-30 GHz,

free band at 60 GHz, and the E-band at 71-76 GHz, 81-86 GHz, and 92-95 GHz (Boccardi, Heath & Lozano 2014).

Generally, propagation characteristics of millimeter waves in terms of possibility of non-line of sight propagation and distance-dependent path-loss do not differ too much from those of microwave radio frequencies (Boccardi, Heath & Lozano 2014). Moreover, rain attenuation and the atmospheric absorption is not a problem for small cell system of order of 200 m, which is the case of most urban environments (Rappaport *et al.* 2013). The only difference is the sensitivity of millimeter waves to the blockages. Interestingly, multiple antenna technology can be a key solution for the millimeter wave system problems. For instance, if multiantenna system is deployed on one side of the millimeter wave communication system, it can eliminate the frequency dependent path-loss. However, if the multiantenna system is deployed in both sides, it can provide array gain as stated in Subsection 1.2.3 to overcome the thermal noise accumulated through this wide-bandwidth system. Furthermore, multiple antenna techniques can reduce the impact of interference on the millimeter wave system, thus, they can improve the performance of the millimeter wave system to operate in noise-limited rather than interference-limited conditions. Moreover, since the wavelength is very short, millimeter wave technology can facilitate other advanced high-gain and steerable antennas techniques at the mobile and base station, such as, massive MIMO which will be addressed in the next subsection. In other words, the integration between millimeter wave and multiple antenna technologies can open the opportunity for future wireless communication systems to achieve multi-gigabit per second.

Even though the large bandwidth of millimeter wave spectrum is about 200 times larger than the microwave spectrum which available currently for the cellular systems (Khan & Pi 2011; Pi & Khan 2012), but it is still a fact that the high data rate which can be realized through this band has not become a widely exploited, at least for the practical application in the cellular communication networks. This field of research after all needs more work efforts and investments to overcome the challenges facing this technology to meet the mobile application requirements. One of the main open issues in this area is the development of low-cost electronic components and equipment to facilitate the efficient energy consumption on millimeter wave frequencies.

1.3.4 Massive MIMO

Massive MIMO is an emerging technology (also known as Large-Scale Antenna Systems (LSAS), large-scale MIMO or hyper-MIMO). It is a multi-user MIMO system where the base station is equipped with large number of antennas. This idea was proposed by Marzetta in (Marzetta 2010). In this technology, generally the number of antennas in the base station is larger than the number of active users for each signaling resource (Boccardi, Heath & Lozano 2014; Lu *et al.* 2013). Massive MIMO can be implemented as a large antenna array, where each active element fed via an optical or electronic digital bus (Larsson *et al.* 2014). Massive MIMO enables for the development of future broadband (fixed and mobile) communication networks. It is expected to be key technology for enhancing both spectral and energy efficiency of wireless communication systems. Moreover, using massive MIMO, the noise and fast fading vanishes, and inter-cell interference can be mitigated with the use of simple precoding techniques (Wang *et al.* 2014).

To clarify the impact of massive MIMO on the communication system, let's assume that we employ massive MIMO in multicell system along with linear matched filter beamforming scheme in the downlink scenario, similar to the setup in (Choi 2013). Now, let's suppose that the random channel vector from the base station to its intended terminal user to be $\mathbf{h}$ which can be written as

$$\mathbf{h} = \sqrt{\iota}\mathbf{u} \tag{1.1}$$

where ι is a factor to consider the large-scale fading effects, and $\mathbf{u} \sim \mathcal{CN}(0, \frac{1}{N}\mathbf{I})$ is the small-scale fading random vector, and N is the number of array antennas.

In the no intra-cell interference scenario, which can be realized by the assignment of orthogonal channels among the same cell users, we can assume, $\mathbf{h}_{k,q}$ denotes the channel vector from the q base station to the user in the cell k. Then, for large N the weight vector of the matched beamforming filter is given by

$$\mathbf{F}_k = \frac{\mathbf{h}_{k,k}}{\|\mathbf{h}_{k,k}\|}. \tag{1.2}$$

The received signal of the user of interest in the kth cell is given by

$$r_k = \mathbf{h}_{k,k}^{\mathcal{H}}\mathbf{F}_k\mathbf{s}_k + \sum_{q\neq k}\mathbf{h}_{k,q}^{\mathcal{H}}\mathbf{F}_q\mathbf{s}_q + n_k, \tag{1.3}$$

where $\mathbf{s}_q$ is the transmitted signal vector from the base station q, and n_k is the received noise at the terminal user at the cell k, with variance σ_k^2.

Therefore, the SINR at the intended user in the kth cell becomes

$$SINR_k = \frac{P_k \|\mathbf{h}_{k,k}\|^2}{\sum_{q \neq k} P_q |\mathbf{h}_{k,q}^{\mathcal{H}} \mathbf{F}_q|^2 + \sigma_k^2}. \tag{1.4}$$

where, P_q is the transmitted power from base station q.

The key idea of the massive MIMO is that, the inter-cell interference (ICI) can mitigated without any cooperation between the base stations. This is because the inner product of the two random vectors $\mathbf{h}_{k,k}$ and $\mathbf{h}_{k,q}$ approaches 0 as $N \to \infty$.

Furthermore, for such system with large N we can apply the following approximation

$$\|\mathbf{h}_{k,q}\|^2 \to \iota_{k,q} \tag{1.5}$$

and

$$\mathbf{u}_{k,q}^{\mathcal{H}} \sim \mathcal{CN}(0, \frac{1}{N}\mathbf{I}) \tag{1.6}$$

which leads to,

$$\begin{aligned} \sum_{q \neq k} P_q |\mathbf{h}_{k,q}^{\mathcal{H}} \mathbf{F}_q|^2 + \sigma_k^2 &= \sum_{q \neq k} P_q \iota_k |\mathbf{u}_{k,q}^{\mathcal{H}} \mathbf{F}_q|^2 + \sigma_k^2 \\ &\approx \frac{1}{N} \sum_{q \neq k} P_q \iota_{k,q} + \sigma_k^2. \end{aligned} \tag{1.7}$$

Hence, the SINR can be approximated as follows

$$SINR_k = \frac{N P_k \iota_{k,k}}{\sum_{q \neq k} P_q \iota_{k,q} + N\sigma_k^2}. \tag{1.8}$$

We notice from the last formula that the small-scale fading term disappear, i.e., the SINR is less fluctuated over time, and this is also one of the advantages of using massive MIMO.

Massive MIMO relies on the spatial multiplexing which on its turn relies on the availability of full and perfect CSI at the transmitter side. In conventional MIMO

systems, such in the LTE systems, the base station transmits pilots to help the terminal-users estimate their channels, then they quantize and feed CSI back to the base station. However, considering the large number of base station antennas in the massive MIMO, the mentioned process of CSI estimation and feedback will not be possible, at least for the high mobility scenarios. This simply because the number of the orthogonal pilots scales with the number of antennas in the base station, which means the downlink and uplink resources will be wasted for transmitting the pilots and the estimated channel responses. Generally, the solution for this problem is to exploit the channel reciprocity between uplink and downlink. Consequently, massive MIMO technology is limited to the systems which operate in TDD mode.

To this end, it is worthy to mention that we will discuss the opportunity of deploying massive MIMO in wireless communication systems that are not necessarily operating on TDD mode. This is can be possible by employing the random precoding strategy with a proper scheduling strategy. Proposal of such system is elaborated in the fifth chapter of this thesis.

1.3.5 Advantages of Massive MIMO

The literature of the research work on the area of massive MIMO presents many advantage of deploying this technology in wireless communication systems. Here we list some of these advantages as below.

- Large multiplexing gain and improved radiation efficiency: massive MIMO can increase the system capacity on order of 10 times or more and enhance the radiated power efficiency about 100 times (Larsson *et al.* 2014). The substantial capacity increase is powered by the large spatial multiplexing gain of the large array antenna in the transmitter. On the other hand, the immense increase of the power efficiency is a direct result of the ability of such massive antenna system to focus its radiated power, by utilizing the very narrow radiation beam pattern (pencil beam) or the high directivity gain of large array antenna. In short, massive MIMO system makes it possible for the base station to collectively add up all the emitted signals at the desired terminal user, and destructively (randomly) elsewhere.
- Inexpensive low-power components: in contrast to the conventional MIMO systems which use expensive ultra-linear 50 Watts amplifiers, massive MIMO

relies on the use of tens or hundreds of low-cost low-power amplifiers with output power of milli-Watts. Therefore, the feeding connecters, such as, the very thick coaxial cables and the large waveguides can be eliminated. In addition, massive MIMO relaxes the constraints on the linearity of the individual amplifiers and the RF chain. The same property which makes the massive MIMO powerful against fading makes it also robust against the failure of one or few antenna elements (Larsson *et al.* 2014).

- Massive MIMO reduces the air interface latency: it is known that multi-path and its fading effects limit the performance of wireless communication systems. For example, if the propagating waves of transmitted signal from the base station traveled through multiple paths and interfered destructively when they reach the desired terminal, then a deep fading will occur. Therefore, the communication system has to wait until a significant change happen to the propagation channel before any data can be received. This consequently makes it hard to build low-latency wireless link. However, massive MIMO as we saw above, significantly reduces the effect of the small-scale fading effects; therefore it helps to reduce the air interface latency of wireless systems (Larsson *et al.* 2014).

1.3.6 Challenges and Limiting Factors of Massive MIMO

There are many issues related to the massive MIMO system need more studies and further addressing, some of these issues are discussed below.

- Pilot contamination: in massive MIMO systems, TDD operation mode is assumed to facilitate channel estimation through the transmitted pilots from the users during the uplink time slots. Ideally, the pilot sequences sent by the users within the same cell and the neighboring cells should be orthogonal. Then, the base stations can estimate correctly the channel vectors of their users in the sense that they are not correlated to the channel vectors of the other users (Lu *et al.* 2013). However, typically, the maximum number of the possible orthogonal sequences is limited by the duration of the channel delay spread and the coherence time (Marzetta 2010). To accommodate larger number of users, pilot reuse policy is used, i.e., non-orthogonal pilot sequences are assigned to the neighboring cells. As a result, the user estimated channel vector for a given cell becomes correlated to the channel

vectors of the users with the non-orthogonal pilot sequences in the neighboring cells. The associated negative consequence of reusing pilots is known as the pilot contamination (Larsson *et al.* 2014).

- Channel reciprocity: in general massive MIMO systems rely on the channel reciprocity between the uplink and downlink to obtain the CSI at the base station. This seems to be a reasonable assumption in the narrowband TDD systems. However, the hardware chains in the terminal users and base station may not reciprocal in the reverse and forward links. This problem can be solved by the calibration of the hardware chains. From other point of view, in the FDD or broadband TDD systems which apply OFDMA and frequency domain scheduling channel reciprocity is no longer valid (Haartsen 2008).

- Propagation models: nearly all the existing research work on massive MIMO assume that as the number of antennas increase, the individual user channels are still spatially uncorrelated and their channel vectors asymptotically become pairwise orthogonal. Also, most of the theoretical studies adopt the i.i.d. Rayleigh fading model to analyze massive MIMO systems. However, some experimental studies have observed that the real antenna correlation is significantly larger than what assumed through the i.i.d. channel assumption. Thus, these empirical results invalidate the hypothesized orthogonality of channel vectors as a result of increasing the MIMO size. This means a proper user scheduling scheme should be a critical component in the design of massive MIMO systems (Lu *et al.* 2013).

1.4 Previous Work

Classically, wireless transceiver designers commonly view interference as an augmentation to the additive Gaussian noise. This assumption is not consistently true; it is valid only if the employed detectors do not take into consideration the interference formation. However, in fact, practical systems have some level of knowledge about interference; because the signals emitted by the interferers belong to discrete constellations (You 2004). In the light of this fact and because of interference management is essential to attain higher spectral efficiency and thereupon higher peak bit rates, researchers have evolved and enhanced abundant of interference-aware mitigation techniques. As discussed in Section 1.3 there are numerous techniques

and approaches that have been lately introduced to mitigate interference in wireless systems, especially in the multiantenan system which we focus on in this thesis. These interference mitigation mechanisms relay on different strategies, e.g., the coordinated transmission/reception approach to avoid interference, as in the CoMP systems (Pateromichelakis *et al.* 2013; Sawahashi *et al.* 2010; Wang *et al.* 2009); but due to the huge complexity, and the overwhelming feedback overhead, also because the associated costly back-haul infrastructure, the implementation of such technology in practice is significantly limited.

Encouraged by the continuously need for new interference mitigation mechanisms, abundant research efforts have been lunched recently to investigate the opportunities of utilizing the large-scale antenna system to mitigate interference in the communication system (Marzetta 2010). However, even though the LSAS has proven its potential to mitigate the inter-cell interference, it is still facing as any other emerging technology critical obstacles, including: pilot contamination and channel estimation problems. These difficulties may limit use of this technology in practice at least in the near future (Larsson *et al.* 2014; Lu *et al.* 2013).

Another example of interference mitigation techniques is a scheme which has recently introduced and grabbed much research concentration, known as (interference alignment) (Cadambe & Jafar 2008; Tresch, Guillaud & Riegler 2009; Yamada & Ohtsuki 2010). Interference alignment is fundamentally established on the concept of designing transmitter and receiver to align interfering signals to each other at receiver side (Lee & Choi 2010). More precisely, vector interference alignment divides the dimensions of the receiver observation space to two subspaces, one of the subspaces is occupied by the desired signal and all the undesired interference are aligned to the other subspace. From the theoretical point of view, interference alignment is claimed to establish optimality to approach Shannon capacity of interference network at high SNR (Gomadam, Cadambe & Jafar 2008). However, the existing interference alignment schemes are facing very challenging problems when it comes to practical implementation. Here we state some of the challenges that considered as encumbrance in practical implementation of interference alignment algorithms:

- Generally, analytical solution for the interference alignment is difficult to obtain. The existing closed-form solutions have been derived for only certain cases with very limited number of users.

- When the closed-form expression exists, perfect channel knowledge is required to obtain it, this is of course requires an overwhelming feedback overhead. In practice, restricted feedback conditions, can lead to imperfect CSIT, which severely affects the system efficiency and performance.
- The required signaling dimension of interference alignment scheme grows exponentially with the total number of users in the system; consequently, a question rises up about the practicality of implementing such a system.
- Although, the distributed interference alignment algorithms require only local channel knowledge at each node, they are yet require an extensive computational complexity due to the iterative manner of finding the optimum solution. In addition, the final values and the convergence speed of the kernel iterative algorithm, which the distributed interference alignment schemes rely on to optimize their objective function, is very sensitive to the initialization conditions.
- To avoid feedback some of interference alignment schemes have been built on the assumption of reciprocity of the wireless network which does not always hold.

Because all of the stated challenges facing aforementioned interference alignment approach, we chose to look for another strategy to mitigate interference. Our fundamental criterion to choose the candidate scheme that limits feedback to the minimum level. Furthermore, it should be applicable with tolerable complexity. We try to avoid feedback because the exhibited overall capacity performance of the feedback-based regimes, such as, the coordinated transmission techniques, or interference alignment schemes, can be misleading when it is compared to open-loop system capacity performance. In other words, feedback in some cases may hurt the system more than improving it. This can be viewed as a resource wasting and consequently a reduction of the pure (net) throughput of the system. Consequently, our first objective is to have a better strategy to mitigate interference with limited feedback. Therefore, we should avoid all interference mitigation processes at the transmitter side, and consider only the approaches with the operations at the receiver side, i.e., the passive interference mitigation strategy, or the receiver centric techniques. At the same time, our second objective is to accomplish this task within a feasible computational complexity, so, the candidate scheme can be implemented in any receiving system.

In a consistent with our stated objectives we encountered a new and actively rising up trend for interference mitigation based on utilizing the intelligence of the terminal nodes to move some of the coordination and mitigation process to the receive side. This approach is pushing towards the device-to-device communications, which can significantly improve the performance and efficiency of the communication networks by enabling the cooperative interference cancellation between the co-located end-nodes. (Doppler *et al.* 2009; Lei *et al.* 2012; Tanbourgi, Jakel & Jondral 2014). Motivated by the interesting idea of utilizing the powerful processing capability of the end-nodes of the current communication systems; also, inspired by the fact that the newly introduced smart-phones are increasingly and vastly adopted by the users of the cellular networks. In this thesis we investigate the opportunities of using the post-processing, i.e., the receive-side interference cancellation strategy, hopefully to find and address comprehensively new schemes to cope with interference in multiantanna systems.

The literature of multi-user detection is full with the traditional methodologies for interference mitigation based on interference canceling at the receive side, where the main goal is to design the decoders in the presence of interference to reduce its effect on the desired signal. This approach includes several schemes, among those techniques: successive interference cancellation for high Signal-to-Interference Power Ratio (SIR) regimes, which suggested for the first time in (Cover 1972). In SIC the signal of interfering users are canceled out sequentially after making a decision on each user's bit. Many schemes employing SIC algorithm have been proposed in literature, such as, multi-stage interference cancellation, see for instance, (Zanella, Chiani & Win 2005) and (Fang & Johansson 2000; Krebs, Joham & Utschick 2014; Miridakis & Vergados 2013; Pedersen *et al.* 1996; Rasmussen, Lim & Johansson 2000). Because of its efficiency SIC scheme is widely used in multiantenna systems, as the V-BLAST algorithm (Foschini 1996; Jankiraman 2004). But, the main disadvantage of SIC is the error propagation, and its relatively large associated delay; therefore, more efficient SIC algorithms have been proposed to decrease its complexity and improve the algorithm robustness against the error propagation, such as, Ordered Successive Interference Cancellation (OSIC) algorithm (Foschini *et al.* 1999; Lin *et al.* 2011; Yang *et al.* 2004). Nevertheless, these proposed algorithms which relay on received SINR to determine the decoding order do not always perfectly utilize the system resources to achieve the highest possible user transmission rate.

On the other hand, when the interfering and desired signals are equal in power, i.e.,

for moderate SIR regimes, parallel interference cancellation (PIC) is performed to detect the signals of desired users. In PIC the interference resulting from the other remaining users accessing the channel is removed simultaneously from the signal of each user. Therefore, all of the system users receive equal treatment to cancel their multi-user interference. Because IC is performed in parallel in PIC algorithm, its associated delay will be small comparing to that for SIC scheme. However, the main drawback of PIC is the cost of the hefty hardware requirements, which limits its practicality for implementation in large communication systems (Bentrcia & Alshebeili 2014; Correal, Buehrer & Woerner 1999; Divsalar, Simon & Raphaeli 1998; Dongning *et al.* 2000; Gu & de Lamare 2014; Han & Liu 2014; Xue *et al.* 1999).

Motivated by the necessary need for an optimal interference mitigation technique considers all ranges of interference levels, a novel interference mitigation scheme proposed recently in (Prasad & Wang 2009), where the authors assumed that each receiver uses a Successive Group Decoding (SGD) which is considered as an extension of the conventional successive decoder. However, instead of decoding only one user at each decoding stage, a subgroup of users is jointly decoded. Considering an interference channel system where a fixed power allocated to all users, the authors of (Prasad & Wang 2009) obtained the decoding strategy that minimizes the outage probability at every receiver and generates the optimal subset of interferers that must be decoded along with the desired user under an imposed complexity constraint.

Here, it is worthy to remind the reader that, successive group decoders have a substantial feature, as they can be implemented with different levels of complexity. In other words, they can be implemented with - as low complexity as- the conventional successive single-user decoder to the high complexity of the maximum likelihood decoder. Therefore, by imposing a constraint on the decoder complexity, the system can adopt the decoder with an adequate complexity that each receiver can sustain; in this stream of research, both of the recently proposed Optimal Successive Group Decoding (OSGD) in (Prasad & Wang 2009), and the Constrained Partial Group Decoding (CPGD) technique which has been proposed in (Chen *et al.* 2012; Gong, Tajer & Wang 2011) employ group decoding strategy in each receiver to decode the desired message conjointly with a part of the interference. Specifically, these decoders exploit the knowledge about the interference to determine which interfering signals (with a constraint on their group size)

should jointly decoded along with the desired signal, while treating the remaining interfering signals as Gaussian noise.

In this thesis we will extensively investigate the openings, and challenges, and propose solutions for deploying these group decoding techniques to mitigate interference in the multiantenna systems. Also, we will assess and analyze the performance of such systems in different wireless communication environments.

1.5 Interference Channel Model

In communication literature, interference channel is defined in (Han & Kobayashi 1981) as the channel of multi pairs of input-output terminals, where each input communicates through a common medium with its respective outputs. Also, the author of (Kramer 2006) presented the interference channel as a model for studying networks with two or more (source-destination) pairs where the signals of the sources interfere with each other at the destination.

For analytical modeling, we consider the temporally uncorrelated discrete model of flat-fading K-user interference channel depicted in Fig. 6. In this thesis we assume that each transmitter is equipped with $N_{ti} \geq 1$ antennas, and intends to communicate with its designated receiver which is equipped with $N_{rk} \geq 1$ antennas. But, due to the broadcasting nature of the wireless channel the transmitted signal is received by all the K receivers. Also we assume the kth receiver is interested only in the signal transmitted by the kth transmitter; however, it is aware of the coding scheme employed by all other users and may choose to decode some or all of them only if it presumes doing that will assist the decoding of its intended user.

Therefore, The received signal of the kth receiver at the nth symbol interval through this K-user interference channel can be expressed by

$$\begin{aligned}(1.9)\qquad \mathbf{y}_k[n] &= \sum_{i=1}^{K} \mathbf{H}_{ki}\mathbf{x}_i[n] + \mathbf{z}_k[n] \\ &= \sum_{i=1}^{K} \mathbf{H}_{ki}\mathbf{V}_i\mathbf{d}_i[n] + \mathbf{z}_k[n] \\ &= \mathbf{H}_{kk}\mathbf{V}_k\mathbf{d}_k[n] + \sum_{i\neq k} \mathbf{H}_{ki}\mathbf{V}_i\mathbf{d}_i[n] + \mathbf{z}_k[n] \quad k \in 1,\cdots,K\end{aligned}$$

where $\mathbf{y}_k$ is the $N_{rk} \times 1$ received vector at user k, $\mathbf{z}_k \sim \mathcal{CN}(0, \sigma^2\mathbf{I})$ is the $N_{rk} \times 1$ complex additive white Gaussian noise (AWGN) vector at user k. $\mathbf{V}_i$ is the $N_{ti} \times S_i$ precoding matrix at transmitter i, and S_i is the number of transmitted streams from user i. $\mathbf{H}_{ki}$ is the $N_{rk} \times N_{ti}$ channel matrix between transmitter i and receiver k, coefficients of $\mathbf{H}_{ki}$ are independent and identically distributed (i.i.d.) complex Gaussian random variables with zero mean and unit variance. $\mathbf{x}_i$ is $N_{ti} \times 1$ unit power transmitted symbol vector of the ith transmitter, $\mathbf{d}_i$ is an $S_i \times 1$ vector indicates the data streams from the ith transmitter. Each transmitter i is subject to an average transmit power constraint, given by $\mathbb{E}[\|\mathbf{x}_i\|^2] \leq P_i$.

The model in (1.9) can be simplified as follows

$$\mathbf{y}_k[n] = \sqrt{P}\mathbf{H}_{kk}\mathbf{x}_k[n] + \sqrt{\alpha P}\sum_{i=1, i\neq k}^{K}\mathbf{H}_{ki}\mathbf{x}_i[n] + \mathbf{z}_k[n], \quad 1 \leq k \leq K \tag{1.10}$$

where P represents the average transmit power allocated to each user. α denotes the cross-talk factor between users, i.e., it represents the relative propagation path loss of the interference channel, or simply the interference-to-signal power ratio. Hereafter, for the sake of simplicity, we omit the symbol interval index n.

As stated above, in this thesis we assume flat fading scenarios, where the fading seen by the kth receiver from the ith transmitter is represented by the $N_{r_k} \times N_{t_i}$ matrix $\mathbf{H}_{ki}$ consists as in (Biglieri *et al.* 2007; Siriteanu *et al.* 2013) of two components, deterministic (i.e., mean) denoted by $\mathbf{H}_D$ and random component represented by $\mathbf{H}_r$

$$\mathbf{H} = \sqrt{\frac{\mathcal{K}}{1+\mathcal{K}}}\mathbf{H}_D + \sqrt{\frac{1}{1+\mathcal{K}}}\mathbf{H}_r \tag{1.11}$$

where $\sqrt{\frac{\mathcal{K}}{1+\mathcal{K}}}$ is the Line of Sight (LOS) component of the channel and $\sqrt{\frac{1}{1+\mathcal{K}}}$ is the fading component, assuming uncorrelated fading. $\mathcal{K}$ is the Ricean $\mathcal{K}$-factor of the channel and is defined as the ratio of the power in the LOS component of the channel to the power in the fading component.

$$\mathcal{K} = \frac{\|\mathbf{H}_D\|^2}{\mathbb{E}\{\|\mathbf{H}_r\|^2\}} \tag{1.12}$$

It is clear that for $\mathcal{K} = 0$, the MIMO channel $\mathbf{H}_{ki}$ has a pure Rayleigh fading, also, if $0 < \mathcal{K} < \infty$, then, $\mathbf{H}_{ki}$ has a Rician fading; while, the case of $\mathcal{K} = \infty$ corresponds to a non-fading channel scenario.

In this work, we use the Kronecker correlation model expressed in (1.13) to simulate the correlation effect in the both ends of the channel, i.e., in the transmit and receive sides. Despite its simplicity, Kronecker model seems to be a reasonable choice when the correlation is quickly vanishing with the distance between the transmit and receive ends (Chuah *et al.* 2002).

$$\mathbf{H}_r = \aleph_r^{\frac{1}{2}} \mathbf{H}_w \aleph_t^{\frac{1}{2}}, \tag{1.13}$$

where $\mathbf{H}_w$ is an $(N_r \times N_t)$ normalized complex Gaussian random matrix, $\aleph_t$, $\aleph_r$, are the deterministic correlation matrices at the transmit and receive end respectively. Also, because of its simplicity and relative accuracy to simulate the realistic antenna inter-element spatial correlation, we adopted the exponential correlation model to generate the transmit and receive correlation matrices, where they can be constructed using a single correlation factor $\rho \in \mathbb{C}$ and $|\rho| \leq 1$ as follows (Chatzinotas, Imran & Hoshyar 2009)

$$\aleph_{ij} = \begin{cases} \rho^{\mathtt{abs}(j-i)} & ,i \leqslant j \\ \left(\rho^{\mathtt{abs}(j-i)}\right)^* & ,i > j \end{cases}. \tag{1.14}$$

In this work, $\mathbf{H}_{ki}$ is assumed to be perfectly known to the kth receiver, but it is unknown to any of the transmitters or any other receiver.

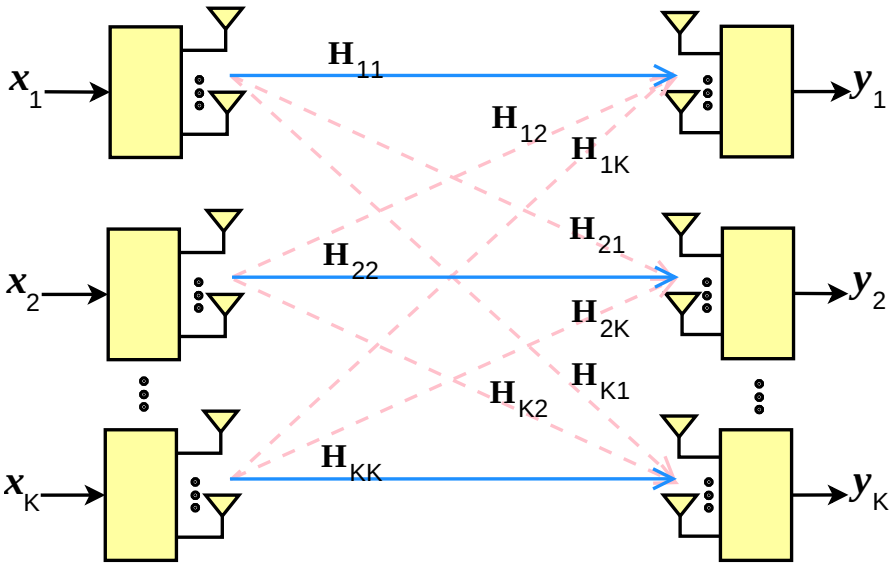

Figure 6. The interference channel.

1.6 Effective Capacity

This section gives a brief review for the basic concepts of the effective capacity. In the field of research dealing with the future wireless networks, modeling wireless channel regarding to the connection Quality of Service (QoS) metrics, such as, delay, and ratio of packet loss, is crucial to promote the QoS of the system. This modeling becomes a necessity as the communication systems are increasingly becoming packet switching based networks. Nevertheless, most of the commonly adopted conventional physical-layer wireless models do not precisely distinguish these QoS metrics; simply because these metric are more related to the link-layer than being physical-layer parameters.

Motivated by this fact, authors of (Wu & Negi 2003) intelligently have proposed and developed a new approach to model the channel QoS which represented by the QoS exponent $\theta \in \mathbb{R}^+$. In their work they have introduced a new terminology called Effective Capacity (EC). The effective capacity can be interpreted as an indication for the data rate that the link can maintain such that the probability of exceeding delay bound asymptotically does not exceed some upper bound. Form other point of view, we can see the effective capacity as the marginal rate between

the ergodic capacity, when the system has no delay limitation, i.e., the QoS exponent $\theta \to 0$, and the outage capacity where the system has no tolerance for the delay, i.e., $\theta \to \infty$ (Duan 2014).

It is important to distinguish between the outage in a link which indicates instantaneous capacity loss, and the effective capacity which indicates the data rate that the link can maintain such that the probability of exceeding delay bound or (equivalently the probability of the length of queuing system) asymptotically does not exceed some upper bound. To see this difference, it is easier show the effective capacity as analogous to the effective bandwidth, where it assesses the wireless channel by two parameters, the probability of non-empty buffer, and the connection QoS exponent θ.

The first metric, i.e., the non-empty buffer probability is equivalent in concept to the marginal CDF or the (outage probability) of the system. However, they are not equal. This is because, the non-empty buffer probability consider the accumulation of the packet in the buffer, while the outage probability which represents the fall of system SNR, or consequently the system capacity below a target rate. Outage probability does not take into account the packet accumulation in the buffer. Since the buffering causes longer busy periods compared with the non-buffered case, the non-empty buffer probability will be larger than the outage probability (Wu & Negi 2003).

Now, to describe the second metric, i.e., the QoS exponent θ, we define $q_l(\infty)$ as the steady length of a queue of a stationary ergodic service process, then, θ is defined as the exponential decaying rate of the distribution of the queue length, i.e., θ describes the decay rate of the probability that the queue length q_l exceeds a certain limit T_q, which can expressed as follows (Duan 2014)

$$\theta = -\lim_{T_q \to \infty} \frac{1}{T_q} \log \Pr(q_l(\infty) \geq T_q) \tag{1.15}$$

Hence, we can have the following expression to approximate the buffer violation probability for large buffer size $T_{q_{max}}$: $\Pr\{Q_l \geq T_{q_{max}}\} \approx e^{-\theta T_{q_{max}}}$, where, Q_l is the distribution of the queue length.

In some systems, constraints on queue length can be transferred to delay limitations. Therefore, we can also have the following approximation: $\Pr\{D \geq D_{max}\} \approx$

$ve^{-\theta\delta_a D_{max}/2}$, where D is the delay experienced by the arriving packet, D_{max} is the delay bound required by the connection, v is a positive constant, δ_a is a constant depends on the service and the arrival rate. (Chang 1994; 2000; Musavian & Aïssa 2010).

It is important to notice that $\theta \to 0$ refers to a system that has no delay constraint. On the other hand, $\theta \to \infty$ corresponds to a system with a rigorous delay constraint. In other words, larger θ implies more restriction on QoS, while smaller θ refers to looser QoS guarantees.

Now, as the effective capacity is defined in (Gursoy 2009; 2011; Musavian & Aïssa 2010) by the maximum fixed rate of arrival that can be supported by some service process, such that, the requirements specified by the QoS exponent θ are statistically guaranteed. Therefore, we can define it mathematically through the cumulant-generating function

$$\Lambda(\theta) = \lim_{t\to\infty} \frac{1}{t} \log_e \mathbb{E}\left\{e^{\theta S(t)}\right\} \tag{1.16}$$

The effective capacity is given as

$$\begin{aligned} \alpha_c(\theta) &= -\frac{\Lambda(-\theta)}{\theta} \\ &= -\lim_{t\to\infty} \frac{1}{\theta t} \log_e \mathbb{E}\left\{e^{-\theta S(t)}\right\} \end{aligned} \tag{1.17}$$

where the QoS exponent θ is defined as in (1.15), $S(t) = \int_0^t r(t)$ is the cumulative service provided by the channel.

Assuming a block fading scenario with a frame duration T, the formula of the effective capacity simplifies to

$$\alpha_c(\theta) = -\frac{1}{\theta T} \log_e \mathbb{E}\left\{e^{-\theta R_s[i]}\right\} \tag{1.18}$$

where the maximum instantaneous achievable service rate of block i is given by $R_s[i] = TB\log_2(1+\digamma[i])$, B is the channel bandwidth, and $\digamma[i]$ is the ith block instantaneous SINR.

Now, with a short-time constraint on the total allocated power P_T to the transmitted

signal vector $\mathbf{x}$, and using the normalized input covariance matrix $\mathbf{Q}_x$ defined as

$$\mathbf{Q}_x = \frac{\mathbb{E}\left\{\mathbf{x}\mathbf{x}^{\mathcal{H}}\right\}}{P_T/B} \tag{1.19}$$

The stochastic service process in a MIMO channel system can be given by

$$B\log_2 \det\left(\mathbf{I} + \frac{P_T}{BN_0}\mathbf{H}\mathbf{Q}_x\mathbf{H}^{\mathcal{H}}\right) = B\log_2 \det\left(\mathbf{I} + N_r\mathtt{SNR}\mathbf{H}\mathbf{Q}_x\mathbf{H}^{\mathcal{H}}\right) \text{ bps} \tag{1.20}$$

where N_0 is the noise power spectral density, N_r is the number of receive antennas, and the signal-to-noise ratio (SNR) defined as

$$\mathtt{SNR} = \frac{\mathbb{E}\left\{\|\mathbf{x}\|^2\right\}}{\mathbb{E}\left\{\|\mathbf{n}\|^2\right\}} = \frac{P_T}{N_r BN_0}. \tag{1.21}$$

Now, we can obtain effective capacity of the closed and open loop MIMO systems. First, we take into account the case of closed loop MIMO system, i.e., the system with the Channel State Information at the Transmitter (CSIT). Therefore, the transmitter can adapt its transmitted power and consequently, $\mathbf{Q}_x$ according to the channel fading. Hence, using (1.18) we can formulate the effective capacity after normalizing it by the receiver dimensionality N_r and the bandwidth B as follows

$$\alpha_c(\mathtt{SNR},\theta) = -\frac{1}{\theta TBN_r}\times \log_e \mathbb{E}\left\{\exp\left(-\theta TB \max_{\mathbf{Q}_x\succeq 0, tr(\mathbf{Q}_x)\leq 1} \log_2 \det\left(\mathbf{I} + N_r\mathtt{SNR}\mathbf{H}\mathbf{Q}_x\mathbf{H}^{\mathcal{H}}\right)\right)\right\} \text{ bps/Hz/dimension} \tag{1.22}$$

From this formula, one can notice that when $\theta \to 0$, QoS constraints turn to be loose, and the effective capacity reaches the ergodic capacity (Gursoy 2011),

$$\lim_{\theta\to 0} \alpha_c(\mathtt{SNR},\theta) = \frac{1}{N_r}\mathbb{E}\left\{\max_{\mathbf{Q}_x\succeq 0, tr(\mathbf{Q}_x)\leq 1} \log_2 \det\left(\mathbf{I} + N_r\mathtt{SNR}\mathbf{H}\mathbf{Q}_x\mathbf{H}^{\mathcal{H}}\right)\right\} \text{ bps/Hz/dimension} \tag{1.23}$$

However, for $\theta > 0$ the ergodic capacity is generally greater than the effective capacity. One can readily see that by applying Jensen's inequality after interchanging

the expectation and the logarithm terms in (1.22)

$$\begin{aligned}\alpha_c(\mathtt{SNR},\theta) &= -\frac{1}{\theta TBN_r}\times \\ &\log_e \mathbb{E}\left\{\exp\left(-\theta TB \max_{\mathbf{Q}_x\succeq 0, tr(\mathbf{Q}_x)\leq 1} \log_2\det\left(\mathbf{I}+N_r\mathtt{SNR}\mathbf{H}\mathbf{Q}_x\mathbf{H}^{\mathcal{H}}\right)\right)\right\} \\ &\leq -\frac{1}{\theta TBN_r}\times \\ &\mathbb{E}\left\{\log_e\exp\left(-\theta TB \max_{\mathbf{Q}_x\succeq 0, tr(\mathbf{Q}_x)\leq 1} \log_2\det\left(\mathbf{I}+N_r\mathtt{SNR}\mathbf{H}\mathbf{Q}_x\mathbf{H}^{\mathcal{H}}\right)\right)\right\} \\ &= \frac{1}{N_r}\mathbb{E}\left\{\max_{\mathbf{Q}_x\succeq 0, tr(\mathbf{Q}_x)\leq 1} \log_2\det\left(\mathbf{I}+N_r\mathtt{SNR}\mathbf{H}\mathbf{Q}_x\mathbf{H}^{\mathcal{H}}\right)\right\} \qquad (1.24)\end{aligned}$$

Second, we consider the case of the open loop MIMO system, i.e., the Channel State Information (CSI) is not available at the transmitter side. Then, in practice, it is preferred to allocate power uniformly across the MIMO antennas, and consequently $\mathbf{Q}_x = \frac{1}{N_t}\mathbf{I}$. Therefore, the effective capacity is given by

(1.25)

$$\alpha_{c,\mathrm{id}}(\mathtt{SNR},\theta) = -\frac{1}{\theta TBN_r}\log_e\mathbb{E}\left\{\exp\left(-\theta TB\log_2\det\left(\mathbf{I}+\frac{N_r}{N_t}\mathtt{SNR}\mathbf{H}\mathbf{H}^{\mathcal{H}}\right)\right)\right\} \quad \text{bps/Hz/dimension}$$

where, the subscript (id) refers to the identical distribution of the power across the antenna elements.

1.7 Brief Review for the Addressed Systems

This section gives a brief review for the fundamentals of the different interference mitigation techniques that we will use in the next chapters to assess the performance of our investigated group decoding schemes.

1.7.1 Water-filling Power Allocation

As described in (Tse & Viswanath 2005), the single-user MIMO channel can be decomposed to a set of non-interfering parallel sub-channels, each of them is corrupted by an independent noise, and with a constrained on the total allocated

power, such that,

$$P_T = \sum_{n_s=1}^{N_{sc}} P_{n_s}, \tag{1.26}$$

where N_{sc} is the number of parallel sub-channels, and P_{n_s} is the allocated power to the n_sth sub-channel. The maximum rate of reliable communication using this scheme is

$$\sum_{n_s=1}^{N_{sc}} \log\left(1+\frac{P_{n_s}|h_{n_s}|^2}{\sigma^2}\right) \tag{1.27}$$

where, h_{n_s} denotes the n_sth sub-channel gain, and σ^2 is the noise variance. It is easy to notice that the sum rate given by (1.27) can be maximized by choosing the (optimal power allocation) as

$$C_{N_{sc}} := \max_{P_1,\dots,P_{N_{sc}}} \sum_{n_s=1}^{N_{sc}} \log\left(1+\frac{P_{n_s}|h_{n_s}|^2}{\sigma^2}\right) \tag{1.28}$$

under the constraint of

$$\sum_{n_s=1}^{N_{sc}} P_{n_s} = P_T, \quad P_{n_s} \geqslant 0, \quad n_s = 1,\dots,N_{sc}. \tag{1.29}$$

Using the Lagrangian method we can solve the problem of the concave objective function in (1.28) as follows

$$\mathcal{L}(\lambda, P_1,\dots,P_{N_{sc}}) := \sum_{n_s=1}^{N_{sc}} \log\left(1+\frac{P_{n_s}|h_{n_s}|^2}{\sigma^2}\right) - \lambda \sum_{n_s=1}^{N_{sc}} P_{n_s}, \tag{1.30}$$

where λ is the Lagrange multiplier. The allocation power optimality condition is given by

$$\frac{\partial \mathcal{L}}{\partial P_{n_s}} = \begin{cases} = 0 & \text{if } P_{n_s} > 0 \\ \leqslant 0 & \text{if } P_{n_s} = 0 \end{cases}$$

By defining $x^+ := \max(x,0)$, then the optimal power allocation which satisfies the optimality condition can be expressed as

$$P_{n_s}^* = \left(\frac{1}{\lambda} - \frac{\sigma^2}{|h_{n_s}|^2}\right)^+, \tag{1.31}$$

Then, a numerical algorithm can be employed to compute the Lagrange multiplier λ to satisfy the total power constraint

$$\sum_{n_s=1}^{N_{sc}} \left(\frac{1}{\lambda} - \frac{\sigma^2}{|h_{n_s}|^2} \right)^+ = P_T. \tag{1.32}$$

Given the channel information, noise variance and using (1.31) transmitter can determine how to optimally allocate power across the sub-channels.

It is worth to notice that water-filling does not allocate all the power to the channels with the highest SNR, instead, it is still provides some power to the the channels with weaker SNR levels. This is because the function $f(\mathtt{SNR}) = \log_2(1+\mathtt{SNR})$ is a concave function, and it can be approximated using

$$\log(1+x) \approx x, \quad x \to 0 \tag{1.33}$$

$$\log(1+x) \approx \log(x), \quad x \gg 1 \tag{1.34}$$

Consequently, the system attains a decaying marginal capacity gain by adding more power to the sub-channels with higher SNR. On the other hand, capacity increases linearly with power in the low SNR levels. Therefore, providing some power to weaker sub-channels can increase the total sum capacity (Adve 2007). However, water-filling scheme does not allocate power to the sub-channels with too low SNR; because, transmitting information through such sub-channels is a waste of power. Then, capacity of water-filling power allocation algorithm is given by

$$C = \sum_{n_s=1}^{N_{sc}} \log_2 \left(1 + \frac{P_{n_s}^* |h_{n_s}|^2}{\sigma^2} \right). \tag{1.35}$$

The above argument also can be seen from other point of view, for instance assuming that the system can concentrate its resources, i.e., the transmitted power in this case, in the times when the channel has high SNR, and then the system can achieve a huge capacity gain. By reflecting this insight into a multi-user system (with large number of users scenario); we can claim that it is most likely to have at any time instance a sub-group of users whose channels are in good condition, then, using a proper selection scheme the multi-user system capacity can be achieved. This

form of diversity is called (opportunistic beamforming) (Viswanath, Tse & Laroia 2002).

Finally, if the SNR of all sub-channels are equal, or the transmitter does not know the channel state information, water-filling algorithm transformed to be an equal power allocation scheme, i.e., $P_{n_s} = P_T/N_{sc}$ and sum capacity in this case is

$$C = \sum_{n_s=1}^{N_{sc}} \log_2 \left(1 + \frac{P_T}{N_{sc}\sigma^2}\right). \tag{1.36}$$

As one can observe, the slope of the log function is less than N_{sc}; then, the sum capacity is significantly larger than the capacity of Single-Input Single-Output (SISO) system.

1.7.2 Interference Alignment Using Minimization of the Interference Leakage (MIL)

Fundamentally, interference alignment schemes are based on the concept of designing transmitter and receiver to align the interfering signals at the receiver side (Lee & Choi 2010). Here we choose one of the recently introduced interference alignment schemes which employs an iterative algorithm to minimize the interference leakage between users. The basic idea of this scheme as represented in (Mohapatra, Nissar & Murthy 2011) is to design an iterative interference alignment algorithm, iterates between two objective functions with a common interference leakage term, to find the locally optimum $\mathbf{v}_k$ and $\mathbf{w}_k$. The minimization of the interference leakage is performed subject to a constraint on the dimension of the desired signal subspace.

Considering the design of the $\mathbf{w}_k$ which is the receiver filter vector at the receiver k, for a fixed precoding vectors $\mathbf{v}_k$ at all transmitters. The received interference plus noise at the receiver k is given by

$$\mathbf{r}_k = \sum_{i=1, i\neq k}^{K} \mathbf{w}_k^{\mathcal{H}} \mathbf{H}_{ki} \mathbf{v}_i \mathbf{x}_i + \mathbf{w}_k^{\mathcal{H}} \mathbf{z}_k. \tag{1.37}$$

When the interference signals are aligned, we need to find $\mathbf{w}_k$ such that

$$\sum_{i=1, i\neq k}^{K} \mathbf{w}_k \mathbf{H}_{k,i} \mathbf{v}_i = 0 \tag{1.38}$$

A reasonable choice for $\mathbf{w}_k$ is the vector that minimizes the interference leakage power at receiver k. There is also a constraint on the dimensionality of the desired signal: $\text{rank}(\mathbf{w}_k\mathbf{H}_{kk}\mathbf{v}_k) = d_k$, where d_k is the Degree of Freedom (DoF) assigned to the kth transmitter. Thus given the channel realization $\mathbf{H}_{kk}$ and the precoding vectors $\mathbf{v}_k$, the optimal receive filter $\mathbf{w}_k$ is designed to minimize the cost function (Mohapatra, Nissar & Murthy 2011)

$$i_k \triangleq tr(\mathbf{w}_k^{\mathcal{H}}\mathbf{Q}_k\mathbf{w}_k) \tag{1.39}$$

such that

$$\mathbf{w}_k^{\mathcal{H}}\mathbf{H}_{kk}\mathbf{v}_k = \beta_k\mathbf{I}_{d_k} \tag{1.40}$$

where $\mathbf{Q}_k$ is the interference plus noise covariance matrix at receiver k, and it is given by

$$\mathbf{Q}_k = \sum_{i=1,i\neq k}^{K} P_i[\mathbf{H}_{ki}\mathbf{v}_i][\mathbf{H}_{ki}\mathbf{v}_i]^{\mathcal{H}} + \mathbf{I}_{N_{r_k}} \tag{1.41}$$

and $\beta_k > 0$ is selected such that $tr(\mathbf{w}_k^{\mathcal{H}}\mathbf{w}_k) = 1$. Here, P_i is the transmit power of user i. The solution to (1.41) is given by (Mohapatra, Nissar & Murthy 2011)

$$\mathbf{w}_k^{opt} = \beta_k\mathbf{Q}_k^{-1}\mathbf{u}_k[\mathbf{u}_k^{\mathcal{H}}\mathbf{Q}_k^{-1}\mathbf{u}_k]^{-1} \tag{1.42}$$

where $\mathbf{u}_k = \mathbf{H}_{kk}\mathbf{v}_k$ is the desired signal subspace of the kth user

$$\beta_k = \frac{1}{\sqrt{tr\{[\mathbf{Q}_k^{-1}\mathbf{u}_k\acute{\mathbf{Q}}_k^{-1}]^{\mathcal{H}}[\mathbf{Q}_k^{-1}\mathbf{u}_k\acute{\mathbf{Q}}_k^{-1}]\}}}, \tag{1.43}$$

and $\acute{\mathbf{Q}}_k = \mathbf{u}_k^{\mathcal{H}}\mathbf{Q}_k^{-1}\mathbf{u}_k$

Now consider designing the precoding vectors $\mathbf{v}_k$ for all transmitters, given the receive filtering vectors $\mathbf{w}_k$ at all receivers. The interference signal due to transmitter k at the unintended receivers is given by

$$\mathbf{s}_{ki} = \mathbf{w}_i\mathbf{H}_{ik}\mathbf{v}_k\mathbf{x}_k, \quad i = 1,2,\cdots,K, i \neq k \tag{1.44}$$

From the feasibility condition for perfect interference alignment, one requires

$$\mathbf{w}_i^{\mathcal{H}}\mathbf{H}_i\mathbf{v}_k = \mathbf{0}, \quad i = 1,2,\cdots,K, i \neq k \tag{1.45}$$

Again, a judicious choice for the precoding vectors would be to select $\mathbf{v}_k$ such that the total interference power at the unintended receives due to transmitter k is minimized. The interference power due to the virtual transmitter k at virtual receiver i is obtained from the squared Frobenius norm of $\mathbf{w}_i^{\mathcal{H}}\mathbf{H}_{ik}\mathbf{v}_k$ as (Mohapatra, Nissar & Murthy 2011)

$$L_{ki} = tr\{P_k\mathbf{v}_k^{\mathcal{H}}[\mathbf{w}_i\mathbf{H}_{ik}]^{\mathcal{H}}[\mathbf{w}_i\mathbf{H}_{ik}]\mathbf{v}_k\}. \tag{1.46}$$

Thus, the total interference power due to the transmitter k is given by

$$\acute{L}_k = tr\{\mathbf{v}_k^{\mathcal{H}}\acute{\Phi}_k\mathbf{v}_k\}. \tag{1.47}$$

where the virtual covariance matrix $\acute{\Phi}_k$ is given by

$$\acute{\Phi}_k = P_k \sum_{i=1,i\neq k}^{K} [\mathbf{w}_i^{\mathcal{H}}\mathbf{H}_{ik}]^{\mathcal{H}}[\mathbf{w}_i^{\mathcal{H}}\mathbf{H}_{ik}]. \tag{1.48}$$

The objective function here is to choose $\mathbf{v}_k$ to minimize $\acute{L}_k$, subject to the desired signal dimension constraint, i.e, $\text{rank}(\mathbf{w}_k^{\mathcal{H}}\mathbf{H}_{kk}\mathbf{v}_k) = d_k$. Including the regularization term the objective function is modified as

$$\acute{L}_k = tr\{\mathbf{v}_k^{\mathcal{H}}\acute{\Phi}_k\mathbf{v}_k + \mathbf{v}_k^{\mathcal{H}}\mathbf{v}_k\}. \tag{1.49}$$

Thus, the constrained optimization is given by

$$\min_{\mathbf{v}_k} \acute{L}_k = tr\{\mathbf{v}_k^{\mathcal{H}}\mathbf{H}_{kk}\mathbf{v}_k\}, \tag{1.50}$$

such that

$$\mathbf{w}_k^{\mathcal{H}}\mathbf{H}_{kk}\mathbf{v}_k = \vartheta_k\mathbf{I}_{d_k} \tag{1.51}$$

and $\vartheta_k > 0$ selected such that $tr(\mathbf{v}_k^{\mathcal{H}}\mathbf{v}_k) = 1$, and

$$\Phi_k = P_k \sum_{i=1,i\neq k}^{K} [\mathbf{w}_i^{\mathcal{H}}\mathbf{H}_{ik}]^{\mathcal{H}}[\mathbf{w}i^{\mathcal{H}}\mathbf{H}_{ik}] + \mathbf{I}_{N_{t_i}}. \tag{1.52}$$

Notice that Φ is the reflected covariance matrix of a virtual channel obtained by interchanging the transmitters and receivers. The optimum solution for $\mathbf{v}_k$ is given by

$$\mathbf{v}_k^{opt} = \vartheta_k \Phi_k^{-1} \mathbf{t}_k^{\mathcal{H}} [\mathbf{t}_k \Phi_k^{-1} \mathbf{t}_k^{\mathcal{H}}]^{-1}, \quad k = 1, 2, \cdots, K \tag{1.53}$$

where $\mathbf{t}_k = \mathbf{w}_k^{\mathcal{H}} \mathbf{H}_{kk}$

$$\vartheta_k = \frac{1}{\sqrt{tr\{[\Phi_k^{-1} \mathbf{t}_k^{\mathcal{H}} \acute{\mathbf{t}}_k^{-1}]^{\mathcal{H}} [\Phi_k^{-1} \mathbf{t}_k^{\mathcal{H}} \acute{\mathbf{t}}_k^{-1}]\}}}, \tag{1.54}$$

and $\acute{\mathbf{t}}_k = \mathbf{t}_k \Phi_k^{-1} \mathbf{t}_k^{\mathcal{H}}$

The iterative Minimum Interference Leakage (MIL) algorithm is summarized as follows

Table 1. The Iterative MIL Algorithm

1	**Initialize** $\mathbf{v}_k, \quad k = 1, 2, \cdots, K$ to be arbitrary precoding vectors
2	**Compute** the matrix $\mathbf{Q}_k$ in (1.41) for $k = 1, 2, \cdots, K$
3	**Obtain** $\mathbf{w}_k, \quad k = 1, 2, \cdots, K$ using (1.42)
4	**Compute** the matrix Φ_k in (1.52) for $k = 1, 2, \cdots, K$
5	**Obtain** $\mathbf{v}_k, \quad k = 1, 2, \cdots, K$ using (1.53)
6	**Repeat** steps 2-5 until convergence of $\sum_{k=1}^{K} J_k$ and $\sum_{k=1}^{K} L_k$

1.7.3 Linear MMSE

Let us briefly describe in this part the design of the linear MMSE receiver for MIMO systems. We consider MSE cost function for the total transmitted data streams

$$J_{MSE} = \mathbb{E}\left[\|\mathbf{x} - \mathbf{G}^{\mathcal{H}}_{\mathbf{mmse}}\mathbf{y}\|^2\right] \tag{1.55}$$

where $\mathbf{G}_{\mathbf{mmse}}$ is the $N_r \times N_t$ MMSE filtering matrix, in order to obtain this matrix, we minimize the cost function by taking the gradient with respect to the filter $\mathbf{G}^*_{\mathbf{mmse}}$ and equate it with zero matrix, this yields

$$\begin{aligned}\mathbf{G}^*_{\mathbf{mmse}} &= \arg\max_{\mathbf{G}_{\mathbf{mmse}}} J_{MSE} \\ &= (\mathbf{H}\mathbf{H}^{\mathcal{H}} + \sigma^2\mathbf{I})^{-1}\mathbf{H},\end{aligned} \tag{1.56}$$

where $\mathbf{I}$ denotes $N_r \times N_r$ identity matrix.

Then, based on the assumption that both of the transmitted signal and the noise ware generated as independent Gaussian variables, the $N_r \times 1$ transmitted vector which estimated at the receiver is given by

$$\hat{\mathbf{x}} = \mathbf{G}^{*\mathcal{H}}_{\mathbf{mmse}}\mathbf{y} \tag{1.57}$$

where $\mathbf{y}$ is the received signal vector.

1.7.4 Successive Interference Cancellation (SIC)

The SIC algorithm of V-BLAST algorithm which proposed in (Foschini 1996) has been proved to be very efficient technique and widely employed scheme in MIMO systems (Jankiraman 2004). Although the ML receiver is considered the optimal scheme that reaches the highest possible diversity order and the best performance (Tse & Viswanath 2005), it is still not the suitable practical scheme to be used, because of its complexity which grows exponentially with the number of transmit antennas and the constellation size of the used modulation scheme. Therefore, the researcher have focused their efforts to propose and investigate other suboptimal schemes that can achieve the trade-off between the performance and complexity (Lin *et al.* 2011).

SIC is suggested for the first time in (Cover 1972). The fundamental idea of SIC is that the users are decoded successively, i.e., after decoding the first user, the effect of its signal subtracted from the received signal, then the second user is decoded and its signal also subtracted from the received signal before decoding the next user, and so on. This procedure is known as the successive (sequential) nulling and canceling (Yang *et al.* 2004). To illustrate this process in more detail let's assume a communication system with two interfering users scenario. When the SIC scheme is employed, the user of interest, say user 1 is decoded treating user 2 as interference, but user 2 is decoded with the advantages that signal of user 1 is already decoded and removed. Thus, this SIC scheme has the advantages in terms of achievable capacity and reliability over the conventional detection schemes, which decode every user treating the other interfering users as noise (Varanasi & Guess 1997). To improve the accuracy and performance of SIC scheme and also to reduce the propagation error from decoding stage to another, an optimal ordering strategy is applied to determine the decoding order in the detection process, this idea has been introduced first in (Foschini *et al.* 1999). This strategy is simply to decode the strongest user first, i.e., the user with the highest SINR is decoded the first. For instance, OSIC algorithm employed by the V-BLAST system is first decodes the strongest signal, then it re-encodes and modulates the estimated symbols of this user, next, it subtracts the effect of this estimated symbols from the receiving signal. After canceling the effect of the first user, OSIC algorithm proceeds to decode the strongest of the remaining signals and cancel its effect, and so on, until it decodes all the transmitted signals. In this manner the weaker user can get higher data rate than if it has to contend with the interference of the strong user. Here, it is worthy to mention that from the information theoretic point of view, user decoding ordering according to their received power is not always the most preferable choice (Tse & Viswanath 2005).

Moreover, the advantage of using SIC with superposition coding over the orthogonal transmission schemes can be obviously seen if the users have unsymmetrical channel gains. To illustrate this point let's assume general two-user downlink system in AWGN channel, with $\|h_1\| < \|h_2\|$, where h_k is the fixed (complex), channel gain corresponding to user k. Under the assumption of using a strategy that superposes the signals of the two users, such as CDMA, then the transmitted signal is the sum of the two signals (Tse & Viswanath 2005), i.e.,

$$x[m] = x_1[m] + x_2[m], \tag{1.58}$$

where $x_k[m]$ is the signal intended for user k. Also, let's assume that P_1 and P_2 are the allocated power for user 1 and 2 respectively, and they are limited by the total transmitted power constrained, such that, $P_1 + P_2 = P$.

Then, at the user 1, the signal of user 2 treated as noise, thus, this user can achieve the following rate

$$R_1 = \log\left(1 + \frac{P_1\|h_1\|^2}{P_2\|h_1\|^2 + N_0}\right) = \log\left(1 + \frac{(P_1 + P_2)\|h_1\|^2}{N_0}\right) - \log\left(1 + \frac{P_2\|h_1\|^2}{N_0}\right). \tag{1.59}$$

On the other hand, at user 2, the receiver which employs SIC first decodes the signal of user 1, i.e., x_1 by treating the signal x_2 as noise, after subtracting the effect of user 1, user 2 can decode its desired signal x_2 reliably with rate of

$$R_2 = \log\left(1 + \frac{P_2\|h_2\|^2}{N_0}\right). \tag{1.60}$$

In contrast, the orthogonal transmission schemes achieve the following rates

$$R_1 = \eta_1 \log\left(1 + \frac{P_1\|h_1\|^2}{\eta_1 N_0}\right). \tag{1.61}$$

and

$$R_2 = (1 - \eta_1)\log\left(1 + \frac{P_2\|h_2\|^2}{(1 - \eta_1)N_0}\right). \tag{1.62}$$

where η_1 is the fraction of the time or bandwidth resources allocated to user 1.

From the above equations, one, can readily see the advantage of using the SIC scheme over the orthogonal transmission approach when the channel gains of the different users are largely varied.

Now, we proceed to illustrate the base-line algorithm of the simple SIC technique based on the MMSE criterion. As stated above, using SIC algorithm, a receiver computes the estimated symbols successively, rather than canceling all the undesired signals together. The structure of SIC algorithm based on the MMSE receiver is shown in Fig. 7.

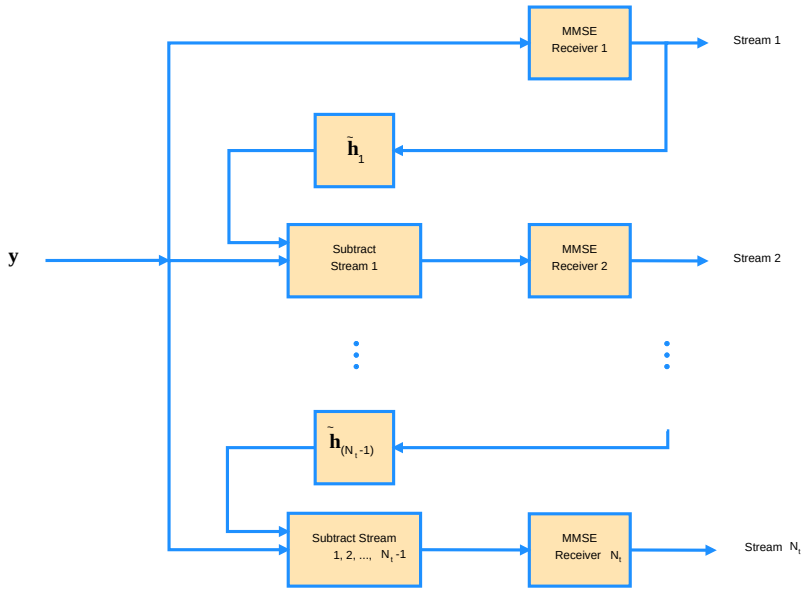

Figure 7. The MMSE-SIC receiver structure

In a multiple antenna system, the algorithm corresponding to the mth antenna stream is mathematically described as follows. When $m = 1$, the expected value of the mth symbol is given by

$$\hat{x}_m^{(f)} = \mathbf{g}_m^{\mathcal{H}} \mathbf{y} \tag{1.63}$$

where $\mathbf{g}_m$ is the mth filtering vector,

$$\mathbf{g}_m^{\mathcal{H}} = (\mathbf{H}\mathbf{H}^{\mathcal{H}} + \sigma^2 \mathbf{I})^{-1} \tilde{\mathbf{h}}_m \tag{1.64}$$

For the remaining streams $m = 2, \ldots, N_t$ we obtain

$$\mathbf{y}^{(m)} = \mathbf{y}^{(m-1)} - \tilde{\mathbf{h}}_{m-1} \hat{x}_{m-1}^{(f)}, \quad \mathbf{y}^{(1)} = \mathbf{y} \tag{1.65}$$

$$\hat{x}_m^{(f)} = \mathbf{g}_m^{\mathcal{H}} \mathbf{y}^{(m)} \tag{1.66}$$

$$\mathbf{g}_m^{\mathcal{H}} = (\tilde{\mathbf{H}}_m \tilde{\mathbf{H}}_m^{\mathcal{H}} + \sigma^2 \mathbf{I})^{-1} \tilde{\mathbf{h}}_m \tag{1.67}$$

where the value $\hat{x}_m^{(f)}$ is the final output corresponding to the antenna stream m, and we design the matrix $\tilde{\mathbf{H}}_m = [\tilde{\mathbf{h}}_m, \tilde{\mathbf{h}}_{m+1}, \ldots, \tilde{\mathbf{h}}_{N_t}]$, which excludes the previous

detected vectors, $\tilde{\mathbf{h}}_1, \tilde{\mathbf{h}}_2, \ldots, \tilde{\mathbf{h}}_{m-1}$ from the matrix $\mathbf{H}$, where the vector $\tilde{\mathbf{h}}_{m-1}\hat{x}_{m-1}^{(f)}$ is the estimated interference to be canceled at iteration m.

As aforementioned, the performance of SIC can be improved by determining the cancellation order, which the algorithm proceeds accordingly. Normally, SIC of MIMO system obtain the order by arranging the received signals powers and start to detect from the antenna stream with the strongest power. In the MIMO system, we produce the cancellation order by arranging a group of values, namely, $\{\tilde{\mathbf{h}}_1, \tilde{\mathbf{h}}_2, \ldots, \tilde{\mathbf{h}}_{N_t}\}$, which corresponds to the columns of the matrix $\mathbf{H}$.

1.7.5 Maximum Likelihood Multi-User Detection (ML-MUD)

Assuming that all of the data symbol vectors are equally likely, then, Maximum Likelihood (ML) scheme is optimal in the sense of minimizing the probability of error of the detected signal (Seethaler, Artes & Hlawatsch 2005). For our system model, the ML detector is given by

$$\hat{\mathbf{x}}_{\mathrm{ML}} = \arg\min_{\mathbf{x}\in\mathcal{D}}\{\|\mathbf{r}_k - \mathbf{y}_k\|^2\} \tag{1.68}$$

where $\hat{\mathbf{x}}_{\mathrm{ML}}$ the ML estimate of the transmitted vector $textbfx$, and the received signal vector at the kth receiver is given by

$$\mathbf{y}_k = \sqrt{P_k}\mathbf{H}_{kk}\mathbf{x}_k + \sqrt{\alpha P_i}\sum_{i=1,i\neq k}^{K}\mathbf{H}_{ki}\mathbf{x}_i \tag{1.69}$$

where P_j the allocated power for the jth transmitter, and $\mathbf{H}_{ki}$ is the channel coefficient matrix between from the ith transmitter to the kth receiver. Each $\mathbf{x}$ represents an $N_t \times 1$ transmit vector, where $\mathbf{x} \triangleq [x_1, \cdots, x_{N_t}]^{\mathcal{T}}$, the mth data symbol x_m is a complex valued, drawn from constellation alphabet $\mathcal{A}_c$, all elements of the vector $\mathbf{x}$ are assumed to be independent and have zero mean unit variance. Also, set $\mathcal{D}$ includes all possible transmitted data vectors $\mathbf{x}$, and its cardinality $|\mathcal{D}| = |\mathcal{A}_c|^{KN_t}$, with an exponential growth with KN_t. One disadvantage of ML detection is related to its optimization problem, where $\mathcal{D}$ is in fact not a convex set (Seethaler, Artes & Hlawatsch 2005). Therefore, the numerical convex optimization methods are not suitable for such a scheme (Seethaler, Artes & Hlawatsch 2005). Because the conventional exhaustive search method to find the optimal solution of (1.68) by evaluating the $\|\mathbf{r}_k - \mathbf{y}_k\|^2$ has a complexity $\mathcal{O}(|\mathcal{A}_c|^{KN_t})$, it is common to consider the maximum likelihood multi-user detection infeasible for

most current communication applications (Dai, Molisch & Poor 2004); recently authors of (Botsinis, Ng & Hanzo 2013) introduced a novel promising approach of designing a low-complexity maximum likelihood multi-user detector employing Quantum Search Algorithms (QSA) for potential application in wireless communication systems. Their presented results show that the employed quantum based MUD search algorithm ties the performance of the conventional optimal Maximum Likelihood Multi-User Detection (ML-MUD). However, this performance achieved with a significant computational complexity reduction compared to the conventional ML-MUD. This can be seen as an opening for using the joint and group detection techniques that can support larger number of users and higher order modulation schemes in the next generation of the communication systems.

1.8 Complexity Issues

In this section, we summarize the computational complexity issues related to the addressed schemes. Starting with few remarks on the complexity of the MIL scheme, we notice that the MIL iterative interference alignment scheme requires a huge computational complexity to compute the transmit precoding and the receiving filtering vectors. For instance, in each iteration, the kernel algorithm of this scheme requires $K(K-1)(N_rN_t+N_r^2)$, and $K(K-1)(N_tN_r+N_t^2)$ complex multiplications, only to compute the covariance matrix in the transmitter and the receiver respectively. Also, since it is an iterative based algorithm, it needs (depending on the initial conditions) a considerable number of iterations L to converge.

To address the convergence of the MIL, we should consider the similarity between the minimized objective functions of step 3 and step 5 of the iterative MIL algorithm in Table 1 as indicated in (Mohapatra, Nissar & Murthy 2011). The objective function minimized in the step 3 represents the total interference plus noise power at receiver of interest. While, the objective function to be minimized in step 5 of the algorithm is the total interference power due to the transmitter of interest. Since these two objective functions are under the same total power constraints; this means, minimizing one of them does not increase the other. In addition, it is stated in (Mohapatra, Nissar & Murthy 2011) that in each iteration, the objective functions will decrease, and they are bounded below by zero. This proves the convergence of both objective functions across all transmitterreceiver pairs. Finally,

since the optimality of the solution to both sub problems is granted, the algorithm is guaranteed to converge to a local optimum.

Nevertheless, it is worthy to noting that the algorithm may not minimize the objective functions to zero, even when the noise variance is zero and the interferences are perfectly aligned, because of the numerical round off errors, but these encountered numerical errors are similar to those for other iterative interference alignment algorithms (Mohapatra, Nissar & Murthy 2011).

On the other hand, complexity of the MMSE receiver per transmit antenna data stream is $O((N_r)^3)$. We notice that the linear MMSE receiver also can be designed as an $N_r \times 1$ filter vector corresponding to each transmit antenna stream. In addition, the complexity of the SIC detector based on MMSE receivers is $O((N_r)^3)$ per transmit antenna data stream.

In contrast with the above mentioned schemes, we can see that the maximum likelihood multi-user detection requires the highest computational complexity, where it uses the exhaustive search to find the optimal solution of its objective function as shown in Subsection 1.7.5. This means the receiver performs its search over all combination of all possible transmitted vectors. Therefore, overall complexity of this scheme grows exponentially with the number of users and the number of transmit antennas. Thus, if we denote the searching set by $\mathcal{D}_t$, then, its size is given by $|\mathcal{A}_c|^{KN_t}$, where $|\mathcal{A}_c|$ is the constellation size of the employed modulation scheme. In other words, the ML arithmetic computational complexity is exponentially increasing with the constellation size and the number of transmit antennas (or the simultaneously transmitted symbols) $O(\mathcal{A}_c^{N_t})$. The MUD-ML overall complexity is $\mathcal{A}_c^{KN_t}(KN_t)^2 + \mathcal{A}_c^{KN_t}(KN_t)$, where $\mathcal{A}_c^{KN_t}(KN_t)^2$ represents the number of multiplication operations and $\mathcal{A}_c^{KN_t}(KN_t)$ represents the number of square operations (Yang *et al.* 2004).

1.9 Contributions of the Thesis

This thesis contributes to the area of interference mitigation via successive group decoding. Specifically, it extensively investigates and assesses the use of the optimal and constrained partial group decoding techniques in the field of interference mitigation and management for various communication setups and environments. Also, it studies the opportunity of using successive group decoding techniques in

the large-scale MIMO systems, where we provide a detailed description for the implementation of such system. Furthermore, through this thesis we comprehensively analyze the performance of the successive group decoding techniques to obtain closed formulas that characterize these systems efficiency in certain practical scenarios.

In this sense, I have successfully presented the most of my research work of this thesis in several conference and journal articles, where, the majority of these papers have been accepted to appear or already published. In all referred papers in this section I was the main author, i.e., the principle researcher, except for (Chen *et al.* 2012) in which I was a coauthor. More detailed description of the contributions of this thesis can be summarized as follows:

- I have studied the capability of the OSGD to mitigate interference in the multiantenna systems, where I have inspected OSGD performance in terms of its (ergodic, and effective) capacity. Also, I have evaluated the minimum required energy per bit, Bit Error Rate (BER), and the outage probability of this scheme under different quality of service (QoS) constraints. In addition, in that study I have considered both the spatially correlated and uncorrelated (Rayleigh and Rician) fading channels. Also, I have explored performance of this scheme in different SNR and SIR environments, where I have considered both the power-limited and bandwidth-limited regimes with various cross-talk values, taking in account several transmit-receive MIMO configurations. This part of my work have been concluded and published in (Abu-Ella & Elmusrati 2014d), and also published with much more details in (Abu-Ella & Elmusrati 2014e), Moreover, I have studied the effect of the Imperfect channel estimation on the performance of the OSGD system. The results of this part of my research work have been submitted through (Abu-Ella & Elmusrati 2014f).

- My second contribution is that I have assessed the performance of the constrained partial group decoding (CPGD) technique in different communication environments. Where I have demonstrated the CPGD capability to manage and mitigate interference comparing to other interference mitigation schemes based on interference alignment strategy. This comparative study is carried out for MIMO interference channel and published in (Abu-Ella & Elmusrati 2014c). Also, prior to this study, I have joined a collaborated

research work to investigate the performance of the constrained group decoding in interference channels, my primary focus in that research was to evaluate the functionality of CPGD scheme comparing to other interference cancellation techniques, and as a result I coauthored (Chen *et al.* 2012).

- Furthermore, I proceeded my research to delve into studying the utilization of the CPGD technique to take advantage of its capability to manage and mitigate interference in uplink multicell MIMO system. Here, also I have assessed the overall system performance and published the results of this part of my work in (Abu-Ella & Wang 2013a).

- I have proposed a new design for the large-scale MIMO transceiver system. I have presented the main challenges facing such Large-Scale MIMO (LS-MIMO) system, and I have proposed solutions for those problems. The transmitters in this proposed downlink system uses a simple fair user scheduling based on limited-feedback algorithm with basic random precodeing algorithm. On the other side, receivers employ constrained partial group decoder (CPGD) to detect their desired signals. Also, I have evaluated the performance of this LS-MIMO downlink system against the total number of users and SNR, using different number of scheduled users and with various group sizes of jointly decoded users, this part of my work was published in (Abu-Ella & Wang 2013b).

- As a part of the analytical work in this thesis, I have derived different closed-form expressions to characterize, generalize and simplify my proposed design and to be used as starting point for the future work. For instance, considering the vital importance of the threshold value related to scheduling algorithm used in the large-scale system, and in consistence with our objective to maintain the system simplicity and minimize the unnecessary computational complexity, I have proposed a closed-form expression to calculate this threshold value instead of computing it through the iterative numerical methods which may not be particularly efficient for large-scale MIMO system. This part of my work was also published in (Abu-Ella & Wang 2013b).

- Motivated by the crucial importance of the group decoding techniques to achieve higher data rates, and also since the large-scale MIMO expected to be a promising key (B4G and 5G) wireless technology, I have obtained a simple closed-form expression allows for a tight approximation to describe

the achieved capacity of OSGD scheme for LS-MIMO systems. Also, I have produced an accurate approximation formula for the rate-outage probability of this system. This part of my research work was accepted to appear in (Abu-Ella & Elmusrati 2014b).

- Finally, considering the importance of the assessment of wireless communication system regarding to the connection quality of service (QoS) as crucial task to promote the user Quality of Experiencece (QoE) in the next-generation wireless networks, I have obtained a simple closed-form expression to formulate the effective capacity of the large-scale OSGD system, which can be used as a tool to analyze the system performance in more realistic way. This part of my work has been submitted to Journal of IEEE Transactions on Wireless Communications (Abu-Ella & Elmusrati 2014a).

1.10 Thesis Organization

The rest of this thesis is organized as follows: Chapter 2 discusses the fundamental concepts of the optimal successive group decoding (OSGD) technique and its performance. Chapter 3 demonstrates the utilization of the CPGD scheme to mitigate interference in the interference channel system. Chapter 4 investigates the usage of CPGD in uplink multicell MIMO system. Chapter 5 introduces a novel proposed large scale MIMO transceiver system design using CPGD. In Chapter 6 we produce several closed-form expressions for ergodic, outage and effective capacity for the large-scale OSGD system. Finally, Chapter 7 concludes this thesis and addresses some practicality matters also layouts the open issues and the prospective points of research associated with this thesis.

2 INTERFERENCE MITIGATION USING OPTIMAL SUCCESSIVE GROUP DECODING

2.1 Introduction

In this chapter we aim to assess the optimal successive group decoder (OSGD) considering different scenarios and in a wide range of testing metrics. We investigate the OSGD in the $K-$user Interference Channel (ICh) and evaluate its capability to mitigate interference. We inspect OSGD performance in terms of its (ergodic and effective) capacity, also, we evaluate its minimum required energy per bit, bit error rate (BER), and outage probability, under different quality of service (QoS) constraints. This chapter considers both the spatially correlated and uncorrelated (Rayleigh and Rician) fading channels. In addition, it explores performance of the OSGD in different SNR and SIR environments, where we consider both the power-limited and bandwidth-limited regimes with various cross-talk values (i.e., for different Interference-to-Signal Power Ratio (ISR) levels), taking into account several transmit-receive multiple-input multiple-output (MIMO) antenna configurations. The obtained numerical results in this chapter show that OSGD technique exhibits very efficient performance to cope with interference in the investigated scenarios, proving by that its competency comparing to the most developed interference cancellation approaches. This makes OSGD a favorable technique for interference reduction; especially, if we bear in mind that OSGD is formed on receive-side processing only. Also, if we contemplate the reduction of its arithmetic complexity, as a result of its innate complexity controlling characteristic, comparing to the large computational complexity of the other optimal interference cancellation schemes, such as, the maximum likelihood multi-user detection (ML-MUD) or the other iterative interference alignment schemes.

The remainder of this chapter is organized as follows: Section 2.2 introduces the idea of the optimal successive group decoding. Section 2.3 discusses the optimality of the OSGD technique. Section 2.4 discusses the complexity of the OSGD technique. Numerical results of the different scenarios in terms of achieved ergodic, outage and effective capacity, minimum required energy per bit, in addition to the bit error rate and outage probability performance evaluation are demonstrated in Section 2.5. Finally, Section 2.6 summarizes this chapter.

2.2 Optimal Successive Group Decoding

Successive group decoder (SGD) was introduced as an extension of the standard successive decoder in which at each stage a subset of users is jointly decoded after treating the transmissions of the remaining users as a Gaussian interference.

In OSGD system, each receiver employs a successive decoding procedure, in each stage a subset of users are jointly decoded, after subtracting the already decoded users from the received signal, and by treating the remaining users as AWGN. This system limits the number of users being jointly decoded at each stage to be at most μ to control the complexity of the decoder. In the remainder of this section, we reproduce the basic concepts of the OSGD according to (Prasad & Wang 2009).

Assuming that the power P_i of each user is pre-specified and is not dependent on the channel realizations. Then, employing the OSGD minimizes the outage probability of each user. Considering the receiver i, the user of interest will be user i, and given the users rates $\mathbf{R}$, and channel realization $\tilde{\mathbf{H}}^{(i)} = [\sqrt{P_1}\mathbf{H}_1^{(i)}, \cdots, \sqrt{P_K}\mathbf{H}_K^{(i)}]$, also, the set of all users' indices $\mathcal{M} \triangleq \{1, \cdots, K\}$, with any disjoint subsets $\mathcal{A}$, $\mathcal{B}$ of $\mathcal{M}$. Then, the validity of the ordered partition $\underline{\mathcal{G}} = \{\mathcal{G}_1, \cdots, \mathcal{G}_p\}$ of any subset of $\mathcal{M}$ for any $p \geq 1$ can be checked according to the following definition

Definition 1: An ordered partition is said to be valid for receiver i if:

- $\mathcal{G}_l \neq \phi$
- $f_i(\mathcal{G}_l) = 1, \quad 1 \leq l \leq p$
- $i \in \mathcal{G}_p$

where, $f_i(\cdot)$ is a bounding function whose purpose is to impose decoding complexity constraint given as

$$f_i(\mathcal{J}) = \begin{cases} 1 & |\mathcal{J}| \leq \mu_i \\ 0 & \text{otherwise} \end{cases}$$

for a specified integer $\mu_i \geq 1$.

By defining a rate-outage as an event where in a decoding stage the rates of the signals to be decoded falls out of the corresponding achievable rate region, and R_i to be the transmission rate of the signal on transmitter i, also, $\mathbf{R} \triangleq [R_i]_{1 \leq i \leq K}$. Then,

the minimum rate margin for decoding $\mathcal{A}$ while treating $\mathcal{B}$ as noise for two disjoint subsets $\mathcal{A}, \mathcal{B} \subseteq \mathcal{M}$ is defined as follows

$$\varepsilon(\tilde{\mathbf{H}}^{(i)}, \mathcal{A}, \mathcal{B}, \mathbf{R}) \triangleq \min_{\mathcal{D} \subseteq \mathcal{A}, \mathcal{D} \neq \phi} \{\triangle\,(\tilde{\mathbf{H}}^{(i)}, \mathcal{D}, \mathcal{B}, \mathbf{R}_{\mathcal{D}})\}, \quad \mathcal{A} \neq \phi \tag{2.1}$$

with $\varepsilon(\tilde{\mathbf{H}}^{(i)}, \phi, \mathcal{B}, \mathbf{R}) = 0$ and

$$\triangle\,(\tilde{\mathbf{H}}^{(i)}, \mathcal{D}, \mathcal{B}, \mathbf{R}_{\mathcal{D}}) \triangleq \log \left| \mathbf{I} + \tilde{\mathbf{H}}_{\mathcal{D}}^{(i)\mathcal{H}} \left(\mathbf{I} + \tilde{\mathbf{H}}_{\mathcal{B}}^{(i)} \tilde{\mathbf{H}}_{\mathcal{B}}^{(i)\mathcal{H}} \right)^{-1} \tilde{\mathbf{H}}_{\mathcal{D}}^{(i)} \right| - \sum_{j \in \mathcal{D}} R_j \tag{2.2}$$

Note that $\mathbf{R}_{\mathcal{D}} \in \mathcal{C}(\tilde{\mathbf{H}}^{(i)}, \mathcal{A}, \mathcal{B})$ if and only if $\varepsilon(\tilde{\mathbf{H}}^{(i)}, \mathcal{D}, \mathcal{B}, \mathbf{R}) \geq 0$. Now, for any valid ordered partition $\underline{\mathcal{G}} = \{\mathcal{G}_1, \cdots, \mathcal{G}_p\} \in \underline{\boldsymbol{\mathcal{Q}}}_i$ we define

$$\varepsilon(\tilde{\mathbf{H}}^{(i)}, \underline{\mathcal{G}}, \mathbf{R}) \triangleq \min_{1 \leqslant l \leqslant p} \left\{ \varepsilon \left(\tilde{\mathbf{H}}^{(i)}, \mathcal{G}_l, \mathcal{M} \backslash \cup_{j=1}^{l} \mathcal{G}_j, \mathbf{R} \right) \right\} \tag{2.3}$$

Now, let $\underline{\boldsymbol{\mathcal{Q}}}_i$ to be the set of all valid ordered partitions of all subsets of $\mathcal{M}$ which contain i, then, the outage event $\mathcal{O}^{(i)}$ occurs for the valid ordered partition $\underline{\mathcal{G}} = \{\mathcal{G}_1, \cdots, \mathcal{G}_p\} \in \underline{\boldsymbol{\mathcal{Q}}}_i$ if and only if

$$\varepsilon(\tilde{\mathbf{H}}^{(i)}, \underline{\mathcal{G}}, \mathbf{R}) < 0. \tag{2.4}$$

Therefore, an OSGD using the partition $\underline{\mathcal{G}} \in \underline{\boldsymbol{\mathcal{Q}}}_i$ will attempt to decode user i if and only if $\varepsilon(\tilde{\mathbf{H}}^{(i)}, \underline{\mathcal{G}}, \mathbf{R}) \geq 0$.

To perform this decoding procedure each receiver i where $1 \leq i \leq K$ employs a greedy algorithm (Algorithm-1) that either declare an outage or yields an optimal valid partition of the OSGD. The involved steps of the successive decoding for the OSGD in the ith receiver are as follows.

1. Initialize with input $\tilde{\mathbf{H}}^{(i)}, \mathbf{R}$
2. Receiver i runs Algorithm-1
3. **If there is no outage**, i.e.,

   $$\mathbf{R}_{\mathcal{G}_l} \in \mathcal{C}(\tilde{\mathbf{H}}^{(i)}, \mathcal{G}_l, \mathcal{M} \backslash \cup_{j=1}^{l} \mathcal{G}_l), \quad \forall 1 \geq l \leq p. \tag{2.5}$$

   Algorithm 1 outputs an optimal partition, $\underline{\mathcal{G}}_{opt} = \{\mathcal{G}_1, \cdots, \mathcal{G}_p\}$. **Then**

For $1 \leq l \leq p$

- **Compute** the noise covariance matrix: $\Phi_{\mathcal{G}_l}^{(i)} = \mathbf{I} + \sum_{j \in \mathcal{M} \setminus \cup_{j=1}^{l} \mathcal{G}_j} \tilde{\mathbf{H}}_j^{(i)} \tilde{\mathbf{H}}_j^{i^{\mathcal{H}}}$ and jointly decode the users in $\mathcal{G}_l$ using the ML rule on $\left\{ \tilde{\mathbf{r}}^{(i)}[n] = \left(\Phi_{\mathcal{G}_l}^{(i)} \right)^{-\frac{1}{2}} \mathbf{y}^{(i)}[n] \right\}_{n=1}^{J}$ assuming the model $\tilde{\mathbf{r}}^{(i)}[n] = \left(\Phi_{\mathcal{G}_l}^{(i)} \right)^{-\frac{1}{2}} \tilde{\mathbf{H}}_{\mathcal{G}_l}^{(i)} \mathbf{x}_{\mathcal{G}_l}[n] + \tilde{\mathbf{z}}^{(i)}[n], \quad 1 \leq n \leq J$ with $\tilde{\mathbf{z}}^{(i)}[n] \sim \mathcal{CN}(\mathbf{0}, \mathbf{I})$.
- **Update** $\left\{ \mathbf{y}^{(i)}[n] \longleftarrow \mathbf{y}^{(i)}[n] - \tilde{\mathbf{H}}_{\mathcal{G}_l}^{(i)} \hat{\mathbf{x}}_{\mathcal{G}_l}^{(i)}[n] \right\}_{n=1}^{J}$, where $\hat{\mathbf{x}}_{\mathcal{G}_l}^{(i)}[n]$ is the decision made corresponding to the nth symbol interval, through the coherence interval of J symbols, in the codeword of the users in the set $\mathcal{G}_l$, which are re-encoded and modulated by receiver i post-processing.

End For

4. **Otherwise**, Algorithm 1 declares an outage for the intended user i.

Table 2. Algorithm 1(a) Partitioning procedure

1	**Initialize** $\mathcal{S} = \mathcal{M}$, $\underline{\mathcal{G}}_{opt}^{(i)} = \phi$
2	Determine a group $\mathcal{G}^* \subseteq \mathcal{S}$ using Algorithm 1(b) after initializing it with user set $\mathcal{S}$ and rates $\mathbf{R}_{\mathcal{S}}$.
3	**If** $\varepsilon(\tilde{\mathbf{H}}^{(i)}, \mathcal{G}^*, \mathcal{S} \setminus \mathcal{G}^*, \mathbf{R}) < 0$ then
4	**Declare** an outage and **Stop**.
5	**else**
6	**Update** $\mathcal{S} \longleftarrow \mathcal{S} \setminus \mathcal{G}^*$ and $\underline{\mathcal{G}}_{opt}^{(i)} \longleftarrow \{\underline{\mathcal{G}}_{opt}^{(i)}, \mathcal{G}^*\}$
7	**If** $i \in \mathcal{G}^*$
8	**Output** $\underline{\mathcal{G}}_{opt}^{(i)}$.
9	**Stop**.
10	**else**
11	**Go to** Step 2
12	**End if**
13	**End if**

Table 3. Algorithm 1(b) Selecting the Optimal Group

1	**Initialize** user set $\mathcal{S}$ and rates $\mathbf{R}_{\mathcal{S}}$
2	Form $\boldsymbol{\mathcal{S}} \triangleq \{\mathcal{G} \subseteq \mathcal{S} : \mathcal{G} \neq \phi, \lvert\mathcal{G}\rvert = \mu_i \text{ or } \mathcal{G} = \mathcal{S}\}$ and set $\boldsymbol{\mathcal{S}}_1 = \phi, \delta = -\infty$.
3	**For** each $\mathcal{G} \in \boldsymbol{\mathcal{S}}$
4	**Repeat**
5	**Update** $\boldsymbol{\mathcal{S}}_1 \longleftarrow \{\boldsymbol{\mathcal{S}}_1, \mathcal{G}\}$.
6	Determine $\xi_{rm} = \min_{\mathcal{W}\subseteq\mathcal{G}, \mathcal{W}\neq\phi} \Delta(\tilde{\mathbf{H}}^{(i)}, \mathcal{W}, \mathcal{S}\backslash\mathcal{G}, \mathbf{R}_{\mathcal{W}})$ and let $\hat{\mathcal{W}}$ be the minimizing set which among all minimizers has the smallest cardinality
7	**If** $\delta < \xi_{rm}$ then set $\mathcal{A} = \mathcal{G}$ and $\delta = \xi_{rm}$.
8	**Update** $\mathcal{G} \longleftarrow \mathcal{G}\backslash\hat{\mathcal{W}}$
9	**Until** $\mathcal{G} = \phi$ or $\mathcal{G} \in \boldsymbol{\mathcal{S}}_1$
10	**End For**
11	**Output** $\mathcal{G}^* = \mathcal{A}, \varepsilon(\tilde{\mathbf{H}}^{(i)}, \mathcal{G}^*, \mathcal{S}\backslash\mathcal{G}^*, \mathbf{R}) = \delta$ and **stop**.

2.3 OSGD Optimality

The OSGD scheme minimizes the outage probability for a given target rate. Or it may be seen as maximizer of the user rate, such that, the outage probability of this user does not exceed a certain upper bound.

To elaborate the above statement more, let's consider the channel realization at the receiver i is given by $\tilde{\mathbf{H}}^{(i)}$, and assume that $\underline{\mathcal{G}}^i = \{\mathcal{G}^i_1, \ldots, \mathcal{G}^i_{p_i}\}$ is any valid ordered partition for the receiver i. Then, according to Theorem 1 in (Prasad & Wang 2009), if Algorithm 1(a) confirms an outage for any channel realization $\tilde{\mathbf{H}}^{(i)}$, then, the maximum rate increment margin will be a negative value, i.e.,

$$\max_{\underline{\mathcal{G}} \in \underline{\boldsymbol{\mathcal{Q}}}_i} \left\{ \varepsilon(\tilde{\mathbf{H}}^{(i)}, \underline{\mathcal{G}}, \mathbf{R}) \right\} < 0. \tag{2.6}$$

where $\underline{\boldsymbol{\mathcal{Q}}}_i$ is the set of all valid partitions at the receiver i.

However, if there is no outage has been declared, then, among all valid ordered partitions, Algorithm 1(a) will determine the optimal ordered partition which maximizes the metric $\varepsilon(\tilde{\mathbf{H}}^{(i)}, \underline{\mathcal{G}}, \mathbf{R})$, i.e.,

$$\underline{\mathcal{G}}^i_{opt} = \arg \max_{\underline{\mathcal{G}} \in \underline{\boldsymbol{\mathcal{Q}}}_i} \left\{ \varepsilon(\tilde{\mathbf{H}}^{(i)}, \underline{\mathcal{G}}, \mathbf{R}) \right\}. \tag{2.7}$$

The proof of the theorem can be followed in (Prasad & Wang 2009).

Building on that, we can eventually come to the conclusion which stated by Theorem 2 in (Prasad & Wang 2009) as follows:

Among all SGDs, OSGD has the lowest outage probability at each receiver.

The proof of this theorem also has been given in same reference. But to explain the last statement we say that, for the receiver i if the OSGD declares an outage, then, any SGD that uses a valid ordered partition from $\underline{\boldsymbol{\mathcal{Q}}}_i$ must also declare an outage for that channel realization. Consequently, since the outage probability is the expectation of the outage event over the set of all channel realizations, the OSGD must minimize the outage probability of the desired user, over all SGDs.

In other words, for any channel realization at the receiver i, and for any valid ordered partition included in $\underline{\boldsymbol{\mathcal{Q}}}_i$, if the OSGD declares an outage, then, all the other SGDs must declare an outage too. Therefore, because the outage probability is the average of the outage event occurrence over the all the channel realization, OSGD does minimize the outage probability over all other SGDs.

This can be seen also as follows, assuming that OSGD has declared an outage for a given channel realization $\tilde{\mathbf{H}}^{(i)}$, then, it follows that we must have, for any valid ordered partitions $\underline{\mathcal{G}} = \{\mathcal{G}_1^i, \ldots, \mathcal{G}_{p_i}^i\} \in \underline{\boldsymbol{\mathcal{Q}}}_i$, the maximum rate margin will be less than zero, i.e., $\max\left\{\varepsilon(\tilde{\mathbf{H}}^{(i)}, \underline{\mathcal{G}}, \mathbf{R})\right\} < 0$. Therefore, the condition in (2.5) is not come true anymore. Consequently, an outage event occurs. Thereupon, we can conclude that any other SGD using any valid ordered partition from $\underline{\boldsymbol{\mathcal{Q}}}_i$ will declare an outage too for that given channel realization, and this affirms the optimality of OSGD scheme (Prasad & Wang 2009).

2.4 Complexity of OSGD

This section discusses the computational complexity of the OSGD and its employed algorithms. Given the users set $\mathcal{S}$ and the group size constraint μ_i, we find that the number of sub-groups that Algorithm-1(b) is examining will be at most $\mathcal{O}\left(|\mathcal{S}|^{\min\{(|\mathcal{S}|-\mu_i)^+, \mu_i\}}\right)$, where $(x)^+ = \max(0, x)$. Also, the loop consists the steps 4 to 9 is repeated at most $|\mathcal{G}|$ times. Therefore, since Algorithm-1(a) will invoke Algorithm-1(b) no more than K times, the complexity of Algorithm-1(a) for fixed group size μ_i is $\mathcal{O}\left(K^{\min\{K-\mu_i+1, \mu_i+1\}}\right)$, which is polynomial in K.

2.5 Simulation Results

In this section we present the numerical results carried out by Monte Carlo simulation of K-user interference channel MIMO OSGD system. Intentionally, we limit the number of users in the simulated scenarios; due to the fact that in many realistic scenarios the number of interfering users which significantly affecting the wireless connection between the access point and its desired user is usually limited. As in the case of downlink cellular system, where there are only limited number of co-channel interfering base stations disturbing the connection between the base station of interest and its desired user. Also, in uplink system, assuming that there is no intra-cell interference, which is a reasonable assumption for the most of the modern cellular systems, where the only source of interference comes from the co-channel users in the other neighboring cells and those users must be close enough to the base station of interest to be considered as interferers; thus we can assume them to be very few too. More importantly, according to (Zhang & Hanzo 2010) which referred to the findings of a field study conducted by the Universal Mobile Telecommunication System network, it is has been stated that, there is no more than three simultaneous interfering signals close to the cell edge. This means, indeed our aforementioned assumption can accommodate realistic scenarios. Therefore, in all of the following simulation setups for the interference channel systems, we assume the number of users K is 3 transmit-receive pairs. One user represented as a desired client and the other two as interfering sources. Another point to mention here is that, for all the following simulations, we have adopted the system model described in Section 1.5.

Finally, referring to the research methodology of this thesis which relays on the numerical simulation, and considering the known fact from the strong law of large numbers that, the expected value of an evaluated quantity can be accurately approximated by the average of a large number of samples (Etemadi 1981; Grinstead & Snell 2003). Also, keeping in mind that, the confidence interval of the estimated value depends on the variance of the evaluated random quantity and the number of simulations, in other words, the error margin of the estimated value for a certain confidence level depends on the sample standard deviation, and the number of samples. For instance, a 95% confidence for the expected value of random variable is limited by the following interval

$$\left[\bar{m}_n - \frac{1.96\bar{s}_n}{\sqrt{n}}, \bar{m}_n + \frac{1.96\bar{s}_n}{\sqrt{n}}\right] \tag{2.8}$$

where $\bar{m}_n, \bar{s}_n$ are the sample mean and sample standard deviation of the random variable using n samples.

Tacking all of that into account, and to fulfill our commitment to produce accurate results, we allow (depending on the sample variance of the evaluated metric) for enough Monte-Carlo simulation runs to ensure the achievement of tight error margin at high level of confidence. In other words, we use large enough number of samples or simulation runs to tighten the error margin of our obtained results. The number of used samples or runs are adequately stated in the context of each simulation setup wherever is necessary.

In the rest of this chapter we aim to investigate the OSGD performance in different scenarios and using a wide range of testing metrics. We inspect the OSGD in the interference channel in terms of it's achieved (ergodic and effective) capacity. Also, we assess its minimum required energy per bit, as well as, we evaluate its BER and outage probability performance. This study considers both the spatially uncorrelated and correlated fading channels with various inter-element correlation factors, under different QoS constraint values. In addition, this part explores the OSGD efficiency in different SNR and SIR environments, (where we consider both the power-limited and bandwidth-limited regimes with different ISR values). All of aforementioned investigation performed with numerous transmit-receive antenna configurations.

2.5.1 Interference Mitigation Capability

In this subsection, we study the OSGD capability to mitigate and suppress interference, so we compare its effective rate per user measured by bit per second per Hertz (bps/Hz) with the achieved rate of a well-known interference alignment scheme which minimizes the leakage interference between users, we point it here by (MIL). This comparison is done using four different MIMO configurations (3×3, 4×4, 6×6 and 8×8), in a high ISR environment, where the α parameter set up to be 1. The normalized QoS exponent which represented by $\hat{\theta} = TB\theta$ chosen to be 3, where B is the bandwidth, T is the block duration, and θ represents the decking rate of the buffering queue. We carry-out the results using two different spatial inter-element correlation factors ($\rho = 0$, and 0.9). From figures (8, 9, 10 and 11), we notice that in all cases OSGD has achieved a higher effective capacity comparing with the MIL scheme. For instance, when $\rho = 0$, for the 3×3 MIMO

configuration, the effective rate per user of the OSGD is 70% higher than that for the MIL. This percentage goes up to 107% in case of the 6×6 MIMO channel. However, when $\rho = 0.9$, this percentages become 79% and 119% for the 3×3 and 6×6 MIMO configurations respectively. This implies that OSGD is less affected by the channel inter-element correlation comparing with the MIL. The overall results in this subsection reveal that OSGD is more effective to suppress interference comparing with the MIL interference alignment scheme.

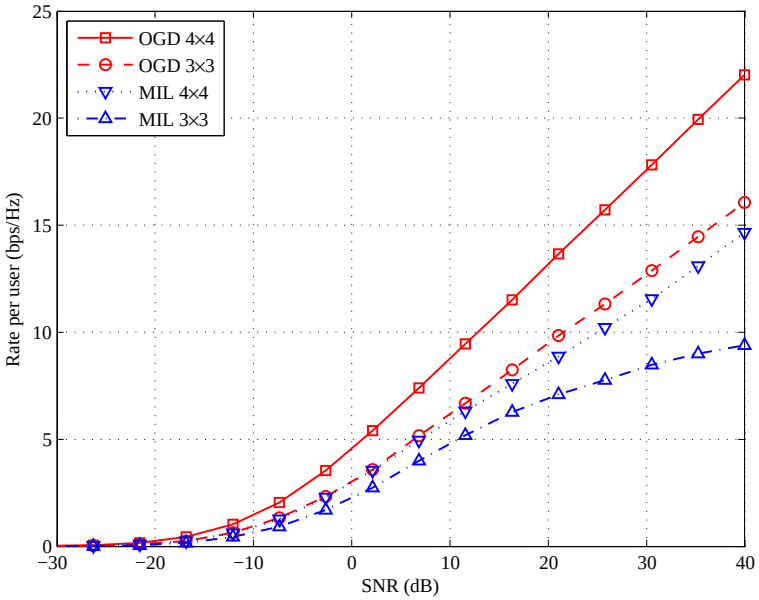

Figure 8. OSGD and MIL effective rate versus SNR (dB), $\alpha = 1$, $(3 \times 3, 4 \times 4)$-MIMO, $\rho = 0$ and the normalized QoS exponent $\hat{\theta} = 3$.

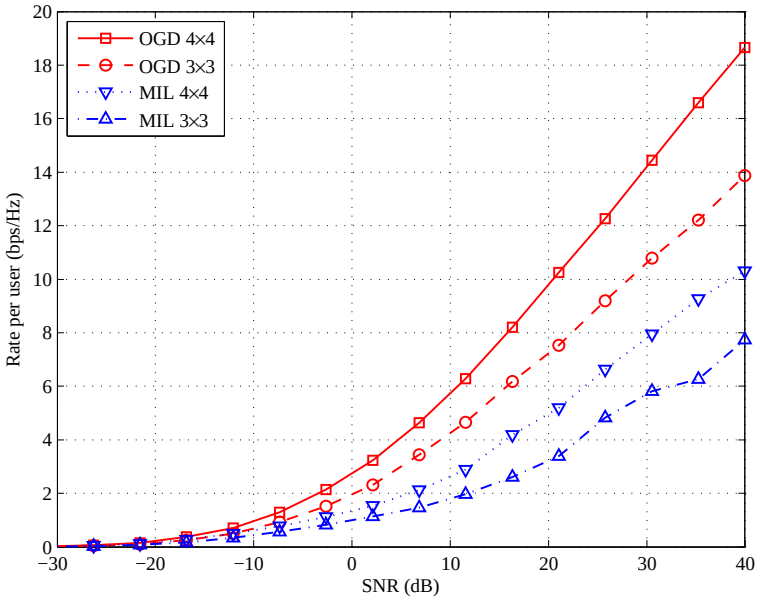

Figure 9. OSGD and MIL effective rate versus SNR (dB), $\alpha = 1$, $(3 \times 3, 4 \times 4)$-MIMO, $\rho = 0.9$ and the normalized QoS exponent $\hat{\theta} = 3$.

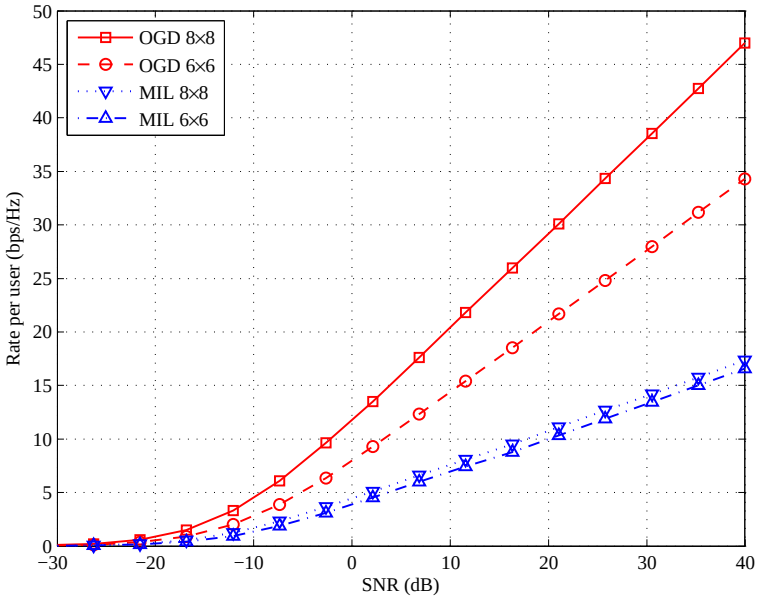

Figure 10. OSGD and MIL effective rate versus SNR (dB), $\alpha = 1$, $(6 \times 6, 8 \times 8)$-MIMO, $\rho = 0$ and the normalized QoS exponent $\hat{\theta} = 3$.

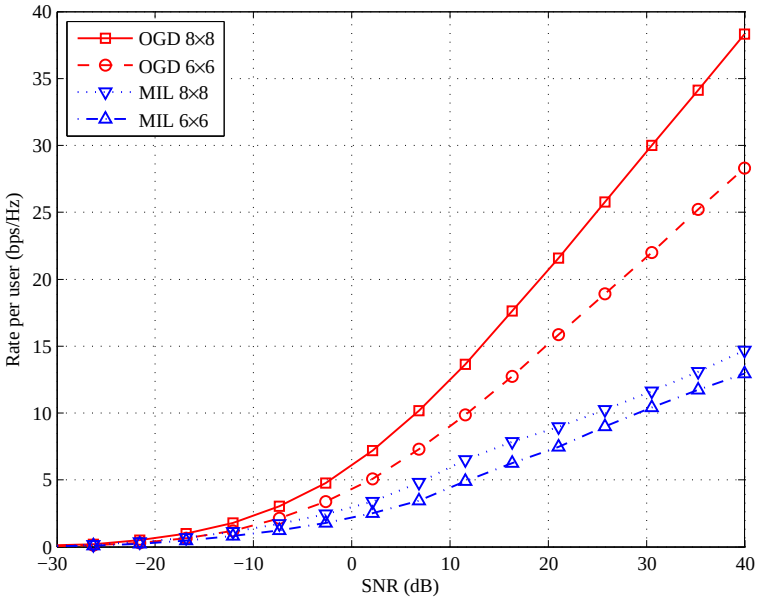

Figure 11. OSGD and MIL effective rate versus SNR (dB), $\alpha = 1$, $(6 \times 6, 8 \times 8)$-MIMO, $\rho = 0.9$ and the normalized QoS exponent $\hat{\theta} = 3$.

2.5.2 Minimum Required Energy Per Bit

Now, with the same aforementioned simulation setup in the previous subsection, we study the minimum required energy per bit $(E_b/N_0)_{min}$ for the OSGD and compare it with that for the MIL interference alignment algorithm. Results of this comparison are presented in figures (12, 13, 14, and 15). Interestingly, we observe that for both OSGD and MIL increasing the inter-element correlation helps the system to work at lower energy per bit, because at low SNR, the two systems benefit from the concentration of the channel eignmodes in only one dominant mode. Also, all the results show that OSGD requires lower minimum energy per bit comparing to the MIL scheme. For instance, the OSGD needs 0.9 dB less energy in case of the highly correlated (3×3) Rayleigh fading channel and this gap increases to be 4.5 dB less required minimum energy per bit in case of (8×8) uncorrelated channel.

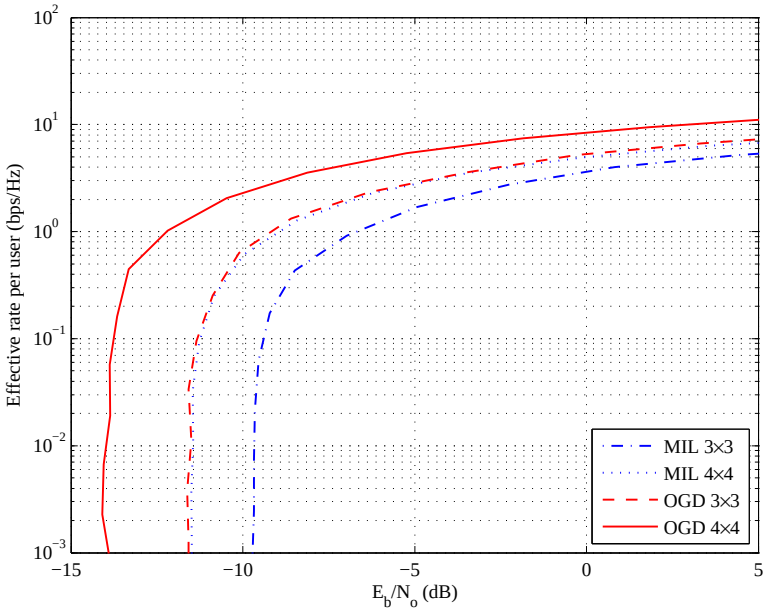

Figure 12. OSGD and MIL effective rate versus E_b/N_o (dB), $\alpha = 1$, $(3\times 3, 4\times 4)$-MIMO, $\rho = 0$ and the normalized QoS exponent $\hat{\theta} = 3$.

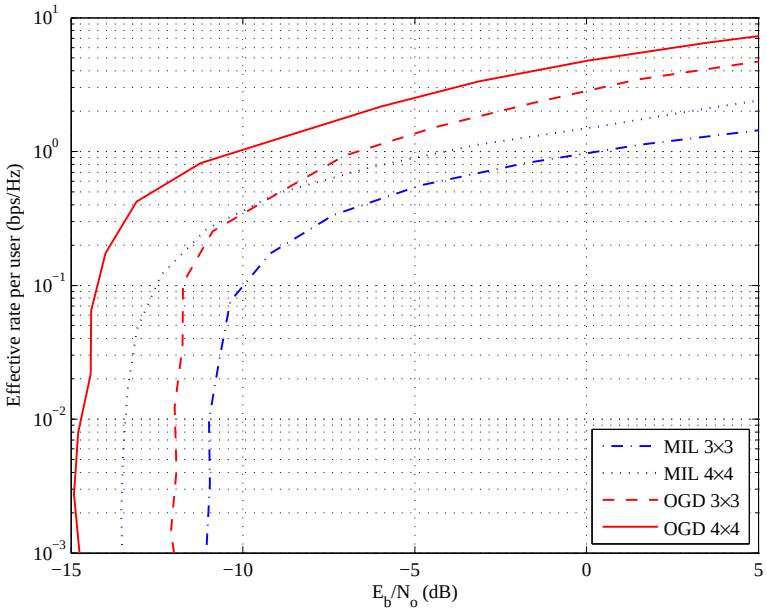

Figure 13. OSGD and MIL effective rate versus E_b/N_o (dB), $\alpha = 1$, $(3\times 3, 4\times 4)$-MIMO, $\rho = 0.9$ and the normalized QoS exponent $\hat{\theta} = 3$.

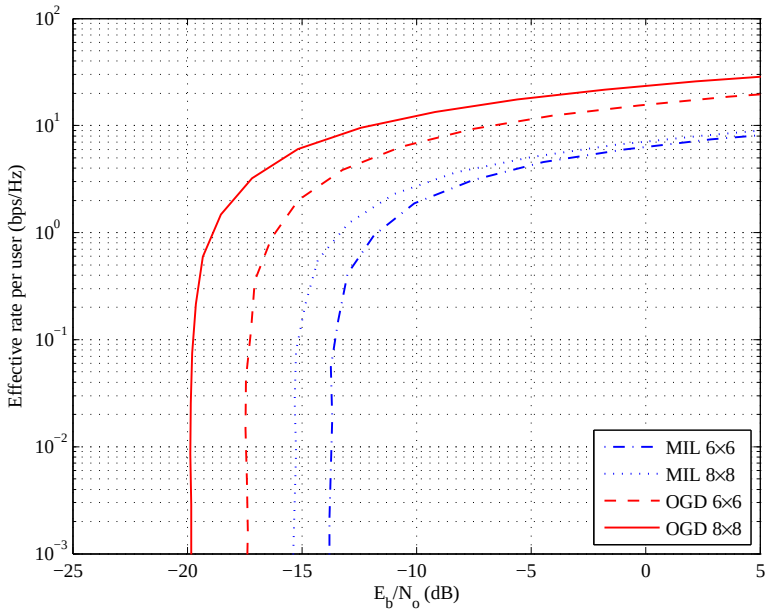

Figure 14. OSGD and MIL effective rate versus E_b/N_o (dB), $\alpha = 1$, $(6\times 6, 8\times 8)$-MIMO, $\rho = 0$ and the normalized QoS exponent $\hat{\theta} = 3$.

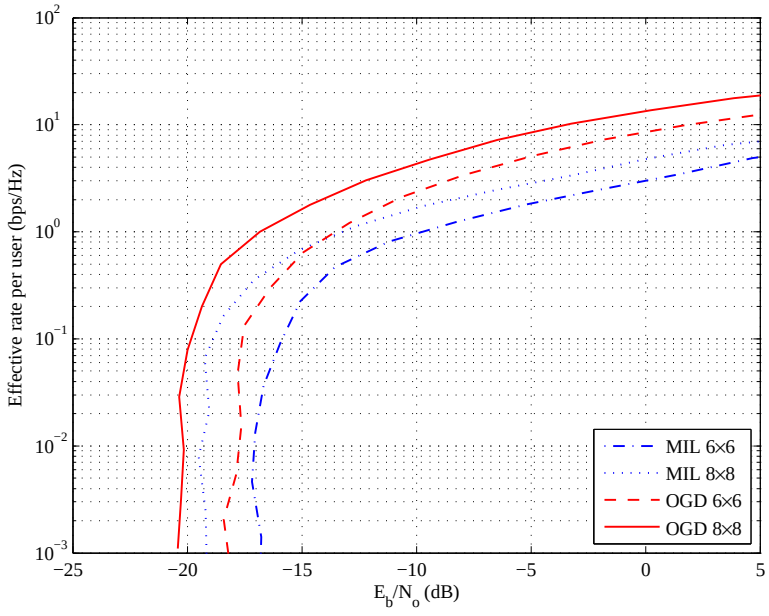

Figure 15. OSGD and MIL effective rate versus E_b/N_o (dB), $\alpha = 1$, $(6\times 6, 8\times 8)$-MIMO, $\rho = 0.9$ and the normalized QoS exponent $\hat{\theta} = 3$.

2.5.3 Achieved Capacity

In this subsection we study the OSGD achieved (ergodic and effective) capacity in (bps/Hz) versus the signal-to-noise ratio SNR in Decibel (dB). We consider the (3×3 and 6×6)-MIMO interference channel, with three different values for the normalized QoS exponents ($\hat{\theta} = 0,5$ and 10), also we use two inter-element correlation factors (0, for the uncorrelated channel and 0.9 for the highly spatial correlated channel). All the comparisons carried out here is for a strong interference environment, where the cross-talk parameter or the ISR α is set to be 1. Figures (16, 17, 18 and 19) present the achieved ergodic and effective capacity result of MMSE receiver and OSGD with group-size (μ) equals 2 and 3 respectively.

Clearly, it can be seen from the figures that OSGD has the highest achieved ergodic and effective capacity in all cases. Also, we can notice that the OSGD with $\mu = 3$ is the least affected scheme by changing the QoS metric $\hat{\theta}$.

Another point to mention here is, we can observe that the achieved capacity of the OSGD becomes lower as the channel becomes more correlated. This can be interpreted as a result of decreasing the degrees of freedom, where, the channel turns out to be less ranked by increasing the correlation between its elements, consequently, its eignmodes tend to concentrate in one dominated mode.

On the other hand, since the MMSE receiver is based on extracting the desired user alone, this case, i.e., increasing the spatial correlation, can be an advantage for such a scheme; thus, it can help increasing its achieved capacity. Nevertheless, the achieved capacity of MMSE receiver in all cases is still far less than that for the OSGD scheme.

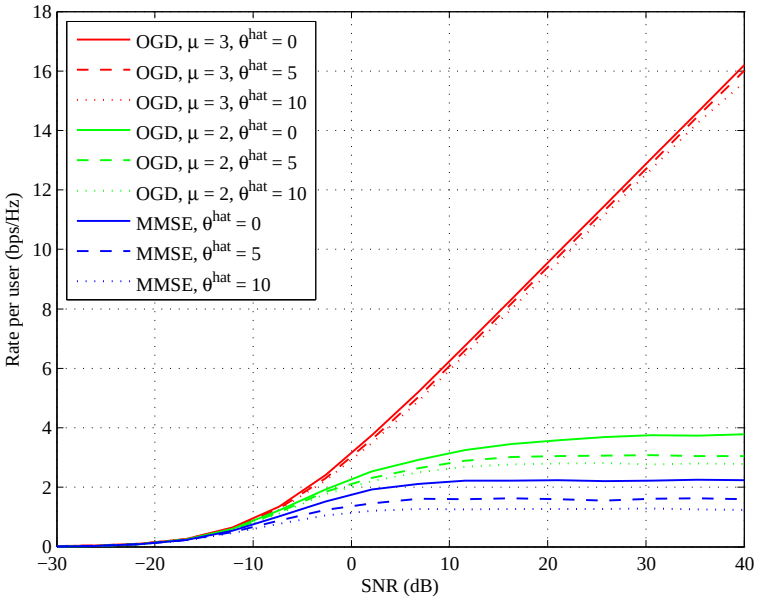

Figure 16. OSGD-$\mu = 2,3$ and MMSE effective rate versus SNR (dB), $\alpha = 1$, $N_t = 3$, $N_r = 3$, $\rho = 0$ and the normalized QoS exponent $\hat{\theta} = 0,5$ and 10.

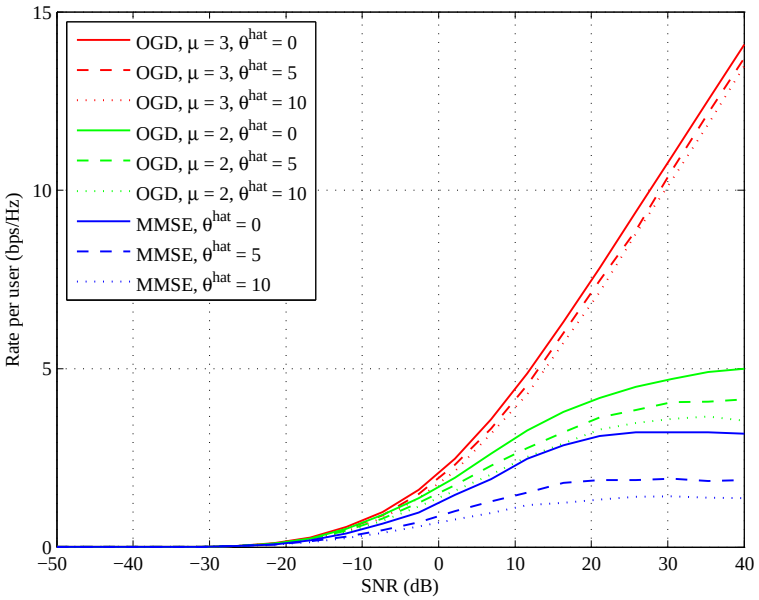

Figure 17. OSGD-$\mu = 2,3$ and MMSE effective rate versus SNR (dB), $\alpha = 1$, $N_t = 3$, $N_r = 3$, $\rho = 0.9$ and the normalized QoS exponent $\hat{\theta} = 0,5$ and 10.

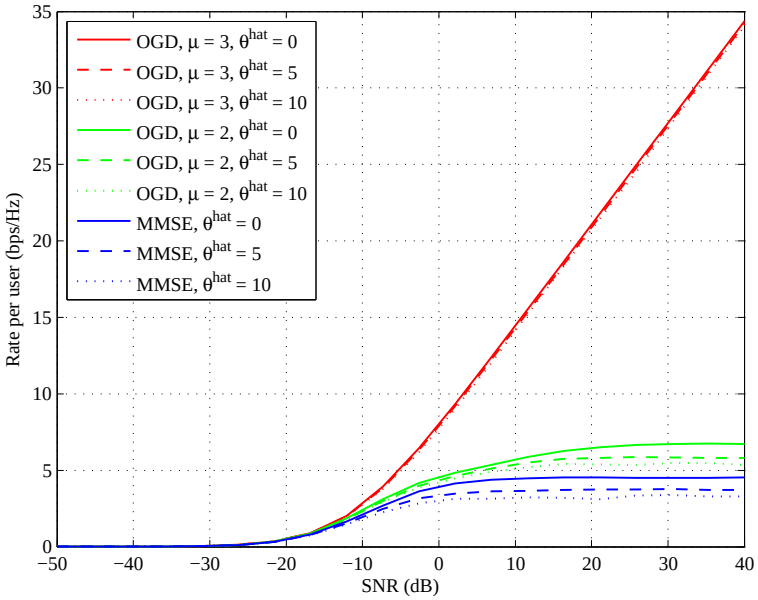

Figure 18. OSGD-$\mu = 2,3$ and MMSE effective rate versus SNR (dB), $\alpha = 1$, $N_t = 6$, $N_r = 6$, $\rho = 0$ and the normalized QoS exponent $\hat{\theta} = 0,5$ and 10.

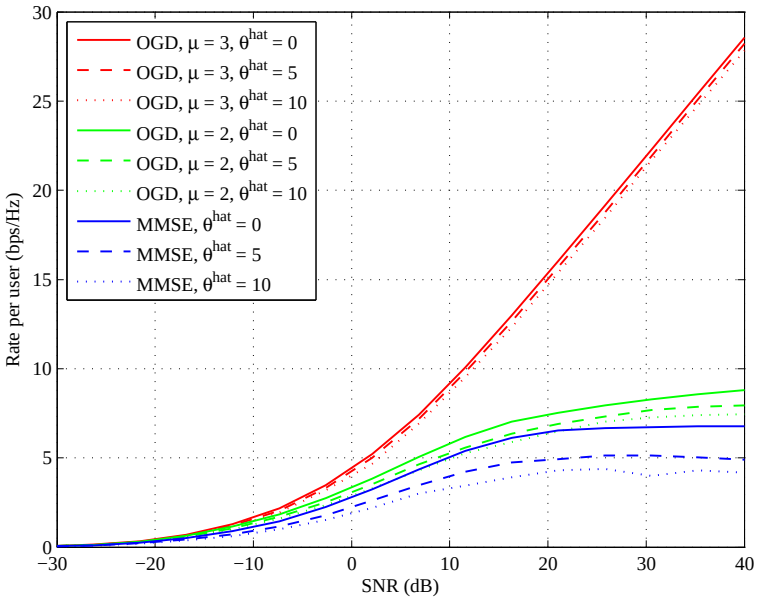

Figure 19. OSGD-$\mu = 2,3$ and MMSE effective rate versus SNR (dB), $\alpha = 1$, $N_t = 6$, $N_r = 6$, $\rho = 0.9$ and the normalized QoS exponent $\hat{\theta} = 0,5$ and 10.

2.5.4 Capacity Upper Bound

In this part, to have a benchmark for our comparison, we contrast the OSGD achieved ergodic capacity per user with the achieved capacity of the single user (i.e., interference-free) $(1 \times 2, 2 \times 2$ and $3 \times 3)$-MIMO uncorrelated channel systems using the equal and adaptive power allocation schemes.

This comparison is carried out for the band-limited and power-limited regimes, i.e., in high and low SNR environments. From the results drawn in figures (20, 21, 22 and 23) which represent the achieved capacity of the three systems, one can see that at very low SNR, OSGD capacity is similar to that for the equal power allocation interference-free system, because in such environment the dominant disturbing factor is the noise not the interference.

However, there is still a gap between the OSGD and the adaptive power allocation scheme which uses the water-filing algorithm to distribute the total power across the antennas. This gap arises because availability of the channel state information at the transmitter (CSIT) for the water-filing scheme helps to allocate the power more intelligently across the paths; while, the OSGD lakes this feature as it is based on a receiver-side processing only, thus, it assumes an equal power allocation in the transmitter side.

More importantly, we ought to remember that the pure (net) throughput of the water-filing scheme is hugely affected by the required feedback. After all, we should also keep in mind that both of the equal and water-filing power allocation systems mentioned here are only a single user systems, i.e., no interference is assumed, and we compare our system, which is working in a strong interference environment, where $\alpha = 1$, with them only because we need to have an upper bound reference for the possible achieved capacity.

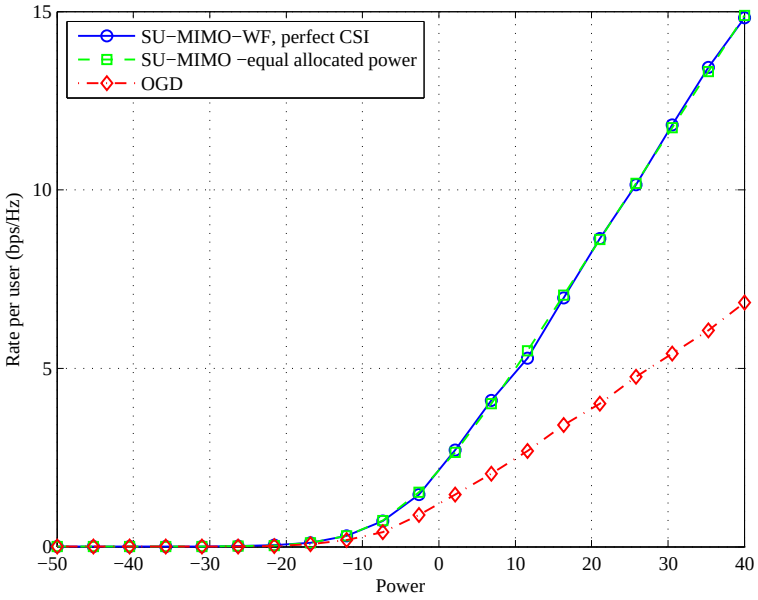

Figure 20. Ergodic rate per user versus SNR (dB) for OSGD, Water filling and Equal power allocation schemes, $N_t = 1, N_r = 2$, and $\alpha = 1$, $\rho = 0$.

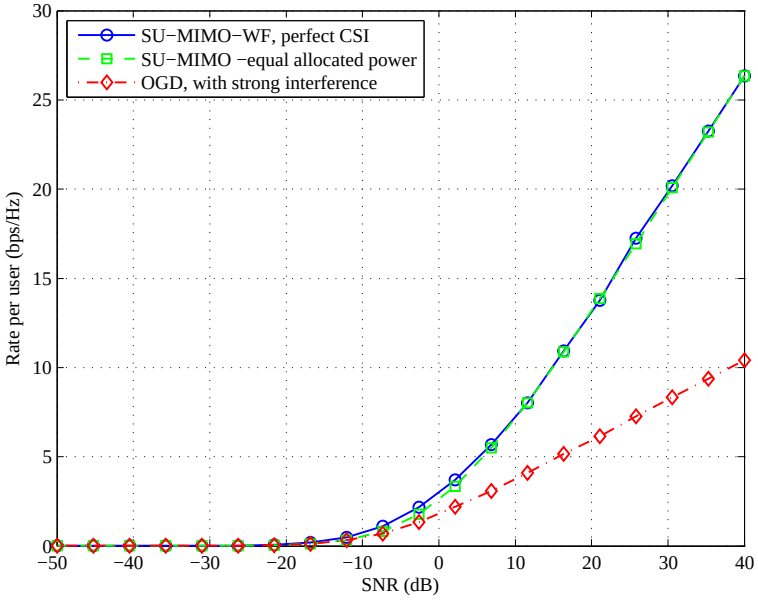

Figure 21. Ergodic rate per user versus SNR (dB) for OSGD, Water filling and Equal power allocation schemes, $N_t = 2, N_r = 2$, and $\alpha = 1$, $\rho = 0$.

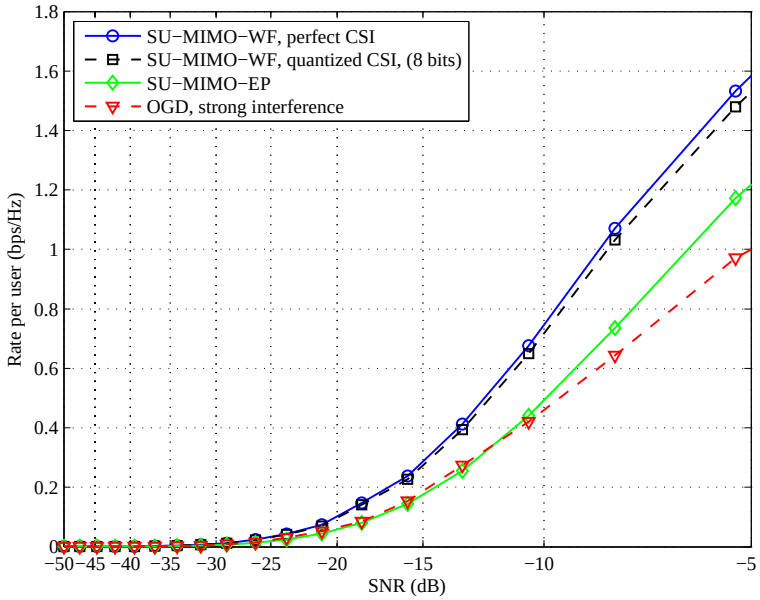

Figure 22. Ergodic rate per user versus SNR (dB) for OSGD, Water filling and Equal power allocation schemes in power-limited regeim, $N_t = 2, N_r = 2$, and $\alpha = 1$, $\rho = 0$.

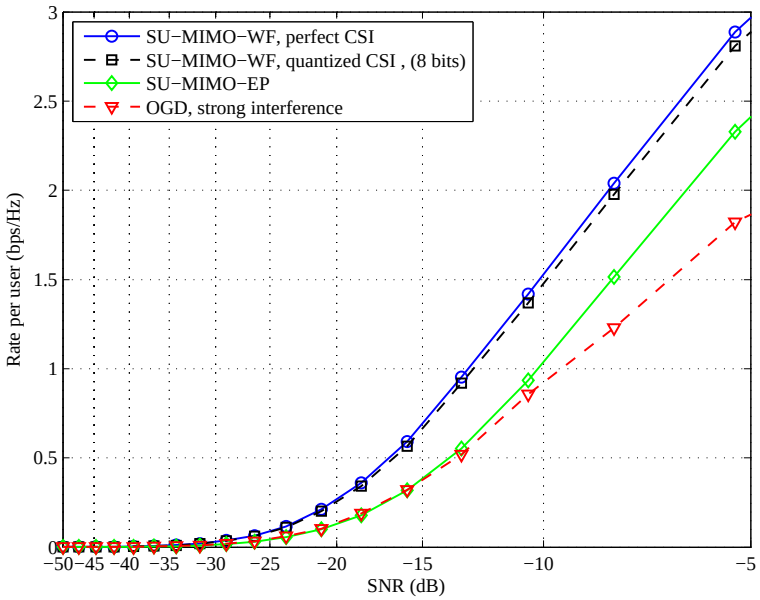

Figure 23. Ergodic rate per user versus SNR (dB) for OSGD, Water filling and Equal power allocation schemes in power-limited regeim, $N_t = 3, N_r = 3$, and $\alpha = 1$, $\rho = 0$.

2.5.5 Effect of the Interference-to-Signal Power Ratio

In this subsection we discuss the effect of changing the cross talk α on the capacity of the OSGD scheme. It is clear that the Interference-to-Signal Power Ratio (ISR) plays a major role in determining the final level of the achieved capacity of any interference channel system, simply because α represents the level of exchanged interference among users. Thus, it is important for our investigation to evaluate the OSGD effectiveness using different values of α. However, to gain deeper insight, we choose to do this task with different SNR levels. In this part, the used interference environment is set up to be (4×4) MIMO fading channel connecting each transmit-receive pair. To avoid any other effects we adjust both of the normalized QoS exponent $\hat{\theta}$ and the antenna inter-element correlation factor ρ to be 0. Figures (24, 25 and 26) present the achieved capacity against a wide decibel range of ISR level for different values of SNR. From the results, it is clear that for high ISR intensities (in the left side of the figures, which represents the scenario of strong interference environment), OSGD with group size $\mu = 3$ outperforms both of the OSGD with $\mu = 2$ and the MMSE receiver. On the other hand, for lower levels of α (on the right side of the figures) there is no difference in the performance of the three schemes; this is simply because in the very low ISR levels OSGD tends to decode its desired user alone, treating the other weak interfering signals as Gaussian noise, i.e., the OSGD converts to MMSE decoder.

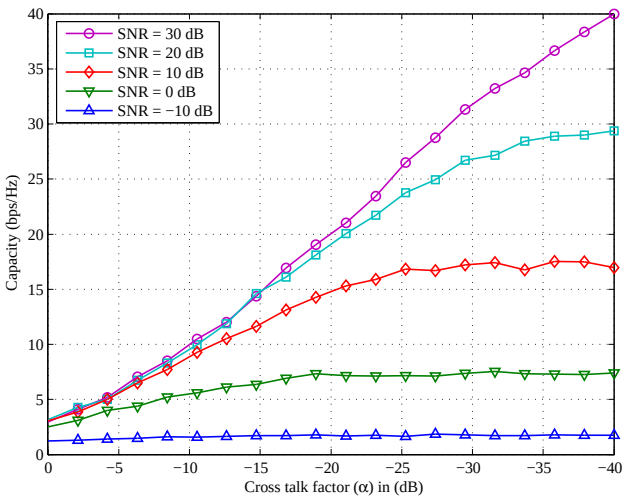

Figure 24. MMSE ergodic capacity versus ISR in different SNR levels, $N_t = 4, N_r = 4$, $\rho = 0$.

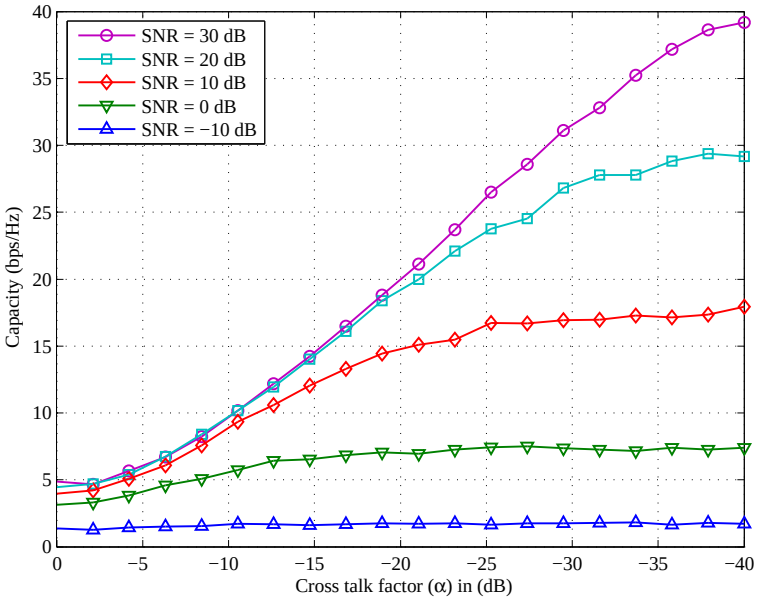

Figure 25. OSGD with $\mu = 2$ ergodic capacity versus ISR in different SNR levels, $N_t = 4, N_r = 4$, $\rho = 0$.

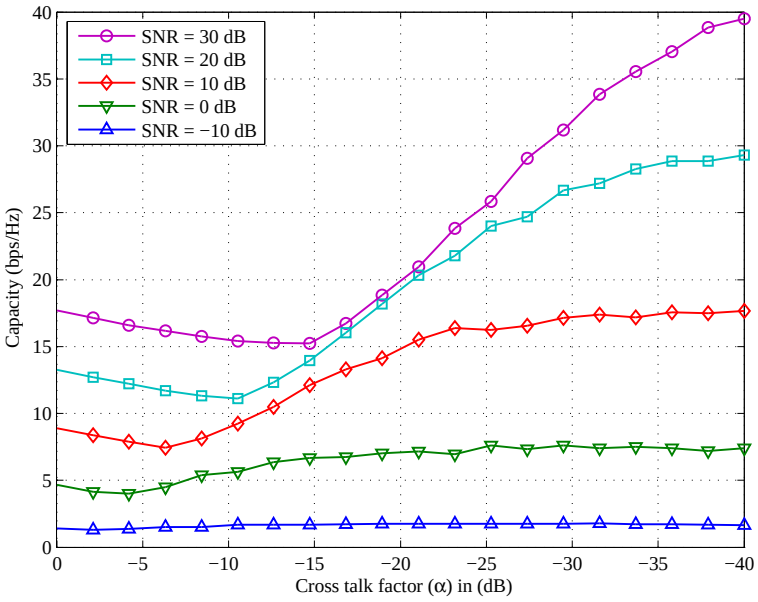

Figure 26. OSGD with $\mu = 3$ ergodic capacity versus ISR in different SNR levels, $N_t = 4, N_r = 4$, $\rho = 0$.

2.5.6 Effect of Number of Antennas

This subsection is focused on the assessment of the effect of number of antennas on the achieved capacity of the different systems. Again, similarly as in the preceding subsection, we set both of $\hat{\theta}$ and ρ to be 0, then, we evaluate the achieved capacity for Signal-User (SU)-MMSE receiver and OSGD with (μ = 2, and 3) against the SNR levels using different sizes of MIMO transmit-receive pairs, the considered MIMO configurations are ($1\times1, 2\times2, 4\times4, 6\times6, 8\times8$ and 10×10). We assume a strong interference environment, where the interference-to-signal ratio $\alpha = 1$. Results of the three systems are shown in figures (27, 28, and 29). From the outcomes, one can see that although the OSGD with group size of 2 is more efficient in exploiting the increase of MIMO antenna size than the MMSE receiver, it is still far away from the efficiency of the OSGD with group size of 3. It is also clear that MMSE is an interference-limited scheme no matter what the MIMO size is. Differently, OSGD with $\mu = 3$ exhibits a noise-limited behavior, revealing its capability to cancel interference completely. In between, we perceive that although OSGD with $\mu = 2$ is not as powerful as the OSGD with $\mu = 3$, but, it succeeds to push its interference-limited behavior to appear at higher SNR levels, demonstrating a moderate interference mitigation capability; yet, it has the complexity reduction advantage over the OSGD with the full group size.

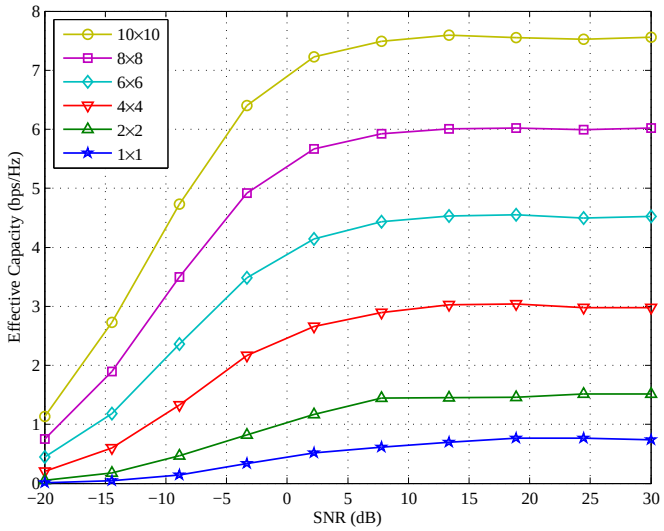

Figure 27. MMSE ergodic capacity versus SNR using different sizes of MIMO configuration, $\rho = 0$ and $\alpha = 1$.

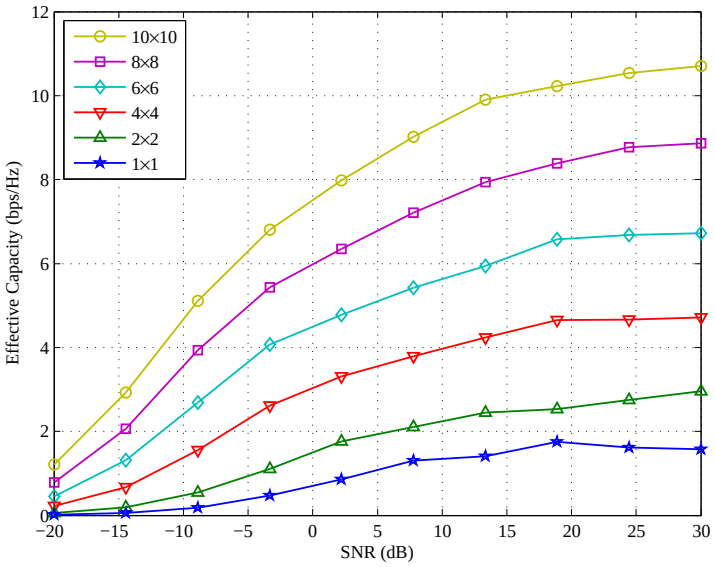

Figure 28. OSGD with $\mu = 2$ ergodic capacity versus SNR using different sizes of MIMO configuration, $\rho = 0$ and $\alpha = 1$.

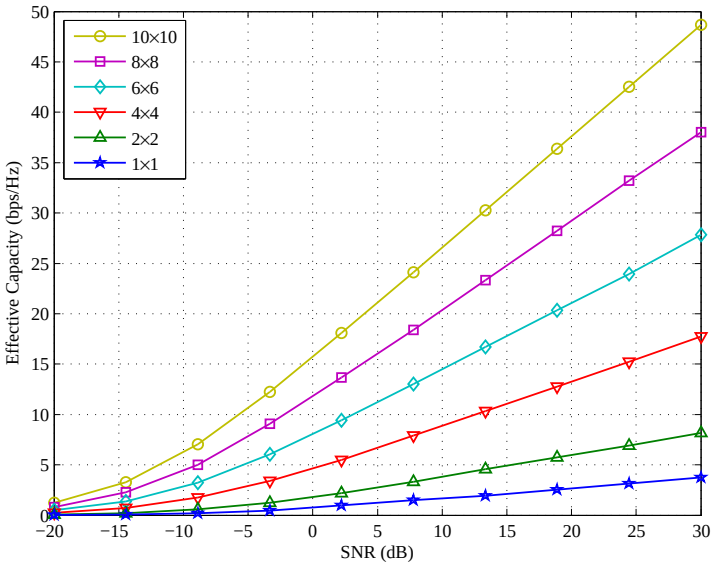

Figure 29. OSGD with $\mu = 3$ ergodic capacity versus SNR using different sizes of MIMO configuration, $\rho = 0$ and $\alpha = 1$.

2.5.7 Effect of Antenna Inter-Element Correlation

In this part, we aim our attention to study the relationship between the antenna inter-element correlation factor ρ and the achieved capacity. In the following scenario, we employ (4×4)-MIMO channel for every transmit-receive pair, with ISR or the cross-talk parameter $\alpha = 1$ and $\hat{\theta} = 0$. From the results in figures (30, 31 and 32), one can notice that for a specific SNR level achieved capacity of OSGD with $\mu = 3$ decreases monotonically with increasing the correlation factor. However, this is not the case for the OSGD with $\mu = 2$ or the MMSE receiver. They exhibit a monotonic decrease of their attained capacity with increasing the correlation factor only at low levels of SNR, but for higher SNR levels, they are interestingly revealing a sudden increase in their capacities in an overshoot-like behavior for short range of correlation values, before they return to steeply decreasing their capacity for higher correlation values. Nevertheless, we can recognize that for all correlation values and SNR combinations the OSGD is the scheme with the highest achieved capacity.

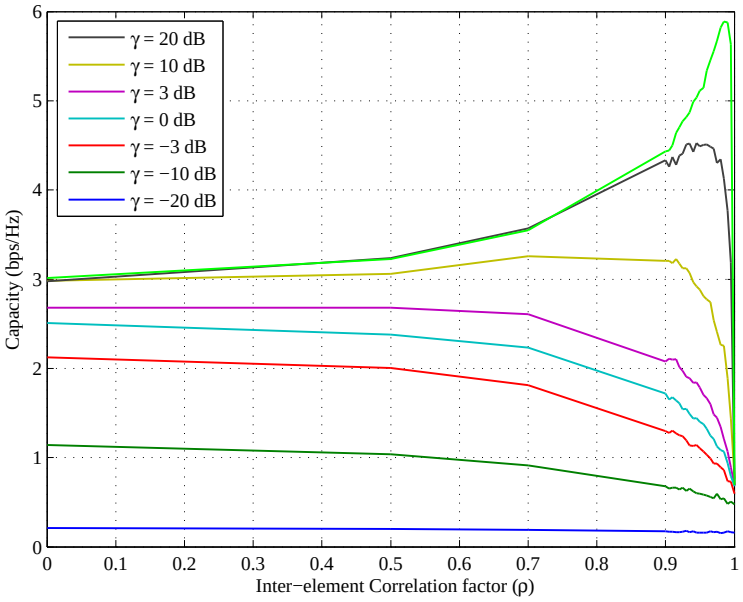

Figure 30. MMSE ergodic capacity versus antenna inter-element correlation factor in different SNR levels, using 4×4 MIMO for each transmit-receive pair.

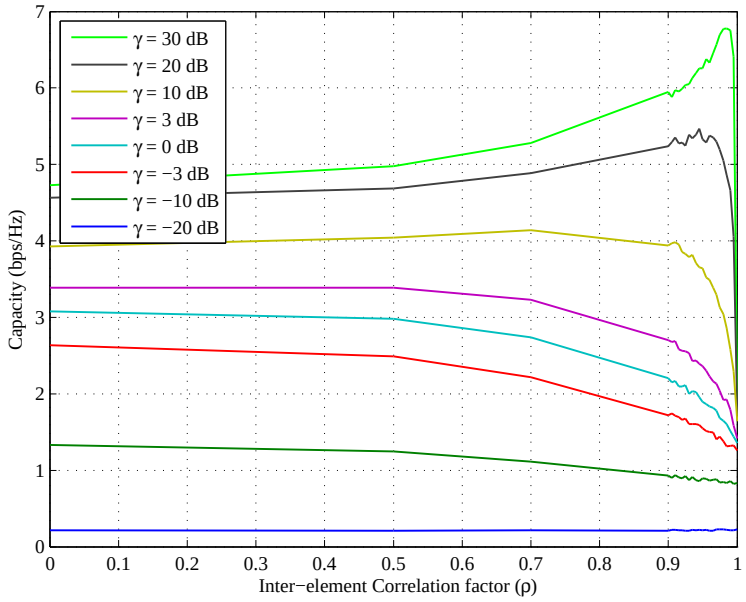

Figure 31. OSGD with $\mu = 2$ ergodic capacity versus antenna inter-element correlation factor in different SNR levels, using 4×4 MIMO for each transmit-receive pair.

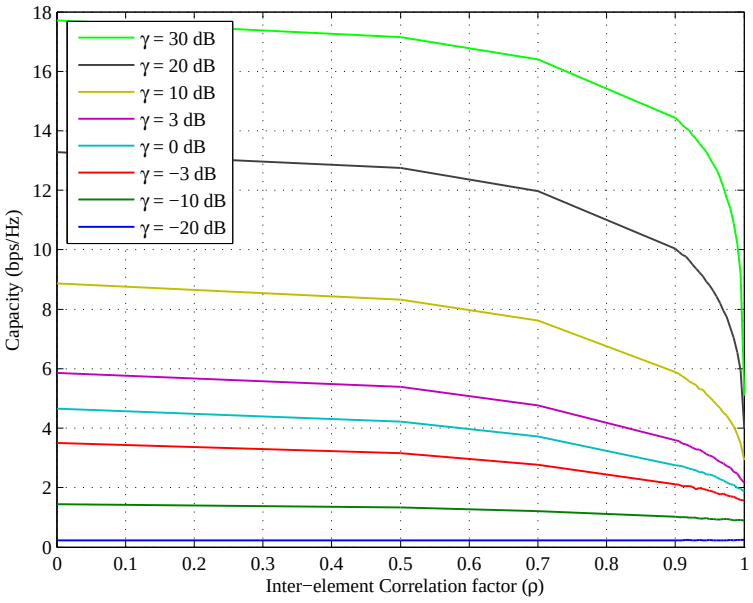

Figure 32. OSGD with $\mu = 3$ ergodic capacity versus antenna inter-element correlation factor in different SNR levels, using 4×4 MIMO for each transmit-receive pair.

2.5.8 Bit Error Rate

This subsection presents the results of BER evaluation for the OSGD scheme in different scenarios, where we conduct this assessment using various SIMO and MIMO configurations, using several correlation factors. In the first scenario, we assume a strong interference environment $\alpha = 1$ with uncorrelated Rayleigh fading, where, single transmit antenna users communicate with their intended receivers which employ OSGD and are equipped in each case with (2, 3, 4, or 5) antennas. The modulation scheme used here is the BPSK, information is decoded and IC process in the receiving side is performed symbol by symbol. The results are depicted in Fig. 33, from which it is obvious that BER is decreasing linearly with the logarithmic scale of $\frac{E_b}{N_0}$. Also, we can readily notice the increase of the diversity gain (which can be inferred from the increase of the absolute slope of the BER curves) by increasing the number of the receive antennas. Now, to get deeper insight on the OSGD efficiency, we choose to compare its performance with the ML-MUD scheme, where all the users are always jointly decoded in the receiver side. Fig. 34 presents the BER performance of the OSGD and ML-MUD in a strong uncorrelated interference environment, but in this case, all of the transmitters and receivers are equipped with multiple antennas. The results displayed in the figure show that at high SNR levels BER performance of the OSGD is slightly deviates from the ML-MUD performance; however, in low SNR levels OSGD exhibits very effective capability to decode its desired users and matches with the ML-MUD scheme. The reason for the slight performance drift is that OSGD tends to be a single decoder at higher SNR levels. On the other hand, Figures (35 and 36) demonstrate the OSGD BER performance for the (4×4 and 5×5) MIMO configuration in a strong interference environment, in this scenario we assume spatial correlation exists between the elements of each antenna. Results in both figures present the BER performance of OSGD and ML-MUD for two different correlation levels, where ($\rho = 0.5$ and 0.9) along with the no correlation case, i.e., $\rho = 0$. All of the presented results clearly prove that BER performance of OSGD is significantly matches the performance of the ML-MUD scheme, especially for the tight specification environments, i.e., for low SNR and higher correlation levels, demonstrating by that the OSGD capability to cope with interference.

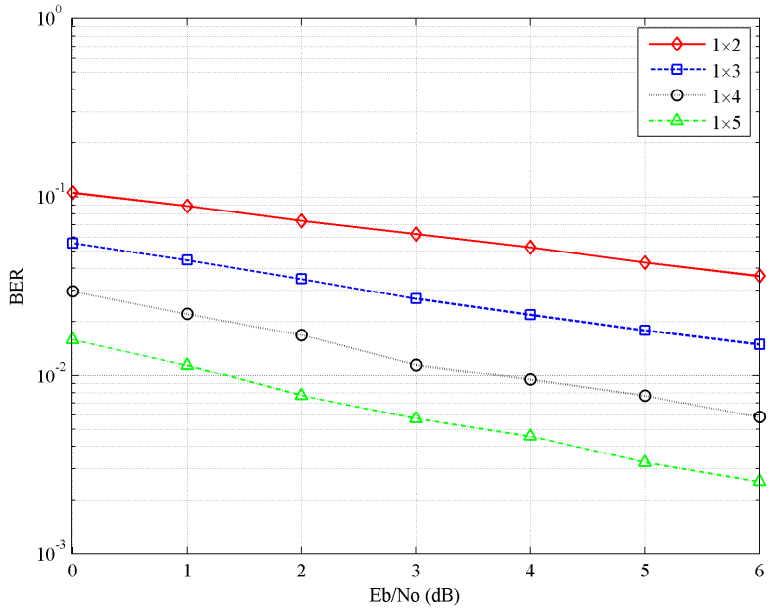

Figure 33. OSGD BER performance versus SNR for $1 \times (2,3,4,5)$ SIMO configurations, with ISR $\alpha = 1$ and receive antenna inter-element correlation $\rho = 0$.

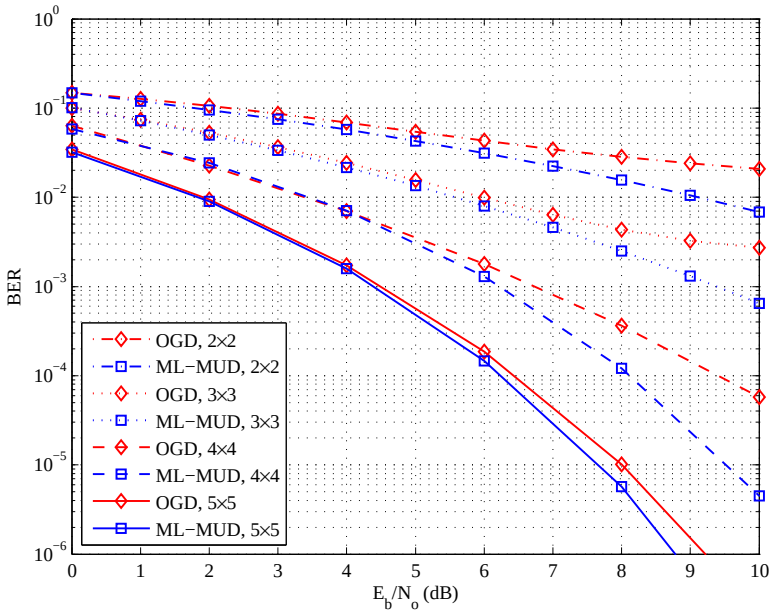

Figure 34. OSGD and ML-MUD BER performance versus SNR for different MIMO configurations, with ISR $\alpha = 1$ and antenna inter-element correlation $\rho = 0$.

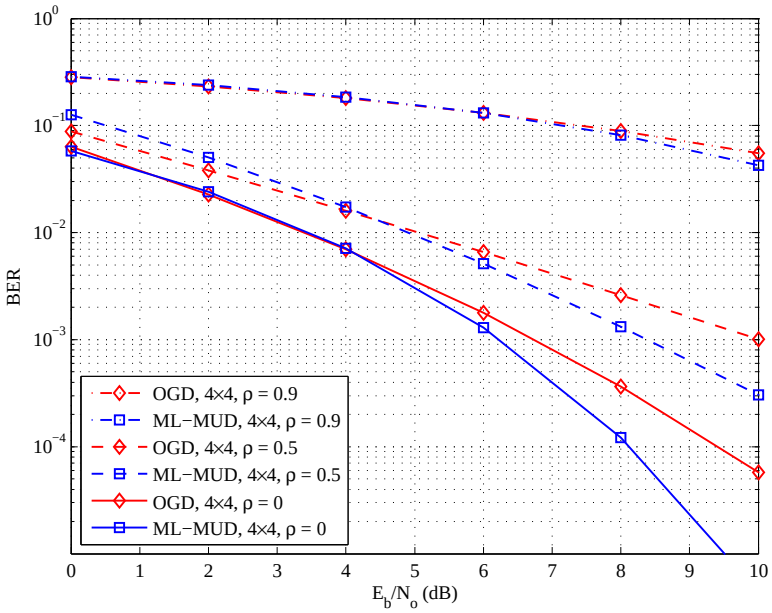

Figure 35. OSGD and ML-MUD BER performance versus SNR for 4×4 MIMO configuration, with ISR $\alpha = 1$ and antenna inter-element correlation $\rho = 0, 0.5$ and 0.9.

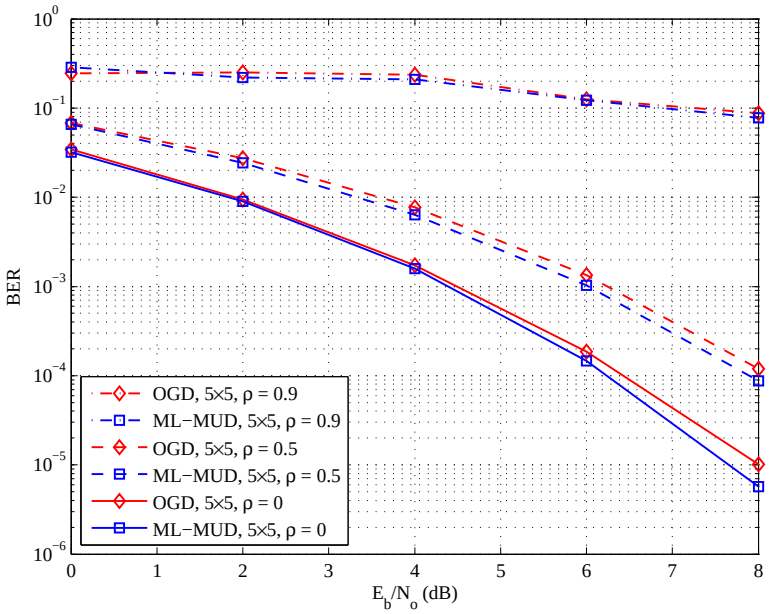

Figure 36. OSGD and ML-MUD BER performance versus SNR for 5×5 MIMO configuration, with ISR $\alpha = 1$ and antenna inter-element correlation $\rho = 0, 0.5$ and 0.9.

2.5.9 Effect of Channel Estimation Error

In this subsection we aim to assess the sensitivity of OSGD system to the channel estimation error. To do so, we evaluate the system BER performance for three CSI error levels (1%, 2% and 5%). The simulation setup of this part considers three different MIMO sizes (3×3, 4×4 and 5×5).

To model the instantaneous estimation error we assume the estimated channel matrix of any user at the receiver of interest is given by

$$\hat{\mathbf{H}} = \mathbf{H} + \mathbf{E}_{ch} \tag{2.9}$$

where $\mathbf{H}$ is the actual normalized channel matrix, and $\mathbf{E}_{ch}$ is the channel estimation error matrix, with $[\mathbf{E}_{ch}]_{i,j} \sim \mathcal{CN}(0, \eta_{ch})$, and η_{ch} is the channel estimation error ratio.

This assessment is carried out for two different scenarios: first, we assume the error occurs in the estimation of all channels, i.e., the desired user channel and the interfering users channels. We represent this case by the solid lines on the figures. In the second case, we presume the error occurs only in the estimation of the interfering users' channels, and this case is represented by the dashed lines on the figures. In both cases we assume a strong interference satiation, where $\alpha = 1$, all the results here carried out for the uncorrelated channel environment. The used modulation scheme is BPSK, and information decoded at the receiver of interest symbol by symbol.

From the results of the first scenario in the figures (37, 38, and 39) one can clearly see that, as the percentage of the error slightly increases, the BER performance largely degrades. Also, we can notice, as the MIMO size increases the effect of the error of CSI estimation relatively increases, see Fig. (40).

Now, to have more comprehensive view, we over plot the results of the first and second scenarios for each MIMO size in figures (41, 42, and 43). From the results, it is obvious that the BER performance of the system in the second scenario is better than that of the first scenario. This is expected because in the second scenario the receiver assumed to estimate its desired user channel perfectly, and the errors only occur in the estimation of undesired users' channels. More importantly, we can notice that, as the MIMO size increases, the effect of undesired users' channels estimation error relatively decreases. This can be readily seen by noticing the

increase of the gap between the BER curves of the first and second scenarios, when the MIMO size increases.

Finally, by observing the results of this section, it is important to notice that, even though increasing the MIMO size makes the system less affected by the interfering users' channel estimation errors; it increases, at the same time, the system sensitivity to the desired user's channel estimation errors.

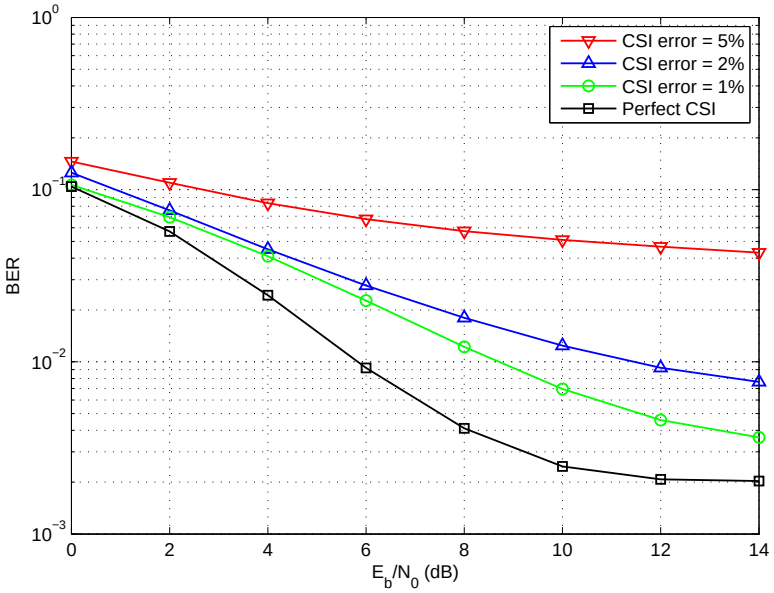

Figure 37. OSGD BER performance versus SNR for the uncorrelated (3×3) MIMO, with ISR $\alpha = 1$, for different estimation errors percentages.

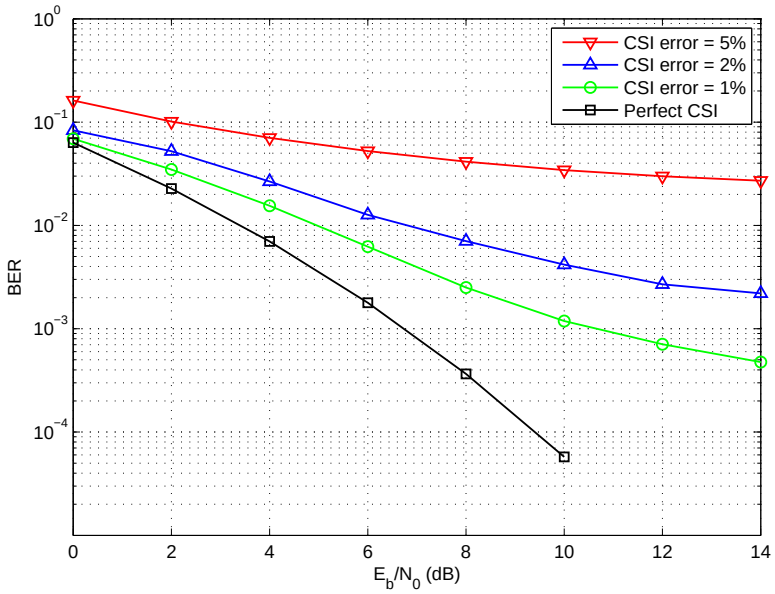

Figure 38. OSGD BER performance versus SNR for the uncorrelated (4×4) MIMO, with ISR $\alpha = 1$, for different estimation errors percentages.

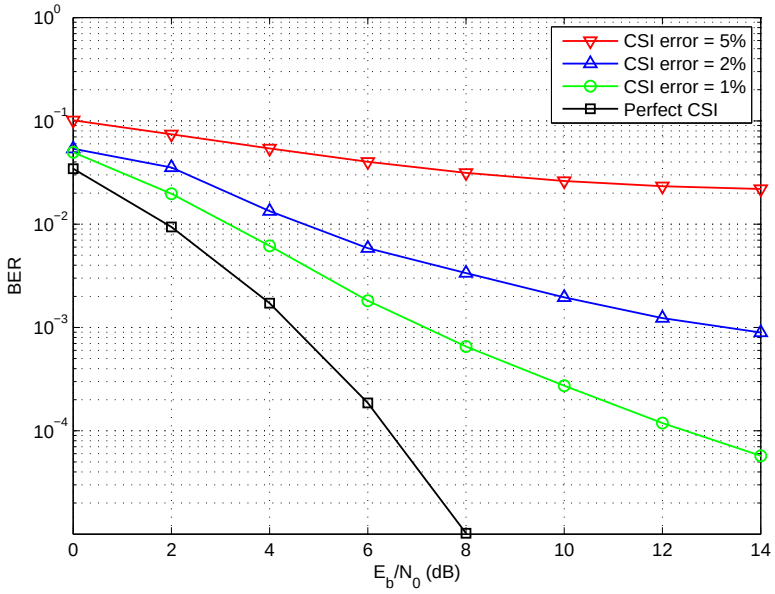

Figure 39. OSGD BER performance versus SNR for the uncorrelated (5×5) MIMO, with ISR $\alpha = 1$, for different estimation errors percentages.

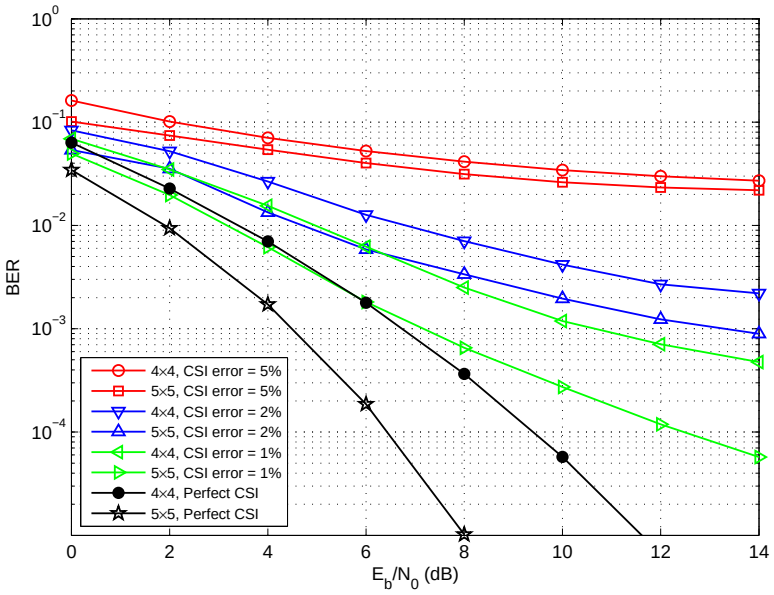

Figure 40. OSGD BER performance versus SNR for the uncorrelated (4×4, 5×5) MIMO, with ISR $\alpha = 1$, for different estimation errors percentages.

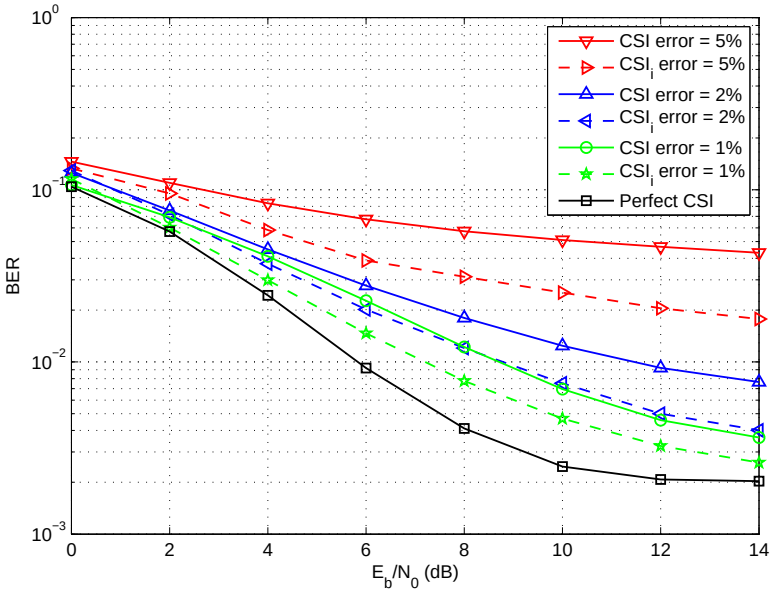

Figure 41. OSGD BER performance versus SNR for the uncorrelated (3×3) MIMO, with ISR $\alpha = 1$, for different estimation errors percentages.

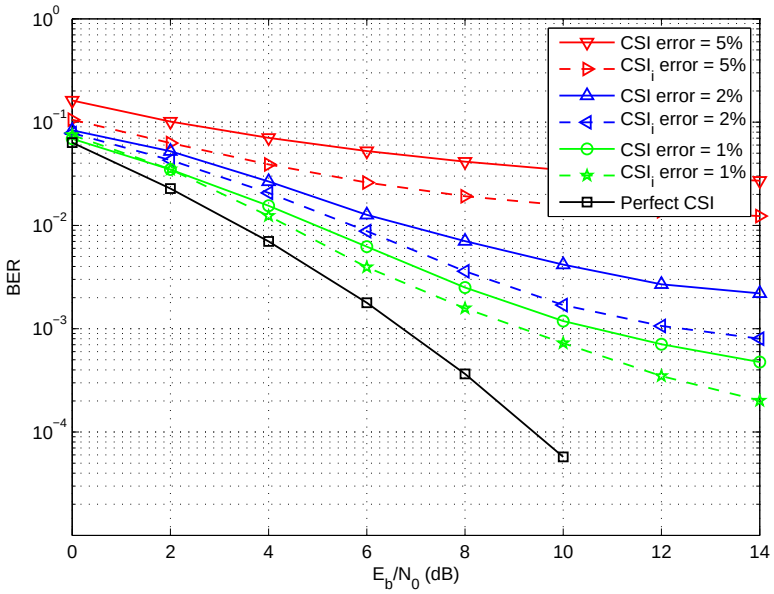

Figure 42. OSGD BER performance versus SNR for the uncorrelated (4×4) MIMO, with ISR $\alpha = 1$, for different estimation errors percentages.

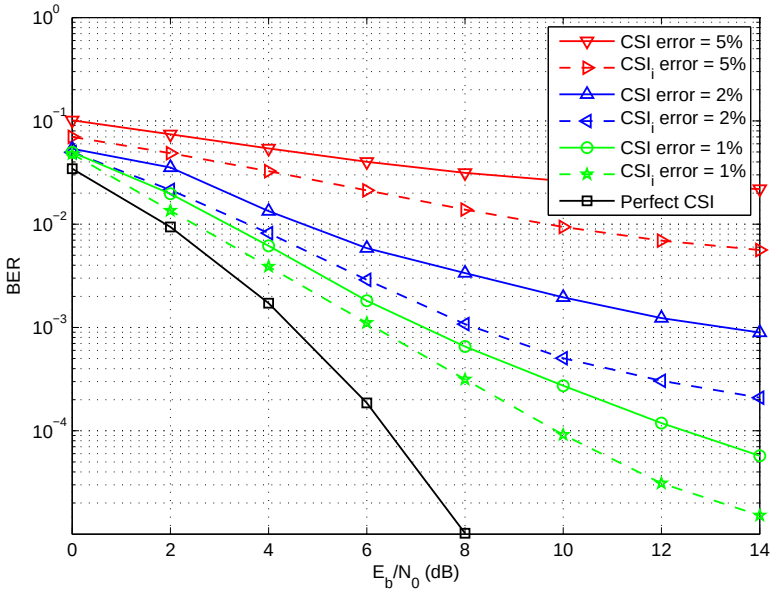

Figure 43. OSGD BER performance versus SNR for the uncorrelated (5×5) MIMO, with ISR $\alpha = 1$, for different estimation errors percentages.

2.5.10 Outage Probability

In this subsection we present the outage probability results of the OSGD scheme for several transmit data target rates, using different MIMO configurations, with various correlation settings, including the (uncorrelated, semi-correlated and fully correlated) scenarios, also for the heterogeneous (Rayleigh and Racian) fading environments. All the results shown in this part are based on a three-user interference system channel, with ISR $\alpha = 1$, where, simulation results of each setup are carried out using 10000 channel realizations.

Results depicted in figures (44, 45 and 46) show the outage probability against the decibel SNR level, using ($2 \times 2, 3 \times 3$ and 4×4) Rayleigh MIMO configuration, for the transmit data target rate of (2, 3, and 4) bps/Hz respectively, in this case we assume no correlation. From the figures we can perceive the increase of the negative slope of the outage probability (which can be appreciated as a diversity gain) as the MIMO size increase. Also, from the multiplexing gain point of view, it can be seen that OSGD efficiently exploits the MIMO dimension to reduce the required power for a specific rate at a predetermined outage level. For instance, at 10^{-3} outage probability for target rate of 4 bps/Hz, the required power is reduced by 10 dB when the 2×2 MIMO is replaced by 3×3 system, further increase of the MIMO dimension to 4×4 yields more 5.5 dB reduction in power to sustain the same data target rate given the aforesaid outage probability. From other point of view, Fig. 47 represents the effect of Rician-Rayleigh channel on the outage probability of the OSGD, for this scenario, we assume that, the channel between the receiver of interest and its desired transmitter is modeled by Rician fading with κ factor equals 10 dB, and the channels between the mentioned receiver and the other two undesired sources are modeled by Rayleigh fading. This assumption is reasonable as indicated in (Siriteanu *et al.* 2013) for indoor and femtocell systems, where the receiver has a direct line of sight component from its intended user and non-line of sight components from the interferers. By comparing the results in Fig. 47 with that in Fig. 46, we do not notice any significant differences in the outage performance, except for the small MIMO dimension, i.e., the (2×2), where we notice less than 1 dB power reduction in the case of existing line of sight (L.O.S.) path between the receiver and its desired transmitter.

Now, to evaluate the effect of the antenna inter-element correlation on the outage probability of the OSGD, we assume that antenna in each end has a strong inter-element correlation $\rho = 0.9$, and we present results of the ($2 \times 2, 3 \times 3$ and

4×4) Rayleigh fading used in this scenario in Fig. 48. Referring again to Fig. 46, to compare its results with those in Fig. 48, one can clearly see that antenna inter-element correlation significantly affects the outage probability of the system. Also, it can be noticed that, the bigger the MIMO dimension the stronger the effect is. In addition, by contrasting the same two figures once more, we notice that, when the correlation exists, it pushes up the required power to achieve certain outage percentage comparing with the no correlation case, say for example, $P_{out} = 10^{-3}$, then, existing of correlation raises the required power by (6, 7 and 7.5) dB, for the ($2 \times 2, 3 \times 3$ and 4×4) MIMO configuration respectively. Finally, to show the effect of antenna inter-element correlation more comprehensively, we choose to look over this effect on the system from different point of views. Thus, we evaluate the outage probability in four different cases: (i) - Non-correlation case, (ii) - Strong spatial correlation between the elements of the receive antenna, and no correlation in the transmit side, (iii)- Strong spatial correlation between the elements of the transmit antenna, and no correlation in the receive side, (iv)- Strong spatial correlation between the elements of each antenna in the transmit and receive sides. This comparison is carried out for two different MIMO dimensions, 2×2 with data target rate of 4 bps/Hz and 8×8 with data target rate of 16 bps/Hz. The results of these cases are shown in figures (49 and 50). From the depicted results, we can observe that, as expected, the best performance is encountered in the non-correlation case, and the worst case is when each antenna in both sides has an inter-element spatial correlation, i.e., the fully correlated case. However, interestingly, although we assume the same correlation intensity for the case (ii) and (iii) which represent the semi-correlation cases, we notice that, performance in case (ii), i.e., when the receive side antenna elements are correlated, exhibits better performance comparing with case (iii), i.e., when the transmit side antenna elements are correlated. This may reflect the ability of OSGD to overcome correlation to improve the system performance as it is a receive-side processing technique.

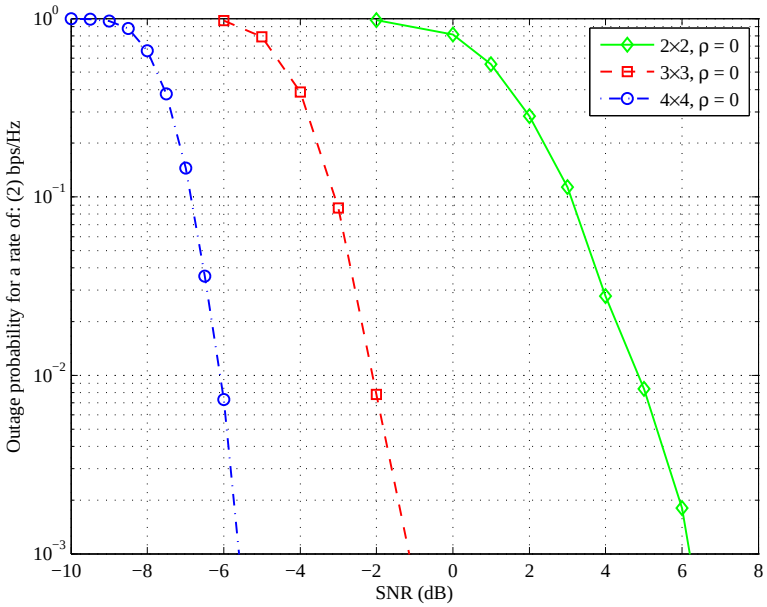

Figure 44. OSGD outage probability performance versus SNR, using rate of 2 bps/Hz, for different MIMO configurations, with ISR $\alpha = 1$ and antenna inter-element correlation $\rho = 0$.

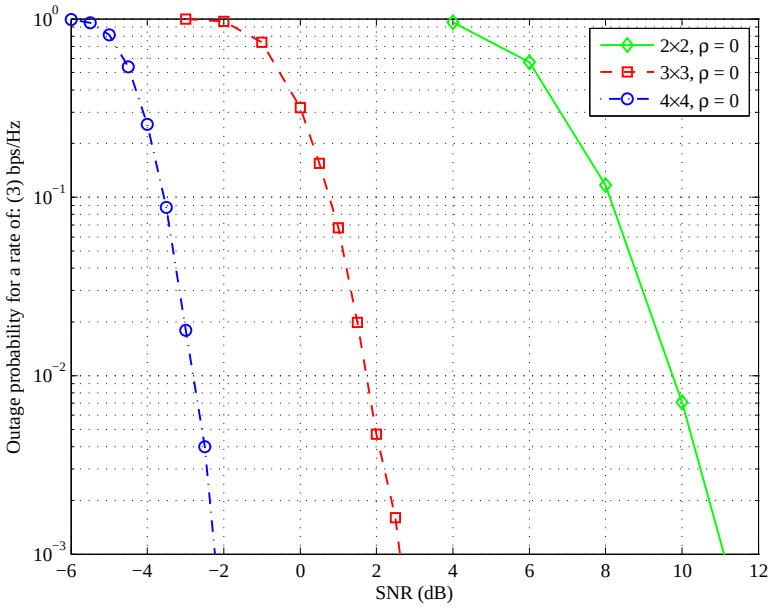

Figure 45. OSGD outage probability performance versus SNR, using rate of 3 bps/Hz, for different MIMO configurations, with ISR $\alpha = 1$ and antenna inter-element correlation $\rho = 0$.

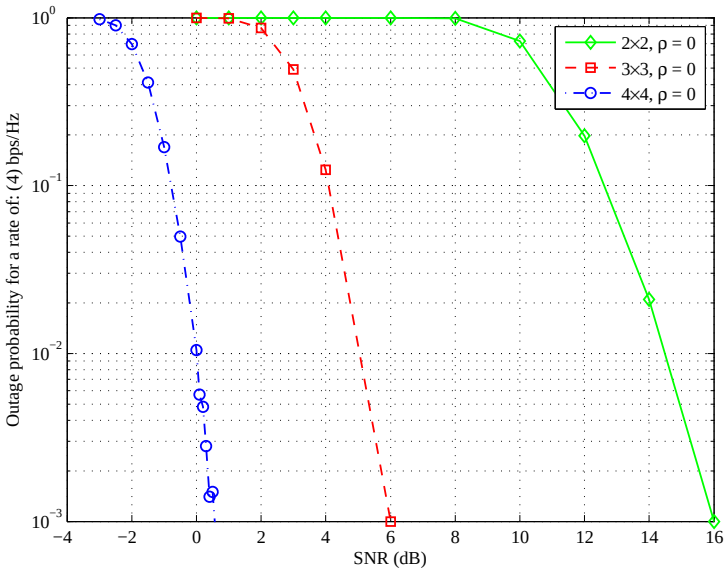

Figure 46. OSGD outage probability performance versus SNR, using rate of 4 bps/Hz, for different MIMO configurations, with ISR $\alpha = 1$ and antenna inter-element correlation $\rho = 0$.

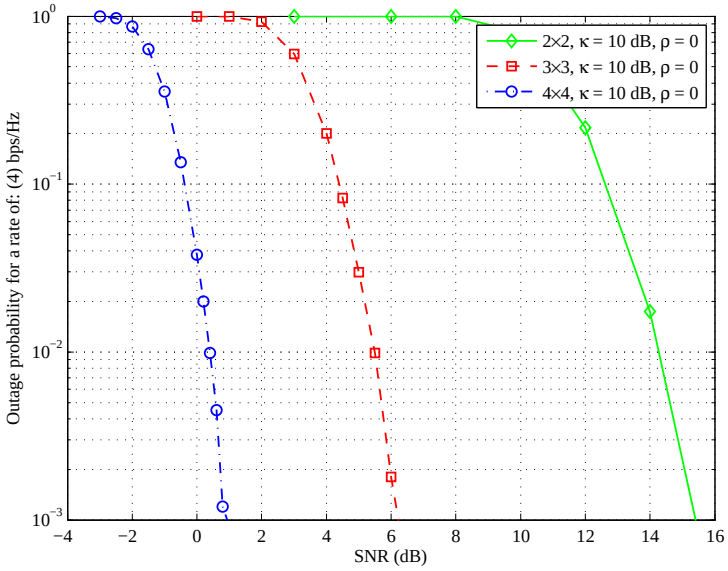

Figure 47. OSGD outage probability performance versus SNR, using rate of 4 bps/Hz, for different MIMO configurations, with ISR $\alpha = 1$, antenna inter-element correlation $\rho = 0$, for the Racian-Rayleigh fading scenario with $\kappa -$ factor $= 10$ dB.

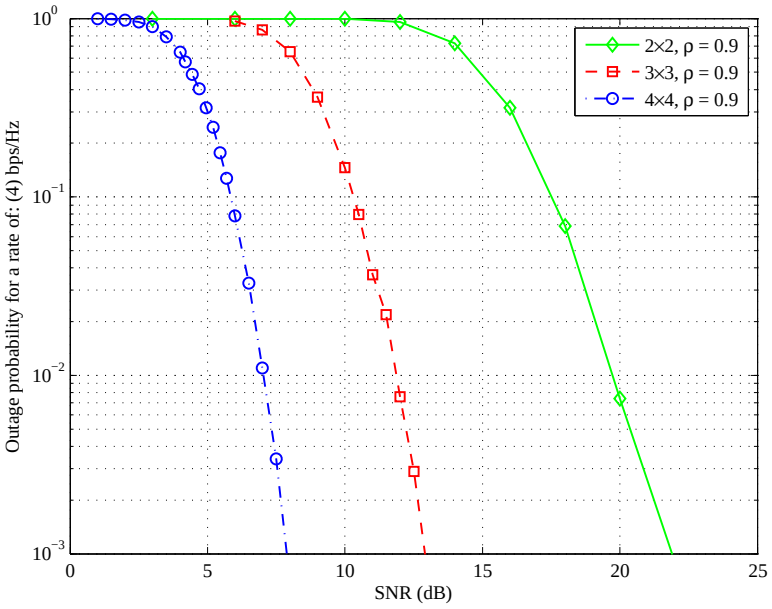

Figure 48. OSGD outage probability performance versus SNR, using rate of 4 bps/Hz, for different MIMO configurations, with ISR $\alpha = 1$ and antenna inter-element correlation $\rho = 0.9$.

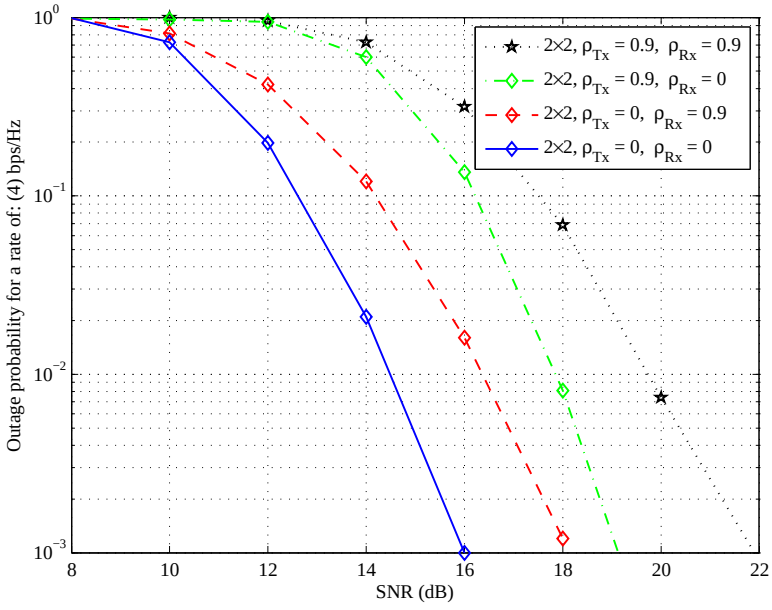

Figure 49. OSGD outage probability performance versus SNR, using rate of 4 bps/Hz, for 2×2 MIMO configuration, with ISR $\alpha = 1$ and different antenna inter-element correlation $\rho = 0$ and 0.9.

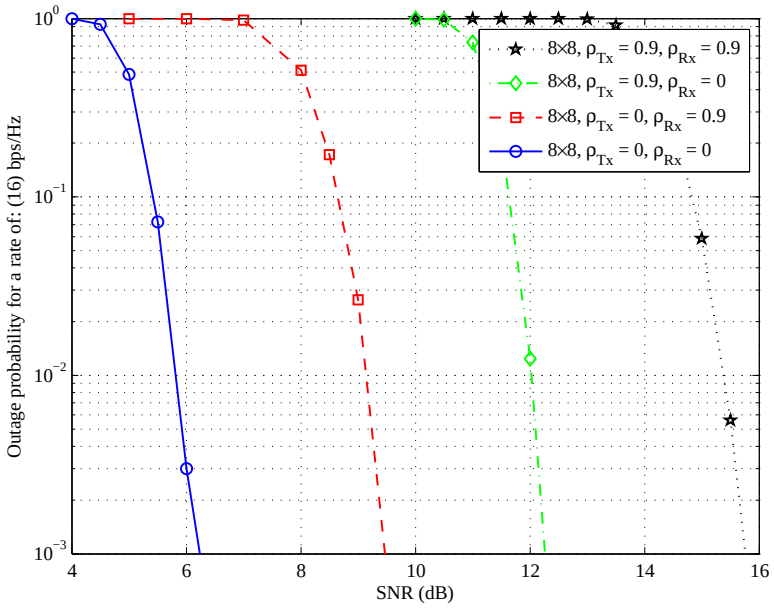

Figure 50. OSGD outage probability performance versus SNR, using rate of 16 bps/Hz, for 8×8 MIMO configuration, with ISR $\alpha = 1$ and different antenna inter-element correlation $\rho = 0$ and 0.9.

2.6 Summary

To summarize our contribution in this chapter, we say that we explored the OSGD in the interference channel environment. In addition, we extensively investigated its performance based on different criteria, among which, achieved ergodic, outage and effective capacity. Also, we evaluated its minimum required energy per bit; we also assessed its BER performance, and outage probability, under different QoS constraints. For generality purposes, this study considered the spatially correlated and uncorrelated (Rayleigh and Rician) fading channels. Moreover, it investigated performance of the OSGD in different SNR and SIR environments, where we considered both the power-limited and bandwidth-limited regimes with different ISR values, as well as it considered various transmit-receive multiple-input multiple-output antenna configurations. To make our results more sensible, we contrasted the outcomes of the aforementioned performance assessment with the results of other well-known interference mitigation approaches, such as, the ML-MUD scheme and the MIL interference alignment technique. Finally, considering the findings of this chapter, which demonstrate effectiveness of the OSGD to mitigate interference; also, because being the OSGD a receiver-based processing

scheme, thus, it does avoid the huge feedback overhead; and beside of its ability to adjust the computational complexity to fit with the processing capability of the employed receivers as a result of its built-in complexity controlling feature; we conclude that OSGD can be a promising candidate for the detection strategy in the interference channel systems.

3 INTERFERENCE MITIGATION USING CONSTRAINED PARTIAL GROUP DECODING

3.1 Introduction

This chapter assesses the performance of the constrained partial group decoding (CPGD) technique in interference channel (IC) environment which we investigated in (Abu-Ella & Elmusrati 2014c). Therefore, the main contribution of this part is to demonstrate the CPGD capability to manage and mitigate interference comparing with other interference mitigation schemes based on interference alignment strategy, such as, Mean Square Error (MSE)-based transceiver proposed in (Shen *et al.* 2010), in addition to other interference alignment techniques including Signal-to-Interference plus Noise Power Ratio Maximization (SINR-MAX) and Interference-to-Noise Power Ratio Minimization (INR-MIN) which are presented in (Lee & Choi 2010) through the MIMO interference channel.

The remainder of this chapter is organized as follows. The Model of MIMO interference channel is described in Section 3.2. Description for the CPGD basic concepts is given in Section 3.3. Brief review for the three addressed interference alignment techniques presented in Section 3.4. Numerical results for achieved capacity and evaluation of BER performance are presented in Section 3.5. Finally, Section 3.6 concludes this chapter.

3.2 System Model

In this chapter, we assume a K-user MIMO interference channel model, where the received signal at the kth user in this system can be expressed by

$$\begin{aligned} \mathbf{y}_k &= \sum_{i=1}^{K} \mathbf{H}_{ki}\mathbf{x}_i + \mathbf{z}_k = \sum_{i=1}^{K} \mathbf{H}_{ki}\mathbf{V}_i\mathbf{d}_i + \mathbf{z}_k \\ &= \mathbf{H}_{kk}\mathbf{V}_k\mathbf{d}_k + \sum_{i\neq k} \mathbf{H}_{ki}\mathbf{V}_i\mathbf{d}_i + \mathbf{z}_k \quad k \in 1,\cdots,K \end{aligned} \tag{3.1}$$

where $\mathbf{y}_k$ is the $N_{rk} \times 1$ received vector at user k, $\mathbf{z}_k \sim \mathcal{CN}(0, \sigma^2\mathbf{I})$ is the $N_{rk} \times 1$ complex additive white Gaussian noise (AWGN) vector at user k,$\mathbf{V}_k$ is the $N_{tk} \times S_k$ precoding matrix at transmitter k, $\mathbf{H}_{ki}$ is the $N_{rk} \times N_{ti}$ channel matrix between transmitter i and receiver k, coefficients of $\mathbf{H}_{ki}$ are independent and identically

distributed (i.i.d.) complex Gaussian random variable with zero mean and unit variance. $\mathbf{x}_i$ is $N_{ti} \times 1$ transmitted vector of the ith transmitter, $\mathbf{d}_k$ is an $S_k \times 1$ vector indicates the data streams from the kth transmitter. Each transmitter i is subject to an average transmit power constraint, given by $\mathbb{E}[\|\mathbf{x}_i\|^2] \leq P_i$.

Assuming that each user deploys a linear receiver, then, estimated data streams at kth receiver are given by

$$\hat{\mathbf{d}}_k = \mathbf{W}_k \mathbf{y}_k = \mathbf{W}_k \sum_{i=1}^{K} \mathbf{H}_{ki} \mathbf{V}_i \mathbf{d}_i + \mathbf{W}_k \mathbf{z}_k \quad k \in 1, \cdots, K \tag{3.2}$$

where $\mathbf{W}_k$ is an $S_k \times N_{rk}$ receiving filter for the kth user.

3.3 Constraint Partial Group Decoding (CPGD)

As described in (Chen *et al.* 2012; Gong, Tajer & Wang 2011), in this scheme each receiver uses a partial group decoder with constrained group size μ to decode its desired message along with a part of the interference. In this chapter we restricted the group size μ to be less than the total number of users K. CPGD technique decreases the complexities of obtaining the best ordered decodable set; also it limits the amount of exchanged information between the users in the system. The CPGD is constructed of two fundamental procedures, which are: Algorithm I in Table 4 make it possible for each receiver to identify its best partition in a distributed way by performing some local processing without any information exchange among different users; and Algorithm II in Table 5 obtains globally optimal rate increment r^* which gives the smallest rate increment that all users suggest.

Now, considering any two disjoint partitions $\mathcal{A}$ and $\mathcal{B}$ of set $\mathcal{M}$, we define $\mathcal{C}_k(\mathcal{A},\mathcal{B})$ as the capacity limit region of the kth receiver, when it jointly decodes the users in $\mathcal{A}$ and treats the users in $\mathcal{B}$ as an AWGN, where the users in $\{\mathcal{M}\backslash(\mathcal{A}\cup\mathcal{B})\}$ are assumed to be already decoded and subtracted in previous stages. Assuming that $\mathbf{H}_{ki}$ represents the channel between the ith transmitter and the kth receiver, then, the rate region $\mathcal{C}_k(\mathcal{A},\mathcal{B})$ can be expressed as

$$\mathcal{C}_k(\mathcal{A},\mathcal{B}) = \left\{ \boldsymbol{R} \in \mathbb{R}_+^{|\mathcal{A}|} : \sum_{i\in\mathcal{D}} R_i \leq \boldsymbol{\mathcal{R}}_k(\mathcal{D},\mathcal{B}), \forall \mathcal{D} \subseteq \mathcal{A} \right\} \tag{3.3}$$

Using the random unitary beamforming vector $\mathbf{v}_i$ at the transmitter i, the rate

$\boldsymbol{\mathcal{R}}_k(\mathcal{D},\mathcal{B})$ is given by

$$\boldsymbol{\mathcal{R}}_k(\mathcal{D},\mathcal{B}) = \log_2\left(1+\gamma_{gap}\frac{\|\mathbf{H}_{k,i\in\mathcal{D}}\mathbf{v}_{i\in\mathcal{D}}\|^2}{\sigma^2+\|\mathbf{H}_{k,i\in\mathcal{B}}\mathbf{v}_{i\in\mathcal{B}}\|^2}\right) \tag{3.4}$$

where γ_{gap} represents the gap between the capacity limit using Gaussian modulation with the infinite-length random codes and the achievable capacity using practical modulation scheme with finite-length codes.

Considering the valid partition $\mathcal{Q}^k = \{\mathcal{G}_1^k,\ldots,\mathcal{G}_{p_k}^k,\mathcal{G}_{p_k+1}^k\}$ of $\mathcal{M}$. Then, we can assume that all users on of this partition can be decoded by the kth receiver if

$$\boldsymbol{R}_{G_m^k} \in \mathcal{C}_k(\mathcal{G}_m^k, \cup_{i=m+1}^{p_k+1}\mathcal{G}_i^k), \forall m \in \{1,\ldots,p_k\} \tag{3.5}$$

For the valid partition $\mathcal{Q}^k$ of the receiver k we define $\mathbf{r}_{G_m^k}^k = [r_i^k]_{i\in\mathcal{G}_m^k}$, Then, the fair rate increment which grantee that all users in $\{\mathcal{G}_1^k,\ldots,\mathcal{G}_{p_k}^k\}$ are decodable at the receiver k is defined by

$$r_k(\mathcal{Q}^k) \triangleq \max r_i^k, \forall i \in \mathcal{M} \tag{3.6}$$

such that

$$\widetilde{\boldsymbol{R}}_{\mathcal{G}_{m^k}} = \boldsymbol{R}_{\mathcal{G}_{m^k}} + \mathbf{r}_{\mathcal{G}_{m^k}}^k \in \mathcal{C}_k(\mathcal{G}_m^k, \cup_{i=m+1}^{p_k+1}\mathcal{G}_i^k), \forall m \in \{1,\ldots,p_k\}, \tag{3.7}$$

Under the fairness (equal rate increment) constraint, and assuming that $\underline{\boldsymbol{\mathcal{Q}}}^k$ ensembles all the valid partitions $\mathcal{Q}^k$, then, at the receiver k the maximum user rate increment is given by

$$r_k^* \triangleq \max_{\mathcal{Q}^k\in\underline{\boldsymbol{\mathcal{Q}}}^k} r_k(\mathcal{Q}^k). \tag{3.8}$$

We can notice that solving (3.8) using the exhaustive search considering all combinations of $\mathcal{Q}^k$ is prohibitively complex. However, by defining the following metric for any two arbitrary disjoint sets $\mathcal{D},\mathcal{B}\subseteq\mathcal{M}$,

$$\triangle_k(\mathcal{D},\mathcal{B}) \triangleq \mathcal{R}_k(\mathcal{D},\mathcal{B}) - \sum_{i\in\mathcal{D}} R_i, \tag{3.9}$$

Authors in (Gong, Tajer & Wang 2011) proposed Algorithm I employed by the receiver k to solve (3.8) and avoid the prohibitive complexity of the exhaustive

search method. This algorithm has two outputs which are: the optimal ordered valid partition $\mathcal{Q}^k_{opt}$ and its optimal rate increment.

It is important to mention that Algorithm I is structured to build the optimal ordered partition $\mathcal{Q}^k_{opt} = \{\mathcal{G}^k_1, \ldots, \mathcal{G}^k_{p_k}, \mathcal{G}^k_{p_k+1}\}$ in a reverse manner, i.e., in the first stage it finds $\mathcal{G}^i_{p_k+1}$ that consists of the indices of the users which will not decoded at the receiver k, and it proceeds in the procedure until it finds the $\mathcal{G}^k_1$ which contains the indices of the users which tolerate the lowest rate increment.

On, the other hand, decoding process starts with decoding users in set $\mathcal{G}^k_1$, when that is done, then, among the remaining users, the set of indices in $\mathcal{G}^k_2$ become the users who will tolerate the least rate increment, this procedure continues until the receiver k decodes the last set of decodable users $\mathcal{G}^k_{p_k}$ which of course contains its desired user.

Now, we can express the fundamental property of Algorithm I as the follows:

Over all possible valid partitions $\underline{\boldsymbol{\mathcal{Q}}}^k$, Algorithm I finds the optimal ordered partition which maximizes $r_k(\mathcal{Q}^k)$, and determines r^*_k , i.e.,

$$\mathcal{Q}^k_{opt} = \{\mathcal{G}^k_1, \ldots, \mathcal{G}^k_{p_k+1}\}$$
$$\arg \max_{\mathcal{Q}^k \in \underline{\boldsymbol{\mathcal{Q}}}^k} r_k(\mathcal{Q}^k)$$

and

$$r^*_k = \max_{\mathcal{Q}^k \in \underline{\boldsymbol{\mathcal{Q}}}^k} r_k(\mathcal{Q}^k)$$

As stated before, the main idea of the CPGD technique is that each receiver in the system locally employs Algorithm I to find its best ordered partition, without any information exchange with other receivers. However, interestingly, the system total sum rate can be optimized through limited feedback between users, by sending scalar value r^*_k obtained by Algorithm I and represent the maximum tolerable rate increment for the receiver k to all other users. Then, the optimal global rate increment can be computed by Algorithm II, this global rate increment is simply the smallest suggested rate increment by all users (Gong, Tajer & Wang 2011).

Table 4. Algorithm I: The Optimal Valid Partition for the Receiver k

1. Initialize $\mathcal{D} = \mathcal{K}$, $\mathcal{G} = \phi$, $p_k = 0$ and $l = 1$
2. repeat
3. Find $\delta_l = \min_{\mathcal{W} \neq \phi, \mathcal{W} \subseteq \mathcal{D}, \lvert\mathcal{W}\rvert \leq \mu} \frac{\Delta_k(\mathcal{W},\mathcal{G})}{\lvert\mathcal{W}\rvert}$
4. Find $\mathcal{G}_l^k = \arg\min_{\mathcal{W} \neq \phi, \mathcal{W} \subseteq \mathcal{D}, \lvert\mathcal{W}\rvert \leq \mu} \frac{\Delta_k(\mathcal{W},\mathcal{G})}{\lvert\mathcal{W}\rvert}$
5. $\mathcal{D} \leftarrow \mathcal{D} \setminus \mathcal{G}_l^k$ and $\mathcal{G} \leftarrow \mathcal{G} \cup \mathcal{G}_l^k$
6. $r_i^k = \delta_l$ for all $i \in \mathcal{G}_l^k$, $p_k \leftarrow p_k + 1$
7. $l \leftarrow l + 1$
8. Until $\mathcal{D} = \phi$
9. Set $\mathcal{Q}_m^k \leftarrow \mathcal{G}_{l-m}^k$ for $1 \leq m \leq p_k$,
and $\mathcal{Q}_{p_{k+1}}^k \leftarrow \cup_{m > p_k} \mathcal{G}_{l-m}^k$
10. Output the rate $\{r_i^k\}$ for $i \in \mathcal{K}$
and the partitions $\mathcal{Q}^k = \{\mathcal{G}_1^k, \cdots, \mathcal{G}_{p_k}^k, \mathcal{G}_{p_{k+1}}^k\}$

Table 5. Algorithm II: Rate Allocation

1. Input $\mathbf{R} = [R_i]_{i \in \mathcal{K}}$
2. for $i = 1, \cdots, K$ do
3. Run Algorithm I to determine $\{r_i^k\}$ for $i \in \mathcal{K}$ and $\mathcal{Q}^k$
4. end for
5. Obtain $r^* = \min_k r_k^*$ where $r_k^* = \max_{i \in \mathcal{K}} r_i^k$
6. Update $\tilde{\mathbf{R}}_i \leftarrow \mathbf{R}_i + r^*$
7. Output $\tilde{\mathbf{R}} = [\tilde{\mathbf{R}}_{i \in \mathcal{K}}]$ and the partitions $\{\mathcal{Q}^1, \cdots, \mathcal{Q}^K\}$.

3.4 Interference Mitigation Techniques Based on Interference Alignment

To assess the interference mitigation capability of the constrained partial group decoding (CPGD) scheme we compare its performance with the different interference alignment-based techniques. This section dedicated to give a brief illustration for the main idea of these interference alignment algorithms.

3.4.1 SUM-MSE Minimization

The objective of this scheme as proposed in (Shen *et al.* 2010) is to jointly design a set of transmit precoding and receiving filter matrices $(\mathbf{V}_k, \mathbf{W}_k), k = 1, \cdots, K$ to minimize the total MSE, i.e., Minimization of the Total Sum of the Mean Square Errors (SUM-MSE-MIN) under the individual transmit power constraints. The

MSE for the kth user is defined as

$$\begin{aligned}\varepsilon_k &= \mathbb{E}[\|\hat{\mathbf{d}}_k - \mathbf{d}_k\|^2] \\ &= \mathbb{E}\left\{tr\left[(\hat{\mathbf{d}}_k - \mathbf{d}_k)(\hat{\mathbf{d}}_k - \mathbf{d}_k)^{\mathcal{H}}\right]\right\} \qquad (3.10)\end{aligned}$$

assuming that

$$\mathbb{E}[\mathbf{d}_i\mathbf{d}_k^{\mathcal{H}}] = \mathbf{0}, \mathbb{E}[\mathbf{d}_i\mathbf{z}_k^{\mathcal{H}}] = \mathbf{0}, \forall\, i \neq k, \mathbb{E}[\mathbf{d}_i\mathbf{d}_i^{\mathcal{H}}] = \mathbf{I}$$

The total MSE can be expressed as

$$\sum_{k=1}^{K}\varepsilon_k = tr\{\sum_{k=1}^{K}\mathbf{W}_k(\sum_{i=1}^{K}\mathbf{H}_{ki}\mathbf{V}_i\mathbf{V}_i^{\mathcal{H}})\mathbf{H}_i^{\mathcal{H}}\mathbf{W}_k^{\mathcal{H}} + K\mathbf{I} \qquad (3.11)$$

$$- \sum_{k=1}^{K}(\mathbf{W}_k\mathbf{H}_{kk}\mathbf{V}_k + \mathbf{V}_k^{\mathcal{H}}\mathbf{H}_{kk}^{\mathcal{H}}\mathbf{W}_k^{\mathcal{H}}) + \sigma^2\sum_{k=1}^{K}\mathbf{W}_k\mathbf{W}_k^{\mathcal{H}}\} \qquad (3.12)$$

The optimization problem is to minimize MSE

$$\min_{\{\mathbf{V}_k;\mathbf{W}_k\}}\sum_{k=1}^{K}\varepsilon_k \qquad (3.13)$$

s.t. $tr(\mathbf{V}_k^{\mathcal{H}}\mathbf{V}_k) \leq P_k \quad \forall k \in \{1,\cdots,K\}$. Therefore, the optimal receive filter for user k is given by

$$\mathbf{W}_k = \Big(\sum_{i=1}^{K}\mathbf{H}_{ki}\mathbf{V}_i\mathbf{V}_i^{\mathcal{H}}\mathbf{H}_{ki}^{\mathcal{H}})^{-1}\mathbf{H}_{kk}\mathbf{V}_k \qquad (3.14)$$

Optimizing the beamforers, subject to the transmit power constraint, gives

$$\mathbf{V}_k = \Big(\sum_{i=1}^{K}\mathbf{H}_{ik}^{\mathcal{H}}\mathbf{W}_i\mathbf{W}_i^{\mathcal{H}}\mathbf{H}_{ik} + \lambda_k\mathbf{I})^{-1}\mathbf{H}_{kk}^{\mathcal{H}}\mathbf{W}_k \qquad (3.15)$$

Now, Lagrange multiplier $\lambda_k \geq 0$ is chosen to make $\|\mathbf{V}_k\|_2^2 \leq 1$. Since $\|\mathbf{V}_k\|^2$ is a convex and decreasing function of λ_k, thus, there exists a unique solution, that can be obtained by an iterative numerical method such as, Newton iteration.

3.4.2 INR Minimization

The basic idea of this scheme as presented in (Lee & Choi 2010) is to design a postprocessing vector to minimize the Interference-to-Noise Power Ratio (INR) at each receiver. Assuming that for the ith transmitter, there is a unitary random beamforming vector $\mathbf{v}_i$ satisfies the constraint $\|\mathbf{v}_i\|^2 = 1$. Then, the received signal obtained after applying the postprocessing vector $\mathbf{w}_k \in \mathbb{C}^{N_{rk}\times 1}$, is given by

$$\mathbf{w}_k^{\mathcal{H}}\mathbf{y}_k = \mathbf{w}_k^{\mathcal{H}}\mathbf{H}_{kk}\mathbf{v}_k x_k + \sqrt{\alpha}\sum_{i=1,i\neq k}^{K}\mathbf{w}_k^{\mathcal{H}}\mathbf{H}_{ki}\mathbf{v}_i x_i + \mathbf{w}_k^{\mathcal{H}}\mathbf{z}_k \tag{3.16}$$

where α is the relative propagation path-loss of the interference channels. Therefore, the average received interference power from each interfering transmitter becomes $P_I = \alpha P_D$. In other words, α is given by

$$\begin{aligned}\alpha &= \frac{P_I}{P_D} \\ &= \frac{INR}{SNR}\end{aligned} \tag{3.17}$$

Therefore, α could be used to represent the ISR. Then the kth-user post-processing vector to minimize INR is given by

$$\begin{aligned}\mathbf{w}_k^{INR} &= \arg\min_{\mathbf{v}\in\mathbb{C}^{N_{rk}\times 1}} P_I\sum_{i\neq k}^{K}|\mathbf{w}^{\mathcal{H}}\mathbf{H}_{ki}\mathbf{v}_i|^2 \\ &= W_{min}(\mathbf{B}_k)\end{aligned} \tag{3.18}$$

where $\mathbf{B}_k$ is given by

$$\mathbf{B}_k = \sum_{i=1,i\neq k}^{K}\mathbf{H}_{ki}\mathbf{v}_i\mathbf{v}_i^{\mathcal{H}}\mathbf{H}_{ki}^{\mathcal{H}} \tag{3.19}$$

and $W_{min}(\mathbf{B}_k)$ is the eigenvector of matrix $(\mathbf{B}_k)$ corresponding to the minimum eigenvalue $\lambda_{min}(\mathbf{B}_k)$.

3.4.3 SINR Maximization

As explained in (Lee & Choi 2010) the aim of this scheme is to design a post-processing vector to maximize the Signal-to-Interference plus Noise Power Ratio (SINR) at each receiver.

The post-processing vector which maximizes the kth-user SINR is given by

$$\mathbf{w}_k^{SINR} = \arg \max_{\mathbf{w} \in \mathbb{C}^{N_{r_k} \times 1}} \frac{P_D |\mathbf{w}^{\mathcal{H}} \mathbf{H}_{ki} \mathbf{v}_k|^2}{1 + \sum_{i \neq k}^{K} P_I |\mathbf{w}^{\mathcal{H}} \mathbf{H}_{ki} \mathbf{v}_i|^2} = W_{max}(\mathbf{C}_k^{-1} \mathbf{D}_k) \tag{3.20}$$

where $W_{max}(\cdot)$ is the eigenvector of matrix $(\cdot)$ corresponding to the maximum eigenvalue $\lambda_{max}(\cdot)$.

$$\mathbf{C}_k = \mathbf{I} + P_I \cdot \mathbf{B}_k \tag{3.21}$$

$$\mathbf{D}_k = P_D \cdot \mathbf{H}_{ki} \mathbf{v}_i \mathbf{v}_i^{\mathcal{H}} \mathbf{H}_{ki}^{\mathcal{H}} \tag{3.22}$$

3.5 Simulation Results

For the sake of clarity, we divide the numerical results of this chapter into two parts: the first part discusses results of the achieved capacity for the four investigated schemes. The second part demonstrates bit error rate (BER) performance evaluation of those techniques.

3.5.1 Achieved Capacity

In this part using simulation results we compare achieved capacity of CPGD, SINR-MAX, INR-MIN and MSE-based schemes. For all systems the number of users K is set to be 3, where each transmitter and receiver is equipped with two antennas. We assume the channel between any transit-receive pair to be a Rayleigh fading channel and is obtained by generating independent and identically distributed (i.i.d.) complex Gaussian random variables with zero mean and unit variance. The constraint of the group size of jointly decoded users μ for the CPGD scheme is fixed to be 2. The interference-to-signal ratio α is adjusted to simulate the moderate and the strong interference environments, thus it is set to be 0.7 and 1.0. Results of this part are depicted in Fig. 51 and Fig. 52 respectively.

From results shown in Fig. 51 which represents a moderate interference environment scenario, one can perceive that for low and moderate SNR levels (i.e., for $SNR < 10$ dB) CPGD achieves the highest capacity. On the other hand, for higher

SNR levels, MSE-based scheme achieves slightly higher capacity than that for CPGD. However, although MSE-based scheme is slightly outperforms CPGD, we should keep in mind that it is built based on an iteratively converging algorithm boosting much higher computational complexity comparing with CPGD. Moreover, MSE-based scheme requires huge feedback to optimize its filters which may significantly reduce the net throughput of the system. From other point of view, Fig. 52 which represents stronger interference environment scenario, where signal-to-interference ratio equals -3 dB. It is obvious that CPGD significantly achieves higher capacity than the SINR-MAX and INR-MIN for all SNR levels. On the other hand, when $SNR > 14$ dB MSE-based starts to achieve slightly higher capacity than CPGD. Here, by contrasting results in Fig. 51 and Fig. 52, we can see the shift from 10 dB to 14 dB that needed for the MSE-based scheme to overcome the CPGD. This implies the ability of CPGD to manage and mitigate interference; especially, in the tight specifications scenario, i.e., in strong interference and low SNR environment.

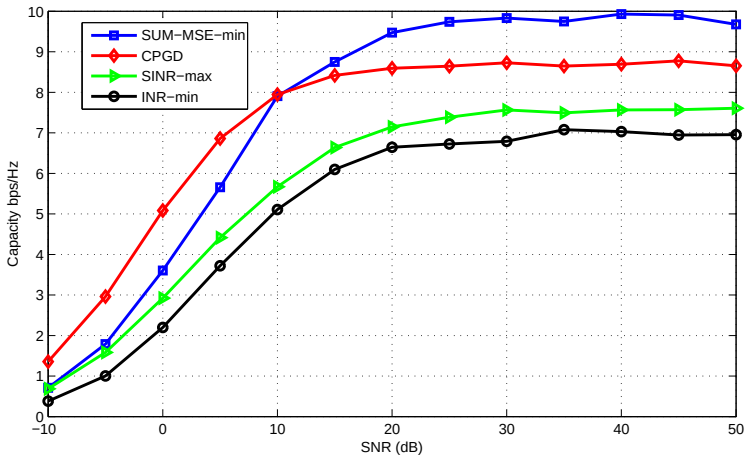

Figure 51. Achieved capacity for the CPGD, SUM-MSE minimization, SINR maximization and INR minimization schemes, for $\alpha = 0.7$.

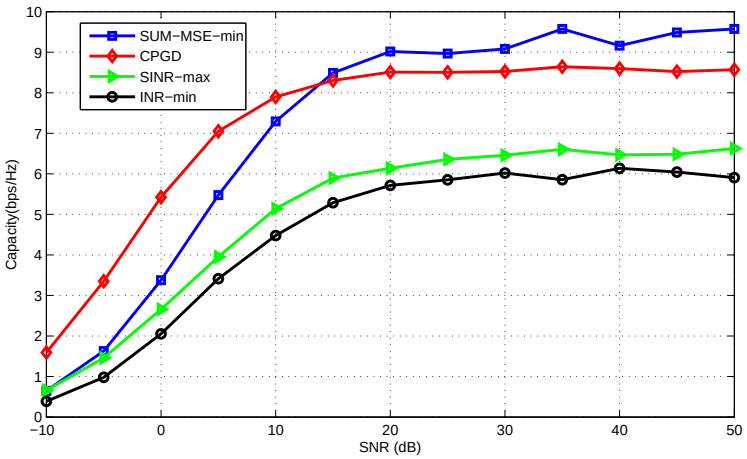

Figure 52. Achieved capacity for the CPGD, SUM-MSE minimization, SINR maximization and INR minimization schemes, for $\alpha = 1.0$.

3.5.2 Bit Error Rate Performance

In this subsection, we evaluate the bit error rate performance of the four addressed schemes. Simulation is conducted for the 3-user MIMO interference channel system, with the same setup in the previous part. However, in this Subsection, all transmitters employ a quadrature phase shift keying (QPSK) modulation, along with Low Density Parity Check (LDPC) code with coding rate $1/2$, using block length of 5400, 64800 bits. The decoding is performed in block-wise manner, after-which the interference cancellation process is taking place. The decoding interference cancellation (IC) in block basis gives a better performance, comparing with the symbol by symbol based IC. However, on the other hand it increases the decoding complexity and the system latency, especially for the very long sequences.

We used two different code-lengths to investigate the effect of the code-length on the system performance. The produced results of this setup are depicted in Fig. 53, and Fig. 54 respectively, the CPGD group size μ is set to be 2.

Fig. 53 shows BER performance of the CPGD, MSE-based, INR-MIN and SINR-MAX schemes, versus average energy per bit to noise power spectral density ratio E_b/N_0, using LDPC code of 5400-bits long. We notice that both of MSE-based

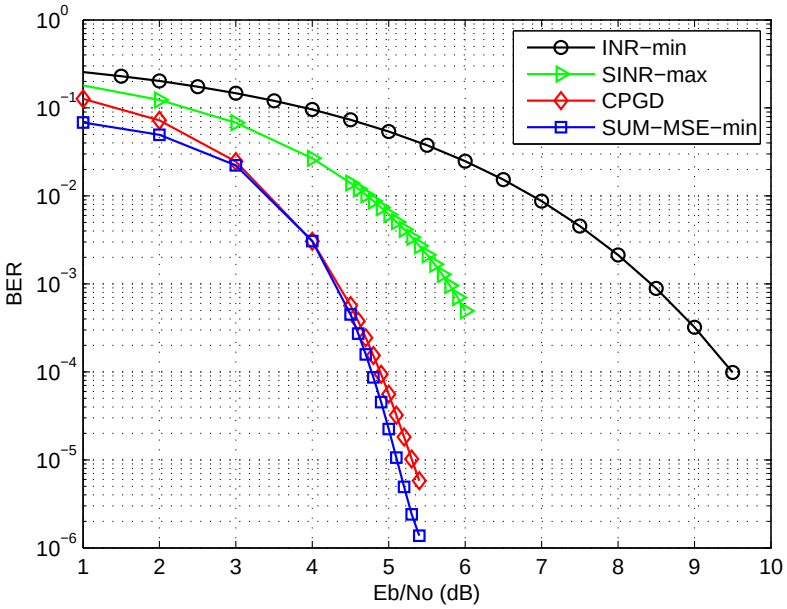

Figure 53. The BER performance of various interference mitigation techniques, using QPSK modulation and LDPC code with block length of 5400 bits and coding rate $1/2$ is used.

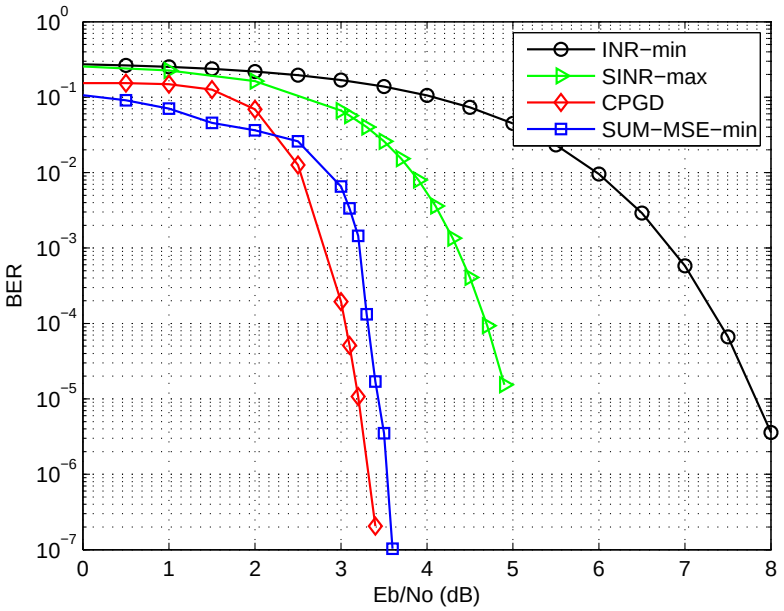

Figure 54. The BER performance of various interference mitigation techniques, using QPSK modulation and LDPC coding with block length of 64800 bits and coding rate $1/2$ is used.

and CPGD almost have identical BER performance and they are significantly outperforming the other two schemes. Similarly, Fig. 54 shows the BER performance of the four schemes against E_b/N_0 but using longer LDPC codes, i.e., with codelength $n = 64800$ bits, which gives as expected better performance. From the figure it is clear that CPGD scheme outperforms all other schemes. The longer code enhances the interference cancellation capability of CPGD, therefore, it overcome all the other schemes even the MSE-based interference alignment scheme. For instance, at BER of 10^{-6}, CPGD has 0.2 dB power gain comparing to MSE-based scheme. Also, CPGD significantly surpasses both of SINR-MAX and INR-MIN. For instance, at BER of 10^{-4}, CPGD has 1.6 dB and 4.4 dB power gain comparing with the SINR-MAX and INR-MIN respectively.

3.6 Summary

In this chapter we have investigated performance of CPGD comparing to three different interference alignment schemes to assess its efficiency to mitigate interference in the MIMO interference channel. Simulation results have shown that for the MIMO interference system, CPGD technique achieved the highest capacity in the tight specification environment, i.e., when the system works in strong interference and low SNR conditions. Furthermore, the evaluation of the bit error rate performance of the four investigated schemes reflected the effectiveness of CPGD technique which considerably outperformed the SINR-MAX, INR-MIN schemes, and it also was shown that using a long-enough LDPC code CPGD outperformed the SUM-MSE-MIN scheme which is feedback-based technique. Therefore, we may conclude this chapter by saying that CPGD can be competitively a promising technique with controlled complexity to mitigate interference in the next generation networks.

4 INTERFERENCE MITIGATION VIA CONSTRAINED PARTIAL GROUP DECODING FOR UPLINK MULTICELL MIMO SYSTEMS

4.1 Introduction

In this chapter, we present the performance of constrained partial group decoding (CPGD) technique which we investigated in (Abu-Ella & Wang 2013a) to assess its capability to manage and mitigate interference in uplink multicell MIMO system. Numerical results show that the CPGD technique exhibits very competitive performance comparing with conventional multiple access Frequency Division Multiple Access (FDMA) and Time Division Multiple Access (TDMA) schemes which are associated with minimum mean square error (MMSE) filtering in terms of achieved per-cell capacity and bit error rate (BER).

The remainder of this chapter is organized as follows. The particular model of MIMO interference channel used in this chapter is described in Section 4.2. Multicell processing and uplink channel model is introduced in Section 4.3. Numerical results for achieved capacity and evaluation of BER performance are presented in Section 4.4. Finally, Section 4.5 summarizes findings of this chapter.

4.2 MIMO Interference Channel Model

The received signal at the kth user through this K-user MIMO interference channel system can be expressed by

$$\begin{aligned} \mathbf{y}_k &= \sum_{i=1}^{K} \mathbf{H}_{ki}\mathbf{x}_i + \mathbf{n}_k \\ &= \mathbf{H}_{kk}\mathbf{V}_k\mathbf{d}_k + \sum_{i\neq k} \mathbf{H}_{ki}\mathbf{V}_i\mathbf{d}_i + \mathbf{n}_k \quad k \in 1,\cdots,K \end{aligned} \tag{4.1}$$

where $\mathbf{y}_k$ is the $N_{rk}\times 1$ received vector at user k, $\mathbf{n}_k \sim \mathcal{CN}(0,\sigma_n^2\mathbf{I})$ is the $N_{rk}\times 1$ complex additive white Gaussian noise (AWGN) vector at user k, $\mathbf{V}_k$ is the $N_{tk}\times S_k$ precoding matrix at transmitter k, $\mathbf{H}_{ki}$ is the $N_{rk}\times N_{ti}$ channel matrix between transmitter i and receiver k, coefficients of $\mathbf{H}_{ki}$ are independent and identically distributed (i.i.d.) complex Gaussian random variable with zero mean and unit variance. $\mathbf{x}_i$ is $N_{ti}\times 1$ transmitted vector from the ith transmitter, $\mathbf{d}_k$ is an $S_k\times 1$

vector indicates the data streams from the kth transmitter. Each transmitter i is subject to an average transmit power constraint, given by $\mathbb{E}[\|\mathbf{x}_i\|^2] \leq P_i$. Assuming that each user applies the linear receiver, then, estimated data streams at kth receiver are given by

$$\begin{aligned} \hat{\mathbf{d}_k} &= \mathbf{W}_k \mathbf{y}_k \\ &= \mathbf{W}_k \sum_{i=1}^{K} \mathbf{H}_{ki} \mathbf{V}_i \mathbf{d}_i + \mathbf{W}_k \mathbf{n}_k \quad k \in 1, \cdots, K \end{aligned} \tag{4.2}$$

where $\mathbf{W}_k$ is an $S_k \times N_{rk}$ receiving filter for the kth user.

4.3 Multi-Cell Processing (MCP)

In this section we focus on the Multi-Cell Processing (MCP) system, or the system based on base stations cooperation. The used multicell model can be seen graphically in Fig. 55.

4.3.1 Uplink Channel Model

To study this system we use the uplink multicell model described in (Chatzinotas, Imran & Tzaras 2008), assuming N_c-cell system, where each cell has a radius R_{di} covered by a Base-Station (BS) and occupied with uniformly distributed K User-Terminals (UT). We also assume that each user and base station are equipped with n_{UT} and n_{BS} antennas respectively. However, for representation simplicity we consider a single antenna users, i.e., $n_{UT} = 1$. Therefore, the received $n_{BS} \times 1$ symbol vector at the nth base station, at time index l is given by:

$$\begin{aligned} \mathbf{y}_n(l) &= \sum_{k=1}^{K} \zeta_{n,k}^{n} \mathbf{G}_{n,k}^{n}(l) \mathbf{x}_{n,k}(l) \\ &+ \sum_{j=1}^{N_c/2} \sum_{k=1}^{K} \zeta_{n-j,k}^{n} \mathbf{G}_{n-j,k}^{n}(l) \mathbf{x}_{n-j,k}(l) \\ &+ \sum_{j=1}^{N_c/2} \sum_{k=1}^{K} \zeta_{n+j,k}^{n} \mathbf{G}_{n+j,k}^{n}(l) \mathbf{x}_{n+j,k}(l) + \mathbf{z}_n(l) \end{aligned} \tag{4.3}$$

which could be written in the generic MIMO Multiple Access Channel (MAC) equation as follows

$$\mathbf{y}(l) = \mathbf{H}(l)\mathbf{x}(l) + \mathbf{z}(l) \tag{4.4}$$

Considering the MIMO BS-UT links, the channel matrix $\mathbf{H}$ can be written as

$$\mathbf{H} = (\Sigma \otimes \mathbb{I}_{n_{BS} \times n_{UT}}) \odot \mathbf{G}_{N_c n_{BS} \times K N_c n_{UT}} \tag{4.5}$$

where $\mathbf{G} \sim \mathcal{CN}(\mathbf{0}, \mathbf{I}_{N_c n_{BS}})$ is a complex Gaussian $N_c n_{BS} \times K N_c n_{UT}$ matrix, comprising the Rayleigh fading coefficients between the $K N_c n_{UT}$ transmit and the $N_c n_{BS}$ receive antennas. Likewise, the variance profile Σ is $N_c \times K N_c$ deterministic matrix, consists of the path-loss coefficients between the $K N_c$ transmitters and the N_c base stations. $\mathbb{I}_{n_{BS} \times n_{UT}}$ is $n_{BS} \times n_{UT}$ matrix of ones.

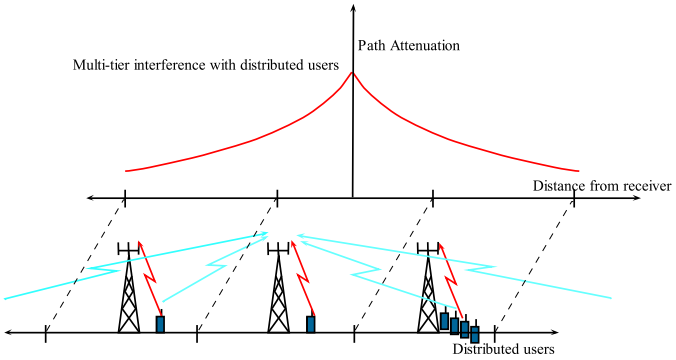

Figure 55. Graphical representation of MCP model: multi-tier interference with distributed users.

4.3.2 MCP Variance Profile Matrix

Having a non-uniform variance is the main characteristic of the MCP channel model. Thus, the MCP channel model is affected by a variance profile which depends on the used path-loss function. Assuming that at reference distance d_0 the path-loss value is L_0, then, the distance dependent power-law path-loss function is given by

$$\begin{aligned} \zeta_{m,k}^{n} &= \zeta(r,t) \\ &= \sqrt{L_0}\left(1 + \frac{d(r,t)}{d_0}\right)^{\frac{-\eta}{2}} \end{aligned} \tag{4.6}$$

where $\zeta_{m,k}^{n}$ is the path-loss coefficient for the link between the kth user of the mth cell and the nth base station. The variable $\zeta(r,t)$ is the (r,t)th element of the variance profile matrix with $r = n/N_c \in (0,1]$ and $t = ((m-1)K + k)/N_c \in (0,K]$

being the normalized row/BS and column/UT indices. Also, $d(r,t)$ represents the distance between the kth user of the mth cell and the nth base station.

4.4 Simulation Results

This section demonstrates numerical results of the uplink multicell system. Assuming that K UTs are distributed uniformly in each cell with radius R_{di} in linear cellular array comprising N_c base station with n_{BS} antennas per base station as in Fig. 56, where a single-antenna users are considered.

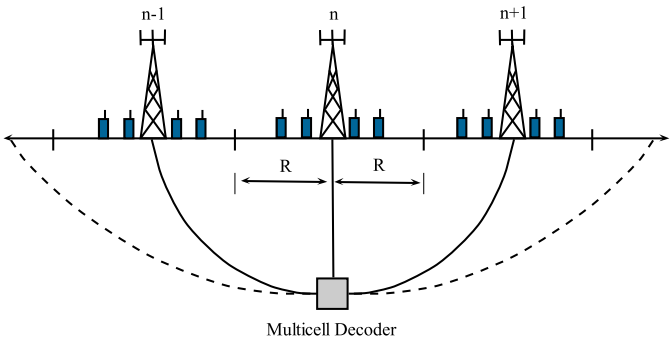

Figure 56. Linear cellular array with fixed number of users per cell.

4.4.1 Per-Cell Sum-Rate

The results are carried out through Monte-Carlo simulation to compute and compare the achieved per-cell sum-rate for the following schemes: 1) Optimal transmission strategy, which is non-orthogonal transmission with power P followed by optimal multicell joint decoding as described in (Chatzinotas, Imran & Tzaras 2008). 2) Multiple access (FDMA and TDMA) with suboptimal MMSE filtering followed by single-user detection scheme. 3) Constrained partial group decoding (CPGD) scheme.

Numerical results are obtained after constructing the channel matrix $\mathbf{H}$. The optimal per-cell sum-rate capacity is calculated by evaluating the following formula

$$C_{opt} = \frac{1}{N_c}\mathbb{E}\left[\log\ \det(\mathbf{I}_{N_c n_{BS}} + \gamma_{gap}\mathbf{H}\mathbf{H}^H)\right] \tag{4.7}$$

Also, the intra-cell orthogonalization channel matrix $\mathbf{H}_o$ is constructed by randomly selecting n_{BS} out of the K users of each cell and constructing the corresponding column vector of $\mathbf{H}$. Then, the achievable per-cell sum-rate with FDMA and linear MMSE filtering is given by

$$C_{mmse}^{FDMA} = -\frac{1}{N_c}\mathbb{E}\left[\sum_{k=1}^{N_c n_{BS}} \log\left[(\mathbf{I}_{N_c n_{BS}} + \gamma_F \mathbf{H}_o^H \mathbf{H}_o)^{-1}\right]_{k,k}\right] \tag{4.8}$$

where the the FDMA transmit SNR γ_F is given by

$$\gamma_F = \frac{\bar{P}}{\sigma^2} \cdot \frac{K}{n_{BS}} \tag{4.9}$$

while the achievable per-cell sum-rate with TDMA and linear MMSE filtering is given by

$$C_{mmse}^{TDMA} = -\frac{1}{N_c}\mathbb{E}\left[\sum_{k=1}^{N_c n_{BS}} \log\left[(\mathbf{I}_{N_c n_{BS}} + \gamma_T \mathbf{H}_o^H \mathbf{H}_o)^{-1}\right]_{k,k}\right] \tag{4.10}$$

where the the TDMA transmit SNR γ_T is given by

$$\gamma_T = \begin{cases} \frac{\bar{P}}{\sigma^2} \cdot \frac{K}{n_{BS}} & PAR \geq \frac{K}{n_{BS}} \\ \frac{\bar{P}}{\sigma^2} \cdot PAR & PAR < \frac{K}{n_{BS}} \end{cases} \tag{4.11}$$

where the *PAR* stands for the peak-to-average power ratio.

The results of the three considered scenarios are obtained using linear cellular configuration of 3 cooperating cells, with 10 single-antenna users in each cell, and each cell has a base station equipped with 3 antennas.

First, the results shown in Fig. 57 display the per-cell sum-rate against the cellular span with the range between (0.1 to 3) *km*. Interestingly, results in this figure show that CPGD scheme reduces the gap between the achieved sum-rate of the optimal non-orthogonal transmission strategy and the achieved sum-rate obtained by the (FDMA and TDMA) with MMSE filtering schemes.

Next, for clearer comparison between the considered schemes, we plot the sum-rate per-cell versus the SNR, as presented in Fig. 58. Results in this figure confirmed the previous results. Where, it is also shown here that the per-cell sum-rate obtained by CPGD is much closer to the optimal achievable capacity compar-

ing with the achieved sum-rate of the (FDMA and TDMA) with MMSE filtering scheme.

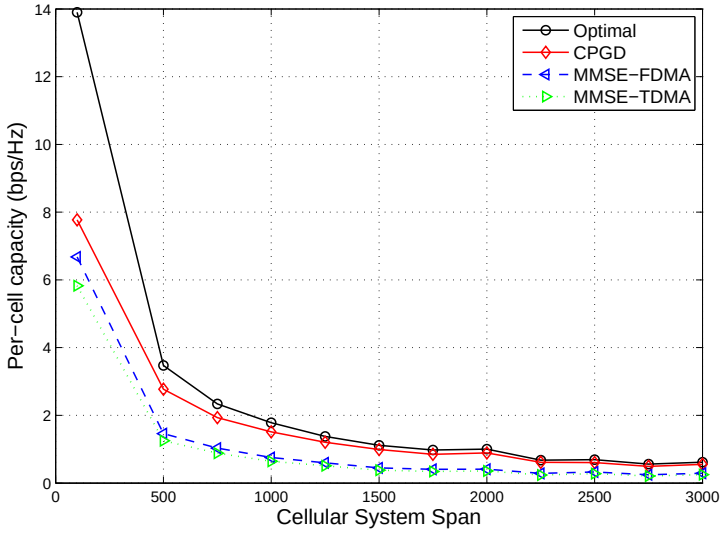

Figure 57. Per-cell capacity versus cell radius R_{di} for fixed number of users per cell, with $K = 10$, $n_{BS} = 3$, $PAR = 2$.

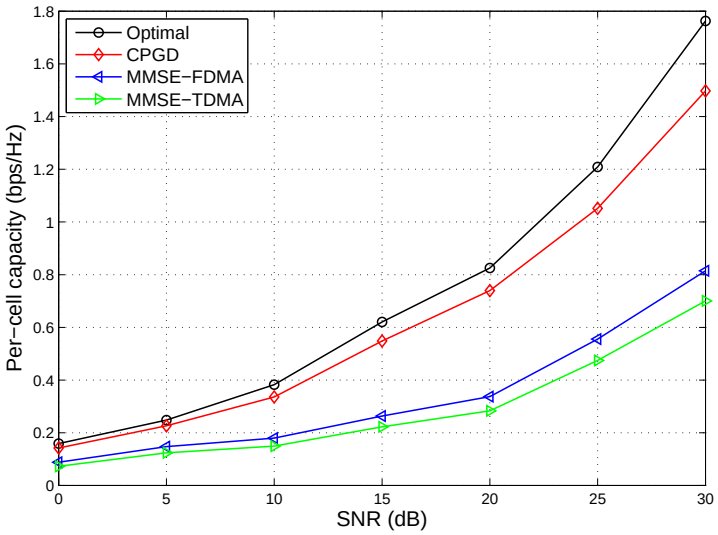

Figure 58. Per-cell capacity versus SNR (dB) for fixed number of users per cell, with $K = 10$, $n_{BS} = 3$, $R_{di} = 1km$.

4.4.2 Bit Error Rate Performance

In this subsection we evaluate BER performance of CPGD in the multi-cell system, to do so we carried out Monte-Carlo simulation for 3-cooperating-cell system, with 250 meters cell radius. Each base station equipped with 3 antennas and we again consider single-antenna users. Every one of those users sends one data stream to its intended base station. We also assume a Rayleigh fading channel model taking into account the users variance profile matrix. In other words, the Rayleigh channel variance is not uniform, but it depends on the path-loss coefficient which is a function of each user's locations. In this part QPSK modulation scheme combined with (64800-bit long) LDPC code with $1/2$ coding rate is used. The decoding is performed in block-wise manner, after-which the interference cancellation process is taking place.

The result of this part is shown in Fig. 59, where it is clear that the CPGD scheme has better BER performance comparing with the MMSE scheme. For instance at BER of 10^{-4}, the CPGD has 1.4 dB power gain comparing with MMSE scheme.

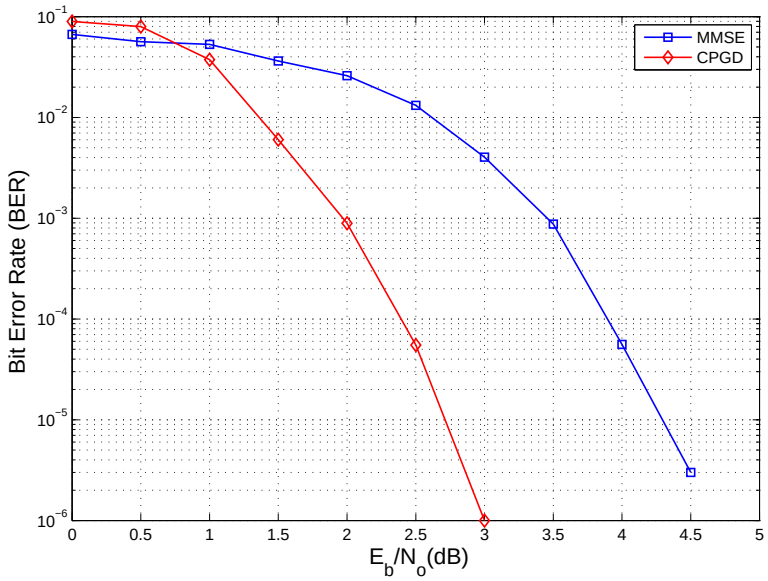

Figure 59. Bit error rate versus E_b/N_o, with $K = 10$, $n_{BS} = 3$, $n_{UT} = 1$, $R_{di} = 250m$.

4.5 Summary

In this chapter we investigated performance of CPGD scheme to mitigate interference in MIMO interference channel for uplink multicell system. We described the MCP model used to assess this system. Then, we demonstrated the capability of CPGD technique to manage and mitigate interference, where simulation results have shown that for uplink multicell MIMO system CPGD scheme has exhibited its superiority over the multiple access (FDMA and TDMA)-MMSE-based techniques in terms of the achieved per-cell sum-rate and bit error rate performance.

5 LARGE-SCALE MIMO TRANSCEIVER SYSTEM

In this chapter we discuss the design of the transceiver system for LS-MIMO wireless communications which we propose in (Abu-Ella & Wang 2013b). We present the main challenges facing this LS-MIMO system; also, we propose solutions for those problems. The transmitters in this proposed downlink system uses a simple fair user scheduling based on limited-feedback algorithm with basic random precodeing algorithm. On the other side, receivers employ constrained partial group decoder (CPGD) to detect their desired signals. Simulation is used to evaluate sum-rate performance of this LS-MIMO downlink system against the total number of users, SNR and for a wide range of the number of employed antennas, using different number of scheduled users and with various group sizes of the jointly decoded users. Numerical results interestingly show an encouraging performance for the proposed transceiver system in this chapter to be considered as a candidate scheme for large-scale MIMO communication systems.

5.1 Introduction

Multiple-Input Multiple-Output (MIMO) system is the backbone of the present communication systems. MIMO started to be the technique to boost the single-user system capacity linearly with increasing the number of antennas. Also, in recent time we see the Single-User MIMO (SU-MIMO) switched to the Multiple-User MIMO (MU-MIMO) Network (Kountouris & Gesbert 2005). Although SU-MIMO and MU-MIMO are still grabbing an intensive research interest, MIMO is practically in use for the modern cellular technology such as 4G wireless systems (Kumari 2010). However, as we need to look at the future of the communication systems, we should open the doors for the (LS-MIMO) systems.

This evolutionary way of looking to the future of communication systems will lead to design antenna arrays consist of small active optical antenna elements, consuming very low power. Nowadays, it is possible that the Long Term Evolution (LTE) system could offer a high peak data rates ($\sim$ 1 Gbps), but the problem is such high data rates still highly random, and the users provided with much lower rates (Rusek *et al.* 2013). Therefore, LS-MIMO can be the solution for the limitation of such LTE system. Moreover, according to (Wang *et al.* 2014), large-scale MIMO expected to be a promising key 5G wireless technology, to facilitate the

achievement of higher data rates, larger network capacity, better energy efficiency, higher spectral efficiency and more flexible mobility for the wireless communication networks.

The literature of wireless communication systems is full of MU-MIMO system design in several ways of implementation and for many different scenarios. However, most efforts in the research have been directed towards small or moderate antenna arrays (Larsson & Stoica 2008). Recently, the emerging field of research of large MIMO systems has grabbed much attention, as it becomes the way to enhance the wireless system performance by exploiting the spatial domain in a better way providing a higher data rates and much better link reliability (Rusek *et al.* 2013). Research tracks in this area includes the energy and spectral efficiency as in (Huh *et al.* 2011; Ngo, Larsson & Marzetta 2011). Also, other researchers have proposed some optimal and near optimal receiving and detection schemes for large MIMO systems as in (Cirkic & Larsson 2012; Kumar *et al.* 2011; Suthisopapan *et al.* 2012). However, there is still much work to be done to propose and investigate other suboptimal, less complicated and more practical large MIMO schemes. Motivated by that, we aim in this chapter to propose and investigate performance of large MIMO transceiver system. Keeping in mind that implementation of such system faces some vital challenges including: channel estimation, precoding, users scheduling, fairness, aggregate feedback and signal detection. All of these issues will be discussed in more details in Section 5.3.

This chapter is organized as follows: the used interference channel model is described in Section 5.2. Section 5.3 discusses the challenges facing the large multi-user MIMO system. The numerical results of this chapter are shown in Section 5.4. Finally, Section 5.5 summarizes this chapter.

5.2 System Model

In multi user downlink system depicted in Fig. 60, we assume that the scheduler selects U users to be served among of total K active users in the system. The received signal by the kth user is given by

$$\mathbf{y}_k = \sqrt{\gamma_{kk}}\,\mathbf{H}_k\mathbf{v}_k\mathbf{x}_k + \sqrt{\gamma_{kl}}\mathbf{H}_k \sum_{l=1,l\neq k}^{U} \mathbf{v}_l\mathbf{x}_l + \mathbf{n}_k, \quad \text{for } k = 1,2,\cdots,U. \tag{5.1}$$

where $\mathbf{x}_k$ is $N_t \times 1$ vector consists of the kth user transmitted signal samples, with $\mathbf{Q}_{x_k} = \mathbb{E}\{\mathbf{x}_k \mathbf{x}_k^{\mathcal{H}}\}$ as covariance matrix, therefore, the total allocated power to user k is given by $P_k = tr\{\mathbf{Q}_{x_k}\}$, where tr denotes the matrix trace. The total sum of allocated power at the base station constrained to satisfy $\sum_k P_k \leq P$. $\mathbf{H}_k \in \mathbb{C}^{N_r \times N_t}$ represents the quasi-static block fading channel matrix, its elements drawn from an i.i.d. complex Gaussian distributed random variable with zero mean and unit variance. The term γ_{kl} is included to account the path-loss and shadowing effects between the transmitter l and the receiver k. $\mathbf{n}_k \in \mathbb{C}^{N_r \times 1}$ is the additive Gaussian noise vector at the receiver k.

The first term of (5.1) represents the actual intended signal vector to be transmitted to the kth user, the second term $\sqrt{\gamma_{kl}}\mathbf{H}_k \sum_{l=1, l\neq k}^{U} \mathbf{v}_l \mathbf{x}_l$ expresses the interference received by the kth user, where $\mathbf{w}_k$ denotes the precoding vector of the kth transmitter.

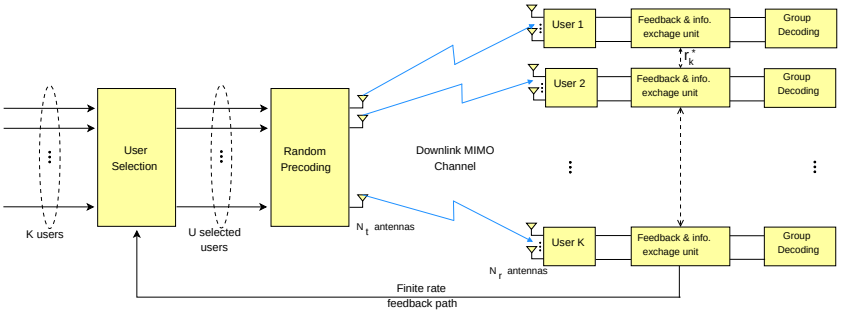

Figure 60. System block diagram for multi-user downlink MIMO channel with limited feedback.

5.3 Large-Scale Multi-User MIMO System Challenges

In this section we present the challenges facing the large-scale multi-user MIMO communication system. As well as, we propose applicable solutions for such problems.

5.3.1 Channel Estimation

Estimating a reliable channel state information (CSI) at the receiver is a critical process in MU-MIMO systems; because the associated complexity grows up with the number of antennas (Duman & Ghrayeb 2007). Nevertheless, estimating the channel matrix $\hat{\mathbf{H}}_k$ of the kth user can be achieved by sending training sequence in the beginning of each transition cycle. For instance, if we assume that the system uses L training symbols for this task, then, by defining $\mathbf{Y}_k \doteq [\mathbf{y}_k(1), \cdots, \mathbf{y}_k(L)]$ and denoting the training symbols by $\mathbf{S}_k \doteq [\mathbf{s}_k(1), \cdots, \mathbf{s}_k(L)]$, the maximum likelihood estimate of $\mathbf{H}_k$ is given by

$$\begin{aligned} \hat{\mathbf{H}}_k &= \arg \min_{\mathbf{H}_k \in \mathbb{C}^{N_r \times N_t}} \|\mathbf{Y}_k - \sqrt{\gamma_{kk}}\,\mathbf{H}\mathbf{S}\|^2 \\ &= \sqrt{\frac{1}{1/\gamma_{kk}}}\mathbf{Y}_k \left(\mathbf{S}\mathbf{S}^{\mathcal{H}}\right)^{-1}. \end{aligned} \tag{5.2}$$

From 5.2 we can see the huge cost of the computational complexity related to such maximum likelihood detector, especially for large-scale system; because of the matrix inversion which requires $\mathcal{O}(L^3)$ complex multiplications. Therefore, we have to avoid using CSI. Alternatively, we will use the received channel quality $\mathbf{H}_k\mathbf{v}_k$ for each user.

5.3.2 Precoding

It is known that the non-linear Dirty Paper Coding (DPC) (Weingarten, Steinberg & Shamai 2006) is the optimal precoding strategy. But, DPC has a prohibitive complexity to implement especially for large MIMO system which we consider. Also, vector perturbation-based methods, such as, the Norm Descent Search (NDS) technique (Mohammed, Chockalingam & Rajan 2008) relay on an iterative algorithm to converge which raises up questions about the complexity and latency constraints of such schemes, especially when they are deployed for large-scale MIMO systems. On the other hand, the linear precoding algorithms including Zero-Forcing (ZF) (Spencer, Swindlehurst & Haardt 2004) and Minimum Mean Square Error (MMSE) (Joham, Utschick & Nossek 2005) require high computational complexity since they involve operations of matrix inversion, which intractable for the considerably large-scale systems. As referred in (Elshokry 2010) it is clear that ZF algorithm requires $N_t^3 + 2N_t^2(N_r - 1) + N_t(N_t - 1)N_r$ and $N_t^3 + 2N_t^2 N_r$ complex additions and multiplications respectively. While, MMSE

scheme involves $N_t^3 + 2N_t^2(N_r - 1) + N_t(N_t - 1)N_r + N_t$ and $N_t^3 + 2N_t^2N_r$ complex additions and multiplications respectively. But the most crucial weak point of such linear precoding techniques, is the indispensable need for the full CSI, where the performance of such systems is significantly affected by accuracy of CSI at the transmitter side. Indeed this is a vital issue, particularly for the large-scale MIMO systems.

As discussed in Chapter 1, in conventional MIMO systems such in the LTE systems, the base station transmits pilots to help the terminal users estimate their channels, then they quantize and feed CSI back to the base station. However, considering the large number of base station antennas in the large-scale MIMO system, the mentioned process of CSI estimation and feedback will not be possible, at least for the high mobility scenarios. This simply because the number of the orthogonal pilots scales with the number of antennas in the base station, this means the downlink and uplink resources will be wasted for transmitting the pilots and the estimated channel responses.

The solution for this problem is to exploit the channel reciprocity between the uplink and downlink. This is however, implies that only the TDD operation mode will be suitable for the large-MIMO systems. But, even though channel reciprocity seems to be a reasonable assumption in the narrowband TDD systems, it is still a fact that hardware chains in the terminal users and base station may not reciprocal in the reverse and forward links. This necessitates the use of additional sophisticated calibration algorithms come with extra latency and computational cost on the system. More importantly, in the broadband TDD systems which apply OFDMA and frequency domain scheduling channel reciprocity is no longer valid (Haartsen 2008).

All of the aforementioned points make us think that the proposal transceiver design should consider a simple precoding strategy avoids all of the stated problems to be suitable for the large-MIMO systems. A practical candidate for the precoding technique is the Random Beamforming (RBF) scheme; we chose this precoding mechanism simply because it avoids the need for the CSI at the base station, and so, all the related problems stated above. Also, because the RBF has been proved to achieve asymptotically optimal growth rate for large systems (Kim *et al.* 2008). The used random precoder generates orthogonal random beams $\mathbf{v}_k \in \mathbb{C}^{(U\times 1)}$ and broadcasts them to all users. The advantage of using orthogonal beams is obvious, to eliminate the intra-cell interference between the simultaneously scheduled

users. The possibly existing inter-cell interference on the other hand, can be effectively mitigated and suppressed by the joint decoding process at the receiver side.

Now, for illustration simplicity we assumed that $N_r = 1$. Thus, as shown in Fig. 61, the transmitted signal at time instance t, resulted from the multiplication of the mth element of the random beam vector and the mth transmit symbol s_m is given by

$$x = \sum_{m=1}^{U} v_m(t)s_m(t), \quad t = 1,2,\cdots,T. \tag{5.3}$$

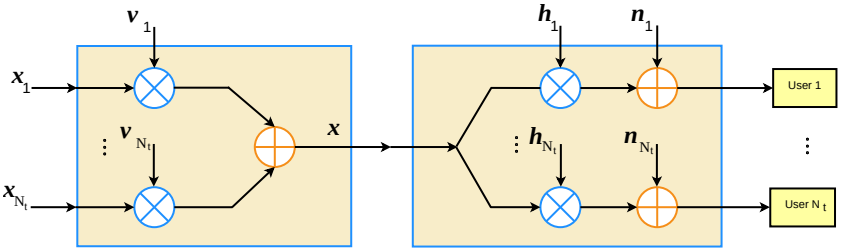

Figure 61. Block diagram of downlink transmission with orthogonal random beamforming.

For the simplicity we drop the time index (t), then, the received signal is given by

$$y_k = \sum_{m=1}^{U} \mathbf{h}_k v_m s_m + n_k. \tag{5.4}$$

Consequently, assuming that $\mathbf{h}_k v_m s_m$ is the desired signal and $\sum_{i\neq m}^{U} \mathbf{h}_k v_i s_i$ is the sum of the interference signals at the kth receiver, then, the SINRs of its mth stream can be computed as follows

$$SINR_{k,m} = \frac{|\mathbf{h}_k v_k|^2}{\frac{1}{SNR\gamma_{kk}} + \sum_{i\neq m}^{U} |\mathbf{h}_k v_i|^2}. \tag{5.5}$$

where, SNR denotes the signal-to-noise ratio at the intended receiver. Motivated by the fact that the reception quality is varied for the different information streams at each user, different scheduling algorithms has been proposed to identify the best matching between the information streams and the users. The following section discusses this issue in more details.

5.3.3 User Scheduling

Considering the difficulty of selecting a subset of users for transmission in the MIMO downlink system, an exhaustive search over all possible combinations of users assure to maximize the system throughput. However, with large number of users, computational complexity prevents implementing such algorithm for practical systems. To solve this problem some practical greedy search algorithms were proposed (Nguyen, Ngoc & Velasquez 2010; Sigdel *et al.* 2009; Wang *et al.* 2011), but the critical problem of this scheme that they are heavily depend on the CSIT. Therefore, using such scheduling algorithms require huge feedback overhead for the signaling phase in the the large-scale MIMO system. Consequently deploying these algorithms will reduce the system net throughput. Thus, we should look for a simple user-selection system utilizes as much as possible the system resources. Accordingly, we decide to use a simple opportunistic-limited feedback technique proposed in (Tajer & Wang 2010). This technique considered to be asymptotically optimal, and exhibits good performance for practical network sizes. So, we use it as a candidate scheduling algorithm for the proposed large-scale MIMO system.

Starting with $N_r = 1$, and without loss of generality, each user is able to decode any information stream among the available N_t streams, while treating the other streams as noise. Then, at the kth user, the mth data stream can be decoded with SINR

$$SINR_{k,m} = \frac{\sqrt{\gamma_{kk}}\,\mathbb{E}\{\|\mathbf{h}_k\mathbf{v}_m\mathbf{x}_m\|^2\}}{\mathbb{E}\{\|\mathbf{n}_k + \sqrt{\gamma_{kl}}\,\sum_{l\neq m}\mathbf{h}_k\mathbf{v}_l\mathbf{x}_l\|^2\}}, \tag{5.6}$$

which can be simplified through the homogenous network assumption to

$$SINR_{k,m} = \frac{\|\mathbf{h}_k\mathbf{v}_m\|^2}{\frac{1}{SNR\gamma_k} + \sum_{l\neq m}\|\mathbf{h}_k\mathbf{v}_l\|^2}, \quad k = 1,\cdots,K, \quad m = 1,\cdots,N_t. \tag{5.7}$$

Now for the kth user, the most favorable beam is defined to be

$$m_k^* = \arg\max_{l\leq m\leq N_t} SINR_{k,m}. \tag{5.8}$$

Considering the quantized value of $SINR_{k,m^*}$, and using the threshold $\beta(\gamma_k, K)$, which is a function of the total number of active users K and the path-loss. The kth user compares its $SINR_{k,m^*}$ with mentioned threshold level. Then, if $SINR_{k,m^*} \geq$

$\beta(\gamma_k, K)$ the user feeds back the index of its most favorable beam m^* to the base-station using $\log_2 N_t$ bits. However, if $SINR_{k,m^*} < \beta(\gamma_k, K)$ the kth user refrains from feeding back its information and so, it will not be considered as a scheduling candidate.

For each beam m, we defined the set B_m consists of the indices of the users who have responded with the integer m as a favorable beam in the feedback stage, i.e.,

(5.9)
$$B_m = \{k | m = \arg\max_{1 \le l \le N_t} SINR_{k,l} \quad \text{and} \quad SINR_{k,m} \ge \beta(\gamma_k, K), \quad k = 1, \cdots, K\}.$$

Now, randomly the base-station chooses one user from the set of users indices B_m for $m = 1, \cdots, N_t$. Then, it schedules this selected user to receive the x_m information stream. Since the sets B_m are mutually exclusive, this guarantees that there is no user assigned to to receive more than one information stream. Although the case of $(|B_m| = 0)$ means that the system did not find any eligible user for the mth beam, and that implies a loss in the sum-rate; it is true that this loss vanishes by increasing the total number of active users.

It is worth to note that using the aforementioned threshold, the cumulative distribution function (CDF) of $SINR_{k,m}$ is given by (Tajer & Wang 2008) as

(5.10)
$$F_k(x) = 1 - \frac{e^{\frac{-x}{SNR\gamma_k}}}{(x+1)^{N_t - 1}}.$$

and by setting the threshold level $\beta(\gamma_k, K)$ such that

(5.11)
$$F_k\{\beta(\gamma_k, K)\} = 1 - \frac{1}{K}.$$

Then, obviously, $F_k(x)$ is monotonically increasing function, and for each K there is a unique solution for $\beta(\gamma_k, K)$. It is shown that for the above choice of the threshold level, this finite-rate feedback scheme achieves the optimal scaling-law of MIMO broadcast channel (Tajer & Wang 2010).

So far, what has been considered is a system with single-antenna users. However, it is shown in (Tajer & Wang 2008) that the system can retain the same gain by slightly modifying the scheduling algorithm for $N_r > 1$. In the modified system, each user can receive more than one information stream x_m, i.e., one stream for

each distinct receive antenna. As a result, we have the scheduling algorithm illustrated in Table 6. This is equivalent to having a network with KN_r users, and all the earlier provided analysis for K users can be straightforward extended for the network with KN_r users. Therefore, for each distinct user, the system sets the threshold level as

$$F_k\{\beta(\gamma_k, K)\} = 1 - \frac{1}{KN_r}. \tag{5.12}$$

Table 6. Scheduling Algorithm with Finite-Rate Feedback

Initialization
1- **for** $k = 1, \cdots, K$ **do**
2- The kth user estimates $\mathbf{h}_k \mathbf{v}_m \quad m = 1, \cdots, N_t$
3- The kth user computes $SINR_{k,m} = \frac{|\mathbf{h}_k \mathbf{v}_m|^2}{\frac{1}{SNR\gamma_k} + \sum_{l \neq k} |\mathbf{h}_k \mathbf{v}_l|^2}$
4- The kth user sets $\beta(\gamma_k, K)$
5- **end for**
Feedback
6- **for** $k = 1, \cdots, K$ **do**
7- The kth user finds $SINR_k^* = \max_{1 \leq m \leq N_t} SINR_{k,m}$
8- The kth user finds $m_k^* = \arg\max_{1 \leq m \leq N_t} SINR_{k,m}$
9- The kth user feeds back m_k^* if $SINR_k^* \geq \beta(\gamma_k, K)$
10- **end for**
User Selection
11- Initialize
12- **for** $m = 1, \cdots, N_t$ **do**
13- $B_m = \{k | m = \arg\max_{1 \leq l \leq N_t} SINR_{k,l}$
and $SINR_{k,m} \geq \beta(\gamma_k, K), \quad k = 1, \cdots, K\}$
14- **while** $k_m^* < 0$ **do**
15 **if** $B_m = \{\ \}$ then set $k_m^* = 0$
16 **else** randomly (uniformly) pick a member of B_m, denote it by k
17 **end if**
18 **if** $k = k_l^*$ or $k = k_{m-1}^*$ then $B_m \leftarrow B_m \backslash k$
19 **else** $k_m^* = k$
20 **end if**
21 **end while**
22- Assign the mth beam to the user k_m^* **if** $k_m^* \neq \{\ \}$
23- **end for**.

One of the essential criteria of designing the user scheduling algorithms is to maintain fairness between all the active users (Airy, Shakkattai & Heath 2003; Gong &

Ming 2006; Lau, Liu & Chen 2002; Sun *et al.* 2008; Torabzadeh & Ajib 2010). Thus we will discuss the fairness issue in the following section.

5.3.4 Fairness

Fairness is an important issue in the multiple access communication system. Where the reception quality for each terminal user, especially in the heterogeneous networks, depends on how the channel directional vector is aligned with the beam direction, and it is also affected by the path-loss and shadowing of the system environment. This means, employing scheduling algorithm based on opportunistic selection of users according to satisfying a minimum level of reception quality could lead to the case when the users with the highest quality of reception dominate the system. Therefore, in our proposed system design we have considered a scheduling strategy with proportional fairness.

The proportional fair scheduling is defined in (Tolga *et al.* 2010) as follows

Definition 2: Scheduling $\Lambda = \{r_i\}$ is said to be proportionally fair if and only if, for any feasible scheduling $\acute{\Lambda} = \{\acute{r}_i\}$, it satisfies:

$$\sum_{i \in U} \frac{\acute{r}_i - r_i}{r_i} \leq 0 \tag{5.13}$$

where r_i is the rate of user i, U is the set of scheduled users. We explain this by saying, a proportional fair schedule is such that any positive change of the rate allocation of users results a negative total change in the system (Tolga *et al.* 2010).

From other point of view, we can see that the proportionally fair allocation Λ maximizes the sum of logarithmic average user rates (Tse 2001)

$$\Lambda = \arg\max_{\acute{\Lambda}} \sum_{i \in U} \log \acute{r}_i. \tag{5.14}$$

In our proposed system design, proportional fairness amongst the users can be sustained by choosing different threshold levels to select different users according to the path-loss and shadowing γ_k. In other words, the system can establish fairness by assigning a lower threshold level for the users who experience higher path-loss and shadowing effects. This SINR threshold level $\beta(\gamma_k, K)$ chosen to satisfy the CDF function in (5.12),

Then, using (5.10) fairness can be explicitly demonstrated as in (Tajer & Wang 2008) as follows

$$\frac{\beta(\gamma_i,K)}{SNR\gamma_i}+(N_t-1)\log\{\beta(\gamma_i,K)\}=\frac{\beta(\gamma_j,K)}{SNR\gamma_j}+(N_t-1)\log\{\beta(\gamma_j,K)\}. \tag{5.15}$$

This implies that if $\gamma_i<\gamma_j$, then, $\beta(\gamma_i,K)<\beta(\gamma_j,K)$. The value of threshold $\beta(\gamma_k,K)$ can be given by an iterative numerical algorithm to solve 5.12). But because of the importance of the threshold value as a critical parameter, the iterative numerical methods may not be particularly efficient for large-scale system. Therefore, to accomplish our goal of sustaining the system simplicity and minimizing the unnecessary computational complexity, we introduce a closed form solution to solve (5.12) instead of using the iterative methods. This closed form solution can be obtained as follows

From (5.10) and (5.12) we get

$$\frac{e^{\frac{\beta(\gamma_k,K)}{SNR\gamma_k}}}{(\beta(\gamma_k,K)+1)^{N_t-1}}=\frac{1}{KN_r} \tag{5.16}$$

Therefore,

$$\beta(\gamma_k,K)=\exp\left(\frac{SNR\gamma_k(\psi_1(1-N_t)-\psi_2)+1}{\psi_3}\right)-1 \tag{5.17}$$

where, $\psi_2=SNR\gamma_k\log(\frac{1}{KN_r})$, $\psi_3=SNR\gamma_k(N_t-1)$, $\psi_1=\mathtt{W}\left(e^{\left((1-\psi)\zeta^{-1}\right)}\zeta^{-1}\right)$, $\mathtt{W}(\cdot)$ stands for the Lambert W-function (Corless *et al.* 1996), and it is defined as follows,

$$\mathtt{W}(x)=xe^{x}. \tag{5.18}$$

To show the effect of the value of the threshold level on the performance of the scheduling algorithm we numerically evaluate (5.17). Results of 32×32 MU-MIMO system depicted in Fig. 62 show the relation between the threshold level and the number of users in different SNRs, for a constant path-loss and shadowing of 0 dB. Also, Fig. 63 shows how the threshold changes with the path-loss and SNRs levels, assuming that the system occupied by 500 users.

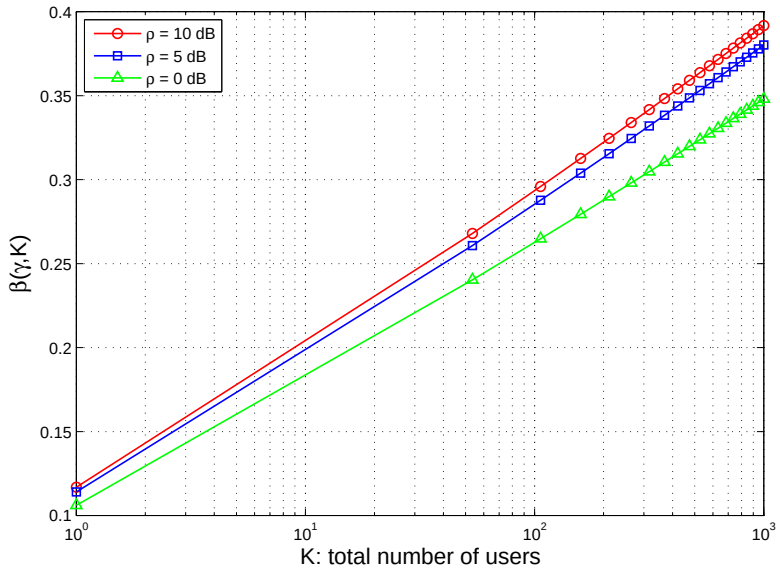

Figure 62. Effect of number of users on the threshold, $N_t = 32$, $N_r = 32$, $\gamma_k = 0$ dB.

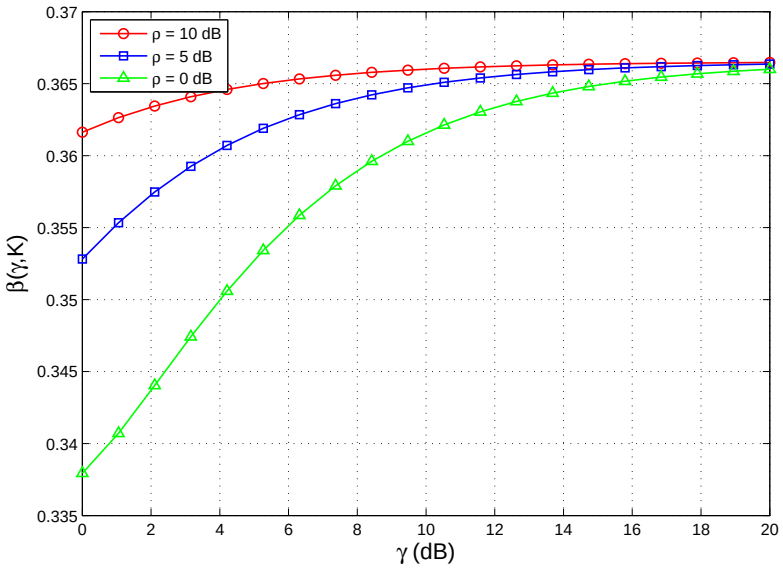

Figure 63. Path loss effect on the threshold, $N_t = 32$, $N_r = 32$, $K = 500$ users.

5.3.5 Aggregate Feedback

In the conventional user scheduling system, there is another challenge arises from the necessity of sending full CSI of the large-scale system back to the transmitter. In fact feeding back CSI for all users in large MU-MIMO severely decreases the system throughput. Therefore, there is an indispensable need for limited feedback technique to overcome this problem (Edfors *et al.* 1998). A good candidate for such system is the opportunistic user scheduling algorithm with finite-rate feedback. In our proposed system users do not feedback their SINR unless they achieve a specific threshold $\beta(\gamma_k, K)$. Therefore, the used scheme does not require all users to feed back their channel quality metric to the base-station and that avoids overloading the feedback channel. In fact, the total amount of imposed feedback is $N_t \log_2 N_t$ which is so far lower than the amount of the required by most existing scheduling algorithms (Tajer, Prasad & Wang 2010).

5.3.6 Signal Detection

In the proposed large-scale MIMO system, interference may exist as an inter-cell interference, since the orthogonal beams will avoid the intra-cell interference. However, for the following simulation cases, we consider a single-cell with non-orthogonal random beams to study the effect of the interference on the system. It is known that conventional detection techniques based on coordinated interference cancellation involve huge amount of exchanged information, impose delay, and extra computational complexity in the system. Motivated by the need for new technique to overcome these challenges by maintaining tolerable delay and reduce the system requirements in terms of its complexity and the amount of exchanged information; we decide to choose a novel constrained partial group decoding technique introduced in (Chen *et al.* 2012; Gong, Tajer & Wang 2011). In this system, as described in Section 3.3, each receiver employs CPGD scheme to decode its desired message along with a part of the interference. CPGD scheme controls the complexities associated with obtaining the best ordered decodable set on one hand, and limits the amount of information exchange on the other hand. CPGD is comprised of two sub-routines: one is employed locally to determine the best partition for each receiver and the suggested rate increment, the other obtains the globally optimal rate increment through a limited feedback process.

5.4 Simulation Results

In this section, we used the simulation layout shown in Fig 64, where we used flat 2-D topology configuration of 12 cells separated by 1 unit. Simulated users are distributed randomly and uniformly on a (15×20) grid, and the cells distinguished as a, b, and c. In this chapter, our concern is to focus on the operations of a particular cell, with number of users, such as, $K \gg N_t$ to account for typical operation scenario of the next-generation packet-based cellular networks. AWGN Gaussian noise is generated by independent and identically distributed (i.i.d.) circularly symmetric random variables, with zero-mean and unit variance. We Assume quasi-static (block) fading model, i.e., the channel vector remaining constant during the scheduling and transmission intervals.

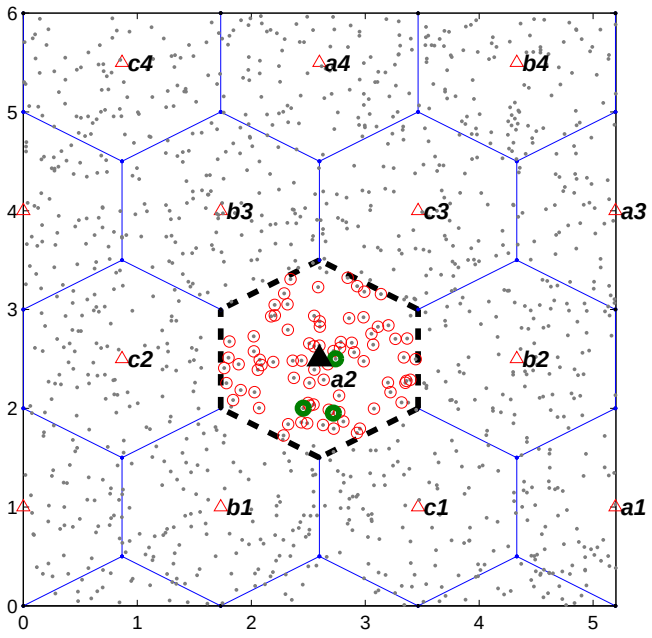

Figure 64. Simulation Layout.

The employed channel model considers the path-loss, log-normal shadow and Rayleigh fading. Depending on the path-loss and shadowing each user assigned to the base-station of the highest average received signal strength, which does not

necessary imply the closest one. At distance d from the base station the overall effect of path-loss and transmit power P is expressed as follows

$$PL(d) = \left(\frac{G_o}{d_o^{\alpha}}\right)\left(1+\left(\frac{d}{d_o}\right)\right)^{-1}, \tag{5.19}$$

where the used setting are: $\alpha = 3.76$, $d_o = \frac{\sqrt{2}}{10}$ and $G_o = 12.94$. The log-normal shadowing is assumed to be with zero mean and shadowing standard deviation $\sigma = 8$ dB.

5.4.1 Single Antenna Users

The following results are produced by simulating single-cell downlink system. Where, the transmitter is equipped with Nt antennas, and uses random precoding algorithm connected to limited feedback-opportunistic scheduler to select U active users, each of them equipped by a single antenna. The receiving system uses a CPGD scheme, with group-size μ represents the number of signals that can be jointly decoded.

First, we aim to observe the throughput versus SNR. Fig. 65 shows the sum rate throughput obtained from 16-antenna system with 4 selected users, each one equipped with single antenna, employs CPGD with un-layered coding scheme and group size $\mu = 1,2,3$ and 4. From the results it is clear that the sum rate throughput increases by increasing the group size. However, it is critical to keep increasing the group-size; because it will increase the processing delay of the decoder. Therefore, in this chapter we constrained the group-size to be 4 at most. Also, Fig. 66 demonstrates clearly the improvement in the system throughput when we switch the group size from 1 to 2. We notice that the highest sum rate in both cases $\mu = 1$ or 2 happens when the system operates with number of selected users closer to the group size. Furthermore, by observing the results shown in Fig. 67, we notice that there is not any sum rate throughput improvement by increasing the number of transmit antennas when the users are equipped with single receiving antenna; because the system capacity is limited by the minimum of transmit or receive antennas numbers.

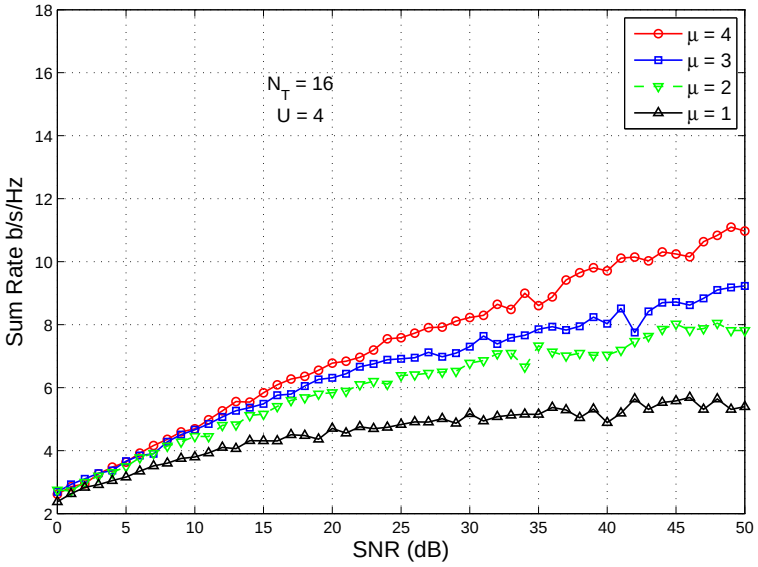

Figure 65. Throughput versus SNR of sixteen-transmit antenna system occupied by four active users employs group decoder with $\mu = 1, 2, 3$ and 4.

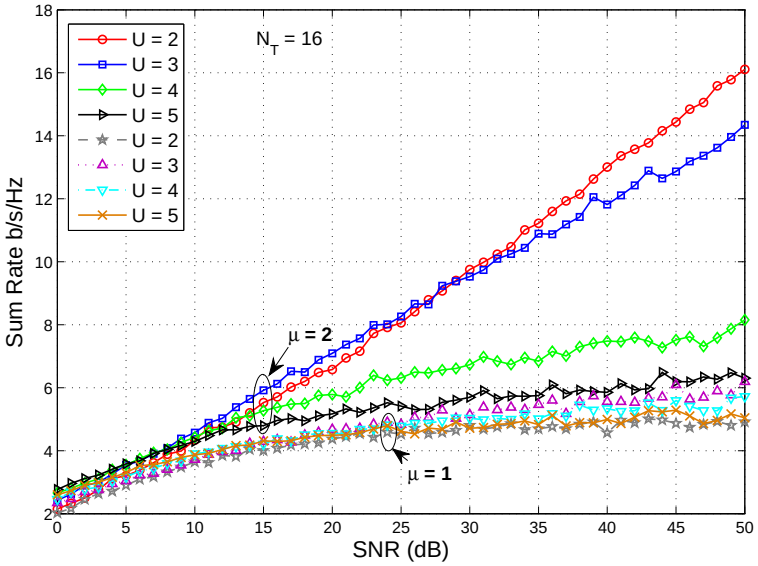

Figure 66. Throughput versus SNR of sixteen-antenna system with (2, 3, 4, 5) active users, using group decoder with $\mu = 1$ and 2.

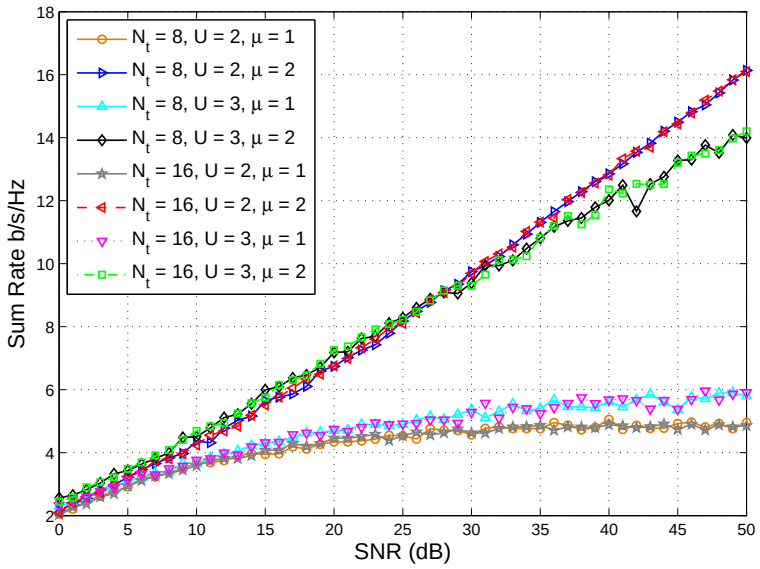

Figure 67. Throughput versus SNR of eight and sixteen-antenna system with (2, 3) active users, using group decoder with $\mu = 1$ and 2.

Second, in this part we intend to view the throughput performance versus the total number of cell users, with SNR of 10 dB. To evaluate the performance of the used opportunistic finite-rate scheduling algorithm comparing to the conventional scheduling techniques, we plot the sum rate throughput obtained by this algorithm and compare it with the throughput achieved using a conventional greedy scheduler. Results of sixteen transmit antenna base station selects 6 single-antenna users to operate simultaneously are shown in Fig. 68. From the Figure, we can perceive that limited feedback algorithm exhibits satisfying performance comparing with the greedy scheduler, but we should keep in mind the huge amount of aggregate feedback to send CSI to the transmitter in case of using the greedy scheme.

From other point of view, to investigate the effect of transmission system size on the throughput, we compare the performance of two systems: one uses eight-transmit antennas, and the other uses sixteen-transmit antennas, both are scheduling 4 users to share the system resources. From the results depicted in Fig. 69, one can see that for small number of users the smaller system, i.e., the system of the 8-transmit antennas performs better and it produces higher sum rate throughput. On the other hand, when the total number of users exceeds a certain point, for instance 300 users in the simulated scenario, the larger system, i.e., the 16-transmit antenna system, starts outperforming the smaller system. This is because the probability

of selecting users align perfectly with the randomly generated beams is increasing with the total population of users.

Now, to inspect the effect of changing the number of scheduled users, we simulate the same previous sixteen-transmit antenna system, with different number of selected users each time. A quick glance on the results in Fig. 70 shows that increasing the number of scheduled users increases the system throughput. However, this is not always the case, i.e., by observing the figure carefully; we can see that the system throughput dramatically increases by increasing the number of scheduled users U until it reaches a maximum level. Then, increasing the number of scheduled users will slightly decrease the system throughput. This is because the number of non-jointly decoded interfering signals will increase by increasing the number of selected users more than the group-size μ. This is will not be the case if orthogonal random beams were used.

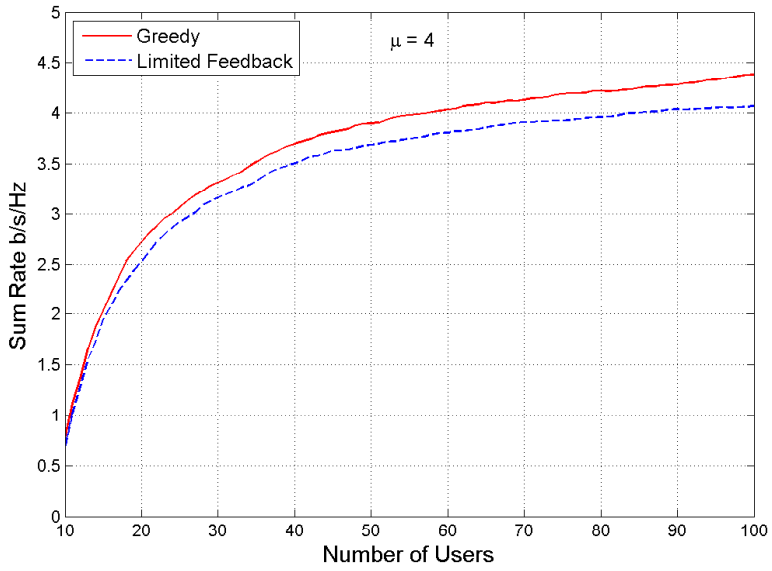

Figure 68. Throughput versus total number of cell users: comparison between greedy scheduler and the limited feedback scheduling scheme.

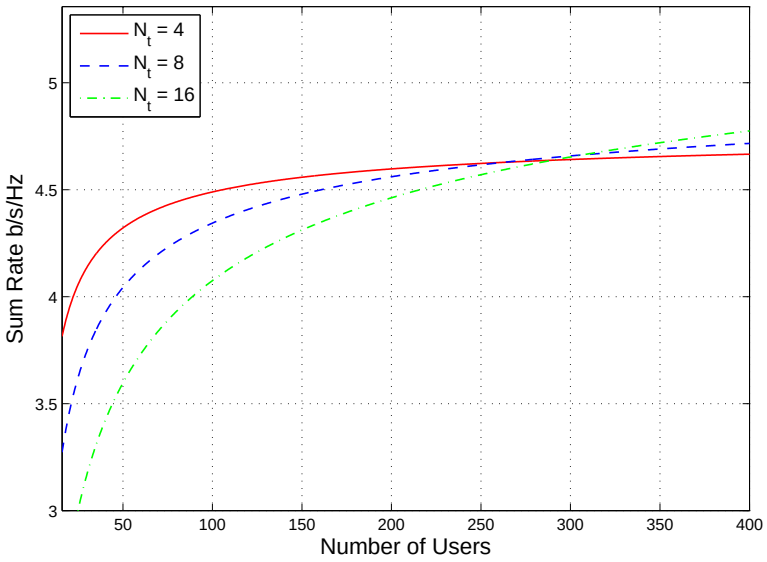

Figure 69. Throughput versus total number of users for three systems with different transmit-antenna size.

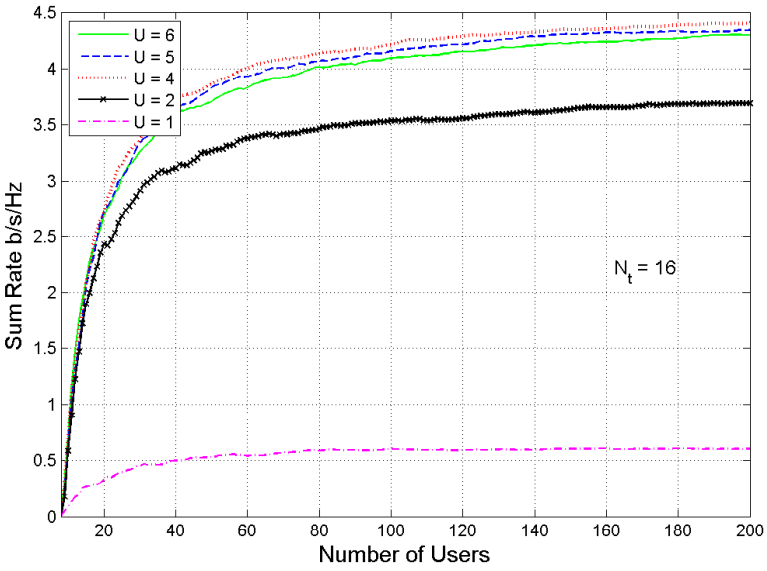

Figure 70. Throughput versus total number of users for sixteen-transmit antenna system uses group decoder with $\mu = 4$ and limited feedback scheduling scheme to select 1, 2, 4, 5 and 6 selected users.

5.4.2 Multiple Antenna Users

As a final step in our evaluation for the proposed system, we upgrade our previously described simulation setup in 5.4.1 to accommodate the performance assessment of a system occupied with multiple-antenna receiving users. The following results are carried out by Monte-Carlo simulation of the single-cell downlink system, with SNR of 10 dB. The transmitter is equipped with N_t antennas, and it uses random precoder connected to opportunistic with limited feedback scheduler to select U active users equals to the number of receive antennas, each user equipped with N_r receive antennas. The receiving system uses CPGD, with different number of transmitters that can be jointly decoded.

In this part we focus to view the system sum-rate throughput performance versus total number of cell-users. As an example, we run the simulation for the previously stated setup using different MIMO sizes: (2×2 up to 16×16), and using $\mu = 2$. Now, using the results shown in Fig. 71, one can see the significant improvement in system throughput with increasing the MIMO size.

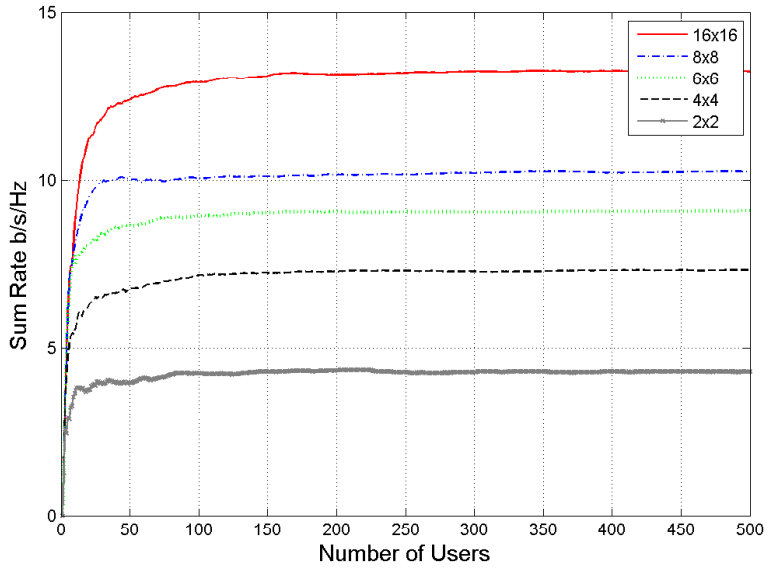

Figure 71. Throughput versus the total number of users for different MIMO sizes using $\mu = 2$.

5.4.3 Deploying Large Antenna Arrays

In this section we investigate the effect of number of system users when the base station deploys relatively large numbers (tens) of antennas. In the simulation setup of this subsection we assume the base station uses 32 and 64-element antenna array, and we consider different SNR levels, i.e., (0, 10 and 20) dB. The CPGD group-size μ is constrained to be 2. The results of this part are depicted in figures (72, and 73). From figures we clearly see that similar to the case of using small or moderate number of antennas in previous subsections, the sum-rate of the system increases with the total number of users in the system. This is because the probability of scheduling users with better aligned channels to the random beams is increasing as the size of the system users population increases. Of course when larger arrays are deployed, much larger over all sum-rate is achieved. In addition, beside it is obvious that the achieved sum-rate increases with SNR, one can also notice that, the slope of the sum-rate curves, i.e., the marginal increase of the sum-rate due to the marginal increase on the total number of users, is slightly faster for the higher SNR level than that for the lower SNR, especially for limited number of users.

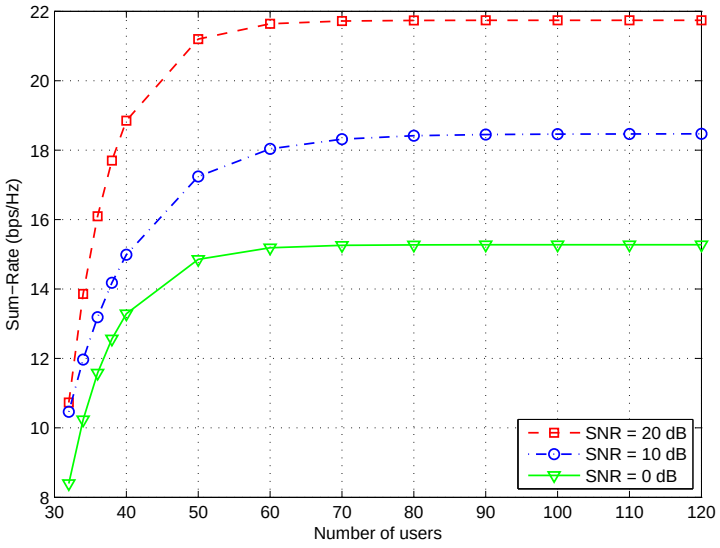

Figure 72. Sum-rate versus the number of users for different SNR levels using $N = 32$, and $\mu = 2$.

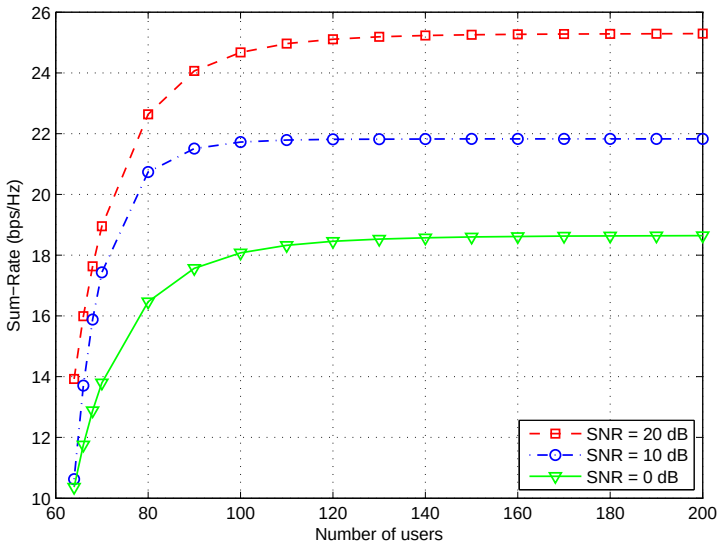

Figure 73. Sum-rate versus the number of users for different SNR levels using $N = 64$, and $\mu = 2$.

5.4.4 Number of Antennas Effect

In this subsection we discuss the effect of increasing the number of antennas on the system throughput. The implemented simulation setup for this part assumes the system occupied with a total of 200 users. All the receivers employ the CPGD scheme with two group-size options ($\mu = 2$ or 3). Also, in this subsection we carry out the results for different SNR levels (0, 10 and 20) dB. The results are depicted in figures (74 and 75) to represent the throughput of the system versus the number of employed antennas at the base station.

From the results shown in Fig. 74 which collected when the receivers employ CPGD scheme with $\mu = 2$, we can observe that the system throughput grows logarithmically with the number of base station antennas. Also, as expected, we can see the logarithmic-increasing trend of the throughput gain with the increase of SNR level.

From other point of view, Fig. 75 shows the results of the system throughput against the number of base station antennas for the two group-size options, i.e., for ($\mu = 2$ and 3). So, we can clearly see the marginal throughput gain of using larger group-size. Moreover, one can also observe that the marginal throughput gain of using larger group-size is slightly enhanced by the increase of the number

of employed antennas, but once again, this marginal gain enhancement is more obvious in the higher SNR levels.

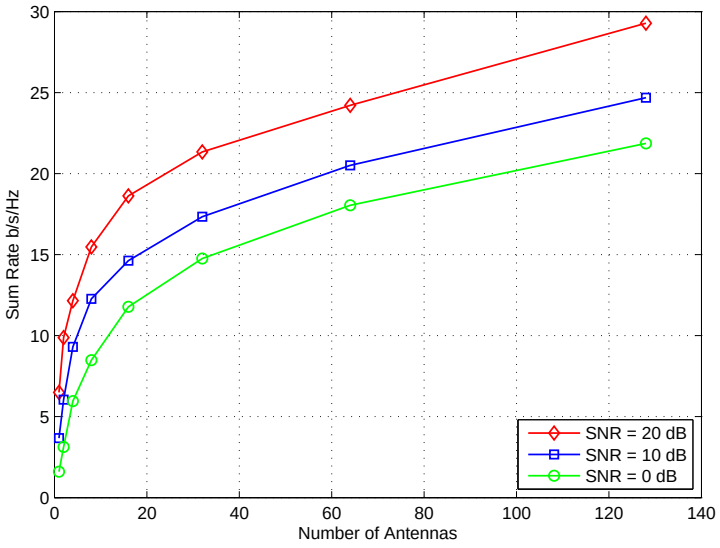

Figure 74. Throughput versus the number of employed antennas for different SNR levels using $K = 200$, and $\mu = 2$.

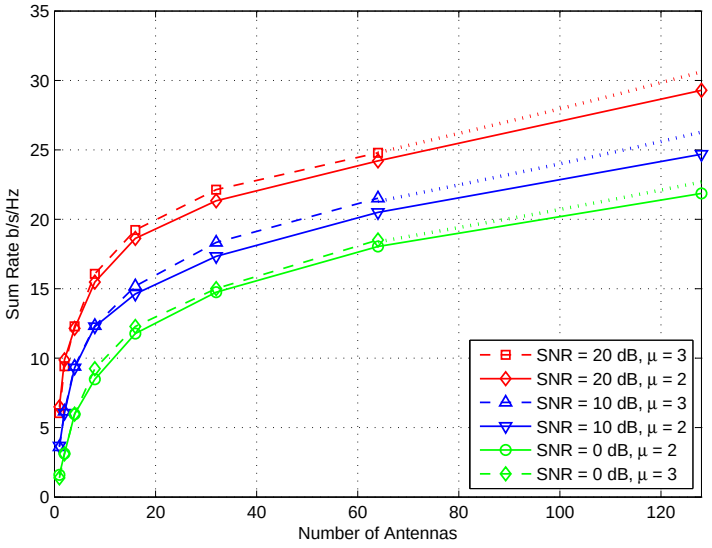

Figure 75. Throughput versus the number of employed antennas for different SNR levels using $K = 200$, and ($\mu = 3$, $\mu = 3$).

5.5 Summary

In this chapter we have proposed a large-scale MIMO wireless transceiver system, where we considered several important challenges facing such LS-MIMO system. We also, constructed downlink communication system with simple fair and limited-feedback user scheduler connected to random precoder. In this proposed system, receivers employ constrained partial group decoder to detect their desired signals. In addition, we evaluated the sum-rate performance of this LS-MIMO downlink system against the total number of users and SNR using various numbers of scheduled users and with different group-sizes of jointly decoded users. Furthermore, we investigated the effect of number of employed base station antennas in the proposed system throughput in different SNR levels and using two group-size options. Interestingly, our findings have shown encouraging performance for such simple transceiver to be candidate scheme for the large-scale MIMO communication systems.

6 TIGHT APPROXIMATION FOR THE ERGODIC AND EFFECTIVE CAPACITY OF LARGE-SCALE OPTIMAL SUCCESSIVE GROUP DECODING SYSTEM

6.1 Introduction

In this chapter we obtain a simple closed-form expression allows for tight approximation for the achieved capacity of the optimal successive group decoding (OSGD). Also, we produce an accurate approximation formula for the rate outage probability of this system. The result of this chapter has been included in our research work in (Abu-Ella & Elmusrati 2014a;b). Although several earlier analytical studies have used Gaussian distribution to model the achieved capacity of large-scale MIMO system based on linear precoding process, see for instance, (Ezio & Giorgio 2003; Guthy, Utschick & Honig 2013; Jung *et al.* 2013; Kamath & Hughes 2005; Smith & Shafi 2004), it is still to the best of our knowledge that there is no exact nor approximate closed-form expression describes the achieved capacity of the large-scale MIMO system which employs the successive group decoding schemes. The deep analysis of this system is avoided as a result of its nonlinear characteristics. However, because of the crucial importance of the group decoding techniques along with the large-scale MIMO, which expected to be a promising key 5G wireless technology (Wang *et al.* 2014), to achieve higher data rates, larger network capacity, better energy efficiency, higher spectral efficiency and more flexible mobility in wireless communication systems; and more importantly, because modeling wireless channel according to the connection quality of service (QoS) is vital for the next generation of wireless networks, we aim also in this chapter to consider the problem of formulating the effective capacity of the large-scale OSGD system.

We accomplished these objectives firstly by using the empirically generated functions to facilitate extracting good approximation for the probability density function of the achieved capacity distribution as a function of SNR and the number of antennas; this leads to the formulation of the rate outage probability of this system. Then, we considered the problem of formulating the effective capacity of the large-scale OSGD system. The last attained formula is essential to give better understanding for performance of the OSGD system, especially in the delay sensitive scenarios or regarding to any other QoS metric.

The reminder of this chapter is organized as follows: Section 6.2 describes the system model which we considered in this chapter. Section 6.3 discusses the formulation of the achieved capacity closed-form expression. Section 6.4 discusses the formulation of the rate outage probability expression. Section 6.5 analyze the effective value of the normally distributed capacity. Then we proceed to formulate the effective capacity of the OSGD system in Section 6.6. After showing the validation of the proposed formulas using numerical results in Section 6.7, we summarize our conclusions in Section 6.8.

6.2 System Model

Figures (76 and 77) represent the layout of the considered three-cell system, where the receiver of interest (UE_1 in the downlink scenario in Fig. 76 or BS_1 in the uplink scenario in Fig. 77) employs the OSGD technique to mitigate co-channel interference coming from the two interfering sources (BS_2, BS_3 in Fig. 76 or UE_2, UE_3 in Fig. 77).

We consider the temporally uncorrelated discrete model of slow-fading channel. In this chapter, we assume that both of the base station of interest and its designated client are equipped with large number (tens) of antennas N. Also, we assume that each base station and its intended client communicate with each other; but, due to the broadcasting nature of the wireless channel, the transmitted signal is received by other unintended destinations. The receiver of interest is only interested in the signal transmitted by its own designated transmitter; however, it is aware of the coding scheme employed by the other two transmitters and may choose to decode one or both of them only if it presumes doing that will assist the decoding of its intended signal. The received signal of this receiver at the nth symbol interval through this interference environment can be expressed by

$$\mathbf{y}[n] = \sqrt{P}\mathbf{H}_d\mathbf{x}_d[n] + \sqrt{\alpha_i P}\sum_{i=1}^{2}\mathbf{H}_i\mathbf{x}_i[n] + \mathbf{z}[n], \tag{6.1}$$

where $\mathbf{y}[n]$ is the $N \times 1$ received signal vector. In this system we assume a quasi-static Rayleigh fading scenario, i.e., the fading seen by the receiver of interest from its intended transmitter $\mathbf{H}_d$ and from the interfering transmitters $\mathbf{H}_i$ have a Rayleigh distribution, where the elements of those channels are generated as a normalized independent and identically distributed (i.i.d.) complex Gaussian random variables with zero mean and unit variance.

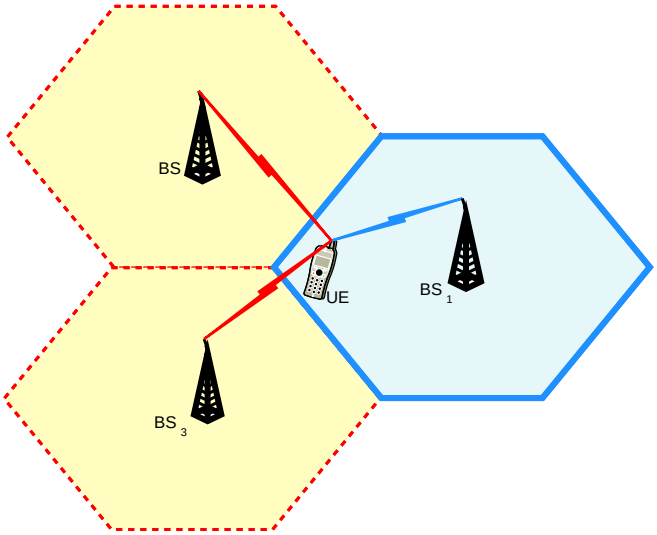

Figure 76. Downlink system

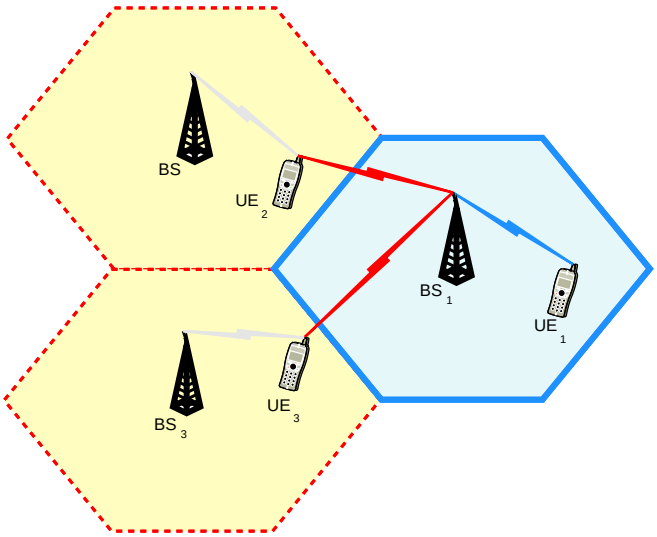

Figure 77. Uplink system

In this chapter, $\mathbf{H}_d$ is assumed to be perfectly known to the receiver of interest, but it is not known to any of the transmitters. $\mathbf{z}[n]$ is the $N \times 1$ complex AWGN vector at the receiver, it is assumed to have i.i.d. $\sim \mathcal{CN}(0,1)$ elements and it is temporally uncorrelated. P denotes the average transmit power from each transmitter. α_i stands for the cross-talk factor from the undesired transmitters, i.e., it represents the relative propagation path-loss of the interference channel, or the interference-to-signal power ratio between the desired user and the ith interfering user. Finally, $\mathbf{x}_d[n]$ and $\mathbf{x}_i[n]$ represents a unit power symbol vector transmitted from the desired and interfering user respectively during the nth time interval.

6.3 Achieved Capacity

6.3.1 Decodable Rate

For any two arbitrary disjoint sets $\mathcal{A}, \mathcal{B} \subseteq \mathcal{M}$, where $\mathcal{M}$ is the set of integer indices of all active users in the system, we assume that the receiver of interest is d. Then, the desired source will be transmitter d, and given the all user's rates $\boldsymbol{R} = [R_j]_{j \in \mathcal{M}}$. The instantaneous achievable rate region $\mathcal{C}_d(\mathcal{A}, \mathcal{B})$ can be described as in (Prasad & Wang 2009) by

$$\mathcal{C}_d(\mathcal{A}, \mathcal{B}) = \left\{ \boldsymbol{R} \in \mathbb{R}_+^{|\mathcal{A}|} : \sum_{j \in \mathcal{D}} R_j \leq \boldsymbol{\mathcal{R}}_d(\mathcal{D}, \mathcal{B}), \forall \mathcal{D} \subseteq \mathcal{A} \right\} \tag{6.2}$$

$$\boldsymbol{\mathcal{R}}_d(\mathcal{D}, \mathcal{B}) \leq \log \left| \mathbf{I} + \tilde{\mathbf{H}}_{\mathcal{D}}^{(d)\mathcal{H}} \left(\mathbf{I} + \tilde{\mathbf{H}}_{\mathcal{B}}^{(d)} \tilde{\mathbf{H}}_{\mathcal{B}}^{(d)\mathcal{H}} \right)^{-1} \tilde{\mathbf{H}}_{\mathcal{D}}^{(d)} \right| \tag{6.3}$$

where the channel realization

$$\tilde{\mathbf{H}}^{(d)} = \left[\sqrt{P}\mathbf{H}_d^{(d)}, \sqrt{\alpha_1 P}\mathbf{H}_1^{(d)}, \sqrt{\alpha_2 P}\mathbf{H}_2^{(d)} \right] \tag{6.4}$$

Considering the valid partition of $\mathcal{M}$ for the user of interest d: $\mathcal{Q}^d = \{\mathcal{G}_1^d, \ldots, \mathcal{G}_{p_d}^d, \mathcal{G}_{p_d+1}^d\}$, we can assume that all users of this partition can be decoded by the desired receiver only if

$$\boldsymbol{R}_{\mathcal{G}_m^d} \in \mathcal{C}_d(\mathcal{G}_m^d, \cup_{j=m+1}^{p_d+1} \mathcal{G}_j^d), \quad \forall m \in \{1, \ldots, p_d\} \tag{6.5}$$

for the valid partition $\mathcal{Q}^d$ of the receiver d we define $\mathbf{r}^d_{\mathcal{G}^d_m} = [r^d_j]_{j\in\mathcal{G}^d_m}$, Then, the fair rate increment which grantee that all users in $\{\mathcal{G}^d_1,\ldots,\mathcal{G}^d_{p_d}\}$ are decodable at the receiver d is defined by

$$r_d(\mathcal{Q}^d) \triangleq \max r^d_j, \quad \forall j \in \mathcal{M} \tag{6.6}$$

such that

$$\widetilde{\boldsymbol{R}}_{\mathcal{G}^d_m} = \boldsymbol{R}_{\mathcal{G}^d_m} + \mathbf{r}^d_{\mathcal{G}^d_m} \in \mathcal{C}_d(\mathcal{G}^d_m, \cup_{j=m+1}^{p_d+1}\mathcal{G}^d_j), \forall m \in \{1,\ldots,p_d\}, \tag{6.7}$$

Under the fairness (equal rate increment) constraint, and assuming that $\underline{\mathcal{Q}}^d$ ensembles all the valid partitions $\mathcal{Q}^d$, then, at the receiver d the maximum user rate increment is given by

$$r^*_{\mathcal{Q}^d} \triangleq \max_{\mathcal{Q}^d\in\underline{\mathcal{Q}}^d} r_d(\mathcal{Q}^d). \tag{6.8}$$

We can notice that solving (6.8) using the exhaustive search considering all combinations of $\mathcal{Q}^d$ is prohibitively complex. However, by defining the following rate margin metric

$$\triangle_d(\mathcal{D},\mathcal{B}) \triangleq \boldsymbol{\mathcal{R}}_d(\mathcal{D},\mathcal{B}) - \sum_{j\in\mathcal{D}} R_j, \tag{6.9}$$

and using the properly designed algorithm proposed in (Gong, Tajer & Wang 2011), we can find the optimal ordered partition $\mathcal{Q}^{d*}$ which minimizes the rate margin $\triangle_d(\mathcal{D},\mathcal{B})$, or equivalently maximizes the rate increment r_d, i.e.,

$$\begin{aligned}\mathcal{Q}^{d*} &= \arg\max_{\mathcal{Q}^d\in\underline{\mathcal{Q}}^d} r_d(\mathcal{Q}^d)\\ &= \arg\min \triangle_d(\mathcal{D},\mathcal{B})\end{aligned} \tag{6.10}$$

This leads to the maximum decodable rate, and therefore,

$$\widetilde{\boldsymbol{R}}_{\mathcal{G}^d_m} = \boldsymbol{R}_{\mathcal{G}^d_m} + \mathbf{r}^*_{\mathcal{G}^d_m}. \tag{6.11}$$

6.3.2 Distribution of Achieved Capacity

The brief description in Section 6.3.1 clarify the nonlinear characteristic of the achievable rate of the OSGD scheme. Therefore, it imposes the difficulty that limits the efforts to establish an analytical formulation of the capacity for such system. However, appertaining to importance of understanding the performance assessment of this system, we approach this problem by the following alternative path, which is, the empirically generated functions using the statistical analysis of large data set of collected observations from the system for wide range of SNR and using various number of antennas, in order to extract good approximation for the distribution of the system achieved capacity as a function of those two fundamental system design parameters.

Here it is worthy to noting that since we use only numerical results of Monte-Carlo simulation to produce the observations (statistics) used in this chapter to characterize the parameters of the system of interest; we therefore, collected according to the metric sample variance large enough number of samples in each considered case to ensure that all of our obtained formulas tightly fit the observations at high level of confidence, i.e., 95% at least.

Through the statistical analysis of the achieved capacity of the OSGD system, we notice that the distribution of the data significantly matches the normal distribution. In fact, among of other possible candidates, we chose the normal distribution because of its mathematical tractability for further analysis.

After choosing the distribution model, we start to look for a good way to estimate the parameters of this distribution. An effective way is the 2-D surface fitting; where we construct, test and modify our model to attain the best, i.e., the most accurate in terms of the mean square error (MSE) and more importantly, the simplest closed-form expression that replicate our large observation set.

Consequently, we claim that the distribution of the achieved capacity by the desired user in the large-scale OSGD system described in Section 6.2 can be tightly approximated by a normal distribution with mean equals μ_c and variance equals σ_c^2, i.e., $C \approx \mathcal{N}(\mu_c, \sigma_c^2)$.

To compute the best estimate for the normal distribution parameters, we used the least squares (LS) method. The basic idea of this approach is to minimize the sum

of the squared error of the estimated values,

$$\sum_i \mathcal{E}_i^2 = \sum_i \left(\mathcal{S}_i - \hat{\mathcal{S}}_i\right)^2 \tag{6.12}$$

where $\mathcal{S}_i$ and $\hat{\mathcal{S}}_i$ are the actual and the estimated sample value a quantity respectively.

6.3.3 Capacity Expected Value

Achieved capacity expected value μ_c or the ergodic capacity of the desired user using the OSGD technique depends on SNR level γ and the number of antennas N. From the statistics of the data that represent the mean value of achieved capacity, we have recognized that it can be modeled tightly at high confidence level $> 95\%$ as follows:

$$\hat{\mu}_c(\gamma, N) = a_m \log_2 \left(1 + \left[2\left(\frac{1}{N}\right)^{b_m} + c_m\right]\gamma\right) N \tag{6.13}$$

The above model can be simplified to the following form

$$\hat{\mu}_c(\gamma, N) = \frac{N}{a_m} \log_2 \left(1 + B_m \gamma\right) \tag{6.14}$$

where

$$B_m = \left[2\left(\frac{1}{N}\right)^{b_m} + c_m\right] \tag{6.15}$$

We can see that OSGD system capacity can be equivalently viewed as the capacity of N/a_m independent sub-channels with weighted SNR. The gap of achieved capacity comparing with capacity of full N-channel system is due to the non-orthogonality between those sub-channels, and the additional SNR loss because of the residual interference which treated as white noise instead of canceling it in case of receiving relatively low interference power. Therefore, for K-interfering users system with large N, it is reasonable to expect B_m to be less than K.

Now, we proceed to compute coefficients, a_m, b_m and c_m using the (LS) algorithm as follows:

$$\{a_m, b_m, c_m\}^{opt} = \arg \min_{a_m, b_m, c_m \in \mathbb{R}} \sum_i \mathcal{E}_i^2(\hat{\mu}_c) \tag{6.16}$$

where

$$\begin{aligned} \mathcal{E}_i(\hat{\mu}_c) &= \mu_c(i) - \hat{\mu}_c(i) \\ &= \mu_c(i) - a_m \log_2 \left(1 + \left[2\left(\frac{1}{N_i}\right)^{b_m} + c_m\right]\gamma_i\right) N_i \end{aligned} \tag{6.17}$$

$$\sum_i \mathcal{E}_i^2(\hat{\mu}_c) = \sum_i \left(\mu_c(i) - a_m \log_2 \left(1 + \left[2\left(\frac{1}{N_i}\right)^{b_m} + c_m\right]\gamma_i\right) N_i\right)^2 \tag{6.18}$$

To find the values of the model coefficients (a, b, and c) correspond to the minimum of the multivariate error function, we take the partial derivative of both sides of (6.18) with respect to each coefficient and force it to zero,

$$\frac{\partial \sum_i \mathcal{E}_i^2(\hat{\mu}_c)}{\partial a_m} = 0, \frac{\partial \sum_i \mathcal{E}_i^2(\hat{\mu}_c)}{\partial b_m} = 0, \frac{\partial \sum_i \mathcal{E}_i^2(\hat{\mu}_c)}{\partial c_m} = 0, \tag{6.19}$$

equivalently we have,

$$\begin{aligned} &\frac{\partial \sum_i \left(\mu_c(i) - a_m \log_2 \left(1 + \left[2\left(\frac{1}{N_i}\right)^{b_m} + c_m\right]\gamma\right) N_i\right)^2}{\partial a_m} = 0 \\ &\frac{\partial \sum_i \left(\mu_c(i) - a_m \log_2 \left(1 + \left[2\left(\frac{1}{N_i}\right)^{b_m} + c_m\right]\gamma\right) N_i\right)^2}{\partial b_m} = 0 \\ &\frac{\partial \sum_i \left(\mu_c(i) - a_m \log_2 \left(1 + \left[2\left(\frac{1}{N_i}\right)^{b_m} + c_m\right]\gamma\right) N_i\right)^2}{\partial c_m} = 0 \end{aligned} \tag{6.20}$$

Finally, by solving the system of equations in (6.20) according to the large set of collected data we have:

$$a_m = \frac{1}{3}, b_m = 3$$

and

$$c_m = \begin{cases} 2.637, & \gamma \leq 1 \\ 2.577, & 1 < \gamma \leq 2 \\ 2.5, & 2 < \gamma \end{cases} .$$

6.3.4 Capacity Variance

In this subsection we aim to model the variance of the achieved capacity σ_c^2. Considering the statistics of the collected data, we notice that the system capacity variance grows with SNR as a result of the increase of the capacity itself with SNR. This increase follows an upper bounded logistic function. From other point of view, through the carefully analysis of the statistics of the collected data, we observe, as expected, that increasing the number of employed antennas slightly decreases the variance of the system capacity. This reduction is tightly following a curve of power function. This behavior is expected, because the number of employed antennas N is a critical effecting factor on the system capacity, i.e., the system capacity is highly and positively correlated with the system size. Hence, in consonance with the law of large number, we expect that increasing the size of this antenna array should decrease the fluctuations (i.e., the variance) of any correlated function.

Therefore, we chose to express the variance using the following model:

$$\hat{\sigma}_c^2(\gamma, N) = \frac{a_v}{1 + (b_v N^{c_v} + d_v)\, \gamma^{-e_v}} \tag{6.21}$$

Then, using the similar steps of the procedure in 6.3.3, we compute the coefficients, a_v, b_v c_v, d_v and e_v through the (LS) algorithm as follows:

$$\{a_v, , b_v, c_v, d_v, e_v\}^{opt} = \arg \min_{a_v, b_v, c_v, d_v, e_v \in \mathbb{R}} \sum_i \mathcal{E}_i^2(\hat{\sigma}_c^2), \tag{6.22}$$

where

$$\begin{aligned} \mathcal{E}_i(\hat{\sigma}_c^2) &= \sigma_c^2(i) - \hat{\sigma}_c^2(i) \\ &= \sigma_c^2(i) - \left(\frac{a_v}{1 + (b_v N^{c_v} + d_v)\, \gamma^{-e_v}} \right) \end{aligned} \tag{6.23}$$

and,

$$\sum_i \mathcal{E}_i^2(\hat{\sigma}_c^2) = \sum_i \left(\sigma_c^2(i) - \left(\frac{a_v}{1 + (b_v N^{c_v} + d_v)\,\gamma^{-e_v}} \right) \right)^2 \tag{6.24}$$

To find the values of the model coefficients (a_v, b_v, c_v, d_v, and e_v) which satisfy the objective function in 6.22, we take the partial derivative of both sides of (6.24) with respect to each coefficient and equate the result with zero,

$$\frac{\partial \sum_i \mathcal{E}_i^2(\hat{\sigma}_c^2)}{\partial a_v} = 0, \frac{\partial \sum_i \mathcal{E}_i^2(\hat{\sigma}_c^2)}{\partial b_v} = 0, \frac{\partial \sum_i \mathcal{E}_i^2(\hat{\sigma}_c^2)}{\partial c_v} = 0, \tag{6.25}$$

$$\frac{\partial \sum_i \mathcal{E}_i^2(\hat{\sigma}_c^2)}{\partial d_v} = 0, \frac{\partial \sum_i \mathcal{E}_i^2(\hat{\sigma}_c^2)}{\partial e_v} = 0, \tag{6.26}$$

equivalently we have,

$$\begin{aligned}
&\frac{\partial \sum_i \left(\sigma_c^2(i) - \left(\frac{a_v}{1+(b_v N^{c_v}+d_v)\gamma^{-e_v}} \right) \right)^2}{\partial a_v} = 0, \\
&\frac{\partial \sum_i \left(\sigma_c^2(i) - \left(\frac{a_v}{1+(b_v N^{c_v}+d_v)\gamma^{-e_v}} \right) \right)^2}{\partial b_v} = 0, \\
&\frac{\partial \sum_i \left(\sigma_c^2(i) - \left(\frac{a_v}{1+(b_v N^{c_v}+d_v)\gamma^{-e_v}} \right) \right)^2}{\partial c_v} = 0, \\
&\frac{\partial \sum_i \left(\sigma_c^2(i) - \left(\frac{a_v}{1+(b_v N^{c_v}+d_v)\gamma^{-e_v}} \right) \right)^2}{\partial d_v} = 0, \\
&\frac{\partial \sum_i \left(\sigma_c^2(i) - \left(\frac{a_v}{1+(b_v N^{c_v}+d_v)\gamma^{-e_v}} \right) \right)^2}{\partial e_v} = 0
\end{aligned} \tag{6.27}$$

Finally, by solving the system of equations in (6.27) according to the collected set of data, we have:

$$a_v = 0.0934, b_v = -3, c_v = -2.5, d_v = \frac{4}{3} \quad \text{and} \quad e_v = 3$$

6.4 Rate Outage Probability

Assuming that the capacity of the user of interest in OSGD system can be accurately approximated by a normal distribution, i.e., $C \approx \mathcal{N}(\hat{\mu}_c, \hat{\sigma}_c^2)$ with mean

$\hat{\mu}_c$ and variance $\hat{\sigma}_c^2$ as expressed in (6.13) and (6.21) respectively. Then, the rate outage probability of this user for a certain target rate R_t can be expressed as the follow:

$$P_{outage}(R_t,\gamma,N) = F_C(R_t|\hat{\mu}_c,\hat{\sigma}_c^2) = \int_{-\infty}^{R_t} \frac{1}{\sqrt{2\pi}\hat{\sigma}_c} e^{\frac{-(c-\hat{\mu}_c)^2}{2\hat{\sigma}_c^2}} dc, \tag{6.28}$$

using the normalized normal distribution, the rate outage probability can be simplified to:

$$P_{outage}(R_t) = 1 - Q(\Upsilon), \tag{6.29}$$

where the normalized target rate Υ is given by

$$\Upsilon = \frac{R_t - \hat{\mu}_c}{\hat{\sigma}_c}. \tag{6.30}$$

6.5 Effective Value of the Normally Distributed Capacity

Assuming a block fading scenario with frame duration T, the formula of the effective capacity can be expressed as follows(Gursoy 2011),

$$\alpha_c \triangleq \frac{-1}{T\theta} \log_e \left(\mathbb{E}\left\{ e^{-T\theta C[i]} \right\} \right) \tag{6.31}$$

where $C[i]$ is the instantaneous achieved capacity sample values.

Now, assuming that the achieved capacity of a system has a normal distribution with mean μ_c and variance σ_c^2, i.e.,

$$C \sim \mathcal{N}(\mu_c, \sigma_c^2), \tag{6.32}$$

and let's define the random variable Z as follows,

$$Z = e^{-\hat{\theta}C} \tag{6.33}$$

where, $\hat{\theta} = T\theta$

To find the effective capacity, we should find the natural logarithm of the expected value of Z. Since C assumed to have normal distribution, then, the distribution of $\hat{\theta}C$ also normal, but with scaled mean and variance, (see (Norstad 1999)).

It is known that if

$$X \sim \mathcal{N}(\mu, \sigma^2), \tag{6.34}$$

then,

$$(aX + b) \sim \mathcal{N}(a\mu + b, a^2\sigma^2). \tag{6.35}$$

Therefore, the distribution of the random variable $\Gamma = -\hat{\theta}C$ can be expressed as follows,

$$\Gamma \sim \mathcal{N}(-\hat{\theta}\mu_c, \hat{\theta}^2\sigma_c^2) \tag{6.36}$$

Subsequently, as it is well know that the exponential of normal random variable has log-normal distribution. Therefore, Z is distributed according to log-normal distribution with corresponding normal distribution mean $-\hat{\theta}\mu_c$ and variance $\hat{\theta}^2\sigma_c^2$, i.e.,

$$\begin{aligned} f_Z(z) &= \frac{1}{z\sigma_z\sqrt{2\pi}} e^{\frac{(-\log(z)-\mu_z)^2}{2\sigma_z^2}} \\ &= \frac{1}{z\hat{\theta}\sigma_c\sqrt{2\pi}} e^{\frac{(-\log(z)-\hat{\theta}\mu_c)^2}{2\hat{\theta}^2\sigma_c^2}} \end{aligned} \tag{6.37}$$

Now, since the expected value of the log-normal random variable Z as shown in (Norstad 1999) is given by,

$$\begin{aligned} \mathbb{E}(Z) &= \mu_z \\ &= e^{\mu + \frac{1}{2}\sigma^2} \end{aligned} \tag{6.38}$$

where μ and σ^2 are the mean and variance of its corresponding normal random variable Γ. It is clear that the expected value of Z is given by

$$\mathbb{E}(Z) = e^{-\hat{\theta}\mu_c + \frac{1}{2}\hat{\theta}^2\sigma_c^2} \tag{6.39}$$

As a final step, we take the natural logarithm of the expected value of Z and multiply it with $\frac{-1}{\hat{\theta}}$, then, we have,

$$\begin{aligned} \alpha_c &= \frac{-1}{\hat{\theta}} \log_e \left(e^{-\hat{\theta}\mu_c + \frac{1}{2}\hat{\theta}^2\sigma_c^2} \right) \\ &= \mu_c - \frac{1}{2}\hat{\theta}\sigma_c^2 \end{aligned} \tag{6.40}$$

The final result represents the effective capacity of the system. Also it reflects the intuitive understanding for the effective capacity, which we can express as follows,

$$\alpha_c = C - \mathcal{E}(\sigma_c^2, \hat{\theta}) \tag{6.41}$$

where $\mathcal{E}(\sigma_c^2, \hat{\theta})$ is rate margin (offset) depends on the variance of the achieved capacity σ_c^2 and the system QoS constraints expressed by the metric $\hat{\theta}$. Therefore, for a very strict QoS requirement, i.e., large $\hat{\theta}$ the gap between the ergodic and effective capacity will increase. On the other hand, when $\hat{\theta} \to 0$, i.e., very loose QoS, effective capacity converges to the ergodic capacity.

6.6 OSGD Effective Capacity

In this part we aim to obtain a closed-form expression for effective capacity of the large-scale OSGD system. According to 6.3.2 the distribution of the achieved capacity of the large-scale OSGD systems can be accurately approximated by normal distribution with mean $\hat{\mu}_c$ and variance $\hat{\sigma^2}_c$. Therefore, we can apply the result in (6.40) to find the effective capacity of this system as follows,

$$C \approx \mathcal{N}(\hat{\mu}_c, \hat{\sigma}_c^2) \tag{6.42}$$

with an expected value $\hat{\mu}_c$ expressed as a function of SNR γ and the number of antennas N as given by (6.13) and with variance expressed in an inverted exponential function of SNR as presented in (6.21).
Now, by invoking the expressions of $\hat{\mu}_c$ and $\hat{\sigma}_c^2$ into (6.40) we have

$$\alpha_c = a_m \log_2 \left(1 + \left[2 \left(\frac{1}{N} \right)^{b_m} + c_m \right] \gamma \right) N - \frac{1}{2}\hat{\theta} \left(\frac{a_v}{1 + (b_v N^{c_v} + d_v)\gamma^{-e_v}} \right) \tag{6.43}$$

which represents the effective capacity for the large-scale OSGD system.

6.7 Numerical Results

This section shows the significant agreement between the obtained closed-form approximation formulas and the Monte-Carlo simulation results of the described system in Section 6.2. In this section we present the numerical results carried out by simulating 3-interfering user system deploying large-scale MIMO OSGD scheme. In all of the following scenarios, we assume strong interference environment, i.e., the $\alpha_i = 1$.

6.7.1 Validation of the Normal Distribution Approximation

The correctness of our proposal of assuming that the normal distribution represents the overall distribution of the achieved capacity of the OSGD system is assured by the close agreement between the proposed and simulated probability density function (p.d.f.) and cumulative distribution function (c.d.f.) of the system achieved capacity considering different number of antennas and also for different SNR levels as depicted in figures (78, 79, 80 and 81).

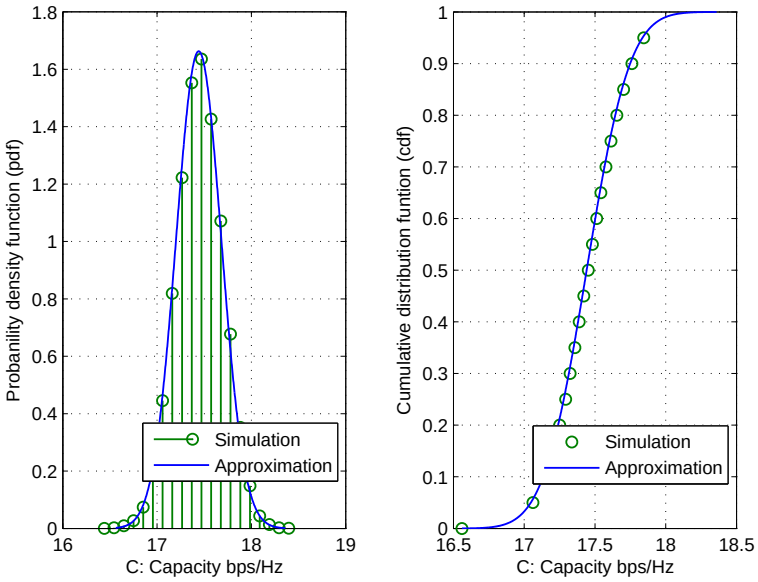

Figure 78. Pdf and CDF of achieved capacity for $SNR = 3$ dB and $N = 20$.

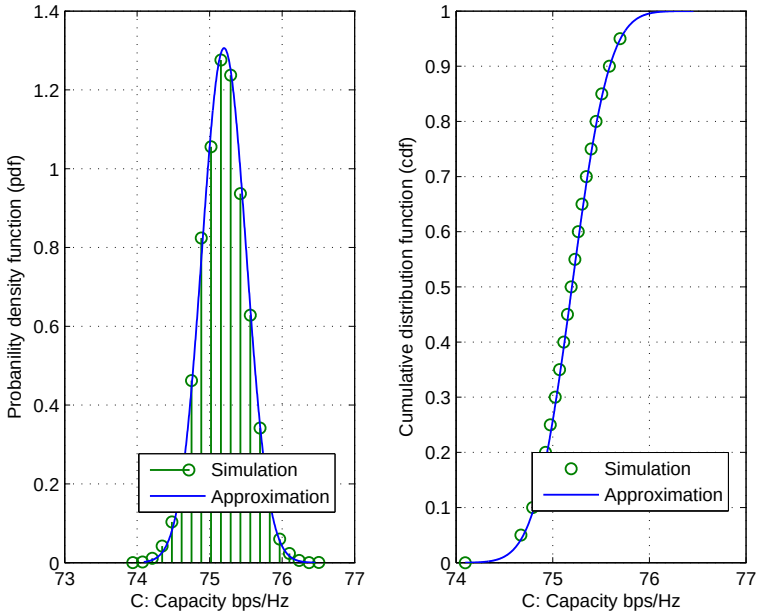

Figure 79. Pdf and CDF of achieved capacity for $SNR = 30$ dB and $N = 20$.

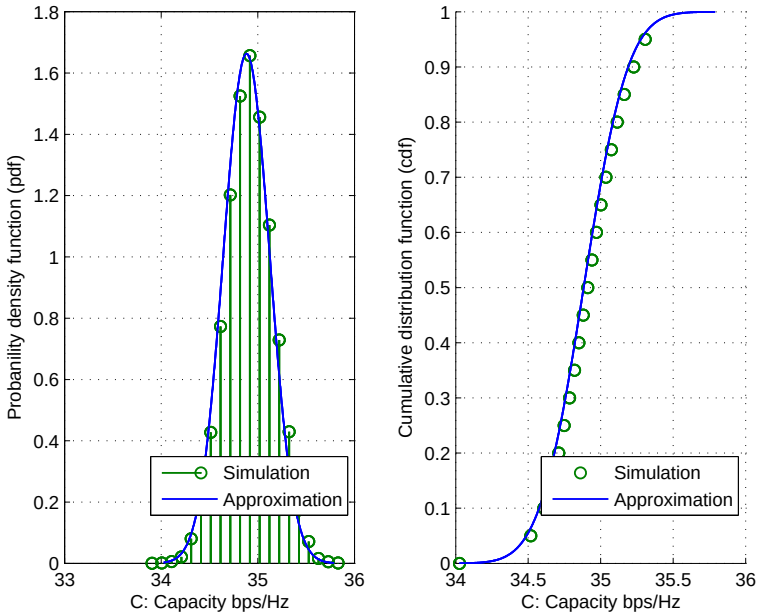

Figure 80. Pdf and CDF of achieved capacity for $SNR = 3$ dB and $N = 40$.

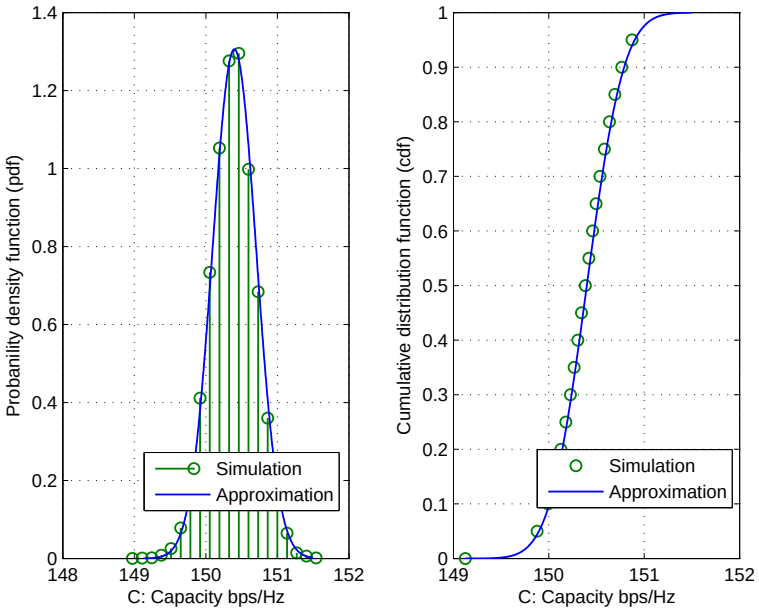

Figure 81. Pdf and CDF of achieved capacity for $SNR = 30$ dB and $N = 40$.

For deeper insight about the goodness of the proposed approximation, we plot the simulation results of the achieved capacity versus the number of antennas N and the SNR in decibel, then, we over plot this graph with a grid of generated points using the proposed approximation formulas in the same figure. The 3-D plots for the mean values of achieved capacity using the simulation and the coordinated points result from the approximation formula in Fig. 82 shows the match between both surfaces. In addition to that, we evaluated the residual between the two surfaces, we compute the MSE between the simulation and the approximation points, and it is found to be less than 8×10^{-3}.

Similarly, Fig. (83 shows the match between the approximation values and the simulation-generated values for the capacity variance. Here also, we compute the MSE between the simulation and the approximation points and it is less than 5×10^{-7}.

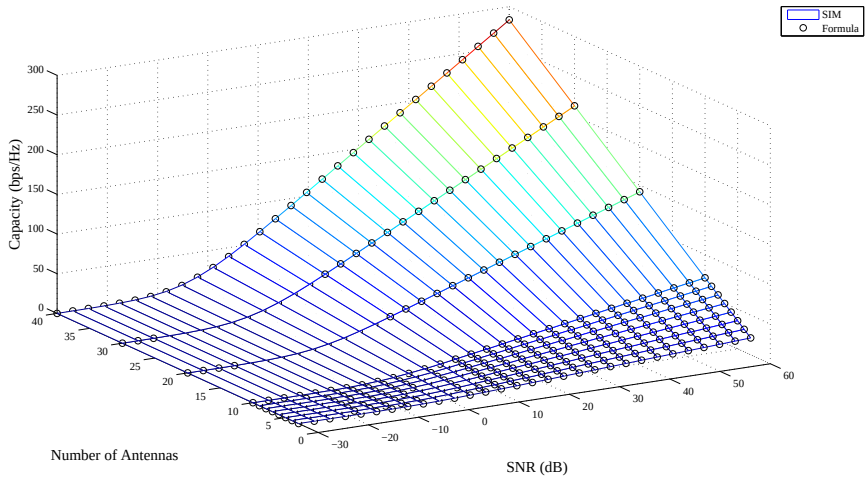

Figure 82. Mean capacity versus SNR (dB) and the number of antennas.

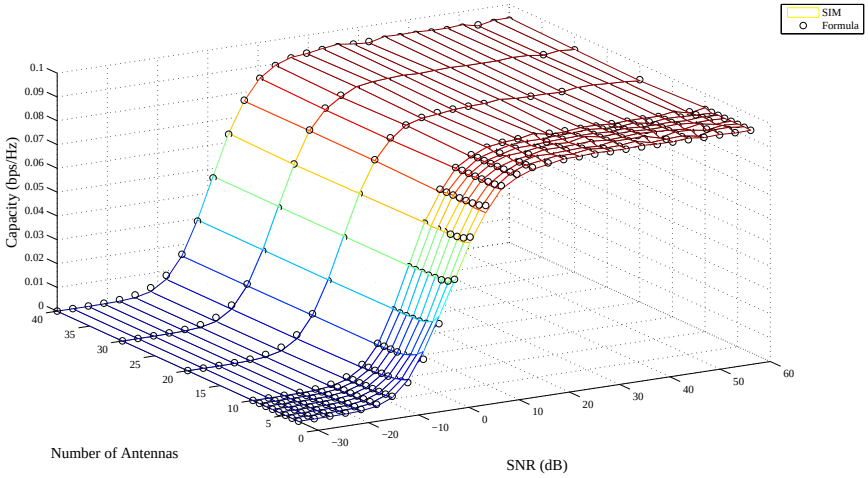

Figure 83. Capacity variance versus SNR (dB) and the number of antennas.

6.7.2 Validation of Rate Outage Probability Formula

In this subsection, we aim to show the goodness of the obtained rate outage probability formula. Therefore, we contrast the results obtained through the simulation of OSGD system in different scenarios with the results generated by the proposed formula. In the first case shown in Fig. 84, we employ (16×16)-MIMO OSGD system with target rate of 20 bps/Hz, and we use also (32×32)-MIMO system with target rate of 30 bps/Hz. In the second case depicted in Fig. 85, we deploy (20×20, 30×30 and 40×40)-MIMO OSGD system to achieve target rate of (20, 30 and 40) bps/Hz respectively. All the considered scenarios reveal good match between the system simulation results and the proposed approximation expression.

6.7.3 Validation of the Effective Capacity Formula

In this subsection we use numerical results obtained from the simulation to validate the proposed closed-form expression for the effective capacity. Therefore, we run the Monte Carlo setup to compute the effective capacity of the large-scale OSGD system. We consider low and high SNR scenarios for different MIMO configuration sizes. In all cases as shown in figures (86, 87, 88, 89 and 90) we can see the close match between the simulated and the analytical results for the effective capacity.

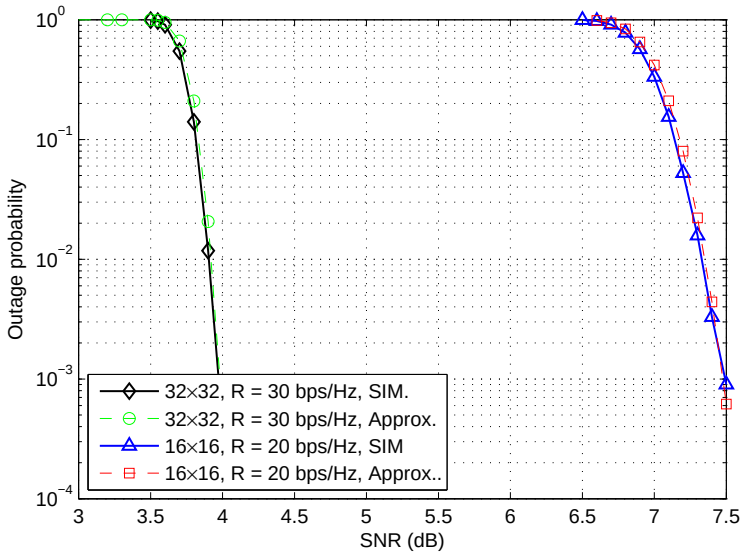

Figure 84. Outage probability of the $(16 \times 16$ and $32 \times 32)$-MIMO OSGD system.

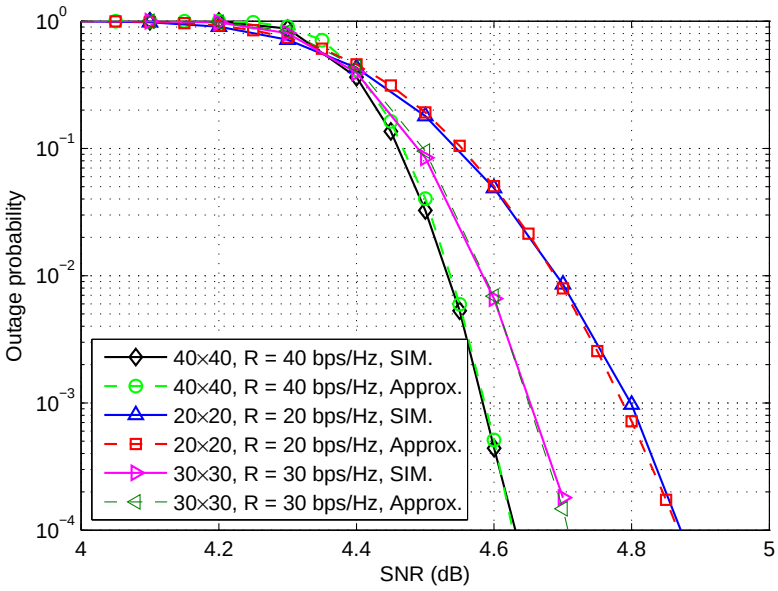

Figure 85. Outage probability of the $(20 \times 20,\ 30 \times 30$ and $40 \times 40)$-MIMO OSGD system.

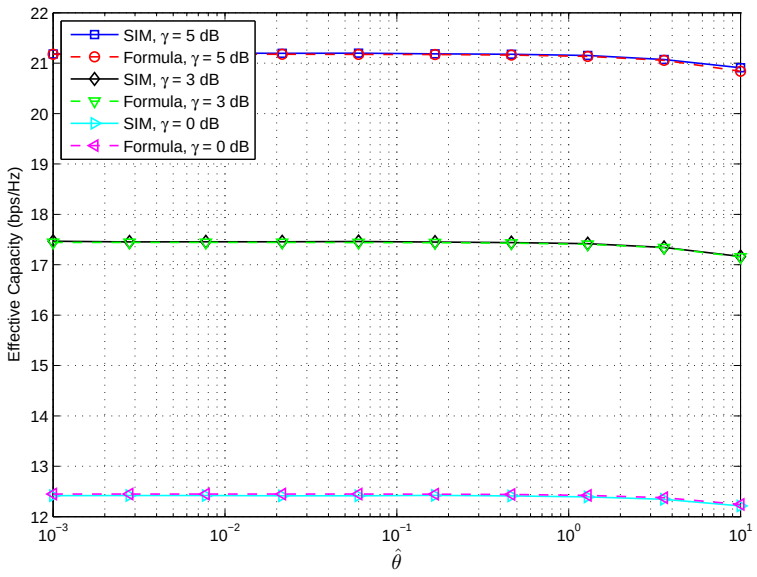

Figure 86. Effective capacity versus $\hat{\theta}$, with different low SNR levels for OSGD using $N = 20$.

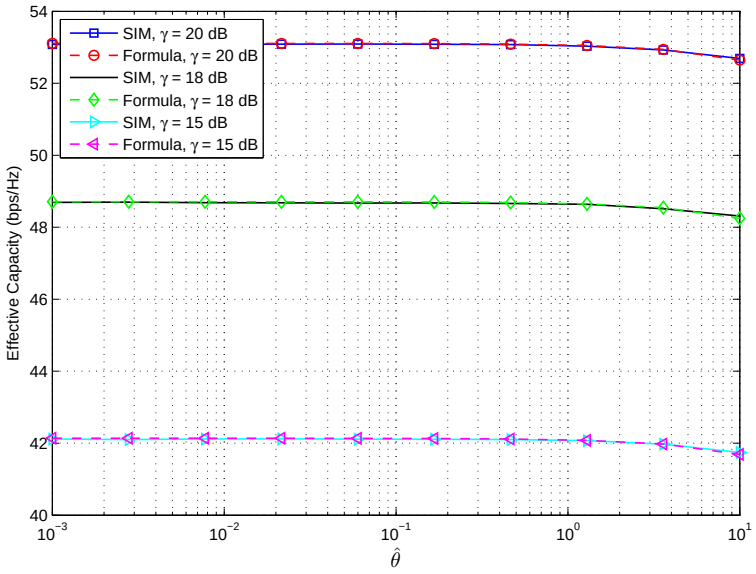

Figure 87. Effective capacity versus $\hat{\theta}$, with different high SNR levels for OSGD using $N = 20$.

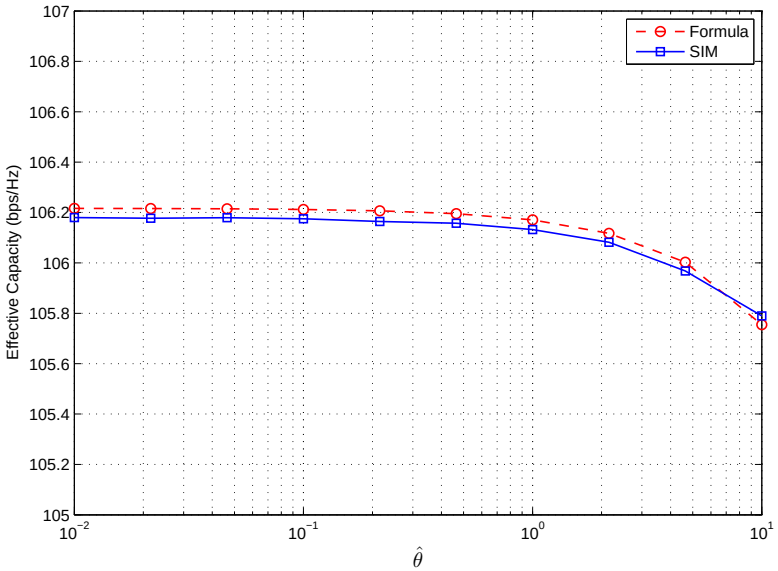

Figure 88. Effective capacity versus $\hat{\theta}$, with SNR = 20 dB levels for OSGD using $N = 40$.

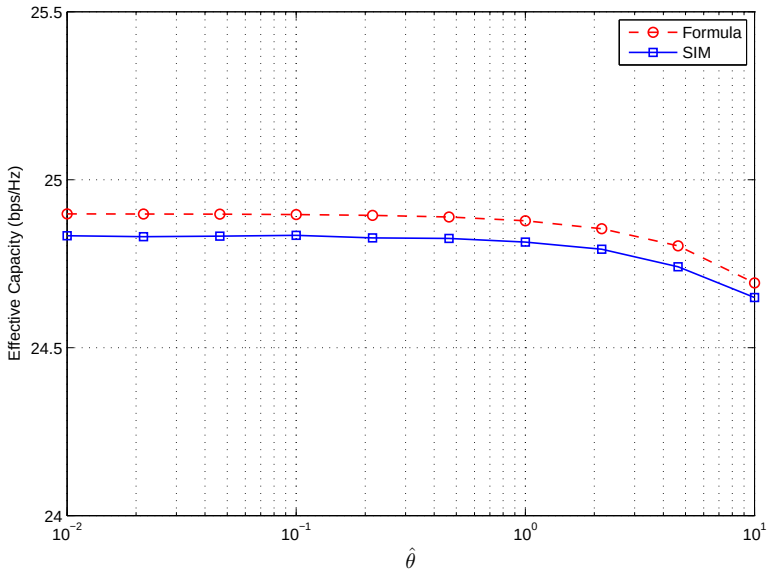

Figure 89. Effective capacity versus $\hat{\theta}$, with SNR = 0 dB levels for OSGD using $N = 40$.

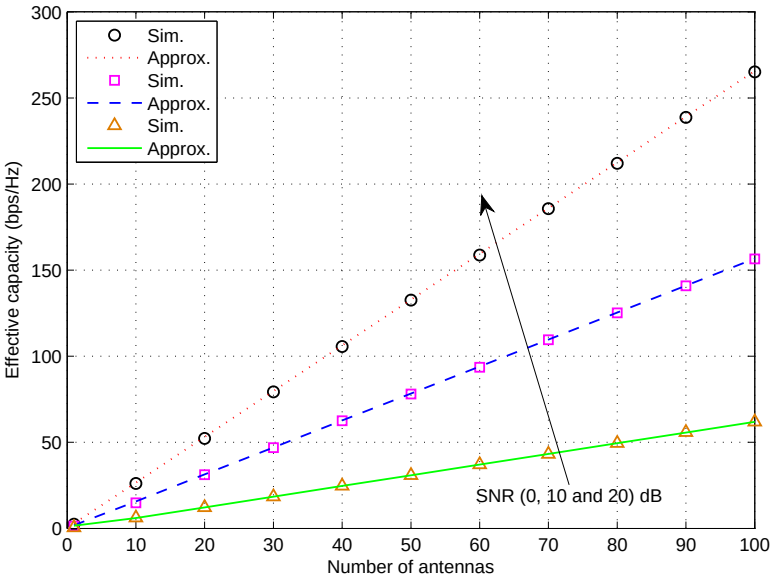

Figure 90. Effective capacity versus number of antennas (N), for OSGD system with SNR $(\gamma = 0, 10$ and $20)$ dB and $\hat{\theta} = 10$.

6.8 Summary

In this chapter we obtained a simple closed-form approximation for the desired user achieved capacity in the large-scale OSGD system. Also we produced a tight approximation expression for the rate outage probability of this system. It is clear that for largely enough system, the mean or ergodic capacity of the system increases linearly with the increase of number of antennas N, and logarithmically with SNR γ. We notice also that the variance of the system capacity is increasing with SNR following an upper bounded logistic model function. On the other hand this variance is inversely and slightly proportional (as a power function) to the increase of the system size N. Finally, in the last part of this chapter, we have proposed a closed-form expression to formulate the effective capacity of the large-scale OSGD system.

7 CONCLUSIONS AND PROSPECTIVE WORK

This chapter summarizes the contributions of this thesis, and it discusses some aspects of the practicality of studied schemes. Also, it outlines the possible prospective research openings related to this work, where some issues seem to be very interesting for more future studies.

7.1 Conclusions

In this thesis we have widely investigated the performance of optimal successive group decoding (OSGD), the recently proposed interference mitigation technique build on the successive group interference cancellation strategy for the multi-antenna systems. Initially, we investigated the OSGD performance in terms of its (ergodic, effective) capacity. Then, we inspected its bit error rate, and outage probability performance in different scenarios. In addition, we evaluated its required energy per bit against different quality of service guarantee levels. In this thesis we take into account both the spatially correlated and uncorrelated (Rayleigh and Rician) fading channels. Likewise, we explored OSGD performance in various SNR and SIR settings, where we considered the power-limited and bandwidth-limited regimes, with different cross-talk values, using several transmit-receive MIMO antenna scales. Our numerical findings in this monograph disclosed that OSGD technique can demonstrate very effective capability to cope with interference in the explored cases, reviling its competency comparing with the other advanced interference cancellation mechanisms. This makes OSGD a promising scheme for interference reduction; essentially, if we recall again that OSGD is a passive interference mitigation technique, i.e., it relies only on receiver-based processing. Additionally, if we ponder in the alleviation of its computational complexity, due to its innate complexity controlling feature, comparing with the large computational cost of its counterpart interference cancellation techniques, e.g., ML-MUD or the iterative interference alignment schemes.

Also, in this work we researched the performance of the CPGD scheme in MIMO interference channel system, in the sake of exploring its capability to suppress interference effects in wireless communication networks. Here also our study outcomes have shown the upper hand of the CPGD comparing to other interference cancellation methods.

By the same token, we delved into exploring the CPGD technique functionality and assessed its capability to manage and mitigate interference in the uplink multicell MIMO system. The obtained achieved per-cell capacity and BER results of this part showed that the CPGD technique enjoys very competitive performance comparing with the classical MMSE-based FDMA and TDMA schemes.

Moreover, we have introduced new large-scale MIMO transceiver design for wireless communication systems, where we presented several major difficulties impaling the practical implementation of this system. As well as, we have suggested solutions for those problems. Interestingly, our findings showed encouraging results for the proposed transceiver system to be a processing choice for the large-scale multiantenna communication systems.

Furthermore, because of the vital importance of the successive group decoding mechanism along with the large-scale MIMO which is expected to be a favorable key 5G wireless technology, to achieve higher data rates, larger network capacity, better energy efficiency, higher spectral efficiency and more flexible mobility in wireless communication networks. We have worked through this thesis to obtained uncomplicated closed-form expression allows for good approximation to describe the achieved capacity of the OSGD with LS-MIMO system. In conjunction, we have produced an accurate approximation formula to describe the rate outage probability of this system. Finally, we have originated a closed-form expression to indicate the effective capacity of the large-scale OSGD scheme as a function of the system SNR and the number of antennas. These explicit forms can give better appreciation for the evaluated performance of this system. Also they simplify the comprehensive characterization of this system according to the QoS requirements.

7.2 Practicality and Other Issues

This thesis is dedicated to study the use of successive group decoding techniques to mitigate interference in multiantenna systems. Through overall this research work our first concern was to consider simplicity and practicality issues. Therefore, we have not confined our options to only considering the most optimal schemes, instead, we were interested also in developing suboptimal techniques that achieve, as best as possible, the trade-off between the system requirements and performance.

The term *system requirements* here includes: feed-back overhead, hardware implementation requirements, and arithmetic computational complexity.

In this thesis we have frequently pointed out the feed-back issue, simply because there is a trade-off between the performance improvement through coordination and the consumed system resources in terms of frequency band or time, i.e., (rate or latency, etc.) which must sacrificed to accomplish this coordination. In this sense, both of OSGD and CPGD schemes require limited information exchange among the different users, i.e., the only level of needed coordination is exchanging rate increment information, which is typically a scalar real value for each user.

Through this thesis, an obvious example for our strategy to limit feed-back is in Chapter 5, where we have proposed the transceiver design for the large-scale MIMO system. We have tried to reduce the feed-back in this system as much as possible. Therefore, we have proposed the use of random precoder, to avoid the need for CSI at the transmitter side. One of the advantages of this proposal design is the operational mode flexibility, since it does not assume the availability of CSI at the transmitter-side. Therefore, this system can work in both operation modes, i.e., FDD and TDD modes, which allows for employing this system in wide range of practical applications. In addition, the scheduling strategy we have deployed in our proposal design relays on a limited feed-back with $(\log_2 N)$-bits for each user, where N is the number of base station antennas.

From other point of view, hardware implementation and construction of OSGD and CPGD systems is preferable; simply because these schemes are originally based on successive interference cancellation algorithms. Of course, the advantage of successive interference cancellation algorithms in terms of hardware complexity is obvious comparing with other schemes, such as, parallel interference cancellation algorithms; especially, for large-scale systems, where the implementation cost related to the scalability of the system is an important limiting factor for the profitable industrial process.

On the other hand, taking into account the associated delay of the conventional serial decoding algorithms, we can say that, both OSGD and CPGD are effectively bridging the gap between the PIC and SIC schemes, since they are based on constrained group instead of single user decoding algorithms.

To elaborate the last point more we say, since decoding techniques considered in this thesis are based on group decoding algorithms, this may raise a question

about the associated complexity of such techniques. Regarding this issue we say, the beauty of the OSGD, and CPGD schemes comes from their substantial feature, as they can be implemented with different levels of complexity, we may call this aspect as (complexity-flexibility) feature. Generally, successive group decoding schemes can be implemented with low complexity as the conventional successive single-user decoder, to the high complexity of maximum likelihood decoder. This feature is controlled through imposing a constraint on the decoding group-size. So, the system can adopt the decoder with the adequate complexity and latency that each receiver can tolerate. Obviously, communication system using these techniques can adapt and enhance its performance depending on the intelligence and the availability of its resources. This can lead to the establishment of very adaptive systems with flexible trade-off between the available resources and enjoyed performance.

Finally, regarding the addressed scheme robustness, we declare that both OSGD and CPGD have no stability concerning issues, since their kernel algorithms are not implemented based on iterative process. This fact leads to the elimination of all related aspects and problems, such as, the convergence speed, the initial values problems, numerical round-off errors, etc.

7.3 Prospective Work

Although we have tried to extensively study the optimal successive, and the constrained partial group decoding techniques, and we have tried to widely investigate their performance to mitigate interference in wireless systems. There are still many open issues related to this work need further investigation, and they are suitable and interesting for future research. Some examples of these topics are listed below.

- Studying the use of successive group decoding techniques in the cognitive radio systems. This study may include several topics, such as, a thorough investigation of utilizing those techniques to mitigate the interference effects caused by the short-time collusion between the primary and the secondary users.
- Also, further and more comprehension studies can be launched using advanced network simulator toolkits, to assess the performance of the addressed techniques in more realistic, i.e., with larger number of users, and with much more complicated scenarios.

- Extending the asymptotic analysis of the investigated systems in this thesis to establish more integrated closed-form expressions to describe the effect of the different parameters, e.g., the strength of the interference, the number of interfering sources, and the spatial correlation coefficient.

- Studying the adaptation of new joint detection schemes with less computational complexity to use them as an alternative for the ML decoder in the case of full group detection mode. Also, studying other semi-optimal, or hybrid adaptive successive decoding schemes to reduce the complexity of determining the substage partitions and decoding order.

- Inspecting the utilization of the quantum searching algorithm and the huge opportunities that they could open for implementing successive group decoding techniques in the future communication networks.

- Another interesting open issue to consider for future work is the utilization of partial coordination between the co-located users. As shown in this thesis, OSGD and CPGD schemes decode the desired user by successive cancellation of the interfering users. However, these techniques still treat the very weak interference as noise. This is can be avoided if the co-located users, who are most likely to have correlated channels, can somehow exchange more information about interference. This information can be used to strengthen the weak interference, so the employed group decoder can totally eliminate it instead of treating it as noise. This can significantly enhance the estimation of desired signal, and also, improve the achieved transmission rate of the intended user.

- Last but not least, the work in this thesis can be used as a starting point to launch comprehensive studies to investigate the opportunities and explore the advantages of the integration between several promising and recently introduced technologies, for example, studying the deployment of successive group interference cancellation techniques at the receive side, which can be facilitated through the utilization of the intelligence of the recently introduced terminal devices. Furthermore, performance of such techniques can be significantly boosted by the use of multiple antennas at the terminal nodes. Also, in its tern, multiantenna technology is potentially applicable for the future end-user nodes through the utilization of the millimeter wave technologies.

REFERENCES

Abu-Ella, O. & Elmusrati, M. (2014). Tight Capacity Approximation of 3-User System using Large-Scale MIMO Optimal Successive Group Decoding. *Submitted to: IEEE Transactions on Wireless Communications*.

Abu-Ella, O. & Elmusrati, M. (2014). Capacity Approximation of Massive MIMO with Optimal Successive Group Decoding System. *Eighth International Conference on Next Generation Mobile Apps, Services and Technologies.* University of Oxford, Oxford, UK. Seb 2014, 254–259.

Abu-Ella, O. & Elmusrati, M. (2014). Partial Constrained Group Decoding: A New Interference Mitigation Technique for the Next Generation Networks. *New Technologies, Mobility and Security (NTMS), 2014 6th International Conference on.* Zayed University, Dubai, UAE. March 2014, 1–5.

Abu-Ella, O. & Elmusrati, M. (2014). Optimal Successive Group Decoding to Mitigate Interference in Wireless Systems. *Distributed Computing in Sensor Systems (DCOSS), 2014 IEEE International Conference on*. Marina Del Rey, CA, USA. May 2014, 322–326.

Abu-Ella, O. & Elmusrati, M. (2014). Interference Mitigation Using Optimal Successive Group Decoding for Interference Channels. *Almadar Journal for Communications, Information Technology, and Applications.* July 2014, 1:1, 37–54.

Abu-Ella, O. & Elmusrati, M. (2014). Performance of the Optimal Successive Group Decoding with Imperfect Channel Estimation. *Submitted to: Antennas and Wireless Propagation Letters, IEEE.*

Abu-Ella, O. & Wang, X. (2013). Interference mitigation via constrained partial group decoding for uplink multicell MIMO systems. *International Conference on Electronics and Communication Engineering (ICECE 2013). World Academy of Science, Engineering and Technology* Istanbul, Turkey. 78:6, 1813–2013.

Abu-Ella, O. & Wang, X. (2013). Large-scale multiple-input-multiple-output transceiver system. *Communications, IET* 7:5, 471–479.

Adve, R. (2007). MIMO systems and transmit diversity. [Web document] [Cited in 2013]. Available at:`http://www.comm.utoronto.ca/~rsadve/Notes/DiversityTransmit.pdf`, 2007.

Airy, M., Shakkattai, S. & Jr. Heath, R. (2003). Spatially greedy scheduling in multi-user MIMO wireless systems. *Signals, Systems and Computers, 2003. Conference Record of the Thirty-Seventh Asilomar Conference on.* 1:11, 982–986.

Alamouti, S. (1998). A simple transmit diversity technique for wireless communications. *Selected Areas in Communications, IEEE Journal on.* 16:8, 1451–1458.

Khan, F. & Pi, J. (2011). Millimeter-wave Mobile Broadband: Unleashing 3-300GHz Spectrum. [Web document] [Cited in 2011]. Available at:`http://wcnc2011.ieee-wcnc.org/tut/t1.pdf`, Samsung, March 28, 2011.

Basir, A. (2013). 3GPP long term evolution (LTE) [Web document]. [Cited in 2013]. Available at:`http://4g-lte-world.blogspot.fi/2012/06/icic-and-eicic.html`, 2012.

Bentrcia, A. & Alshebeili, S. (2014). Competitive linear parallel interference cancellation detection based on monotone line-search techniques. *Signal Processing, IET.* 8:5, 521–529.

Biglieri, E., Calderbank, R., Constantinides, A., Goldsmith, A., Paulraj, A. & Poor, H. (2007). *MIMO Wireless Communications.* Cambridge University Press, New York, NY, USA, 2007.

Boccardi, F., Heath, R.W., Lozano, A., Marzetta, T.L. & Popovski, P. (2014). Five disruptive technology directions for 5G. *Communications Magazine, IEEE.* 52:2, 74–80.

Botsinis, P., Ng, S. & Hanzo, L. (2013). Quantum search algorithms, quantum wireless, and a low-complexity maximum likelihood iterative quantum multi-user detector design. *Access, IEEE.* 1, 94–122.

Brennan, D. G. (1959). Linear Diversity Combining Techniques. *Proceedings of the IRE.* 47:6, 1075–1102.

Brydon, A. (2014). Opportunities and threats from LTE Device-to-Device (D2D) communication [Web document]. [Cited in 2014]. Available at:`http://www.unwiredinsight.com/2014/lte-d2d`, 28 FEBRUARY 2014.

Cadambe, V.R.; Jafar, S.A. (2008). Interference Alignment and Spatial Degrees of Freedom for the K User Interference Channel. *Communications, 2008. ICC '08. IEEE International Conference on*, 19–23.

Chang, C., (1994). Stability, queue length, and delay of deterministic and stochastic queueing networks. *Automatic Control, IEEE Transactions on.* 39:5, 913–931.

Chang, C. (2000). *Performance Guarantees in Communication Networks.* Springer-Verlag, London, UK, UK, 2000.

Chatzinotas, S., Imran, & Hoshyar, R. (2009). On the multicell processing capacity of the cellular MIMO uplink channel in correlated rayleigh fading environment. *Wireless Communications, IEEE Transactions on.* 8:7, 3704–3715.

Chatzinotas, S., Imran, M. & Tzaras, C. (2008). Uplink capacity of MIMO cellular systems with multicell processing. *Wireless Communication Systems. 2008. ISWCS '08. IEEE International Symposium on.* 453–457.

Chen, Y., Yu, G., Zhang, Z., Chen, H.-H, & Qiu, P. (2008). On cognitive radio networks with opportunistic power control strategies in fading channels. *IEEE Transactions on Wireless Communications.* 7:7, 2752–2761.

Choi, J. (2013). Precoding and Massive MIMO [Web document]. [Cited in 2014]. Available at:`http://www.mobile.ecei.tohoku.ac.jp/COE/workshop_2013_10/pdf/Choi.pdf`, Oct., 2013.

Chuah, C., Tse, D., Kahn, J. & Valenzuela, R. (2002). Capacity scaling in MIMO wireless systems under correlated fading. Information Theory. *Information Theory, IEEE Transactions on.* 48:3, 637–650.

Cirkic, M. & Larsson, E. G. (2012). SUMIS: A Near-Optimal Soft-Ouput MIMO Detector at Low and Fixed Complexity. *CoRR abs/1207.3316*.

Corless, R. M., Gonnet, G. H., Hare, D. E. G., Jeffrey, D. J. & Knuth, D. E. (1996). On the Lambert W Function. *In Advanced in Computational Mathematics.* 5, 329–359.

Correal, N.S., Buehrer, R.M. & Woerner, B.D. (1999). A DSP-based DS-CDMA multiuser receiver employing partial parallel interference cancellation. *Selected Areas in Communications, IEEE Journal on.* 17:4, 613–630.

Cover, T. (1972). Broadcast channels. *Information Theory, IEEE Transactions on.* 18:1, 2–14.

Dai, H., Molisch, A. F. & Poor, H. V. (2004). Downlink capacity of interference-limited MIMO systems with joint detection. *IEEE Transactions on Wireless Communications.* 3:2, 442–453.

Divsalar, D., Simon, M. K. & Raphaeli, D. (1998). Improved parallel interference cancellation for CDMA. *Communications, IEEE Transactions on.* 46:2, 258–268.

Dongning, G., Rasmussen, L.K., Sumei, S. & Lim, T.J. (2000). A matrix-algebraic approach to linear parallel interference cancellation in CDMA. *Communications, IEEE Transactions on.* 48:1, 152–161.

Doppler, K., Rinne, M., Wijting, C., Ribeiro, C.B. & Hugl, K. (2009). Device-to-device communication as an underlay to LTE-advanced networks. *IEEE Communications Magazine.* 47:12, 42–49.

Duan, R. (2014). On Performance Analysis of Cognitive Radios. *University of Vaasa, ACTA WASAENSIA 293, COMPUTER SCIENCES 10, TELECOMMUNICATION ENGINEERING*.

Duman, T. M. & Ghrayeb, A. (2007). *Coding for MIMO communication systems.* John Wiley and Sons, Ltd.

Edfors, O., Sandell, M., van de Beek, J.-J., Wilson, S. K. & Börjesson, P. O. (1998). OFDM channel estimation by singular value decomposition. *IEEE Transactions on Communications.* 46:7, 931–339.

Elshokry, A. (2010). *Complexity and performance evaluation of detection schemes for spatial multiplexing MIMO systems*. Master's Thesis, Faculty of Engineering, Islamic University Gaza, 2010.

Etemadi, N. (1981). An elementary proof of the strong law of large numbers. *Zeitschrift für Wahrscheinlichkeitstheorie und Verwandte Gebiete.* 55:1, 119–122.

Ezio, B. & Giorgio, T. (2003). Large-system analyses of multiple-antenna system capacities. *Journal of Communications and Networks.* 5:2, 96–103.

Fang, L. & Milstein, L:B. (2000). Successive interference cancellation in multi-carrier DS/CDMA. *Communications, IEEE Transactions on.* 48:9, 1530–1540.

Foschini, G. (1996). Layered space-time architecture for wireless communication in a fading environment when using multi-element antennas. *Bell Labs Tech. J.* 1:2, 41–59.

Foschini, G.J., Golden, G.D., Valenzuela, R.A & Wolniansky, P.W. (1999). Simplified processing for high spectral efficiency wireless communication employing multi-element arrays. *Selected Areas in Communications, IEEE Journal on.* 17:11, 1841–1852.

García, M. & Oberli, C. (2009). Intercarrier Interference in OFDM: A General Model for Transmissions in Mobile Environments with Imperfect Synchronization. *EURASIP J. Wireless Comm. and Networking.* 2009.

Godara, L.C. (1997). Applications of antenna arrays to mobile communications I: Performance improvement, feasibility, and system considerations. *Proceedings of the IEEE.* 85:7, 1031–1060.

Gomadam, K. S., Cadambe, V. R. & Jafar, S. A. (2008). Approaching the Capacity of Wireless Networks through Distributed Interference Alignment. *in 'GLOBECOM', IEEE.* 7:7, 4260–4265.

Gong, C., Abu-Ella, O., Wang, X. & Tajer, A. (2012). Constrained Group Decoder for Interference Channels. *JCM.* 7:5, 382–390.

Gong, C., Tajer, A. & Wang, X. (2011). Interference Channel with Constrained Partial Group Decoding. *IEEE Transactions on Communications.* 59:11, 3059–3071.

Gong, C. & Ming, Z. (2006). Linear programming in multi-user scheduling for MIMO broadcast channels. *IET International Conference on.* Nov, 1–4.

Gore, D., Gorokhov, A. & Paulraj, A. (2002). Joint MMSE versus V-BLAST and antenna selection. *Signals, Systems and Computers, 2002. Conference Record of the Thirty-Sixth Asilomar Conference on.* 1, 505–509.

Grinstead, C.M. & Snell, J.L. (2003). *Introduction to Probability*. AMS.

Gu, J. & de Lamare, R.C. (2014). Joint parallel interference cancellation and relay selection algorithms based on greedy techniques for cooperative DS-CDMA systems. *Acoustics, Speech and Signal Processing (ICASSP), 2014 IEEE International Conference on.* May, 2754–2758.

Gursoy, M. C. (2009). MIMO Wireless Communications under Statistical Queueing Constraints. *Allerton 2009. 47th Annual Allerton Conference on.* , 1153–1160.

Gursoy, M. C. (2011). MIMO Wireless Communications Under Statistical Queueing Constraints. *IEEE Transactions on Information Theory.* 57:9, 5897–5917.

Guthy, C., Utschick, W. & Honig, M.L. (2013). Large System Analysis of Sum Capacity in the Gaussian MIMO Broadcast Channel. *Selected Areas in Communications, IEEE Journal on.* 31:2, 149–159.

Haartsen, J.C. (2008). Impact of non-reciprocal channel conditions in broadband TDD systems. *Personal, Indoor and Mobile Radio Communications, 2008. PIMRC 2008. IEEE 19th International Symposium on.* Sep, 15–18.

Hamza, A.S., Khalifa, S.S., H.S. Hamza,H.S. & Elsayed, K. (2013). A survey on inter-cell interference coordination techniques in ofdma-based cellular networks. *Communications Surveys Tutorials, IEEE.* 15:4, 1642–1670.

Han, T. S. & Kobayashi, K. (1981). A new achievable rate region for the interference channel. *IEEE Transactions on Information Theory.* 27:1, 49–60.

Han, F. & Liu, K.J.R. (2014). A Multiuser TRDMA Uplink System with 2D Parallel Interference Cancellation. *Communications, IEEE Transactions on.* 62:3, 1011–1022.

Harrington, R.F. & Lepage, W.R. (1952). Directional Antenna Arrays of Elements Circularly Disposed About a Cylindrical Reflector. *Proceedings of the IRE.* 40:1, 83–86.

Huh, H., Caire, G., Papadopoulos, H. C. & Ramprashad, S. A. (2011). Achieving Massive MIMO Spectral Efficiency with a Not-so-Large Number of Antennas. *IEEE Transactions on Wireless Communications.* 11:9, 3226-3239.

Jankiraman, M. (2004). *Space-Time Codes and MIMO Systems.* Artech House, Inc., Norwood, MA, USA.

Joham, M., Utschick, W. & Nossek, J. A. (2005). Linear transmit processing in MIMO communications systems. *IEEE Transactions on Signal Processing.* 53:(8-1), 2700–2712.

Joshi, S.A.; Rukmini, T.S.; Mahesh, H.M. (2011). Error rate analysis of the V-BLAST MIMO channels using interference cancellation detectors. *Signal Processing, Communication, Computing and Networking Technologies (ICSCCN), 2011 International Conference on.*, 614–618

Jung, M., Kim, T., Min, K., Kim, Y., Lee, J. & Choi, S. (2013). Asymptotic Distribution of System Capacity in Multiuser MIMO Systems with Large Number of Antennas. *Vehicular Technology Conference (VTC) Spring), 2013 IEEE 77th*, 1–5.

Kamath, M.A. & Hughes, B.L. (2005). The asymptotic capacity of multiple-antenna Rayleigh-fading channels. *Information Theory, IEEE Transactions on.* 51:12, 4325–4333.

Kim, Y., Chae, H., Kim, K., Yang, J. & Kim, D. (2008). Performance analysis of random beamforming for MIMO broadcast channel: Outage probability approach. *In Convergence and Hybrid Information Technology, 2008. ICCIT '08. Third International Conference on.* 2, 317–323.

Kountouris, M. & Gesbert, D. (2005). Robust multi-user opportunistic beamforming for sparse networks. *In Signal Processing Advances in Wireless Communications, 2005 IEEE 6th Workshop on* , 975–979.

Kramer, G., (2006). Review of rate regions for interference channels. *In Communications, 2006 International Zurich Seminar on*, 162–165.

Krebs, A., Joham, M. & Utschick, W. (2014). An adaptive MMSE-SIC soft detector with error regularization for iterative MIMO receivers. *Acoustics, Speech and Signal Processing (ICASSP), 2014 IEEE International Conference on.* May 2014, 1961–1965.

Kumar, A., Chandrasekaran, S., Chockalingam, A. & Rajan, B. S. (2011). Near-optimal large-MIMO detection using randomized mcmc and randomized search algorithms. *In Communications (ICC), 2011 IEEE International Conference on*, 1–5.

Kumari, J. (2010). MIMO-ofdm for 4G wireless systems. *In International Journal of Engineering Science and Technology.* 2, 2886–2889

Larsson, E. ,Edfors, O., Tufvesson, F. & Marzetta, T. (2014). Massive MIMO for next generation wireless systems. *Communications Magazine, IEEE* 52:2, 186–195.

Larsson, E. G. & Stoica, P. (2008). *Space-Time Block Coding for Wireless Communications*. Cambridge University Press, New York, NY, USA, 1st edition.

Lau, V.K.N., Liu, Y., & Chen, T.-A. (2002). Optimal multi-user space time scheduling for wireless communications. *In Vehicular Technology Conference, 2002. Proceedings. VTC 2002-Fall.* 4, 1939–1942

Lee, J. H. & Choi, W. (2010). Opportunistic Interference Aligned User Selection in Multiuser MIMO Interference Channels. *in GLOBECOM , IEEE*, 1-5.

Lee, J.; Toumpakaris, D. & Yu, W. (2011). Interference Mitigation via Joint Detection. *IEEE Journal on Selected Areas in Communications.* 29:6, 1172–1184.

Lei, L., Zhong, Z., Lin, C. & Shen, X. (2012). Operator controlled device-to-device communications in LTE-advanced networks. *IEEE Wireless Communications.* 19:3, 96–104.

Lin, H., Tang, Y., Guan, L. & Shao, S. (2011). Ordered Successive Interference Cancellation (OSIC) in V-BLAST Systems with Asynchronous Transmission Mode. *Wireless Personal Communications.* 60, 263–275.

Lu, L., Li, G., Swindlehurst, A., Ashikhmin, A. & Zhang, R. (2013). An Overview of Massive MIMO: Benefits and Challenges. *Selected Topics in Signal Processing, IEEE Journal of.* 99, 1–18.

Luo, Z-Q., Shum, W-Y. & Zhao, G. (2004). User capacity analysis of space division multiple access channel. *Signals, Systems and Computers, 2004. Conference Record of the Thirty-Seventh Asilomar Conference on.* 1, 223–227.

Marzetta, T.L. (2010). Noncooperative Cellular Wireless with Unlimited Numbers of Base Station Antennas. *Wireless Communications, IEEE Transactions on.* 9:11, 3590–3600.

Mietzner, J.; Schober, R.; Lampe, L.; Gerstacker, W.H. & Hoeher, P.A., (2009). Multiple-antenna techniques for wireless communications - a comprehensive literature survey. *Communications Surveys & Tutorials, IEEE.* 11:2, 87–105.

Miridakis, N.I & Vergados, D.D. (2013). A Survey on the Successive Interference Cancellation Performance for Single-Antenna and Multiple-Antenna OFDM Systems. *Communications Surveys & Tutorials, IEEE.* 15:1, 312–335.

Mohammed, S. K., Chockalingam, A. & Rajan, B. S. (2008). A Low-Complexity Precoder for Large Multiuser MISO Systems. *in 'VTC Spring' , IEEE*, 797-801.

Mohapatra, P.; Nissar, K. E. & Murthy, C. R. (2011). Interference Alignment Algorithms for the K User Constant MIMO Interference Channel. *IEEE Transactions on Signal Processing.* 59:11, 5499–5508.

Musavian, L. & Aïssa, S. (2010). Effective capacity of delay-constrained cognitive radio in Nakagami fading channels. *IEEE Transactions on Wireless Communications.* 9:3, 1054–1062.

National Communications System Technology & Standards Division (1991). Telecommunications: Glossary of Telecommunication Terms [Web document]. [Cited in 2013]. General Services Administration Information Technology Service. Available at:`http://www.its.bldrdoc.gov/fs-1037/fs-1037c.htm`, 1991.

Ngo, H. Q., Larsson, E. G. & Marzetta, T. L. (2011). Energy and Spectral Efficiency of Very Large Multiuser MIMO Systems. *CoRR abs/1112.3810*.

Nguyen-Le, H. Le-Ngoc, T. & Canonne-Velasquez, L. (2010). Heterogeneous multiuser transmission with bem-based limited feedback over doubly selective MIMO downlink channels. *In Telecommunications (ICT), 2010 IEEE 17th International Conference on*, 350–355.

Norstad, J. (1999). The Normal and Lognormal Distributions. *John Norstad. Probability review.* [Web document] [Feb. 2014]. Available at: `http://www.norstad.org/finance/normdist.pdf`.

Pateromichelakis, E., Shariat, M., ul Quddus, A. & Tafazolli, R. (2013). On the Evolution of Multi-Cell Scheduling in 3GPP LTE / LTE-A.. *IEEE Communications Surveys and Tutorials.* 15:2, 701–717.

Paulraj, A. & Kailath, T. (1994). Increasing capacity in wireless broadcast systems using distributed transmission/directional reception (DTDR). *U.S. Patent 5,345,599*, Sep. 06, 1994.

Pedersen, K.I., Kolding, T.E., Seskar, I. & Holtzman, J:M. (1996). Practical implementation of successive interference cancellation in DS/CDMA systems. *Universal Personal Communications, 1996. Record., 1996 5th IEEE International Conference on.* 1, 321–325.

Petrus, P., Ertel, R.B. & Reed, J.H. (1998). Capacity enhancement using adaptive arrays in an AMPS system. *Vehicular Technology, IEEE Transactions on.* 47:3, 717–727.

Phelts, R. E. & Enge, P. (2000). The case for narrowband receivers. *In Proceedings of the 2000 National Technical Meeting, Institute of Navigation, January*.

Pi, Z. & Khan, F. (2012). A millimeter-wave massive MIMO system for next generation mobile broadband. *Signals, Systems and Computers (ASILOMAR), 2012 Conference Record of the Forty Sixth Asilomar Conference on.* Nov., 693–698.

Prasad, N. & Wang, X. (2009). Outage minimization and rate allocation for the multiuser Gaussian interference channels with successive group decoding. *IEEE Transactions on Information Theory.* 55:12, 5540–5557.

Rappaport, T.S., Sun, S., Mayzus, R., Zhao, H., Azar, Y., Wang, K., Wong, G.N., Schulz, J.K., Samimi, M. & Gutierrez, F. (2013). Millimeter Wave Mobile Communications for 5G Cellular: It Will Work!. *Access, IEEE.* 1, 335–349.

Rasmussen, L.K., Lim, T.J. & Johansson, A-L. (2000). A matrix-algebraic approach to successive interference cancellation in CDMA. *Communications, IEEE Transactions on.* 48:1, 145–151.

Rugini, L., Banelli, P. & Leus, G. (2005). Simple equalization of time-varying channels for OFDM. *IEEE Communications Letters.* 9:7, 619–621.

Rusek, F.; Persson, D.; Lau, B. K.; Larsson, E. G.; Marzetta, T. L.; Edfors, O. & Tufvesson, F. (2013). Scaling Up MIMO: Opportunities and Challenges with Very Large Arrays. *IEEE Signal Process. Mag.* 30:1, 40–60.

Sawahashi,M.; Kishiyama, Y.; Morimoto, A.; Nishikawa, D. & Tanno, M. (2010). Coordinated multipoint transmission/reception techniques for LTE-advanced [Coordinated and Distributed MIMO]. *Wireless Communications, IEEE.* 17:3, 26–34.

Seethaler, D., Artes, H. & Hlawatsch, F. (2005). Detection techniques for MIMO spatial multiplexing systems. *Elektrotechnik und Informationstechnik (E & I).* 122:3, 91–96.

Sfar, S., Letaief, K.B. (2003). Group ordered successive interference cancellation for multiuser detection in MIMO CDMA systems. *Wireless Communications and Networking, 2003. (WCNC 2003).* 2:3, 888–893.

Singh, S., Kumar, A., Khurmi, S.S. & Singh, T. (2012). Coordinated Multipoint (CoMP) Reception and Transmission for LTE-Advanced/4G. *International Journal of Computer Sci ence And Technology (IJCST).* 3:2, 212–217.

Shen, H., Li, B., Tao, M. & Wang, X. (2010). MSE-Based Transceiver Designs for the MIMO Interference Channel. *IEEE Transactions on Wireless Communications.* 9:11, 3480–3489.

Shi, Q., Fang, Y. & Wang, M. (2009). A novel ICI self-cancellation scheme for OFDM systems. *In Wireless Communications, Networking and Mobile Computing WiCom '09. 5th International Conference on*, 1–4.

Sigdel, S., Elliott, R. C., Krzymien, W. A. & Al-Shalash, M. (2009). Greedy and Genetic User Scheduling Algorithms for Multiuser MIMO Systems with Block Diagonalization. *in 70th 'VTC Fall' , IEEE*, 1–6.

Siriteanu, C., Blostein, S. D., Takemura, A.; Shin, H. & Yousefi, S. (2013). Exact Performance Analysis of MIMO Zero Forcing Detection for Transmit Correlated Rician Rayleigh Fading. *CoRR abs/1307.2958.*

Smith, P. & Shafi, M. (2004). An approximate capacity distribution for MIMO systems. *Communications, IEEE Transactions on.* 52:6, 887–890.

Spencer, Q. H., Swindlehurst, A. L. & Haardt, M. (2004). multiplexing in multiuser MIMO channels. *IEEE Transactions on Signal Processing.* 52:2, 461–471.

Sun, H., Wang, D., Xie, Y. & You, X. (2008). Performance analysis of multi-user scheduling over time-varying channel. *In Communications, Circuits and Systems, 2008. ICCCAS 2008. International Conference on.* May, 144–147.

Suthisopapan, P., Kasai, K., Meesomboon, A. & Imtawil, V. (2012). Near Capacity Approaching for Large MIMO Systems by Non-Binary LDPC Codes with MMSE Detection. *CoRR abs/1203.0960.*

Tajer, A., Prasad, N. & Wang, X. (2010). Beamforming and rate allocation in MISO cognitive radio networks. *IEEE Transactions on Signal Processing.* 58:1, 362–377.

Tajer, A. & Wang, X. (2008). Opportunistic multi-antenna downlink transmission with finite-rate feedback. *In Communication, Control, and Computing, 2008, 46th Annual Allerton Conference on.* Sep., 79–86.

Tajer, A.& Wang, X. (2010). Downlink multiuser MIMO with limited feedback orthogonal random beamforming. *In Technical Report: Department of Electrical Engineering, Columbia University.*

Tanbourgi, R., Jakel, H. & Jondral, F.K. (2014). Cooperative interference cancellation using device-to-device communications. *Communications Magazine, IEEE.* 52:6, 118–124.

Tolga, G., Chenxi, Z., Jonathan, A.R. & Anthony, E. (2010). Proportional Fair Scheduling Algorithm in OFDMA-Based Wireless Systems with QoS Constraints. *JOURNAL OF COMMUNICATIONS AND NETWORKS.* 12:1, 30–42.

Torabzadeh, M. & Ajib, W. (2010). Packet Scheduling and Fairness for Multiuser MIMO Systems. *IEEE T. Vehicular Technology* 59:3, 1330–1340.

Tresch, R., Guillaud, M. & Riegler, E. (2009). On the Achievability of Interference Alignment in the K-User Constant MIMO Interference Channel. *In Statistical Signal Processing, 2009. SSP '09. IEEE/SP 15th Workshop on.* Sep., 277–280.

Tsang, C.-S & Nguyen, T. M. (2004). Survey of signal processing techniques for interference suppression in communication. *In Aerospace Conference, 2004. Proceedings. 2004 IEEE.* 2, 1347–1354.

Tse, D. (2001). Multiuser diversity in wireless networks [Web document]. [Cited in 2014]. Available at:`http://www.eecs.berkly.edu/dtse/stanford416.ps`, Apr. 2001.

Tse, D. & Viswanath, P. (2005). *Fundamentals of Wireless Communication*. Cambridge University Press, New York, NY, USA.

Van Dierendonck, A. J, Fenton, P. & Ford, T. (1992). Theory and Performance of Narrow Correlator Spacing in a GPS Receiver. *IEEE T. Vehicular Technology.* 39:3, 265–283.

Van Nee, R. D. J., Siereveld, J., Fenton, P. C. & Townsend, B. R. (1994). The Multipath Estimating Delay Lock Loop: Approaching Theoretical Accuracy Limits. *Proc. of the IEEE Position Location and Navigation Symposium (PLANS).* 27, 246–251.

Varanasi, M.K. & Guess, T. (1997). Optimum decision feedback multiuser equalization with successive decoding achieves the total capacity of the Gaussian

multiple-access channel. *Signals, Systems & Computers, 1997. Conference Record of the Thirty-First Asilomar Conference on.* 2, 1405–1409.

Viswanath, P., Tse, D. & Laroia, R. (2002). Opportunistic beamforming using dumb antennas. *Information Theory, IEEE Transactions on.* 48:6, 1277–1294.

Vucetic, B., Li, Y. & Hardjawana, W. (2013). Spectrally efficient cooperative precoding and beamforming for multi-user MIMO systems. [Web document] [Cited in 2013] Available at:`http://www.cel.usyd.edu.au/research/allresearch/projects.phtml?group=tc`.

Wang, C. -X., P., Haider, F., Gao, X., You, X.-H, Yang, Y., Yuan, D., Aggoune, H. M., Haas, H., Fletcher, S., & Hepsaydir, E. (2014). Cellular architecture and key technologies for 5G wireless communication networks. *Communications Magazine, IEEE.* 52:2, 122–130.

Wang, C. -L., Huang, Y. -C. & Shen, P. -C. (2006). An intercarrier interference suppression technique using time-domain windowing for ofdm systems. *In Vehicular Technology Conference, 2006. VTC 2006-Spring. IEEE 63rd.* 5, 2518–2522.

Wang, J. & Milstein, L. B. (1995). CDMA overlay situations for microcellular mobile communications. *IEEE Transactions on Communications.* 43:234, 603–614.

Wang, Q., Jiang, D. Liu, G. & Yan, Z. (2009). Coordinated Multiple Points Transmission for LTE-Advanced Systems," Wireless Communications, Networking and Mobile Computing. *WiCom '09. 5th International Conference on.* Sep., 1–4.

Wang, Y., Feng, W., Li, Y., Zhou, S. & 0001, J. W. (2011). Coordinated User Scheduling for Multi-Cell Distributed Antenna Systems. *in 'GLOBECOM', IEEE* , 1–5.

Weingarten, H., Steinberg, Y. & Shamai, S. (2006). The Capacity Region of the Gaussian Multiple-Input Multiple-Output Broadcast Channel. *IEEE Transactions on Information Theory.* 52:9, 3936–3964.

Weitzen, J.A., Kilpatrick, J.A. & Mui, S.Y. (1992). Large scale space diversity in a widely spaced network of meteor scatter communication systems and its application to mobile communications. *Vehicular Technology, IEEE Transactions on.* 41:4, 455–460.

Widrow, B., Mantey, P.E., Griffiths, L.J. & Goode, B.B. (1967). Adaptive antenna systems. *Proceedings of the IEEE* 55:12, 2143–2159.

Winters, J.H., Salz, J. & Gitlin, R.D. (1994). The impact of antenna diversity on the capacity of wireless communication systems. *Communications, IEEE Transactions on.* 42:234, 1740–1751.

Wu, D. & Negi, R. (2003). Effective capacity: a wireless link model for support of quality of service. *IEEE Transactions on Wireless Communications.* 2:4, 630–643.

Xue, G., Weng, J., Le-Ngoc, T. & Tahar, S. (1999). Adaptive multistage parallel interference cancellation for CDMA. *Selected Areas in Communications, IEEE Journal on.* 17:10, 1815–1827.

Yamada, M. & Ohtsuki, T. (2010). Interference alignment in the $2 \times (1 + N)$ MIMO model. *In GLOBECOM Workshops (GC Wkshps), 2010 IEEE*, 1963–1967.

Yang, L., Ming, C., Cheng, S. & Wang, H. (2004). Combined maximum likelihood and ordered successive interference cancellation grouped detection algorithm for multistream MIMO. *In Spread Spectrum Techniques and Applications, 2004 IEEE Eighth International Symposium on*, 250–254.

You, X. -H (2004). Future: towards beyond 3G mobile communications. *In Emerging Technologies: Frontiers of Mobile and Wireless Communication, 2004. Proceedings of the IEEE 6th Circuits and Systems Symposium on.* 1, 1–5.

Yu, W., Ginis, G. & Cioffi, J. M. (2002). Distributed multiuser power control for digital subscriber lines. *IEEE Journal on Selected Areas in Communications.* 20:5, 1105–1115.

Zanella, A., Chiani, M. & Win, M. Z. (2005). MMSE reception and successive interference cancellation for MIMO systems with high spectral efficiency. *IEEE Transactions on Wireless Communications.* 4:3, 1244–1253.

Zhang, R. & Hanzo, L. (2010). Wireless cellular networks. *Vehicular Technology Magazine, IEEE.* 5:4, 31–39.

Zheng, L. & Tse, D.N.C. (2003). Diversity and multiplexing: a fundamental tradeoff in multiple-antenna channels. *IEEE Trans. Inf. Theory.* 49:5, 1073–1096.